

UCLA

UCLA Electronic Theses and Dissertations

Title

Estimating Radiation Dose Metrics for Patients Undergoing Tube Current Modulation CT Scans

Permalink

<https://escholarship.org/uc/item/6f0592k5>

Author

McMillan, Kyle

Publication Date

2015

Peer reviewed|Thesis/dissertation

UNIVERSITY OF CALIFORNIA

Los Angeles

Estimating Radiation Dose Metrics for Patients
Undergoing Tube Current Modulation CT Scans

A dissertation submitted in partial satisfaction of the
requirements for the degree Doctor of Philosophy
in Biomedical Physics

by

Kyle Lorin McMillan

2015

© Copyright by
Kyle Lorin McMillan
2015

ABSTRACT OF THE DISSERTATION

Estimating Radiation Dose Metrics for Patients
Undergoing Tube Current Modulation CT Scans

by

Kyle Lorin McMillan

Doctor of Philosophy in Biomedical Physics

University of California, Los Angeles, 2015

Professor Michael McNitt-Gray, Chair

Computed tomography (CT) has long been a powerful tool in the diagnosis of disease, identification of tumors and guidance of interventional procedures. With CT examinations comes the concern of radiation exposure and the associated risks. In order to properly understand those risks on a patient-specific level, organ dose must be quantified for each CT scan. Some of the most widely used organ dose estimates are derived from fixed tube current (FTC) scans of a standard sized idealized patient model. However, in current clinical practice, patient size varies from neonates weighing just a few kg to morbidly obese patients weighing over 200 kg, and nearly all CT exams are performed with tube current modulation (TCM), a scanning technique that adjusts scanner output according to changes in patient attenuation. Methods to account for TCM in CT organ dose estimates have been previously demonstrated, but these methods are limited in scope and/or restricted to idealized TCM profiles that are not based on physical

observations and not scanner specific (e.g. don't account for tube limits, scanner-specific effects, etc.).

The goal of this work was to develop methods to estimate organ doses to patients undergoing CT scans that take into account both the patient size as well as the effects of TCM. This work started with the development and validation of methods to estimate scanner-specific TCM schemes for any voxelized patient model. An approach was developed to generate estimated TCM schemes that match actual TCM schemes that would have been acquired on the scanner for any patient model. Using this approach, TCM schemes were then generated for a variety of body CT protocols for a set of reference voxelized phantoms for which TCM information does not currently exist. These are whole body patient models representing a variety of sizes, ages and genders that have all radiosensitive organs identified. TCM schemes for these models facilitated Monte Carlo-based estimates of fully-, partially- and indirectly-irradiated organ dose from TCM CT exams. By accounting for the effects of patient size in the organ dose estimates, a comprehensive set of patient-specific dose estimates from TCM CT exams was developed. These patient-specific organ dose estimates from TCM CT exams will provide a more complete understanding of the dose impact and risks associated with modern body CT scanning protocols.

The dissertation of Kyle Lorin McMillan is approved.

Christopher Cagnon

James Lamb

Jianwei Miao

Michael McNitt-Gray, Committee Chair

University of California, Los Angeles

2015

I dedicate this dissertation to my wife Candice. Without her endless love and support, I would never have been able to realize my academic dreams.

TABLE OF CONTENTS

Chapter 1: Introduction	1
1.1 Background and Significance	1
1.2 Current State of the Art	3
1.3 Overview	5
1.4 References	9
Chapter 2: Specific Aims	14
Chapter 3: Monte Carlo Dosimetry Package	15
3.1 Introduction	15
3.2 Development	15
3.3 Validation	24
3.4 References	32
Chapter 4: GSF and ICRP Reference Voxelized Phantoms	35
4.1 Introduction	35
4.2 Physical Characteristics	36
4.3 Image Characteristics	38
4.4 Organ and Material Descriptions	39
4.5 Breast and Bone Dose Considerations	43
4.6 Reference Voxelized Phantom Modifications	44
4.7 References	46
Chapter 5: Determining Patient Size Data from CT Localizer Radiograph	48
5.1 Introduction	48
5.2 Methods	49
5.3 Results	58
5.4 Discussion	60
5.5 References	62
Chapter 6: Estimating Tube Current Modulation Schemes Using Patient Size Data from Topogram	64
6.1 Introduction	64
6.2 Methods	67
6.3 Results	87
6.4 Discussion	91
6.5 References	95
Chapter 7: Estimating Tube Current Modulation Schemes Using Patient Size Data from Simulated Topogram	98
7.1 Introduction	98
7.2 Methods	99
7.3 Results	112
7.4 Discussion	117
7.5 References	120
Chapter 8: Tube Current Modulation Monte Carlo Dose Simulations with GSF and ICRP Reference Voxelized Phantoms	121
8.1 Introduction	121
8.2 Methods	122
8.3 Results	132

8.4 Discussion	134
8.5 References	135
Chapter 9: Size-Specific, Scan Technique-Independent Organ Dose and Effective Dose Estimates in Tube Current Modulation CT Examinations	137
9.1 Introduction	137
9.2 Methods	140
9.3 Results	150
9.4 Discussion	156
9.5 References	160
Chapter 10: Accuracy and Generalizability of Size-Specific, Scan Technique-Independent Organ Dose Estimates In Tube Current Modulation CT Examinations	162
10.1 Introduction	162
10.2 Methods	163
10.3 Results	169
10.4 Discussion	174
10.5 References	177
Chapter 11: Size-Specific Fetal Dose Estimates in Tube Current Modulation CT Examinations of Pregnant Patients	179
11.1 Introduction	179
11.2 Methods	181
11.3 Results	187
11.4 Discussion	190
11.5 References	194
Chapter 12: Conclusion	196
12.1 Contributions	196
12.2 Future Work	198
Appendix A: Organ Irradiation Percentages for Protocols of Interest	200
A.1 Abdomen	200
A.2 Abdomen/Pelvis	201
A.3 Chest	202
A.4 Chest/Abdomen/Pelvis (CAP)	203
Appendix B: Estimates of Organ Dose and ICRP Publication 103 Calculations of Effective Dose for GSF and ICRP Reference Voxelized Phantoms	204
B.1 Baby	204
B.2 Child	205
B.3 Donna	206
B.4 Frank	207
B.5 Golem	208
B.6 Helga	209
B.7 Irene	210
B.8 ICRP Female (Regina)	211
B.9 ICRP Male (Rex)	212
B.10 Visible Human	213
Appendix C: Estimates of Organ Dose and ICRP Publication 60 Calculations of Effective Dose for GSF and ICRP Reference Voxelized Phantoms	214
C.1 Baby	214

C.2 Child.....	215
C.3 Donna.....	216
C.4 Frank.....	217
C.5 Golem.....	218
C.6 Helga.....	219
C.7 Irene.....	220
C.8 ICRP Female (Regina).....	221
C.9 ICRP Male (Rex).....	222
C.10 Visible Human.....	223
Appendix D: Estimates of WED_{protocol} and WED_{organ} for Protocols of Interest.....	224
D.1 WED_{protocol} – All Protocols.....	224
D.2 WED_{organ} – Abdomen.....	225
D.3 WED_{organ} – Abdomen/Pelvis.....	226
D.4 WED_{organ} – Chest.....	227
D.5 WED_{organ} – Chest/Abdomen/Pelvis (CAP).....	228
Appendix E: Estimates of $CTDI_{\text{vol,protocol}}$ and $CTDI_{\text{vol,organ}}$ for Protocols of Interest.....	229
E.1 $CTDI_{\text{vol,protocol}}$ – All Protocols.....	229
E.2 $CTDI_{\text{vol,organ}}$ – Abdomen.....	230
E.3 $CTDI_{\text{vol,organ}}$ – Abdomen/Pelvis.....	231
E.4 $CTDI_{\text{vol,organ}}$ – Chest.....	232
E.5 $CTDI_{\text{vol,organ}}$ – Chest/Abdomen/Pelvis (CAP).....	233

LIST OF FIGURES

Figure 1.1. Overview of objectives from this dissertation. The development of methods to estimate scanner-specific TCM schemes will be discussed in Chapters 5-7. TCM schemes will be determined for a set of pediatric and adult reference voxelized phantoms in Chapter 8. Size-specific, scan technique-independent organ dose and effective dose estimates determined from TCM Monte Carlo simulations of the reference voxelized phantoms will be discussed in Chapter 9.....	7
Figure 3.1. Example of TCM scheme extracted from the raw projection data of a patient who underwent a clinically indicated chest CT exam on a Siemens Sensation 64 scanner.	19
Figure 3.2. (Left) Breasts and lungs contoured from axial image of patient who underwent chest CT exam. (Right) Monte Carlo representation of the patient with all non-contoured regions identified as a specific tissue using Hounsfield lookup table.	21
Figure 3.3. Pyramid diagram of different levels of validation. Level 1 involves simple phantoms that are homogeneous in composition. Level 2 involves phantoms that are heterogeneous in composition or shape (or even both).....	25
Figure 3.4. (Left) Diagram of AAPM Report 195 Case #4: Computer tomography with simple solids. (Right) Diagram of AAPM Report 195 Case #5: Computed tomography with a voxelized solid.	26
Figure 3.5. 16 cm head and 32 cm body CTDI phantoms.	28
Figure 3.6. (Left) Elliptical phantom. (Middle) Rectangular water phantom. (Right) Anthropomorphic phantom.	30
Figure 3.7. (Left) TLD (red) segmented from axial image of patient who underwent VC exam. (Right) Zoomed in view of TLD segmentation.	31
Figure 4.1. Cross-sectional images of the GSF and ICRP reference voxelized phantoms (a) Baby, (b) Child, (c) Donna, (d) Frank, (e) Golem, (f) Helga, (g) Irene, (h) Visible Human, (i) ICRP Male (Rex) and (j) ICRP Female (Regina).	38
Figure 4.2. Example of modifications made to the Visible Human reference voxelized phantom: (a) Original reference voxelized phantom with arms, (b) arms removed and (c) arms removed and shoulders modified to represent “arms up” anatomy.	45
Figure 5.1. DICOM field (0029,1140) from Siemens topogram.	50
Figure 5.2. Siemens topogram evaluated as a text file reveals array of numbers inferred to be patient size data. This is assumed to be the data stored in DICOM field (0029.1140).....	52
Figure 5.3. AP, LAT and $D_{w,topo}$ overlaid on topograms of patients who underwent abdomen/pelvis (left) and chest (right) CT examinations.....	55
Figure 5.4. $D_{w,topo}$ and $D_{w,image}$ overlaid on topograms of patients who underwent abdomen/pelvis (left) and chest (right) CT examinations.	57
Figure 6.1. AP and LAT water-equivalent estimates of patient size extracted from the topogram of an adult patient who underwent a clinically indicated chest CT examination. This patient will be used as an example throughout the development of the methods to estimate scanner-specific TCM schemes presented in this investigation.	68
Figure 6.2. (Left) Patient size data extracted from topogram. (Right) Maximum patient attenuation at each table position calculated from patient size data using Eq. (6.1).	70

Figure 6.3. Different strength settings used by Siemens to adjust tube current relative to QRM defined at a reference patient attenuation. Image courtesy of Ronald Booiij, Department of Radiology, Erasmus MC, Rotterdam, The Netherlands.	72
Figure 6.4. (Left) Patient attenuation calculated from size data extracted from topogram. (Right) Tube current profile calculated from patient attenuation data using Eq. (6.2) at all table positions with corresponding axial CT images.	73
Figure 6.5. (Left) Patient size data extracted from topogram. (Right) Angular attenuation profile determined from patient size data. The blue dots are the AP and LAT locations, and the green lines are the interpolated patient size.	75
Figure 6.6. (Left) Angular attenuation profile determined from patient size data extracted from topogram. (Right) Angular modulation scheme calculated from angular attenuation data using Eq. (6.5) at all table positions with corresponding axial CT images.	77
Figure 6.7. Estimated and actual TCM schemes for adult chest patient. Estimated TCM scheme calculated from control curve and angular modulation scheme from Fig. 6.4 and Fig. 6.6, respectively. Actual TCM scheme extracted from raw projection data.	79
Figure 6.8. Estimated and actual TCM schemes from Fig. 6.7 with areas of disagreement labeled: (1) estimated tube current is too high in the shoulders (high attenuation region) and (2) estimated tube current does not increase fast enough moving into the abdomen from the thorax.	80
Figure 6.9. Estimated and actual TCM schemes of adult chest patient will modifications to account for tube limits and increasing attenuation applied to the estimate TCM scheme.	83
Figure 6.10. Central slice of axial images of smallest (left) and largest (right) chest patients used in the validation study. Both images were reconstructed in a 500 mm field of view.	86
Figure 6.11. Central slice of axial images of smallest (left) and largest (right) abdomen/pelvis patients used in the validation study. Both images were reconstructed in a 500 mm field of view.	86
Figure 6.12. Estimated and actual TCM schemes for pediatric (left) and adult (right) chest patients.	91
Figure 6.13. Estimated and actual TCM schemes for pediatric (left) and adult (right) abdomen/pelvis patients.	91
Figure 6.14. TCM schemes for 80 kVp pediatric abdomen/pelvis patient estimated using “Average” (left) and stronger response (right).	93
Figure 6.15. Estimated and actual TCM schemes for Sensation 16 (left) and Definition Flash (right) chest patients.	94
Figure 6.16. Available methods to generate Siemens TCM schemes. This investigation introduces methods to estimate TCM schemes using patient size data extracted from the topogram.	95
Figure 7.1. Diagram of AP projectional imaging setup.	101
Figure 7.2. Air scan and patient scan fluence profiles at a particular table location for an adult patient who underwent a clinically indicated chest CT examination. This patient will be used as an example throughout the development of the methods to estimate Siemens patient attenuation information presented in this investigation.	103
Figure 7.3. (Left) Air scan and patient scan fluence profiles. (Right) Patient attenuation profile along the detector calculated by dividing the fluence profile from the air scan by the fluence profile from the patient scan.	104

Figure 7.4. (Left) Patient attenuation profile calculated from air scan and patient scan fluence profiles. (Right) Moving average filter with span of 5 cm applied to patient attenuation profile to eliminate any spurious peaks caused by strong local attenuations.	105
Figure 7.5. (Left) Patient attenuation profile (represented as a bar plot with each bar representing the attenuation value at each detector element) before outside air and table threshold applied. (Right) Patient attenuation profile with outside air and table detector elements eliminated by a threshold value of 1.8.	106
Figure 7.6. (Left) Patient attenuation profile after outside and table threshold applied. (Right) Patient attenuation profile with low-attenuation region detector elements eliminated by a threshold value of 9% of the maximum attenuation from the attenuation profile.	108
Figure 7.7. Diagram of scanner geometry with all components of Eq. (7.5) labeled.	111
Figure 7.8. (Left) Estimated AP and LAT dimensions of patient size compared with AP and LAT dimensions of patient size extracted from the topogram of a patient who underwent a clinically indicated chest CT exam. (Right) Estimated AP and LAT dimensions of patient size compared with AP and LAT dimensions of patient size extracted from the topogram of a patient who underwent a clinically indicated abdomen/pelvis CT exam. (Note: The estimated patient attenuation data (solid lines) was derived from the patient's axial image data and therefore does not include the extra anatomy before and after the scan range in the patient's actual topogram (dashed lines).)	113
Figure 7.9. (Left) TCM from simulated topogram and actual TCM scheme for chest patient. (Right) TCM from simulated topogram and actual TCM scheme for abdomen/pelvis patient.	114
Figure 7.10. Available methods to generate Siemens TCM schemes. This investigation introduces methods to estimate TCM schemes using patient size calculated from a simulated topogram.	120
Figure 8.1. AP and LAT dimensions of patient size determined from the whole body simulated topogram of the Visible Human reference voxelized phantom.	123
Figure 8.2. Visible Human reference voxelized phantom TCM schemes for abdomen (top left), abdomen/pelvis (top right), chest (bottom left) and CAP (bottom right) protocols.	126
Figure 9.1. Patient size data for Visible Human reference voxelized phantom. Chest protocol scan range, central table position of scan range and lung extent annotated on size data. WED_{protocol} calculated as the WED at the table location at the center of the scan range. WED_{organ} calculated as the average WED over all table positions within the anatomical extent of the lungs.	143
Figure 9.2. Chest protocol TCM scheme and FTC profile for Visible Human reference voxelized phantom. Chest protocol scan range and lung extent annotated on tube current profiles. $CTDI_{\text{vol,protocol}}$ based on the average tube current across the entire chest scan range. $CTDI_{\text{vol,organ}}$ based on the average tube current across all slices containing the lungs.	144
Figure 10.1. Comparison of simulated liver dose for patients scanned on Siemens, GE and Toshiba scanners and liver dose estimated using TCM, FTC and SSDE conversion coefficients for the protocol-specific (left) and organ-specific (right) approaches.	171
Figure 10.2. Comparison of simulated kidney dose for patients scanned on Siemens, GE and Toshiba scanners and kidney dose estimated using TCM, FTC and SSDE conversion coefficients for the protocol-specific (left) and organ-specific (right) approaches.	171

Figure 10.3. Comparison of simulated spleen dose for patients scanned on Siemens, GE and Toshiba scanners and spleen dose estimated using TCM, FTC and SSDE conversion coefficients for the protocol-specific (left) and organ-specific (right) approaches.	172
Figure 10.4. Comparison of simulated lung dose for patients scanned on Siemens, GE and Toshiba scanners and lung dose estimated using TCM, FTC and SSDE conversion coefficients for the protocol-specific (left) and organ-specific (right) approaches.	173
Figure 10.5. Comparison of simulated breast dose for patients scanned on Siemens, GE and Toshiba scanners and breast dose estimated using TCM, FTC and SSDE conversion coefficients for the protocol-specific (left) and organ-specific (right) approaches.	174
Figure 11.1. Axial (left) and sagittal (right) images of a pregnant patient at a gestational age of 24 weeks who underwent a clinically indicated abdomen/pelvis CT examination.	182
Figure 11.2. (Center) Gestational sac (yellow), uterus (pink) and fetus (red) segmented from the images of a pregnant patient. (Right) Monte Carlo representation of the patient with all voxels assigned to a specific tissue type [5].	183
Figure 11.3. Estimated TCM scheme for a pregnant patient who received a clinically indicated CT examination. The TCM scheme is overlaid on an image of the simulated CT localizer radiograph of the pregnant patient. The portion of the scan range in which the fetus is located is indicated with blue dashed lines.	185
Figure 11.4. FTC and TCM $CTDI_{vol}$ -normalized fetal doses determined from detail Monte Carlo simulations as well as TCM, FTC and SSDE conversion coefficients (fits).	189

LIST OF TABLES

Table 4.1. Physical characteristics of GSF and ICRP reference voxelized phantoms. Data in parentheses refers to the weight or height of the reference voxelized phantom. Data not in parentheses refers to the weight or height of the actual patient whose images were used to create the phantom.	37
Table 4.2. Image characteristics of GSF and ICRP reference voxelized phantoms.	39
Table 4.3. Organs and respective tissue weighting factors used in the ICRP Publication 103 calculation of effective dose. All primary organs have their own weighting factor while the average dose to all remainder organs has a weighting factor of 0.12.	41
Table 4.4. Organs and respective tissue weighting factors used in the ICRP Publication 60 calculation of effective dose. All primary organs have their own weighting factor while the average dose to all remainder organs has a weighting factor of 0.05.	42
Table 4.5. Organ substitutes for ICRP 103/ICRP 60 organs not identified in all GSF and ICRP reference voxelized phantoms.	42
Table 5.1. Comparison of two estimates of WED ($D_{w,image}$ and $D_{w,topo}$).	59
Table 5.2. Comparison of SSDE calculated using two estimates of WED ($D_{w,image}$ and $D_{w,topo}$).	60
Table 6.1. Protocol-specific reference attenuation for protocols of interest in this investigation. Corresponding water-equivalent length given in parentheses.	71
Table 6.2. Modulation index limits as a function of gantry rotation time.	76
Table 6.3. Tube current limits for various tube voltages for the Sensation 64 CT scanner.	82
Table 6.4. Patient size and scan techniques for validation patients.	85
Table 6.5. Comparison of average tube current between actual and estimated TCM schemes.	88
Table 6.6. Comparison of lung and breast dose from Monte Carlo simulations of chest CT exams using actual and estimated TCM schemes.	89
Table 6.7. Comparison of liver, kidney and spleen dose from Monte Carlo simulations of abdomen/pelvis CT exams using actual and estimated TCM schemes.	90
Table 7.1. Comparison of average tube current between actual and estimated TCM schemes.	115
Table 7.2. Comparison of lung and breast dose from Monte Carlo simulations of chest CT exams using actual and estimated TCM schemes.	116
Table 7.3. Comparison of liver, kidney and spleen dose from Monte Carlo simulations of abdomen/pelvis CT exams using actual and estimated TCM schemes.	117
Table 8.1. Scan ranges for protocols used in this investigation.	124
Table 8.2. Technical settings used for all Monte Carlo simulations.	125
Table 8.3. Protocol-specific adult reference attenuation values for protocols of interest in this investigation. Corresponding water-equivalent length given in parentheses. For Siemens Definition class scanners, both pediatric and adult patients are scanned with the same set of reference attenuation values. For Siemens Sensation class scanners, pediatric patients are scanned with a different set of reference attenuation values. In this investigation, a Definition Flash scanner model was used in the simulations, so both pediatric and adult reference voxelized phantoms were scanned with this set of reference attenuation values.	125
Table 8.4. Organs of interest whose doses are tallied within each of the Monte Carlo simulations in this investigation. Anatomical substitutes are given in parentheses.	127
Table 8.5. Criteria for organ irradiation classification for each organ for a given protocol.	128

Table 8.6. Organ irradiation classifications for abdomen protocol. ICRP Publication 103 and ICRP Publication 60 tissue weighting factors for each organ are also presented.....	129
Table 8.7. Organ irradiation classifications for abdomen/pelvis protocol. ICRP Publication 103 and ICRP Publication 60 tissue weighting factors for each organ are also presented.....	130
Table 8.8. Organ irradiation classifications for chest protocol. ICRP Publication 103 and ICRP Publication 60 tissue weighting factors for each organ are also presented.....	131
Table 8.9. Organ irradiation classifications for CAP protocol. ICRP Publication 103 and ICRP Publication 60 tissue weighting factors for each organ are also presented.....	132
Table 8.10. Simulated organ doses and ICRP Publication 103 calculations of effective dose for the Visible Human reference voxelized phantom. Values are tabulated for both TCM and FTC for all protocols used in this investigation.....	133
Table 9.1. Age-specific k-factor values for protocols of interest in this investigation.....	149
Table 9.2. Exponential regression coefficients and R^2 for each organ for abdomen protocol. ..	151
Table 9.3. Exponential regression coefficients and R^2 for each organ for abdomen/pelvis protocol.....	152
Table 9.4. Exponential regression coefficients and R^2 for each organ for chest protocol.....	153
Table 9.5. Exponential regression coefficients and R^2 for each organ for CAP protocol.....	154
Table 9.6. Exponential regression coefficients and R^2 for ICRP 103 calculation of effective dose.....	154
Table 9.7. Exponential regression coefficients and R^2 for ICRP 60 calculation of effective dose.....	155
Table 9.8. Mean error across all reference voxelized phantoms between ICRP Publication 103 calculations of effective dose from the simulated organ doses (Appendix B) and effective doses determined using the various estimation methods.....	155
Table 9.9. Mean error across all reference voxelized phantoms between ICRP Publication 60 calculations of effective dose from the simulated organ doses (Appendix C) and effective doses determined using the various estimation methods.....	156
Table 10.1. Summary of patient image data used in this investigation.....	164
Table 10.2. Exponential regression coefficients and R^2 for organs of interest within the abdomen/pelvis protocol.....	166
Table 10.3. Exponential regression coefficients and R^2 for organs of interest within the chest protocol.....	166
Table 10.4. Mean error and SD of error across scanner-specific and pooled patients between simulated liver dose for an abdomen/pelvis scan and liver dose estimated using TCM, FTC and SSDE conversion coefficients for the same scan. Errors evaluated for conversion coefficients determined using the protocol-specific and organ-specific approaches.....	170
Table 10.5. Mean error and SD of error across scanner-specific and pooled patients between simulated kidney dose for an abdomen/pelvis scan and kidney dose estimated using TCM, FTC and SSDE conversion coefficients for the same scan. Errors evaluated for conversion coefficients determined using the protocol-specific and organ-specific approaches.....	170
Table 10.6. Mean error and SD of error across scanner-specific and pooled patients between simulated spleen dose for an abdomen/pelvis scan and spleen dose estimated using TCM, FTC and SSDE conversion coefficients for the same scan. Errors evaluated for conversion coefficients determined using the protocol-specific and organ-specific approaches.....	170
Table 10.7. Mean error and SD of error across scanner-specific and pooled patients between simulated lung dose for a chest scan and lung dose estimated using TCM, FTC and SSDE	

conversion coefficients for the same scan. Errors evaluated for conversion coefficients determined using the protocol-specific and organ-specific approaches.	173
Table 10.8. Mean error and SD of error across scanner-specific and pooled patients between simulated breast dose for a chest scan and breast dose estimated using TCM, FTC and SSDE conversion coefficients for the same scan. Errors evaluated for conversion coefficients determined using the protocol-specific and organ-specific approaches.....	173
Table 11.1. Technical settings used for all Monte Carlo simulations.....	185
Table 11.2. Patient characteristics and fetal doses for pregnant patients used in this investigation.	188
Table 11.3. Exponential regression coefficients and R^2 for fetal dose estimation.	189
Table 11.4. Error between simulated fetal dose and fetal dose estimated using TCM, FTC and SSDE conversion coefficients.....	190

ACKNOWLEDGEMENTS

First and foremost I'd like to thank my advisor, Dr. Mike McNitt-Gray. Mike has been a constant source of support and encouragement throughout my doctoral studies. He always pushed me to dig deeper into problems, and because of that, I was able to develop solutions for problems I thought were unsolvable. He helped me develop the skills and scientific curiosity that will serve as a strong foundation for all my future research endeavors.

I want to thank all the members of the Monte Carlo Dose Group, especially Dr. Chris Cagnon, Dr. John DeMarco and Dr. Maryam Bostani. Chris's passion and enthusiasm has always given me total confidence in my work. Even when results were bad, Chris helped me see that all data is exciting in some way, shape or form. John's skepticism of good results has always pushed me to develop clear and concise arguments to defend my work. It's truly hard to express how thankful I am for the support Maryam has provided over the years. To me she is a great colleague, teacher and role model, but more than anything, she is a great friend.

I would like to thank Dr. Eric Brubaker and Dr. Pete Marleau for providing me with my first opportunities to undertake original research. The two summers spent at Sandia National Laboratories prior to my arrival at UCLA provided me with a wealth of tools necessary to develop and execute a research plan. I am especially thankful for their patience in teaching me computer programming.

I would also like to thank my family, especially my parents, Mike and Lauren McMillan, for all their support and encouragement over the years. I am eternally grateful for all the sacrifices they made so that I could pursue my studies to the highest level.

I would like to acknowledge financial support provided by the National Institute of Biomedical Imaging and Bioengineering Training Grant T32EB002101. I would also like to

acknowledge and thank my colleagues at the Mayo Clinic, Dr. Cynthia McCollough, Dr. Lifeng Yu and Dr. Shuai Leng, for their collaborations and research support in the form of the National Institutes of Health Grant R01-EB017095.

VITA

- 2010 B.S.E., Nuclear Engineering and Radiological Sciences
University of Michigan, Ann Arbor
Ann Arbor, Michigan
- 2011 M.S.E., Nuclear Engineering and Radiological Sciences
University of Michigan, Ann Arbor
Ann Arbor, Michigan
- 2011 – 2015 Graduate Student Researcher
University of California, Los Angeles
Los Angeles, California
- 2014 M.S., Biomedical Physics
University of California, Los Angeles
Los Angeles, California

SELECTED PUBLICATIONS

- I. Sechopoulos, E. S. M. Ali, A. Badal, A. Badano, J. M. Boone, I. S. Kyprianou, E. Mainegra-Hing, **K. L. McMillan**, M. F. McNitt-Gray, D. W. O. Rogers, E. Samei, A. C. Turner, “Monte Carlo reference data sets for imaging research: Executive summary of the report of AAPM Research Committee Task Group 195,” *Med. Phys.*, 42(5), 5679 (2015).
- M. Bostani, J. W. Mueller, **K. McMillan**, D. D. Cody, C. H. Cagnon, J. J. DeMarco, M. F. McNitt-Gray, “Accuracy of Monte Carlo simulations compared to in-vivo MDCT dosimetry,” *Med. Phys.*, 42(2), 1080-1086 (2015).
- M. Bostani, **K. McMillan**, P. Lu, H. Kim, C. H. Cagnon, J. J. DeMarco, M. F. McNitt-Gray, “Attenuation-based size metric for estimating organ dose to patients undergoing tube current modulated CT exams,” *Med. Phys.*, 42(2), 958-968 (2015).
- K. McMillan**, M. Bostani, C. Cagnon, M. Zankl, A. R. Sepahdari, M. McNitt-Gray, “Size specific, scanner-independent organ dose estimates in contiguous axial and helical head CT examinations,” *Med. Phys.*, 41(12), 121909 (2014).
- M. Bostani, **K. McMillan**, J. J. DeMarco, C. H. Cagnon, M. F. McNitt-Gray, “Validation of a Monte Carlo model used for simulating tube current modulation in computed tomography over a wide range of phantom conditions/challenges,” *Med. Phys.*, 41(11), 112101 (2014).
- K. McMillan**, M. McNitt-Gray, D. Ruan, “Development and validation of a measurement-based source model for kilovoltage cone-beam CT Monte Carlo dosimetry simulations,” *Med. Phys.*, 40(11), 111907 (2013).

M. Khatonabadi, H. J. Kim, P. Lu, **K. L. McMillan**, C. H. Cagnon, J. J. DeMarco, M. F. McNitt-Gray, "The feasibility of a regional CT DIvol to estimate organ dose from tube current modulated CT exams," *Med. Phys.*, 40(5), 051903 (2013).

SELECTED PRESENTATIONS

K. McMillan, M. Bostani, E. Angel, M. McNitt-Gray, "Size-Specific, Scanner-Independent Fetal Dose Estimates in Abdominal and Pelvic CT Examinations of Pregnant Patients," AAPM 57th Annual Meeting, Anaheim, CA, July 12-16, 2015.

K. McMillan, M. Bostani, C. McCollough, M. McNitt-Gray, "Accurate Predication of CT Tube Current Modulation: Estimating Tube Current Modulation Schemes for Voxelized Patient Models Used in Monte Carlo Simulations," AAPM 57th Annual Meeting, Anaheim, CA, July 12-16, 2015.

K. McMillan, M. Bostani, C. H. McCollough, M. F. McNitt-Gray, "Estimating Organ Dose from Tube Current Modulated CT Exams Using Size Data Available in the DICOM Header of CT Localizer Radiographs and Regional Scanner Output," 100th Scientific Assembly and Annual Meeting of the Radiological Society of North America, Chicago, IL, November 30-December 5, 2014.

K. McMillan, M. Bostani, M. Zankl, C. H. Cagnon, J. J. DeMarco, M. F. McNitt-Gray, "Dose to Partially Irradiated Organs as a Function of Z-axis Over-Ranging and Scan Over-Prescription for Chest CT Examinations," 100th Scientific Assembly and Annual Meeting of the Radiological Society of North America, Chicago, IL, November 30-December 5, 2014.

K. McMillan, M. Bostani, M. Zankl, C. H. Cagnon, J. J. DeMarco, M. F. McNitt-Gray, "Quantifying the Effects of Patient Size, Scanner Selection and Scan Start Location on Organ Dose Estimates in Contiguous Axial Head CT Examination," 100th Scientific Assembly and Annual Meeting of the Radiological Society of North America, Chicago, IL, November 30-December 5, 2014.

K. McMillan, M. Bostani, M. Zankl, J. DeMarco, C. Cagnon, M. McNitt-Gray, "Attenuation-Based Size Adjusted, Scanner-Independent Organ Dose Estimates for Head CT Exams: TG 204 for Head CT," AAPM 56th Annual Meeting, Austin, TX, July 20-24, 2014.

K. McMillan, M. Bostani, C. McCollough, M. McNitt-Gray, "Calculating SSDE from CT Exams Using Size Data Available in the DICOM Header of CT Localizer Radiographs," AAPM 56th Annual Meeting, Austin, TX, July 20-24, 2014.

K. McMillan, M. Khatonabadi, M. Zankl, J. DeMarco, C. Cagnon, M. McNitt-Gray, "Patient-specific, scanner-independent organ dose estimates for head CT exams," SPIE Medical Imaging Conference, San Diego, CA, February 15-20, 2014.

Chapter 1: Introduction

1.1 Background and Significance

From the first computed tomography (CT) scanner introduced in 1972 for head imaging to the development of 320 slice CT scanners in the late 2000s capable of acquiring images of large volumes of the body in a matter of seconds, CT technology has improved dramatically over the years. Technological advancements have increased the utility and usage of CT scanning [1]. A consequence of CT's increased usage is increased radiation dose to the population.

In a 2003 survey conducted in the UK, CT's contribution to the total effective population's radiation dose was estimated to be 47% even though CT only represented 9% of all x-ray diagnostic examinations [2]. A 2006 report by the National Council on Radiation Protection and Measurements (NCRP) estimated that exposure to ionizing radiation in the United States increased seven fold between the 1980s and 2006 with approximately half of that increase due to CT imaging [3]. This NCRP report also estimated the total number of CT scans performed in the United States in 2006 to be 67 million. Those 67 millions CT scans represented only 17% of all procedures utilizing ionizing radiation yet contributed to 49% of the population's collective effective dose.

The concern with CT is the biological risk associated with exposure to ionizing radiation [4-7]. There are two kinds of biological risk: (1) deterministic effects and (2) stochastic effects. Deterministic effects describe the immediate effects of the absorbed dose when exceeding a certain threshold (on the order of Gy). These effects can include hair loss, skin reddening (erythema), sterility and cataracts [8]. Stochastic effects describe potential long-term effects of

radiation exposure, most notably carcinogenesis (i.e. initiation of cancer formation) [9]. The interaction of ionizing radiation with cells can lead to DNA strand breaks. If not repaired correctly, these strand breaks could result in cell proliferation with genetic mutations that could lead to carcinogenesis. Ionizing radiation from CT scanning is considered to be low-dose (on the order of mGy), so thresholds for deterministic effects are rarely exceeded. Instead, stochastic effects are of primary concern for CT.

International Commission on Radiological Protection (ICRP) Publication 60 and ICRP Publication 103 provide models that allow for the estimation of the lifetime risk of cancer resulting from any specified dose of ionizing radiation [10,11]. The risk models are based on effective dose. Effective dose is the tissue-weighted sum of the equivalent doses in all specified tissues and organs of the body. Equivalent dose is absorbed dose that takes into account the radiobiological effectiveness (RBE) of the radiation [12]. Because CT x-rays are considered to be low linear energy transfer (LET) radiation, the RBE for CT x-rays is approximately 1. Therefore, equivalent dose equals absorbed dose for CT x-rays. Effective dose takes into account the type of radiation and the radiosensitivity of each organ (tissue weighting factors), but it is sex-averaged and age-independent, so it is not intended for estimating an individual patient risk. Rather, effective dose is intended for assessing radiation risk for an entire population [13-15]. It is well established, though, that sex and age of exposure are important factors in the risk of cancer induction from ionizing radiation exposure [16].

Biological Effects of Ionizing Radiation 7th Report (BEIR VII) presents models that allow for the estimation of the lifetime risk of cancer resulting from any specified dose of ionizing radiation that take into account sex and age of exposure [17]. BEIR VII risk models were developed using atomic bomb survivor data as well as medical and occupational radiation

studies. In ICRP Publication 60 and ICRP Publication 103, the risk models are based on effective dose, but in BEIR VII, the risk models are based on individual organ dose. Because of this, cancer site-specific (i.e. organ-specific) risk estimates are provided in BEIR VII. This is especially important for risk assessment from CT exposure because various tissues of the body receive substantially different doses [16-18]. For example, for a routine chest CT examination, the lungs will be fully-irradiated, but the colon may be partially- or indirectly-irradiated. Therefore, a separate assessment of lung and colon risk is of considerable interest.

The high frequency of CT procedures coupled with the fact that radiation exposure from CT scans has been identified as a significant component of the total medical radiation exposure globally warrants the need for accurate quantification of radiation dose from CT examinations [19]. In particular, the determination of organ dose from CT exams is essential to understanding the patient-specific risk from a CT scan [5,6].

1.2 Current State of the Art

Monte Carlo simulations have proven to be a useful tool for estimating organ dose from CT exams because all major components of the scanner can be explicitly modeled with varying levels of detail (i.e. energy spectrum, bowtie filtration, beam collimation, helical or axial source movement, etc.) [20-22]. Although the physical components of a CT scanner play a role in the accuracy of Monte Carlo simulations, the most important component that needs to be modeled is tube current modulation (TCM). TCM is a scanning technique that adapts tube current to the attenuation of the body region [23]. Tube current is increased in regions of high attenuation (e.g. shoulders or pelvis) and decreased in regions of low attenuation (i.e. lungs). Virtually all clinical

protocols have implemented TCM as a means to reduce patient dose while maintaining acceptable image quality [23,24]. Studies have shown TCM to reduce scanner output upwards of 91% when compared with fixed tube current (FTC) [24,25]. The potentially large differences between dose from TCM and FTC scans highlights the need to incorporate TCM into dose estimates to ensure an accurate representation of actual patient dose.

Numerous efforts have been made to better quantify dose to patients undergoing CT examinations through the use of Monte Carlo simulations. Focus has centered on tools that use a database of predetermined, Monte Carlo-based dose estimates to provide rapid dose estimates for any scan technique or scan range. While this generalized approach to dose quantification enables the investigation of dose for variable scan conditions, the dose estimates are based on a summation of FTC single axial scans, and thus modern scanning techniques, such as TCM, are not accounted for in these dose estimates [26-28]. Graphics processing unit (GPU)-based Monte Carlo dose simulation software has also been developed. While this facilitates near real-time CT imaging dose calculations, dose estimates are based on a library of deformable patient phantoms for which no TCM data exists [29,30]. Additionally, Monte Carlo simulations have been used to describe the relationship between CT dose and patient size [31-36]. While these relationships provide robust estimates of dose for any patient size, they are developed from FTC Monte Carlo simulations and therefore do not specifically address TCM dose estimates.

Early efforts to model TCM concentrated on the development of idealized, attenuation-based TCM profiles [37,38]. These models were later incorporated into Monte Carlo simulations to estimate organ dose from TCM CT examinations [39-42]. Even though TCM algorithms for each major CT manufacturer are based on the idea that tube current will be adjusted in response to changes in patient attenuation, they tend to differ in implementation, so the major limitation of

models of idealized TCM profiles is that they do not represent any manufacturer-specific TCM schemes [43]. Therefore, organ doses estimated using these TCM schemes are themselves idealized and not necessarily the organ doses the patient model would have received had they been scanned on an actual CT scanner.

Other studies extracted TCM profiles from the raw projection data of a CT scanner and modeled them in Monte Carlo simulations [44-46]. These TCM profiles are the actual TCM profiles generated for a given patient's anatomy, and therefore, organ dose estimated using these TCM schemes can be considered accurate estimates of the true organ dose for a TCM CT examination. For these studies, though, organ dose estimates are limited to organs that are fully-irradiated and can be easily segmented from the CT image data. Because of this, the scope of these studies is severely narrowed, and dose metrics related to risk, such as effective dose, are unable to be calculated. Additionally, these studies are limited by the fact that manufacturer cooperation is necessary to obtain the tools to properly read the raw projection data and extract the relevant TCM information.

1.3 Overview

Given the limitations of current Monte Carlo-based methods to estimate organ dose from TCM CT examinations, the advancement of Monte Carlo simulations that incorporate TCM has been recognized as a high priority. The bottleneck that remains for accurate estimates of organ dose from TCM CT exams is the ability to estimate scanner-specific TCM schemes.

In order to overcome these limitations, the primary objective of this dissertation is to develop methods to estimate Siemens TCM schemes for any voxelized patient model. Voxelized

patient models, including computational phantoms, have long played a significant role in the analysis of radiation dose from CT scans. There currently exist a large number of detailed computational phantoms (e.g. GSF, XCAT, RPI, UF/NCI) that model a variety of patient sizes, including special patient populations such as pregnant patients [47]. To date, no validated TCM data exists for any of these models that accurately describes the actual TCM that would be applied in patient scans, particularly for TCM schemes that take into account machine limits, anatomy-specific limits and on-line feedback. This is a substantial limitation as the vast majority of current clinical CT scanning, and especially body scanning, employs some form of TCM. Without validated TCM schemes, the utility of such computational phantoms for CT dosimetry applications is limited to the realm of FTC scans, which are not common clinically. Figure 1.1 shows an outline of the “Development” of methods to estimate scanner-specific TCM schemes. Patient size calculated by Siemens from the CT localizer radiograph (i.e. topogram) will be discussed in Chapter 5. This size data serves as the input to TCM scheme estimation methods described in Chapter 6. In order to determine patient size in the Siemens manner for voxelized patient models that were not scanned on Siemens scanners, methods to simulate a Siemens topogram for any patient anatomy are described in Chapter 7.

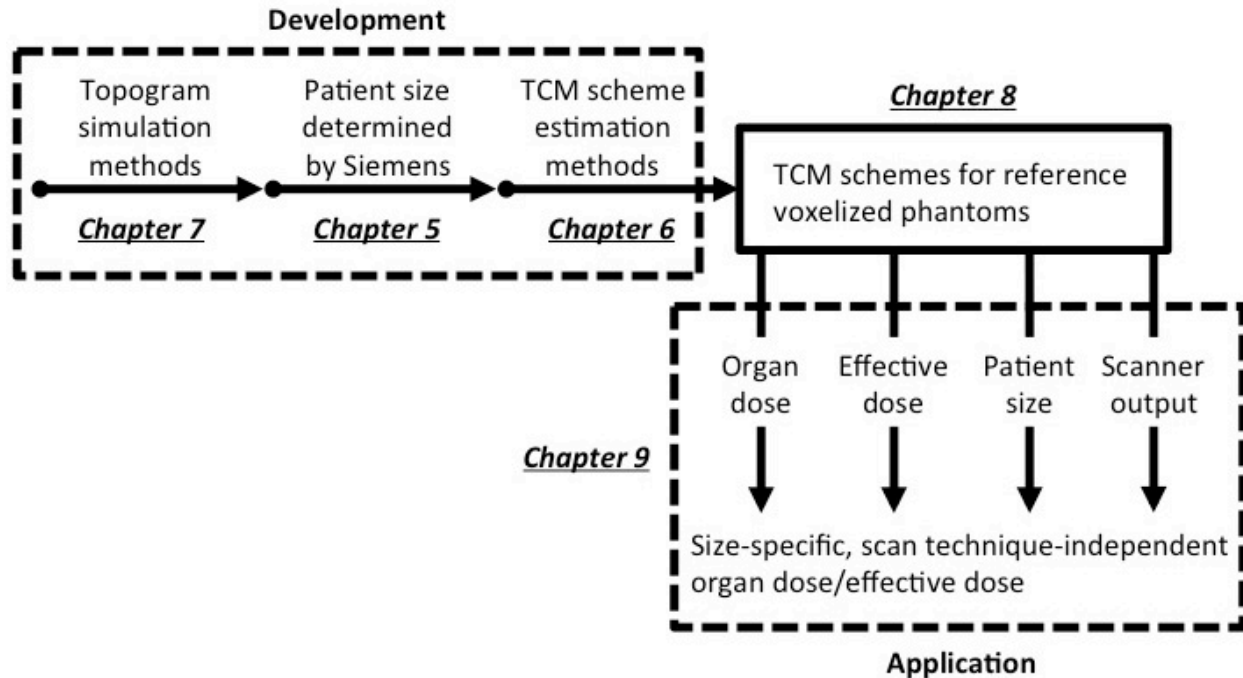


Figure 1.1. Overview of objectives from this dissertation. The development of methods to estimate scanner-specific TCM schemes will be discussed in Chapters 5-7. TCM schemes will be determined for a set of pediatric and adult reference voxelized phantoms in Chapter 8. Size-specific, scan technique-independent organ dose and effective dose estimates determined from TCM Monte Carlo simulations of the reference voxelized phantoms will be discussed in Chapter 9.

The next objective of this dissertation is to determine patient-specific, scan technique-independent radiation dose metrics based on easily measurable or reported patient and scanner metrics. In FTC scans, it has been shown that organ dose normalized to account for scanner-specific effects correlates strongly with patient size [32,33]. Therefore, a simple measurement of patient size coupled with a scanner output metric can be used in conjunction with predetermined scanner output-to-organ dose conversion coefficients to derive accurate estimates of organ dose for a given patient scanned under given conditions. Because of the variation of scanner output across different regions of the body, applying the FTC organ dose conversion coefficients to TCM scans may not be appropriate. Instead, a new set of conversion coefficients specific to TCM may need to be determined. First, scanner-specific TCM schemes for a set of pediatric and

adult reference voxelized phantoms from which all radiosensitive organs have been previously identified will be determined (Chapter 8). These TCM schemes will then be incorporated into detailed Monte Carlo simulations of organ dose from TCM CT exams. Performing these simulations across a set of voxelized patient models representing a variety of sizes, ages and genders, relationships between scanner output-normalized organ dose and patient size will be developed. These size-specific organ dose estimates could be used to quickly estimate organ dose for any fully-, partially- or indirectly-irradiated organ for a given routine TCM CT examination. Additionally, because organ dose can be estimated for all radiosensitive organs, estimates of size-specific effective dose can also be calculated. Size-specific dose estimates will simplify the TCM dose estimation problem while providing the most accurate information possible. Figure 1.1 shows an outline of the “Application” of TCM schemes estimated for a set of reference voxelized phantoms (Chapter 9). Monte Carlo simulations can be used to estimate organ doses that can then be used to calculate effective dose. Using simulated topograms determined using methods from Chapter 7, patient size can be determined for each voxelized phantom. Scanner output metrics can be determined directly from the estimated TCM schemes for each voxelized phantom.

In Chapter 2, the specific aims of this dissertation will be explicitly defined. The Monte Carlo methods employed throughout this dissertation will be described in Chapter 3. The reference voxelized phantoms mentioned above will be described in detail in Chapter 4. In Chapter 10, organ doses estimated using the size-specific organ dose estimates determined in Chapter 9 will be compared with “gold standard” organ doses derived from detailed Monte Carlo simulation of TCM CT examinations. In Chapter 11, the methods for estimating size-specific organ dose will be extended to determine size-specific fetal dose estimates for pregnant patient

who undergo clinically indicated TCM CT examinations. Finally, in Chapter 12, the conclusions of this dissertation will be presented.

1.4 References

1. J Adam, "Changes in the computed tomography patient population," *European Radiology Supplements* **16**, D38 (2006).
2. P. C. Shrimpton *et al.*, "National survey of doses from CT in the UK: 2003," *Br. J. Radiol.* **79**, 968-980 (2006).
3. F. A. Mettler *et al.*, "Medical radiation exposure in the U.S. in 2006: preliminary results," *Health Phys.* **95**, 502-507 (2008).
4. D. J. Brenner, C. D. Elliston, E. J. Hall, W. E. Berdon, "Estimated Risks of Radiation-Induced Fatal Cancer from Pediatric CT," *Am. J. Roentgenol.* **176**, 289-296 (2001).
5. M. S. Pearce *et al.*, "Radiation exposure from CT scans in childhood and subsequent risk of leukaemia and brain tumours: a retrospective cohort study," *Lancet* **380**, 499-505 (2012).
6. J. D. Mathews *et al.*, "Cancer risk in 680,000 people exposed to computed tomography scans in childhood or adolescence: data linkage study of 11 million Australians," *BMJ* **346**, 1-18 (2013).
7. D. J. Brenner, C. D. Elliston, "Estimated Radiation Risks Potentially Associated with Full-Body CT Screening," *Radiology* **232**, 735-738 (2004).
8. N. Hamada, Y. Fujimichi, "Classification of radiation effects for dose limitation purposes: history, current situation and future prospects," *J. Radiat. Res.* **55**, 629-640 (2014).

9. S. Ma, B. Kong, B. Liu, X. Liu, "Biological effects of low-dose radiation from computed tomography scanning," *Int. J. Radiat. Biol.* **89**, 326-333 (2013).
10. International Commission on Radiological Protection, "1990 Recommendations of the International Commission on Radiological Protection," ICRP Publication 60 (1991).
11. International Commission on Radiological Protection, "The 2007 Recommendations of the International Commission on Radiological Protection," ICRP Publication 103 (2007).
12. International Commission on Radiological Protection, "Relative biological effectiveness (RBE), quality factor (Q), and radiation weighting factor (w(R)). A report of the International Commission on Radiological Protection," *Ann. ICRP* **33**, 1-117 (2003).
13. American Association of Physicists in Medicine, "The Measurement, Reporting, and Management of Radiation Dose in CT," AAPM Report 96 (2008).
14. A. J. Einstein, M. J. Henzlova, S. Rajagopalan, "Estimating risk of cancer associated with radiation exposure from 64-slice computed tomography coronary angiography," *JAMA* **298**, 317-323 (2007).
15. J. D. Harrison, C. Streffer, "The ICRP protection quantities, equivalent and effective dose: their basis and application," *Radiat. Prot. Dosimetry* **127**, 12-18 (2007).
16. D. Brenner, E. Hall, "Computed tomography – An increasing source of radiation exposure," *N. Engl. J. Med.* **357**, 2277-2284 (2007).
17. Committee to Assess Health Risks from Exposure to Low Levels of Ionizing Radiation, "Health Risks from Exposure to Low Levels of Ionizing Radiation: BEIR VII Phase 2," National Research Council (2005).
18. C. J. Martin, "Effective dose: how should it be applied to medical exposures?" *Br. J. Radiol.* **80**, 639-647 (2007).

19. National Council on Radiation Protection and Measurements, "Ionizing radiation exposure of the population of the United States," NCRP Report No. 160 (2009).
20. G. Jarry, J. J. DeMarco, U. Beifuss, C. H. Cagnon, M. F. McNitt-Gray, "A Monte Carlo-based method to estimate radiation dose from spiral CT: from phantom testing to patient-specific models," *Phys. Med. Biol.* **48**, 2645-2663 (2003).
21. A. C. Turner *et al.*, "A method to generate equivalent energy spectra and filtration models based on measurements for multidetector CT Monte Carlo dosimetry simulations," *Med. Phys.* **36**, 2154-2164 (2009).
22. K. McMillan, M. McNitt-Gray, D. Ruan, "Development and validation of a measurement-based source model for kilovoltage cone-beam CT Monte Carlo dosimetry simulations," *Med. Phys.* **40**, 111907 (2013).
23. C. H. McCollough, M. R. Bruesewitz, J. M. Kofler Jr., "CT dose reduction and dose management tools: overview of available options," *Radiographics* **26**, 503-512 (2006).
24. M. K. Kalra *et al.*, "Techniques and Applications of Automatic Tube Current Modulation for CT," *Radiology* **233**, 649-657 (2004).
25. M. K. Kalra *et al.*, "Comparison of z-axis automatic tube current modulation technique with fixed tube current CT scanning of abdomen and pelvis," *Radiology* **232**, 347-353 (2004).
26. Y. Gao, P. F. Caracappa, X. G. Xu, "How to Use VirtualDose to Track Patient Organ Doses," *Health Phys.* **107**, S100 (2014).
27. D. G. Jones, P. C. Shrimpton, "Normalised organ doses for X-ray computed tomography calculated using Monte Carlo techniques," NRPB-SR250 (1993).
28. G. Stamm, H. D. Nagel, "CT-expo – a novel program for dose evaluation in CT," *Rofo.* **174**, 1570-1576 (2002).

29. H. Lin *et al.*, “Formation of Computational Phantoms from CT Numbers for Use in the ARCHER Monte Carlo Code,” *Health Phys.* **107**, S98 (2014).
30. T. Liu *et al.*, “Monte Carlo CT Dose Calculation: A Comparison Between Experiment and Simulation Using ARCHER-CT,” *Med. Phys.* **41**, 424 (2014).
31. A. C. Turner *et al.*, “The feasibility of a scanner-independent technique to estimate organ dose from MDCT scans: Using CTDIvol to account for differences between scanners,” *Med. Phys.* **37**, 1816-1825 (2010).
32. A. C. Turner *et al.*, “The feasibility of patient size-corrected, scanner-independent organ dose estimates for abdominal CT exams,” *Med. Phys.* **38**, 820-829 (2011).
33. K. McMillan *et al.*, “Size-specific, scanner-independent organ dose estimates in contiguous axial and helical head CT examinations,” *Med. Phys.* **41**, 121909 (2014).
34. J. J. DeMarco *et al.*, “Estimating radiation doses from multidetector CT using Monte Carlo simulations: effects of different size voxelized patient models on magnitudes of organ and effective dose,” *Phys. Med. Biol.* **52**, 2583-2597 (2007).
35. E. Angel *et al.*, “Radiation Dose to the Fetus for Pregnant Patients Undergoing Multidetector CT Imaging: Monte Carlo Simulations Estimating Fetal Dose for a Range of Gestational Age and Patient Size,” *Radiology* **249**, 220-227 (2008).
36. American Association of Physicists in Medicine, “Size-Specific Dose Estimates (SSDE) in Pediatric and Adult Body CT Examinations,” AAPM Report 204 (2011).
37. M. Gies, W. A. Kalender, H. Wolf, C. Suess, “Dose reduction in CT by anatomically adapted tube current modulation. I. Simulation studies,” *Med. Phys.* **26**, 2235-2247 (1999).
38. W. A. Kalender, H. Wolf, C. Suess, “Dose reduction in CT by anatomically adapted tube current modulation. II. Phantom measurements,” *Med. Phys.* **26**, 2248-2253 (1999).

39. H. Schlattl, M. Zankl, J. Becker, C. Hoeschen, "Dose conversion coefficients for CT examinations of adults with automatic tube current modulation," *Phys. Med. Biol.* **55**, 6243-6261 (2010).
40. H. Schattl, M. Zankl, J. Becker, C. Hoeschen, "Dose conversion coefficient for pediatric CT examinations with automatic tube current modulation," *Phys. Med. Biol.* **57**, 6309-6326 (2012).
41. X. Li, W. P. Segars, E. Samei, "The impact on CT dose of the variability in tube current modulation technology: a theoretical investigation," *Phys. Med. Biol.* **58**, 4525-4548 (2014).
42. X. Tian *et al.*, "Prospective estimation of organ dose in CT under tube current modulation," *Med. Phys.* **42**, 1575-1585 (2015).
43. N. Keat, "CT scanner automatic exposure control systems," MHRA Report 05016 (2005).
44. E. Angel *et al.*, "Monte Carlo simulations to assess the effects of tube current modulation on breast dose for multidetector CT," *Phys. Med. Biol.* **54**, 497-512 (2009).
45. M. Khatonabadi *et al.*, "A comparison of methods to estimate organ doses in CT when utilizing approximations to the tube current modulation function," *Med. Phys.* **39**, 5212-5228 (2012).
46. M. Khatonabadi *et al.*, "The feasibility of a regional CTDIvol to estimate organ dose from tube current modulated CT exams," *Med. Phys.* **40**, 051903 (2013).
47. X. G. Xu, "An exponential growth of computational phantom research in radiation protection, imaging, and radiotherapy: a review of the fifty-year history," *Phys. Med. Biol.* **59**, 233-302 (2014).

Chapter 2: Specific Aims

The goal of this dissertation is to develop methods to estimate organ dose to patients undergoing CT scans that take into account both the patient size as well as the effects of tube current modulation (TCM). This work starts with the development and validation of methods to predict scanner-specific TCM schemes for any patient anatomy. This allows realistic TCM schemes that take into account machine limits, anatomy-specific limits and on-line feedback to be modeled. TCM schemes are then generated for a variety of reference voxelized phantoms for which TCM information does not currently exist. These are whole body patient models representing a variety of sizes, ages and genders that have all radiosensitive organs identified. TCM schemes for these models facilitate Monte Carlo-based estimates of fully-, partially- and indirectly-irradiated organ dose from TCM CT exams. The ability to create validated TCM schemes for these models will aid in modernizing Monte Carlo simulations performed using detailed reference voxelized phantoms (or computational phantoms), will allow the generalization of TCM schemes to all patient models and will help create new sets of dosimetry data from which estimates of patient dose (effective dose, SSDE, etc.) may be derived.

The overall hypothesis of this research is that it is possible to reasonably estimate dose to any organ for TCM CT exams. The specific aims of this study are:

SA-1 To develop and validate methods to estimate scanner-specific TCM schemes for any voxelized patient model.

SA-2 To develop a comprehensive set of patient-specific dose estimates from TCM CT exams.

Chapter 3: Monte Carlo Dosimetry Package

3.1 Introduction

Monte Carlo simulations have proven to be a powerful tool for estimating organ dose from CT examinations [32-44]. All major components of the CT scanner can be modeled with great detail (e.g. energy spectrum, beam collimation, helical or axial source movement) [5-7]. Patient models can also be incorporated into the simulations with detailed anatomical descriptions (e.g. organ-specific material composition and electron density) [7].

Monte Carlo simulations are used extensively throughout this dissertation. Methods have been previously developed to allow for the simulation of advanced CT capabilities [21,9]. Significant validation work has been performed to ensure the accuracy of these developments [21,10,11]. The purpose of this chapter was to characterize the major components of the Monte Carlo simulations used within this dissertation and describe all validation experiments previously performed to quantify the accuracy of the simulations.

3.2 Development

3.2.1 Monte Carlo Simulation Engine

The Monte Carlo software package MCNPX (Monte Carlo N-Particle eXtended version 2.7.0) is used as the simulation engine for this dissertation [12]. Within all simulations, the detailed

photon transport mode with a low-energy cutoff of 1 keV is used. The detailed physics treatment includes coherent scattering and accounts for fluorescent photons after photoelectric absorption. Form factors and Compton profiles are used to account for electron binding effects, and analog capture is always used. The incoherent, coherent, and photoelectric cross section data are based on ENDF/B-VII (Evaluated Nuclear Data File) [13].

3.2.2 CT Source Model

Modifications are made to the standard MCNPX code in order to appropriately model the possible x-ray source position, energy, initial trajectory, and attenuation due to the bowtie filter for a variety of CT scanners [5,21]. Specifically, modifications are made to the MCNPX file “source.F” to create custom source subroutines specific to CT scanning.

In order to properly model a CT scanner in a Monte Carlo simulation, detailed information related to the scanner energy spectrum and bowtie filter geometry is necessary. This information is typically proprietary and therefore not readily available to research groups. A measurement-based “equivalent” source model was previously developed by Turner *et al.* to overcome this limitation [21]. The equivalent source model has two components: (1) equivalent spectrum module and (2) equivalent bowtie filter module. The goal of the equivalent spectrum module is to generate an x-ray photon spectrum (equivalent spectrum) with a calculated beam behavior that best matches a half-value layer (HVL) value measured experimentally, and in doing so takes into account the spectrum off the anode and any inherent filtration of the system (include x-ray tube housing). The goal of the equivalent bowtie filter module is to generate a description of the attenuation profile of the bowtie filter such that a resultant equivalent bowtie

filter attenuates the equivalent spectrum in the same manner that the actual bowtie filter attenuates the actual x-ray spectrum. This module is based on attenuation profile measurements made along the length of the bowtie filter. By using a measurement-based model to determine the energy spectrum and bowtie filter description, the method can be applied for any CT scanner from any manufacturer.

Using the equivalent spectrum and equivalent bowtie filter as inputs to the Monte Carlo simulation, the photon's initial trajectory is first randomly selected from an energy cumulative distribution function created from the equivalent spectrum. Next, the initial position of the photon is randomly selected from all possible positions along the simulated scan length (single axial, contiguous axial, helical). An acceptable fan angle and longitudinal beam width (i.e. cone angle) value is then randomly sampled. The direction of the photon is specified by the components of a unit vector in a direction randomly selected from the set of all possible trajectories for a given start position, fan angle, and longitudinal beam width. Finally, attenuation due to the bowtie filter is modeled by adjusting the statistical weighting factor of each photon. The path length of a photon through the bowtie for a given trajectory is linearly interpolated from the bowtie filter description (equivalent aluminum (Al) path length as a function of trajectory angle) generated from the equivalent bowtie profile module. Using this path length and the linear attenuation coefficients for Al, the resulting exponential attenuation factor is calculated. Multiplying this exponential attenuation factor by an initial particle weight (default value of 1) yields the new weighting factor for that photon in MCNPX.

3.2.3 Modeling Tube Current Modulation

Methods were previously developed to incorporate tube current modulation (TCM) into the Monte Carlo simulations [9]. Whether the TCM scheme is extracted from the raw projection data of a patient who underwent an actual CT scan or is estimated using methods discussed later in this dissertation, TCM schemes are described by three components: (1) Table location, z , (2) tube angle (0-360°), θ , and (3) tube current, I . Tube current is defined as a function of tube angle and table position, $I(\theta, z)$. Table location, tube angle and tube current data is recorded in a text file that serves as an input to the Monte Carlo simulations. Figure 3.1 shows an example of a TCM scheme extracted from the raw projection data of a patient who underwent a clinically indicated chest CT examination.

When TCM is used within the Monte Carlo simulations, the TCM information (table location, tube angle, tube current) is first loaded into the simulation from the text file. Next, all tube current values are normalized by the maximum tube current value. Then, an index number ranging from 1 to the length of the text file is randomly sampled. The table position, tube angle and normalized tube current corresponding to that index are used to set the initial position, trajectory and initial particle weight of the simulated photon, respectively. Finally, photon energy and bowtie filter attenuation are determined according to the methodology outlined in Section 3.2.2.

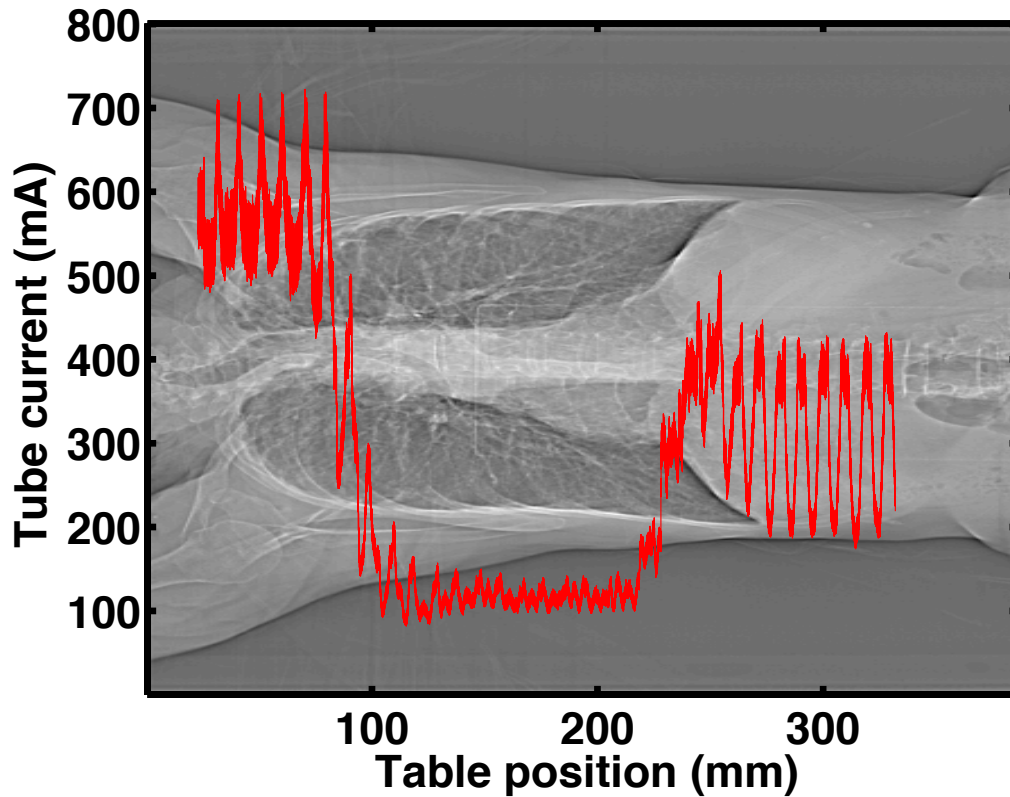


Figure 3.1. Example of TCM scheme extracted from the raw projection data of a patient who underwent a clinically indicated chest CT exam on a Siemens Sensation 64 scanner.

3.2.4 Voxelized Patient Models

In order to use Monte Carlo simulations to determine organ doses, organ volumes must be identified in the patient models incorporated into the Monte Carlo simulations. For patient models derived from the CT images of patients who are actually scanned, anatomically structures are segmented from the axial images using manual, semi-automated and automated contouring tools [14]. All voxels within each of the contoured regions are identified as belonging to a specific organ or anatomical structure. All voxels outside of the contoured regions are identified

as a specific tissue type (lung, fat, water, muscle, bone, air) using a Hounsfield number lookup table [15]. Figure 3.2 shows an example of organs segmented from the axial images of a patient (left) and the Monte Carlo representation of the patient with all non-contoured regions identified as a specific tissue type (right).

Each voxel is assigned an integer identification number corresponding to the organ or tissue type identified for that voxel. Each organ identification number is assigned a material description (i.e. weight fractions and density) based on the elemental compositions and physical characteristics of tissue substitutes from ICRU (International Commission on Radiation Units and Measurements) Report 44 [16]. Patient models are then incorporated into Monte Carlo simulations as a 3D matrix of identification numbers with each identification number having a corresponding material description.

Within this dissertation, organs doses are tallied using both actual patients and reference voxelized phantoms. For actual patients, organs are identified using the methodology described above. For reference voxelized phantoms, which are described in extensive detail in Chapter 4, all organs and anatomical structures are already identified.

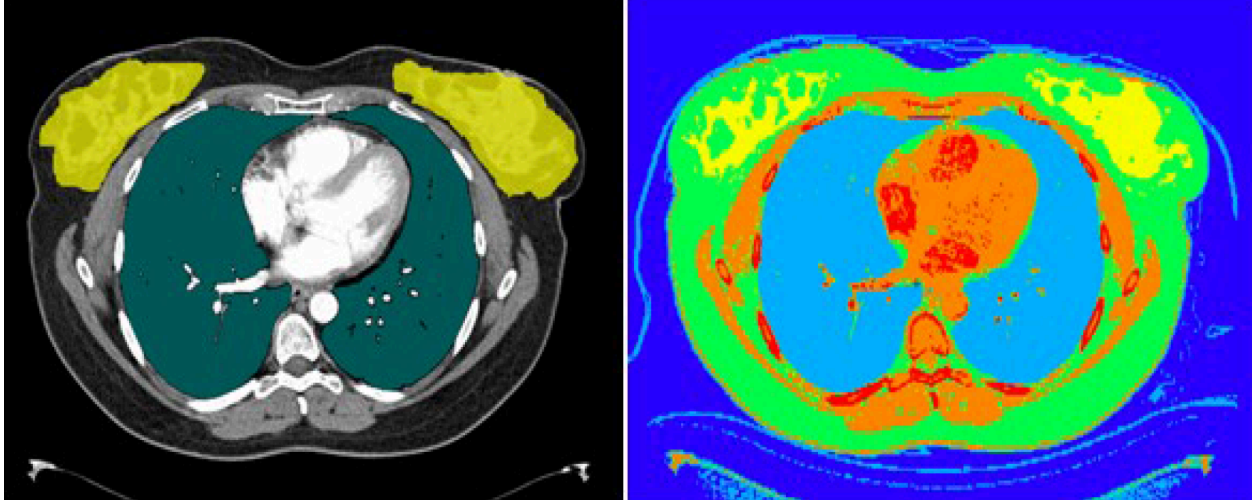


Figure 3.2. (Left) Breasts and lungs contoured from axial image of patient who underwent chest CT exam. (Right) Monte Carlo representation of the patient with all non-contoured regions identified as a specific tissue using Hounsfield lookup table.

3.2.5 Dose Calculations

Simulation physics options are set so that the photon transport mode does not explicitly create photoelectrons but instead assumes all secondary electrons deposit their energy at the photon interaction site, which is reasonable given the incident photon energy distribution for a diagnostic CT beam (< 150 kVp). This assumption satisfies charged particle equilibrium and allows absorbed dose to be approximated as collision kerma, which is calculated in each volume of interest by tallying the photon energy fluence and multiplying by the material-specific and energy-dependent mass energy-absorption coefficient. The mass energy-absorption coefficients used in this investigation are referenced from Hubbell and Seltzer [17]. Simulated dose is defined as:

$$D_{sim} = \left[\sum_{E=0}^{kVp} \left(\psi_E \times \left(\mu_{en} / \rho \right)_{E,material} \right) \right] \times CF_{MeV/g \rightarrow mGy} \quad (3.1)$$

where ψ_E is the photon energy fluence for a given energy E , $\left(\mu_{en} / \rho \right)_{E,material}$ is the material-specific and energy-dependent mass energy-absorption coefficient and $CF_{MeV/g \rightarrow mGy}$ is the conversion factor to go from MeV/g to mGy.

Normalization factors are required to convert simulated dose values (mGy per particle) to absolute dose normalized on a tube current time product basis (mGy per total mAs). In order to do this, air scan measurements (mGy per total mAs) and corresponding simulations (mGy per particle) are performed using the appropriate beam energy and nominal collimation for the given scanner. For air scan measurements, the 100 mm pencil ionization chamber is attached to the patient table such that the active portion of the chamber is extended beyond the edge of the table at the scanner isocenter and therefore essentially “free-in-air.” A CT dose index ($CTID_{100}$) in air measurement is then made. A corresponding simulation using an ionization chamber model at isocenter is then performed in MCNPX. By dividing the air scan measurement by the air scan simulation, a normalization factor (particles per total mAs) is uniquely determined for each combination of scanner, beam energy and nominal collimation, similar to that described by DeMarco *et al.* [18]. The normalization factor to convert simulated dose to absolute dose is defined as:

$$NF_{kVp,NT} = \frac{\left(CTDI_{air,measured} \right)_{kVp,NT}}{\left(CTDI_{air,simulated} \right)_{kVp,NT}} \quad (3.2)$$

where kVp is the beam energy, NT is the nominal collimation, $(CTDI_{air,measured})_{kVp,NT}$ is the measured $CTID_{100}$ in air and $(CTDI_{air,simulated})_{kVp,NT}$ is the simulated $CTID_{100}$ in air. Dose simulation results are then multiplied by the appropriate normalization factor to yield simulated dose in units of mGy per total mAs. Although normalization factors can be calculated using measurements and simulations within some phantom, the advantage of air scan normalization factors is that the chamber position is reproducible in a locally homogeneous dose region void of any nearby attenuating mediums such as the patient table [19].

In order to obtain absolute dose in units of mGy, the calculated dose in units of mGy per total mAs must be multiplied by the total mAs for a given scan length (total mAs = mAs per rotation \times number of rotations). For fixed tube current (FTC) simulations, the mAs per rotation is based on the average tube current across the scan length (a constant value). For TCM simulations, the maximum tube current within a simulated TCM exam is used in the conversion to absolute dose because, as described in Section 3.2.3, the initial photon weighting factors used in the simulation are based on instantaneous tube current values relative to the maximum tube current over the entire scan length. After all correction and normalization factors have been applied to the Monte Carlo dose simulation output, the resultant absolute dose is defined as:

$$D_{abs} = D_{sim} \times NF_{kVp,NT} \times I \times t \times \left[\text{Scan length} / (\text{Pitch} \times NT) \right] \quad (3.3)$$

where I is the average tube current across the scan length for FTC simulations and maximum tube current across the scan length for TCM simulations, t is the rotation time and $\text{Scan length} / (\text{Pitch} \times NT)$ is the number of rotations.

3.3 Validation

The purpose of this section is to outline the previous validation work that has been performed. The validation studies are broken down into five levels (Level 0 – Level 4), with Level 0 being the most basic validation and Level 4 being the most advanced. All, though, are deemed necessary to ensure the CT source model can accurately estimate dose for nearly any CT scanning scenario. Figure 3.3 shows a pyramid diagram highlighting the different level of validation. At the base is a comparison of the CT source model to other code systems. This is the foundation of the validation work. At the top of the pyramid is TCM validation. This is the highest level of validation for the CT source model. All levels of validation are described in detail below.

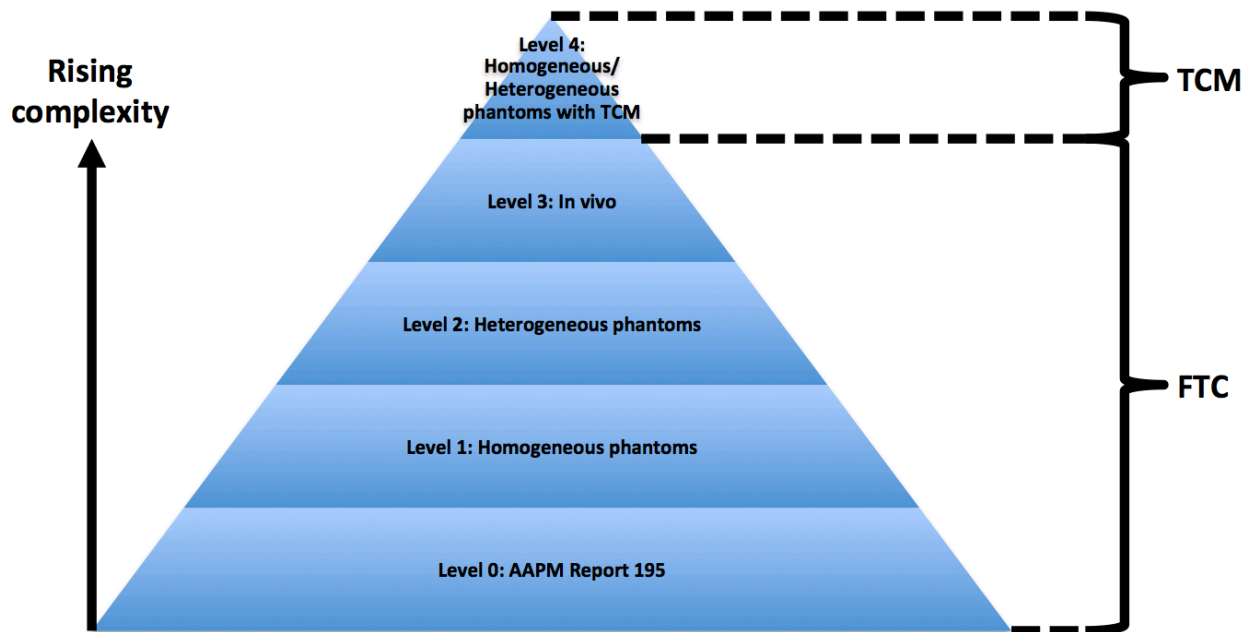


Figure 3.3. Pyramid diagram of different levels of validation. Level 1 involves simple phantoms that are homogeneous in composition. Level 2 involves phantoms that are heterogeneous in composition or shape (or even both).

3.3.1 AAPM Report 195 (Level 0)

Organized in 2009, the goal of AAPM Task Group 195 was to develop a set of Monte Carlo benchmark studies that could be performed by a variety of widely used Monte Carlo code systems, including EGSnrc, Penelope, GEANT4 and MCNP. Summarized in AAPM Report 195, the result of this task group was an in-depth comparison of the different code systems for the different benchmark studies [20].

Two of the studies in AAPM Report 195 were directly related to Monte Carlo simulations of CT systems: (1) Computed tomography with simple solids (Case #4) and (2) computed tomography with a voxelized solid (Case #5). Figure 3.4 shows diagrams of the two scenarios. For all scenarios, geometry and material descriptions as well as tally regions were specified. The

source description, including spectrum description and source rotation conditions, was also specified. Additionally, for simplicity, no bowtie filter was used any of the simulations. In the first study, absorbed dose was tallied in a simple CTDI phantom. In the second study, organ dose was tallied in a complex, voxelized CT phantom. Strong agreement (differences < 5%) was observed between the different code systems for all scenarios tested. The MCNP results were actually generated using the CT source model described in this dissertation, so AAPM Report 195 effectively serves as a validation of the CT source model against other code systems. The limitation of this validation, though, is that it is a comparison between simulated results for different codes rather than a comparison between simulated and measured results. A detailed comparison of simulations to analogous measurements is necessary to ensure that the simulation is properly modeling all the complexities that go into accurately estimating absorbed dose. Additionally, TCM is not taken into account in these scenarios.

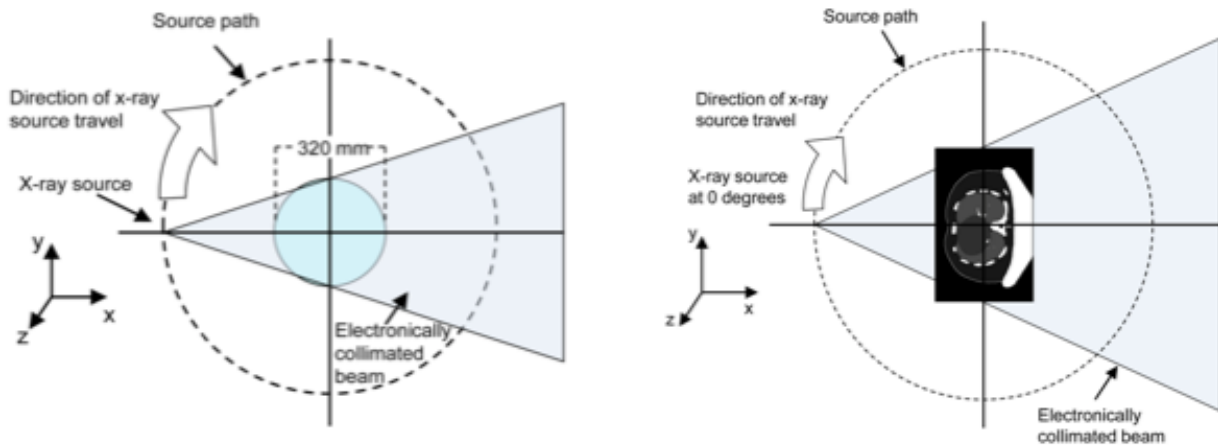


Figure 3.4. (Left) Diagram of AAPM Report 195 Case #4: Computer tomography with simple solids. (Right) Diagram of AAPM Report 195 Case #5: Computed tomography with a voxelized solid.

3.3.2 Homogeneous Phantoms (Level 1)

A comparison of simulated and measured dose within a simple, homogeneous phantom has always been the standard for establishing the baseline accuracy of Monte Carlo simulations against physical measurements. The CT source model used in this work was previously validated against measured dose within the head (16 cm) and body (32 cm) PMMA (poly methyl methacrylate) CTDI phantoms [21]. Figure 3.5 shows the two CTDI phantoms. $CTDI_{100}$ was measured at center and periphery positions for a variety of beam energy and bowtie filter combinations for 64-slice multi-detector CT scanners from four major manufacturers (Siemens, Toshiba, GE and Philips). Corresponding simulations were then performed. CTDI phantom geometry was incorporated into the Monte Carlo simulations using standard geometric shape definitions in MCNPX.

A root mean square error of 5% between simulated and measured dose was observed for all scenarios. By restricting the validation to simple objects, this work validates the CT source model without introducing potential geometry errors caused by modeling more complex geometries. The limitation of homogeneous phantoms is that they do not properly model the geometric complexity or material inhomogeneity of human anatomy. Additionally, only FTC simulations and measurements are performed, so this work does not validate the TCM capabilities of the CT source model.



Figure 3.5. 16 cm head and 32 cm body CTDI phantoms.

3.3.3 Heterogeneous Phantoms (Level 2)

In order to validate the ability to properly model complex human anatomy within Monte Carlo simulations, validation against measurements using phantoms of different sizes and material compositions is necessary. The CT source model used in this work was previously validated against measurements within the following heterogeneous phantoms: (1) Elliptical phantom, (2) rectangular water phantom and (3) anthropomorphic phantom [10]. Figure 3.6 shows the three heterogeneous phantoms. The elliptical phantom is comprised of fat, lung and muscle equivalent material sections. Measurements were made with a thimble ionization chamber at center and periphery locations within the phantom. A thimble ionization chamber with an active volume of 0.6 cm^3 was utilized along with a calibrated electrometer for all measurements. The 0.6 cm^3

chamber's small volume can serve as an approximate point dosimeter and was small enough to fit in all of phantom geometries described in this validation study. The rectangular water phantom consists of slabs of water equivalent material typically used in radiation therapy calibration measurements. Measurements were made with the thimble ionization inserted into a central hole in the slabs. Additional measurements were made with the ionization chamber attached to the surface of the phantom. The anthropomorphic phantom is a torso phantom made up of lung, fat, muscle and bone equivalent materials. Measurements were made with the thimble ionization chamber placed both inside and on the surface of the anthropomorphic phantom. Corresponding simulations were then performed. Elliptical and rectangular water phantom geometry was incorporated into the Monte Carlo simulations using standard geometric shape definitions in MCNPX. Anthropomorphic phantom geometry was incorporated into the simulations using the voxelized patient model methodology outlined in Section 3.2.4.

A root mean square error of 5.05% between simulated and measured dose was observed for all scenarios. While this further validates the CT source model and validates the ability to properly model more complex geometries within the Monte Carlo simulations, this validation work was only done for FTC scans, and therefore, the TCM capabilities of the CT source model are not validated by this work.

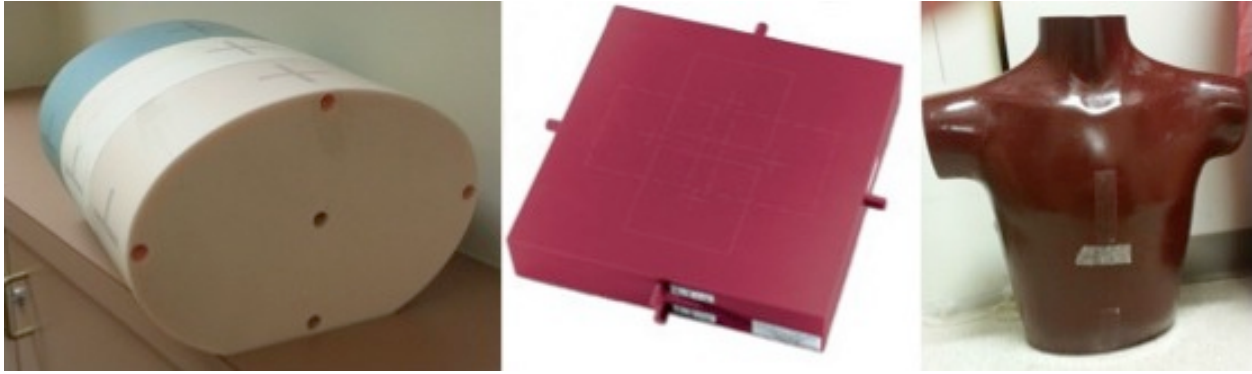


Figure 3.6. (Left) Elliptical phantom. (Middle) Rectangular water phantom. (Right) Anthropomorphic phantom.

3.3.4 *In Vivo* (Level 3)

In order to validate the ability of a Monte Carlo code system to estimate dose within an actual patient, *in vivo* validation is necessary. The CT source model used in this work was previously validated, in conjunction with researchers at MD Anderson Cancer Center, against dose measurements made within patients undergoing virtual colonoscopy (VC) exams [11,21]. Dose was measured using thermoluminescent dosimeters (TLDs) placed within a tube that was placed within the rectum of 10 patients who underwent the VC procedure. Corresponding simulations were then performed. Monte Carlo patient models were created from images of the 10 patients using the methodology outlined in Section 3.2.4. The TLD was segmented from the images and identified as muscle tissue (TLD material was muscle equivalent). Figure 3.7 shows the TLD segmented from the images of one of the patients who underwent the VC procedure.

An average percent error of 7.43% between simulated and measured dose was observed for all scenarios. This validation provides extensive credibility to the methods used to model patient geometry and material composition. Like previous validation work, the major limitation

of this validation study is that the VC dose measurements and simulations were performed using FTC, not TCM.

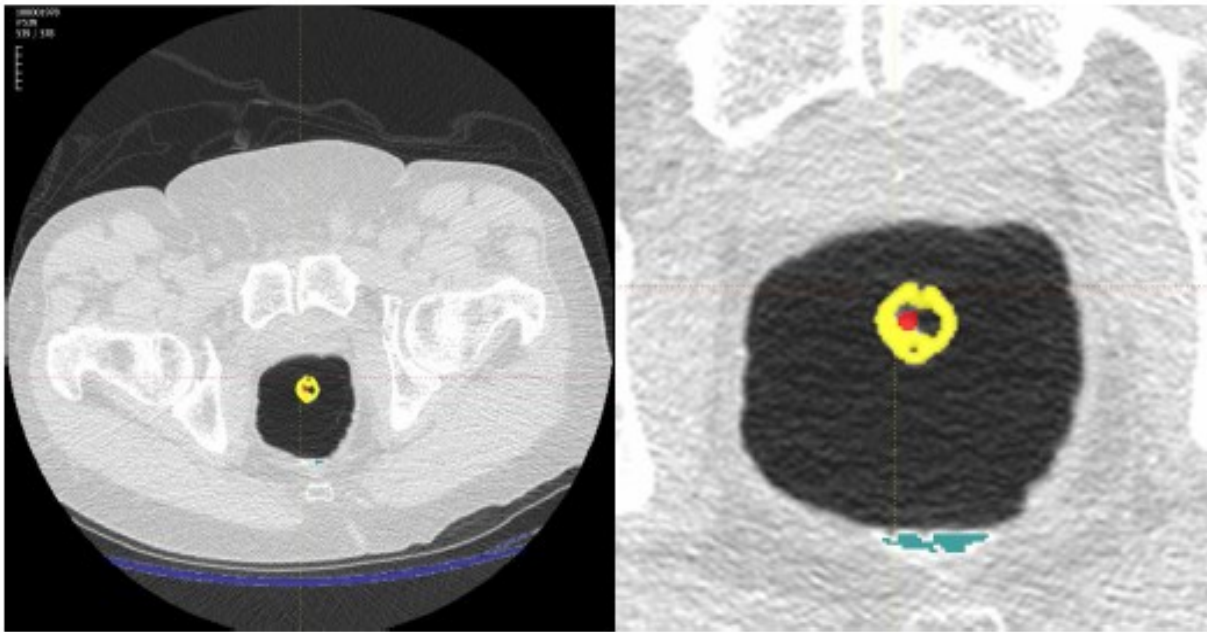


Figure 3.7. (Left) TLD (red) segmented from axial image of patient who underwent VC exam. (Right) Zoomed in view of TLD segmentation.

3.3.5 Homogeneous and Heterogeneous Phantoms with Tube Current Modulation (Level 4)

Up until this point, all validation was performed using FTC. Therefore, the TCM methods described in Section 3.2.3 were not explicitly validated. Because of this, a comprehensive validation of TCM simulations was performed [10]. All homogeneous and heterogeneous phantom measurements described in Section 3.3.2 and 3.3.3 for FTC were also performed using TCM. TCM schemes for these phantom measurements were extracted from the raw projection

data, and, using the methodology outlined in Section 3.2.3 to incorporate TCM into the simulations, corresponding TCM simulations were performed.

A root mean square error of 4.49% between simulated and measured dose was observed for all scenarios. This validation study validates the methods used to simulate TCM and provides a capstone to the extensive validation work performed previously. With this level of validation, there is confidence in the CT source model to move on to organ dose assessment.

3.4 References

1. A. C. Turner *et al.*, “The feasibility of patient size-corrected, scanner-independent organ dose estimates for abdominal CT exams,” *Med. Phys.* **38**, 820-829 (2011).
2. K. McMillan *et al.*, “Size-specific, scanner-independent organ dose estimates in contiguous axial and helical head CT examinations,” *Med. Phys.* **41**, 121909 (2014).
3. E. Angel *et al.*, “Radiation dose to the fetus for pregnant patients undergoing multidetector CT imaging: Monte Carlo simulations estimating fetal dose for a range of gestational age and patient size,” *Radiology* **249**, 220-227 (2010).
4. E. Angel *et al.*, “Monte Carlo simulations to assess the effects of tube current modulation on breast dose for multidetector CT,” *Phys. Med. Biol.* **54**, 497-512 (2009).
5. G. Jarry, *et al.*, “A Monte Carlo-based method to estimate radiation dose from spiral CT: from phantom testing to patient-specific models,” *Phys. Med. Biol.* **48**, 2645-2663 (2003).
6. J. J. DeMarco, *et al.*, “A Monte Carlo based method to estimate radiation dose from multidetector CT (MDCT): cylindrical and anthropomorphic phantoms,” *Phys. Med. Biol.* **50**, 3989-4004 (2005).

7. J. J. DeMarco, *et al.*, “Estimating radiation doses from multidetector CT using Monte Carlo simulations: effects of different size voxelized patient models on magnitudes of organ and effective dose,” *Phys. Med. Biol.* **52**, 2583-2597 (2007).
8. A. C. Turner *et al.*, “A method to generate equivalent energy spectra and filtration models based on measurements for multidetector CT Monte Carlo dosimetry simulations,” *Med. Phys.* **36**, 2154-2164 (2009).
9. E. Angel, *et al.*, “Monte Carlo simulations to assess the effects of tube current modulation on breast dose for multidetector CT,” *Phys. Med. Biol.* **54**, 497-512 (2009).
10. M. Bostani, *et al.*, “Validation of a Monte Carlo model used for simulating tube current modulation in computed tomography over a wide range of phantom conditions/challenges,” *Med. Phys.* **41**, 112101 (2014).
11. M. Bostani, *et al.*, “Accuracy of Monte Carlo simulations compared to in-vivo MDCT dosimetry,” *Med. Phys.* **42**, 1080-1086 (2015).
12. D. B. Pelowitz, MCNPX User’s Manual Version 2.7.0, Los Alamos National Laboratory Report LA-CP-11-00438 (LANL, Los Alamos, NM, 2011).
13. M. B. Chadwick *et al.*, “ENDF/B-VII.1: Nuclear data for science and technology: Cross sections, covariances, fission product yields and decay data,” *Nucl. Data Sheets* **112**, 2887–2996 (2011).
14. L. N. Tran, *et al.* “Comparison of treatment response classifications between unidimensional, bidimensional, and volumetric measurements of metastatic lung lesions on chest computed tomography. *Acad. Radiol.* **11**, 1355-1360 (2004).
15. J. J. DeMarco, T.D. Solberg, J. B. Smathers, “A CT-based Monte Carlo simulation tool for dosimetry planning and analysis,” *Med. Phys.* **25**, 1-11 (1998).

16. International Commission on Radiation Units and Measurements, “Tissue substitutes in radiation dosimetry and measurement,” ICRU Report No. 44 (ICRU 1989).
17. J. H. Hubbell and S. M. Seltzer, “Tables of x-ray mass attenuation coefficients and mass energy-absorption coefficients,” available at:
<http://physics.nist.gov/PhysRefData/XrayMassCoef/cover.html> (2004).
18. J. J. DeMarco, *et al.*, “A Monte Carlo based method to estimate radiation dose from multidetector CT (MCDT): Cylindrical and anthropomorphic phantoms,” *Phys. Med. Biol.* **50**, 3989–4004 (2005).
19. G. Zhang, *et al.*, “Monte Carlo modeling for dose assessment in cone beam CT for oral and maxillofacial applications,” *Med. Phys.* **40**, 072103 (2013).
20. American Association of Physicists in Medicine, “Monte Carlo Reference Data Sets for Imaging Research,” AAPM Report 195 (2015).
21. J. W. Mueller *et al.*, “In vivo CT dosimetry during CT colonography,” *Am. J. Roentgenol.* **202**, 703-710 (2014).

Chapter 4: GSF and ICRP Reference Voxelized Phantoms

4.1 Introduction

Reference voxelized phantoms are models of patient anatomy based on CT or MRI images from high-resolution scans of an individual. Individual organs and anatomical structures are segmented from the images, so the resultant reference voxelized phantoms are a 3D matrix of voxels with each voxel belonging to a particular organ or anatomical structure. Reference voxelized phantoms have long played a significant role in CT dosimetry, specifically Monte Carlo simulations of CT dose [7-33]. For CT dosimetry, the most useful dose metric for understanding the dose impact of a CT scan is organ-specific dose. In order to quantify organ doses for patients who undergo CT examinations, there are two options: (1) Segment individual organs from the patient's axial images or (2) use reference voxelized phantoms with all radiosensitive organs identified. While patient-specific organ segmentation offers the most patient-specific dose assessment, axial images are only available for anatomy that was scanned, so some organs of interest may be partially within the scan range or completely outside of the scan range. For those organs, accurate organ dose assessment based on the patient's axial images is not possible because of incomplete segmentation. Organ dose assessment using reference voxelized phantoms, on the other hand, does not suffer the limitations caused by the inability to identify partially- or indirectly-irradiated organs from an individual patient's axial images. Reference voxelized phantoms are based on whole-body scans, so regardless of the scan range, organ doses in all radiosensitive organs can be quantified. This not only facilitates the assessment of partially- and indirectly-irradiated organ dose but also allows for the calculation of

effective dose. The major limitation of reference voxelized phantoms is that they are not patient-specific but rather representative of certain patient sizes and ages. As will be discussed in Chapter 9, though, reference voxelized phantoms of different sizes can be used to derive relationships between patient size and dose.

Within this dissertation, there are two groups of reference voxelized phantoms that will be used: GSF and ICRP (International Commission on Radiological Protection) reference voxelized phantoms [5,6]. The GSF family of reference voxelized phantoms is a set of 8 patient models that includes both pediatric and adult models. The ICRP reference voxelized phantoms consist of a male and female reference voxelized phantom representing the ICRP Adult Reference Male and Female, respectively. The purpose of this chapter was to describe the characteristics of these reference voxelized phantoms and outline how these reference voxelized phantoms are incorporated into Monte Carlo simulations of organ dose.

4.2 Physical Characteristics

Table 4.1 outlines the physical characteristics of the GSF and ICRP reference voxelized phantoms [5,6]. As described in the ‘Range’ category of Table 4.1, some of the reference voxelized phantoms were distributed as whole-body models and some were distributed with anatomy below the thighs excluded. For those phantoms with anatomy excluded, a weight and height are provided for both the individual that was scanned and the phantom. For Frank, there is no information available about the patient whose images were used to construct the reference voxelized phantom, so only the weight and height of the reference voxelized phantom are tabulated. Figure 4.1 shows cross-sectional images of each of the reference voxelized phantoms.

Table 4.1. Physical characteristics of GSF and ICRP reference voxelized phantoms. Data in parentheses refers to the weight or height of the reference voxelized phantom. Data not in parentheses refers to the weight or height of the actual patient whose images were used to create the phantom.

	Phantom	Gender	Age	Range	Weight (kg)	Height (cm)
GSF	Baby	Female	8 weeks	Whole body	4.2	57
	Child	Female	7 years	Whole body	21.7	115
	Donna	Female	40 years	Whole body	79	170
	Frank	Male	48 years	Torso and head	(65.4)	(96.5)
	Golem	Male	38 years	Whole body	68.9	176
	Helga	Female	26 years	From mid thighs upwards	81 (76.8)	170 (114)
	Irene	Female	32 years	Whole body	51	163
	Visible Human	Male	38 years	From knees upwards	103.2 (87.8)	180 (125)
ICRP	ICRP Male (Rex)	Male	38 years	Whole body	73	176
	ICRP Female (Regina)	Female	43 years	Whole body	59	167

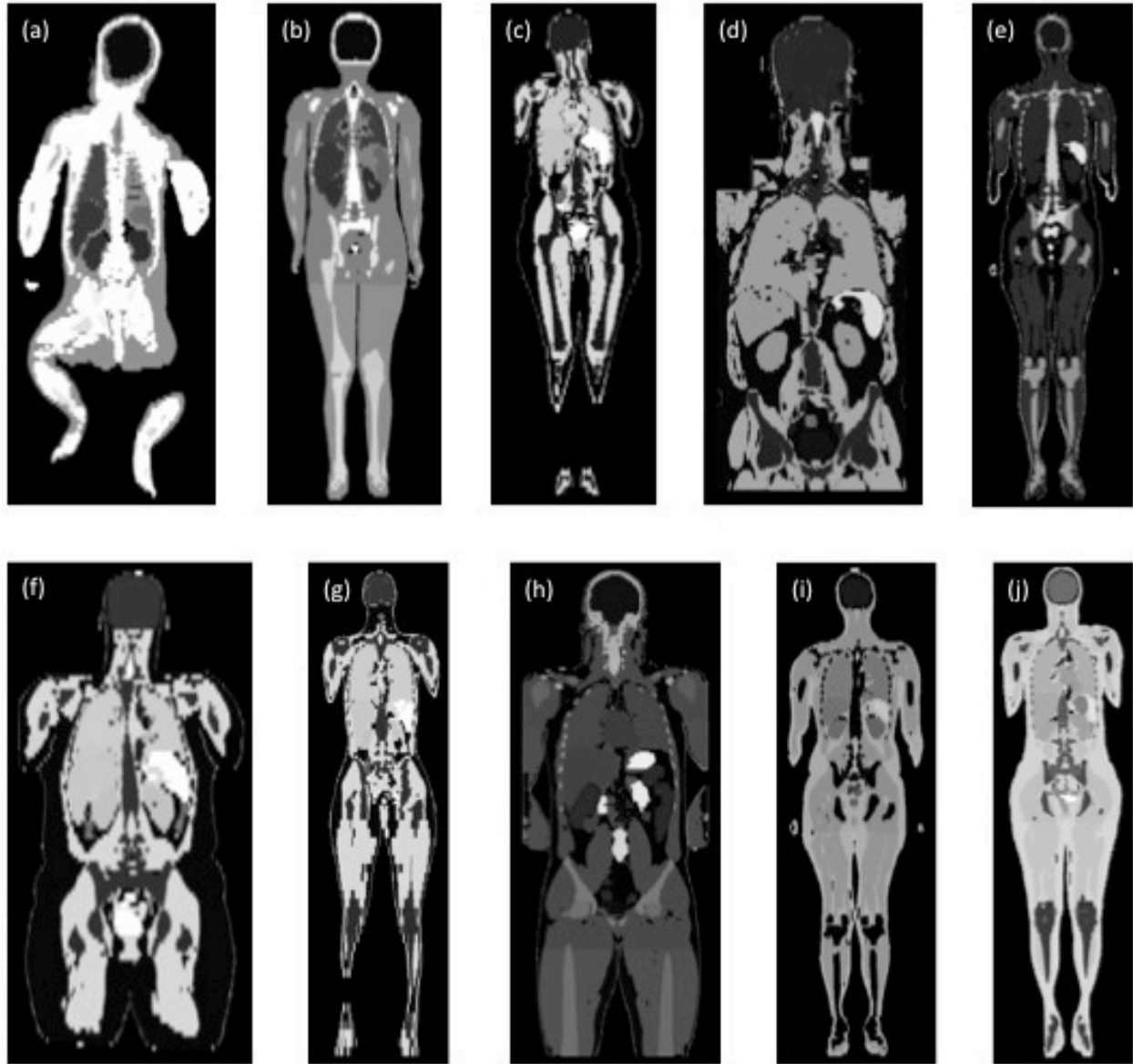


Figure 4.1. Cross-sectional images of the GSF and ICRP reference voxelized phantoms (a) Baby, (b) Child, (c) Donna, (d) Frank, (e) Golem, (f) Helga, (g) Irene, (h) Visible Human, (i) ICRP Male (Rex) and (j) ICRP Female (Regina).

4.3 Image Characteristics

Table 4.2 shows the image characteristics of the GSF and ICRP reference voxelized phantoms [5,6]. Each reference voxelized phantom consists of a large number of contiguous slices with

slice thicknesses ranging from 4 mm to 10 mm. In-plane matrix resolution ranges from 256 x 256 to 512 x 512 pixels.

Table 4.2. Image characteristics of GSF and ICRP reference voxelized phantoms.

	Phantom	# of images	Slice thickness (mm)	In-plane resolution	Voxel size (mm ³)
GSF	Baby	142	4	267 x 138	2.89
	Child	144	8	256 x 256	18.97
	Donna	179	10	256 x 256	35.15
	Frank	193	5	512 x 512	2.75
	Golem	220	8	256 x 256	34.61
	Helga	114	10	512 x 512	9.60
	Irene	348	5	262 x 132	17.57
	Visible Human	250	5	512 x 512	4.27
ICRP	ICRP Male (Rex)	222	8	254 x 127	36.53
	ICRP Female (Regina)	348	4.84	299 x 137	15.24

4.4 Organ and Material Descriptions

As many as 141 individual organs and anatomical structures are identified within each of the GSF and ICRP reference voxelized phantoms. Of considerable interest are organs whose doses are used to calculate effective dose. Table 4.3 lists the organs and respective tissue weighting factors used in the ICRP Publication 103 calculation of effective dose [11]. Table 4.4 lists the organs and respective tissue weighting factors used in the ICRP Publication 60 calculation of effective dose [10]. Of the organs listed in Tables 4.3 and 4.4, nearly all are identified in the GSF and ICRP reference voxelized phantoms. There are, however, a handful of radiosensitive organs of interest that have not been identified in all 10 GSF and ICRP reference voxelized phantoms.

For those organs, appropriate anatomical substitutes are suggested based on relative anatomical location. Table 4.5 lists the organs from Tables 4.3 and 4.4 that are not identified in every reference voxelized phantom along with the anatomical substitutes used in their absence. For example, if the salivary glands are not identified in the reference voxelized phantom, dose to the brain is used as a surrogate for dose to the salivary glands. The only organ that is not identified in all reference voxelized phantoms for which an anatomical substitute is not suggested is the breast. There are no superficial organs in the same region of the chest as the breasts that can be used as an appropriate substitute. Only 3 of the 10 patient models used in this investigation do not have the breast identified (Child, Golem, Visible Human).

Table 4.3. Organs and respective tissue weighting factors used in the ICRP Publication 103 calculation of effective dose. All primary organs have their own weighting factor while the average dose to all remainder organs has a weighting factor of 0.12.

	Organ	ICRP 103 Tissue Weighting Factor (w_T)
Primary organs	Breast	0.12
	Colon	0.12
	Lung	0.12
	Red marrow (RBM)	0.12
	Stomach	0.12
	Gonads	0.08
	Bladder	0.04
	Esophagus	0.04
	Liver	0.04
	Thyroid	0.04
	Bone surface	0.01
	Brain	0.01
	Salivary glands	0.01
	Skin	0.01
	Remainder organs	Adrenals
Extrathoracic (ET) region		
Gall bladder		
Heart		
Kidneys		
Lymphatic nodes		
Muscle		0.12
Oral mucosa		
Pancreas		
Prostate/Uterus		
Small intestine		
Spleen		
Thymus		

Table 4.4. Organs and respective tissue weighting factors used in the ICRP Publication 60 calculation of effective dose. All primary organs have their own weighting factor while the average dose to all remainder organs has a weighting factor of 0.05.

	Organ	ICRP 60 Tissue Weighting Factor (w_T)
Primary organs	Gonads	0.20
	Colon	0.12
	Lung	0.12
	Red bone marrow (RBM)	0.12
	Stomach	0.12
	Bladder	0.05
	Breast	0.05
	Esophagus	0.05
	Liver	0.05
	Thyroid	0.05
	Bone surface	0.01
	Skin	0.01
	Remainder organs	Adrenals
Brain		
Kidneys		
Muscle		
Pancreas		0.05
Prostate/Uterus		
Small intestine		
Spleen		
Thymus		

Table 4.5. Organ substitutes for ICRP 103/ICRP 60 organs not identified in all GSF and ICRP reference voxelized phantoms.

ICRP 103/ICRP 60 organs	Organ substitutes
Breast	---
Gonads	Prostate (Male)/Uterus (Female)
Esophagus	Thymus
Salivary glands	Brain
Extrathoracic (ET) region	Thyroid
Gall bladder	Pancreas
Lymphatic nodes	Muscle
Oral mucosa	Brain
Small intestine	Stomach or duodenum/ileum

Each voxel within the GSF and ICRP reference voxelized phantoms is assigned an integer identification number corresponding to the particular organ or anatomical structure the voxel represents. As described in Section 3.2.4, in order to incorporate the reference voxelized phantoms into Monte Carlo simulations, each organ identification number is assigned a material description (i.e. weight fractions and density) based on the elemental compositions and physical characteristics of tissue substitutes from ICRU (International Commission on Radiation Units and Measurements) Report 44 [16]. For all skeletal tissue, homogeneous bone (HB) composition and density (1.4 g/cm^3) is used [10]. For lungs, a density of 0.048 g/cm^3 is used to better represent the most common density of lung tissue that would result from the application of a Hounsfield number to electron density lookup table on lung tissue pixels in a CT image [15].

4.5 Breast and Bone Dose Considerations

For all organs, organ dose is calculated according to the methodology outlined in Section 3.2.5. While some reference voxelized phantoms have both glandular and adipose breast tissue identified, breast dose is tallied within glandular breast tissue voxels only. Because the identification of bone marrow voxels is difficult/impossible in clinical CT images, red bone marrow (RBM) and bone surface are not explicitly segmented in the GSF and ICRP reference voxelized phantoms. Instead, HB voxels are used to determine skeletal tissues doses [12]. Dose to the bone surface is estimated as the dose to the HB voxels. Dose to RBM is approximated as dose to the HB voxels multiplied by the ratio of the mass energy-absorption coefficients of RBM and HB. Dose to RBM is defined as:

$$D_{RBM} = D_{HB} \times \frac{(\mu_{en}/\rho)_{RBM}}{(\mu_{en}/\rho)_{HB}} \quad (4.1)$$

where D_{HB} is the dose the HB voxels, $(\mu_{en}/\rho)_{RBM}$ is the mass energy-absorption coefficient of RBM and $(\mu_{en}/\rho)_{HB}$ is the mass energy-absorption coefficient of HB. As described in Eq. (3.1) from Section 3.2.5, D_{HB} is calculated as the product of the photon energy fluence in HB voxels, ψ_{HB} , and $(\mu_{en}/\rho)_{HB}$. Therefore, dose to RBM can be redefined as:

$$D_{RBM} = \psi_{HB} \times (\mu_{en}/\rho)_{RBM} \quad (4.2)$$

4.6 Reference Voxelized Phantom Modifications

All GSF and ICRP reference voxelized phantoms are based on scans of patient who had their arms at their sides at the time of scanning. While arms are almost always raised above the head for any routine body scanning protocol (e.g. abdomen, abdomen/pelvis, chest, chest/abdomen/pelvis), most of the individuals used to construct the reference voxelized phantoms suffered from leukemia and had to undergo whole-body irradiation, so “arms up” was not necessarily a consideration. Because the arms are usually raised above the head for body scanning, it is important to replicate that behavior in the voxels phantoms to ensure the realistic simulation of organ dose.

For all reference voxelized phantoms, arm tissue (skin, muscle and bone) is identified below the shoulders. By setting the voxel identification numbers of arm tissue to the voxel

identification number of air, the arm tissue can be eliminated from the side of the body. When the arms are raised above the head, the shoulders are also raised, so in order to recreate this anatomical positioning, the shoulders are edited using a custom tool designed in MeVisLab. Figure 4.2 shows the progression of modifications to the Visible Human reference voxelized phantom from the original reference voxelized phantom (a) to the reference voxelized phantoms sans arms (b) to finally the reference voxelized phantom with the shouldered edited (c). The fully-modified reference voxelized phantoms are the reference voxelized phantoms that will be used in all Monte Carlo simulations described in this dissertation.

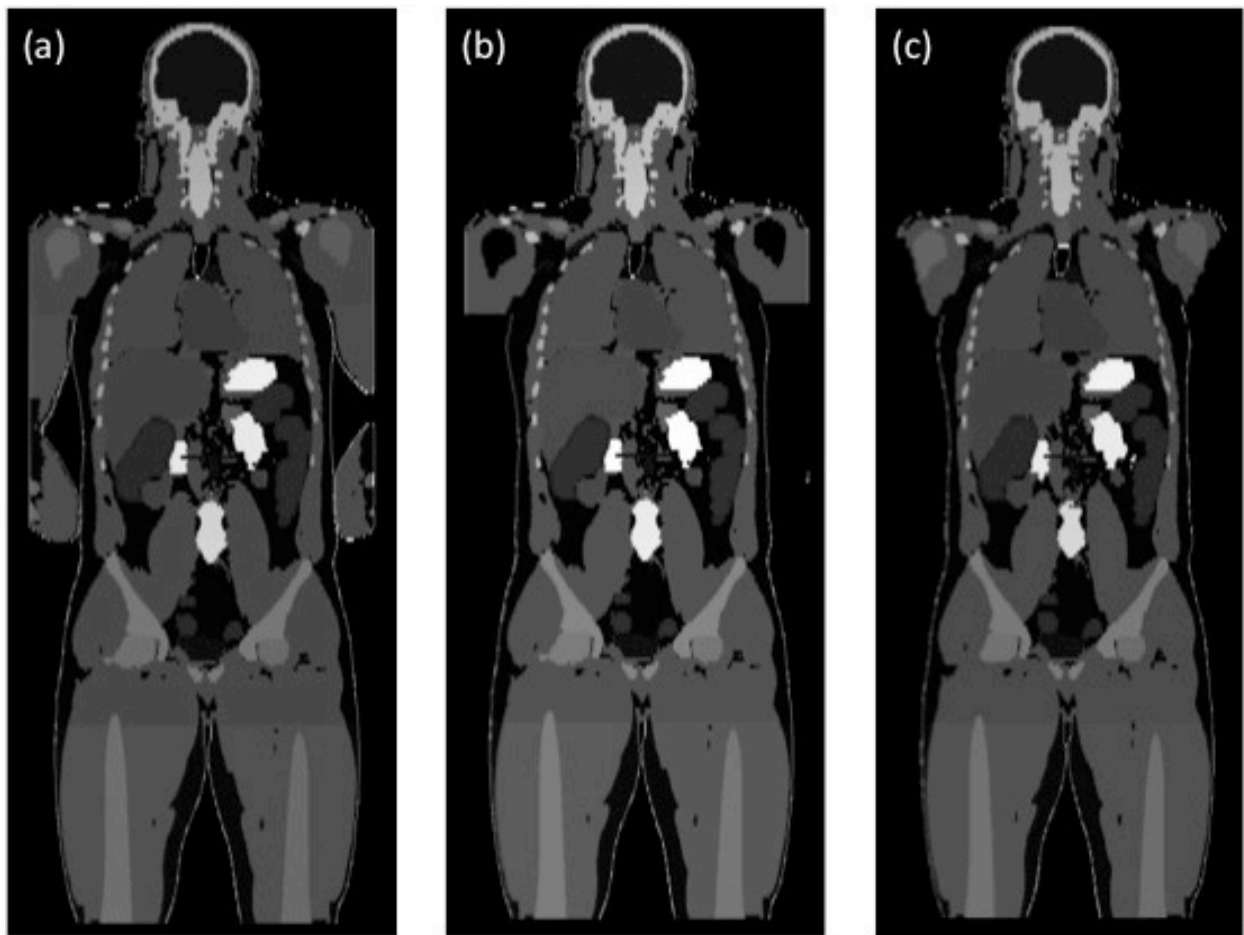


Figure 4.2. Example of modifications made to the Visible Human reference voxelized phantom: (a) Original reference voxelized phantom with arms, (b) arms removed and (c) arms removed and shoulders modified to represent “arms up” anatomy.

4.7 References

1. J. J. DeMarco, *et al.*, “Estimating radiation doses from multidetector CT using Monte Carlo simulations: effects of different size voxelized patient models on magnitudes of organ and effective dose,” *Phys. Med. Biol.* 52, 2583-2597 (2007).
2. A. C. Turner *et al.*, “The feasibility of a scanner-independent technique to estimate organ dose from MDCT scans: Using CTDIvol to account for differences between scanners,” *Med. Phys.* 37, 1816-1825 (2010).
3. A. C. Turner *et al.*, “The feasibility of patient size-corrected, scanner-independent organ dose estimates for abdominal CT exams,” *Med. Phys.* 38, 820-829 (2011).
4. K. McMillan *et al.*, “Size-specific, scanner-independent organ dose estimates in contiguous axial and helical head CT examinations,” *Med. Phys.* 41, 121909 (2014).
5. N. Petoussi-Henss, M. Zankl, U. Fill, D. Regulla, “The GSF family of voxel phantoms,” *Phys. Med. Biol.* 47, 89-106 (2002).
6. International Commission on Radiological Protection, “Adult Reference Computation Phantoms,” ICRP Publication 110 (2009).
7. International Commission on Radiological Protection, “The 2007 Recommendations of the International Commission on Radiological Protection,” ICRP Publication 103 (2007).
8. International Commission on Radiological Protection, “1990 Recommendations of the International Commission on Radiological Protection,” ICRP Publication 60 (1991).
9. International Commission on Radiation Units and Measurements, “Tissue substitutes in radiation dosimetry and measurement,” ICRU Report No. 44 (ICRU 1989).

10. M. Cristy, K. F. Eckerman, "Specific absorbed fractions of energy at various ages from internal photon sources," Oak Ridge National Laboratory Report TM-8381, Vol. I-VII (ORNL, Oak Ridge, TN, 1987).
11. J. J. DeMarco, T.D. Solberg, J. B. Smathers, "A CT-based Monte Carlo simulation tool for dosimetry planning and analysis," *Med. Phys.* 25, 1-11 (1998).
12. M. Rosenstein, "Organ doses in diagnostic radiology," Food and Drug Administration Report 76-8030 (FDA, Rockville, MD, 1976).

Chapter 5: Determining Patient Size Data from CT Localizer Radiograph

5.1 Introduction

TCM is a scanning technique that adapts tube current to the attenuation (i.e. size) of the body region [1]. Tube current is increased in regions of high attenuation (e.g. shoulders or pelvis) and decreased in regions of low attenuation (i.e. lungs). Virtually all clinical protocols have implemented TCM as a means to reduce patient dose while maintaining acceptable image quality [1,2]. In order to understand how a tube current modulation (TCM) algorithm modulates tube current in response to changes in patient size, it is first necessary to understand what patient size metric is being acquired by the scanner to drive the TCM algorithm. While it is understood that TCM algorithms utilize an attenuation-based size metric, it is still unclear exactly what that size metric is [2].

Before CT images are acquired, a CT localizer radiograph is obtained. This projectional image aids in properly aligning the patient and setting the appropriate scan range. Based on the scanner manufacturer and the scan protocol, either an anterior-posterior (AP) radiograph, lateral (LAT) radiograph or both are acquired. Patient attenuation is derived from these projectional images and is then used within all scanner-specific algorithms that require knowledge of patient attenuation, such as TCM [2]. The exact location where this attenuation information is stored and the form of this attenuation information, though, remains a mystery. Numerous efforts have been undertaken to estimate attenuation-based size metrics from CT localizer radiographs and axial images, but these are all retrospective estimates of patient size and therefore do not necessarily correspond to the attenuation-based size estimated by the scanner during image acquisition [3-5].

The purpose of this investigation was to determine the exact patient size data utilized by the scanner, specifically size data that may be created and then stored in the CT localizer radiograph's DICOM header. Efforts focused on defining the patient size data determined for Siemens CT scanners. Once patient size estimates were determined, for a series of patients who underwent clinically indicated abdomen/pelvis and chest CT examinations, patient size estimates were compared with an attenuation-based patient size metric currently accepted by the medical physics community as accurate estimate of patient size ("gold standard"). In addition to this direct comparison of patient size, an indirect comparison of patient size was performed by comparing size-specific dose estimates (SSDE) calculated using the patient size metrics [36]. A quantitative assessment of the relative agreement between both patient size and SSDE calculations established a practical definition of the attenuation-based patient size data determined by Siemens CT scanners.

5.2 Methods

5.2.1 Size Data in CT Localizer Radiograph

The goal of this investigation was to determine if patient size data is stored on a Siemens scanner in a form that is easily accessible. The most likely location of the patient size information is the CT localizer radiograph (the "topogram" for Siemens CT scanners). Patient attenuation information is determined during the acquisition of the topogram, so it is reasonable to assume that the topogram would contain that information [1].

All CT images are traditionally stored according to the Digital Imaging and Communications in Medicine (DICOM) standard [7]. As part of the standard, each image includes a “header” that contains a series of fields with information about scan acquisition parameters and other quantitative and textual data. If patient attenuation is stored on the scanner in a usable form, it is likely to be stored within the header of the topogram. Evaluating the DICOM header of a Siemens topogram, a specific DICOM field stood out, DICOM tag (0029,1140). Fig. 5.1 shows the full expansion of this private field. At multiple locations within the field and subfields, the words “ATTENUATION” and “AEC” were identified. AEC stands for “automatic exposure control,” another term for TCM. These are clues that indicate that this may be the DICOM field where information related to the patient attenuation used to drive the Siemens TCM algorithm may be stored.

▼ Unknown	0029,1140	SIEMENS MEDCOM HEADER\SOM 5 TPOS\SOM 5 NULLPOSITION\VB...OM HEADER\SOM 5 AEC\SOM 5 ATTENUATION\VB10A 20030626\
▼ Item		SIEMENS MEDCOM HEADER\SOM 5 TPOS\SOM 5 NULLPOSITION\VB10A 20030626\~000016125M
Unknown	0029,0010	SIEMENS MEDCOM HEADER
Unknown	0029,1041	SOM 5 TPOS
Unknown	0029,1042	SOM 5 NULLPOSITION
Unknown	0029,1043	VB10A 20030626
Unknown	0029,1044	~000016125M
▼ Item		SIEMENS MEDCOM HEADER\SOM 5 AEC\SOM 5 ATTENUATION\VB10A 20030626\
Unknown	0029,0010	SIEMENS MEDCOM HEADER
Unknown	0029,1041	SOM 5 AEC
Unknown	0029,1042	SOM 5 ATTENUATION
Unknown	0029,1043	VB10A 20030626
Unknown	0029,1044	

Figure 5.1. DICOM field (0029,1140) from Siemens topogram.

Evaluation of the DICOM header in a standard DICOM reader failed to yield any quantitative information related to the patient attenuation. This may be due in part to the absence of information for subfield (0029,1044) as observed in Fig. 5.1. Because of this, an alternative approach to evaluate the information in the DICOM header of the topogram was suggested. Instead of opening the topogram image in a DICOM reader, the image was instead opened in a text editor. Any text editor can be used (e.g. Notepad, TextEdit). By evaluating the image as a

text file, the information contained in the subfield (0029,1044) was now visible. Fig. 5.2 shows what that subfield information looks like when the topogram image is evaluated as a text file. The data is an array of numbers with a set of leading zeros and a single decimal place. Because the data is saved in a standard form, a regular expression match algorithm can be employed in a variety of programming languages (e.g. Matlab, Python, etc.) to extract this array of numbers.

```

topogram.dcm
DICMUL20BUI1.2.840.10008.5.1.4.1.1.2UI81.3.12.2.1107.5.1.4.54023.30000012020320143200000001249UI1.2.840.1
0008.1.2.1UI1.3.12.2.1107.5.1.4SHSIEMENS_S5VB30B CS
ISO_IR 100CS&ORIGINAL\PRIMARY\LOCALIZER\CT_SOM5
TOPUI1.2.840.10008.5.1.4.1.1.2UI81.3.12.2.1107.5.1.4.54023.30000012020320143200000001249 DA20120131!
DA20120131"DA20120131#DA201201310TM080237.125000 1TM081258.515000 2TM081253.578396 3TM081258.515000
PSH`CSCTpLOSIEMENS êPNêLO
Sensation 64!STForce Anonymity PNfemale_chest 5 topo 2 3 2012 LO
Anonymous 0DA@CS0 CSCHEST PDS0.6 `DS120 êDS500` L0syngo CT 2007SDS512 DS1040DS570 DS0 0DS161
@CSCWPIS4047QIS35RIS141 `SH0 pIS4 êDS1.2 DA20120131TM062940.000000 SHT20sQCSFFS
UI81.3.12.2.1107.5.1.4.54023.30000012020320143200000001247
UI81.3.12.2.1107.5.1.4.54023.30000012020320143200000001248 SH IS2 IS1 IS1 2DS-255.5\ -161\ -1.5
7DS1\6.123031769e-017\0\0\0\ -1 RUI81.3.12.2.1107.5.1.4.54023.30000012020320143200000001246 @LO ADS1
(US(CS
MONOCHROME2 (US(US(0DS1\1 (US(US
(US
(US(PDS50\300(QDS350\2000(RDS-1024 (SDS1 (ULOWINDOW1\WINDOW2 )LOSIEMENS CSA HEADER)LOSIEMENS MEDCOM
HEADER )CSSOM 5 ) LO
VA10A 971201)OBRLT3024FD` t@FDç` |ÉÂ@SL`SL»
SLFDx@SLQSLSL2SL+LT
CHESTFDÂ@FD FD!SL`SL%SL
'FDN@)SLZ+LT265340901,SL`-SL/FD333333,,?0LTP30F5SL6CST 7SL8SL`9SL;SL<SL=FDÂ@>SL‡(?SLFDFDÂU"o_î?
FD·zÆG· 0IS0 SLA
SL1
SL`~`~`~`CS
END! )@SQ""`~{x)LOSIEMENS MEDCOM HEADER )ACS
SOM 5 TPOS)BLOSOM 5 NULLPOSITION(CLOVB10A 20030626)DOB
-000016125M`+ë!)LOSIEMENS MEDCOM HEADER )ACS
SOM 5 AEC )BLOSOM 5 ATTENUATION )CLOVB10A 20030626)DOB.!00000014.3 00000014.1 00000014.1 00000014.0
00000014.0 00000014.0 00000013.9 00000013.9 00000013.9 00000013.8 00000013.7 00000013.7 00000013.6
00000013.7 00000013.7 00000013.8 00000013.8 00000013.8 00000013.8 00000013.9 00000014.0 00000014.1
00000014.0 00000013.9 00000013.9 00000013.8 00000013.9 00000014.0 00000014.0 00000014.0
00000014.0 00000014.0 00000014.0 00000014.0 00000013.9 00000013.8 00000013.9 00000013.9 00000014.0
00000014.1 00000014.0 00000013.9 00000014.0 00000014.0 00000014.0 00000014.0 00000013.9 00000013.9
00000013.9 00000014.0 00000014.0 00000014.0 00000014.0 00000014.0 00000014.3 00000014.5 00000014.8
00000015.1 00000015.3 00000015.4 00000015.5 00000015.6 00000015.8 00000015.9 00000015.9 00000015.8
00000015.8 00000015.8 00000015.8 00000015.8 00000015.9 00000015.9 00000016.1 00000016.2 00000016.4
00000016.6 00000016.7 00000016.9 00000017.1 00000017.2 00000017.4 00000017.4 00000017.9 00000018.0
00000017.9 00000017.9 00000017.8 00000017.8 00000017.8 00000017.7 00000017.7 00000017.9 00000017.6
00000017.6 00000017.6 00000017.6 00000017.7 00000017.7 00000017.8 00000018.1 00000018.0 00000018.0
00000018.1 00000018.4 00000018.4 00000018.4 00000018.5 00000018.7 00000018.8 00000018.8 00000018.9
00000018.9 00000018.9 00000018.9 00000018.9 00000018.8 00000018.8 00000019.1 00000019.0 00000018.8
00000018.8 00000018.8 00000018.8 00000018.6 00000018.6 00000018.6 00000018.6 00000018.5 00000018.3
00000018.1 00000018.0 00000017.9 00000018.0 00000018.0 00000017.9 00000017.9 00000017.9 00000017.9
00000017.8 00000017.8 00000017.6 00000017.6 00000017.5 00000017.5 00000017.6 00000017.6 00000017.7
00000017.7 00000017.9 00000017.7 00000017.6 00000017.6 00000017.6 00000017.6 00000017.6 00000017.7
00000017.7 00000017.6 00000017.6 00000017.6 00000017.6 00000017.6 00000017.6 00000017.6 00000017.6
00000017.5 00000017.5 00000017.5 00000017.5 00000017.6 00000017.6 00000017.6 00000017.6 00000017.5
00000017.4 00000017.4 00000017.3 00000017.3 00000017.3 00000017.4 00000017.4 00000017.4 00000017.4
00000017.7 00000017.7 00000017.8 00000017.8 00000017.9 00000018.0 00000018.0 00000018.1 00000018.1
00000018.2 00000018.3 00000018.4 00000018.5 00000018.4 00000018.3 00000018.3 00000018.4 00000018.4
00000018.5 00000018.5 00000018.5 00000018.6 00000018.7 00000018.6 00000018.6 00000018.6 00000018.5
00000018.4 00000018.3 00000018.3 00000018.4 00000018.4 00000018.4 00000018.4 00000018.4 00000018.4
00000018.4 00000018.4 00000018.4 00000018.3 00000018.3 00000018.3 00000018.3 00000018.3 00000018.3
00000018.3 00000018.3 00000018.2 00000018.2 00000018.3 00000018.3 00000018.3 00000018.3 00000018.3

```

Figure 5.2. Siemens topogram evaluated as a text file reveals array of numbers inferred to be patient size data. This is assumed to be the data stored in DICOM field (0029.1140).

When the numbers were extracted, it was revealed that the length of numbers was exactly two times the length of the topogram. This was true for every topogram evaluated. In other words, if the length of the topogram is 512 mm, there are 1024 numbers in the array. The exact

relationship between topogram length and the length of numbers found in the DICOM header of the topogram offers clues as to what this information is conveying. As mentioned earlier, depending on the manufacturer and scan protocol, a certain topogram or set of topograms will be acquired [1]. Regardless of the protocol, Siemens only requires a single topogram to initiate the Siemens TCM algorithm. Patient attenuation is explicitly measured in the direction of the topogram (AP or LAT) and calculated in the orthogonal direction. Therefore, for a given topogram, it was hypothesized that the extracted numbers represent the AP and LAT patient attenuation information in 1 mm resolution. The first half of the numbers corresponds to patient attenuation in the direction that the topogram was acquired. The second half of the numbers corresponds to patient attenuation in the orthogonal direction. For example, for a 512 mm AP topogram with 1024 numbers extracted from the DICOM header of the topogram, the first 512 numbers correspond to AP patient attenuation, and the next 512 numbers correspond to LAT patient attenuation. If a LAT topogram had been acquired, the opposite would be true.

While there is now context as to why the length of patient attenuation data extracted from the DICOM header of the topogram is two times the length of the topogram, it is still unclear exactly what attenuation-based patient size metric the numbers represent. A common attenuation-based patient size metric is water equivalent diameter (WED) [20]. Conventionally measured retrospectively from the topogram or axial image data, WED expresses patient attenuation in terms of the diameter of a cylinder of water having the same average attenuation as the patient. WED calculated from axial images is defined as:

$$D_{w,image} = 2 \sqrt{\left(\frac{1}{1000} \overline{CT(x,y)_{ROI}} + 1 \right) \times \frac{A_{ROI}}{\pi}} \quad (5.1)$$

where $\overline{CT(x,y)}_{ROI}$ is the mean CT number within a region of interest (ROI) of the image and

A_{ROI} is the total area of the ROI defined as:

$$A_{ROI} = N_{pixel} \times A_{pixel} \quad (5.2)$$

where N_{pixel} is the number of pixels in the ROI and A_{pixel} is the area of each pixel [4,5,20,9].

When calculating $D_{w,image}$, it is important to define the ROI to include the entire patient while minimizing the amount of other attenuating materials, such as the CT table. This is especially true for small pediatric patients where attenuation due to the CT table can make up a nontrivial percentage of the total attenuation of the patient [10].

Given the popularity of WED as an attenuation-based measurement of patient size in CT imaging, it was hypothesized the AP and LAT attenuation data extracted from the DICOM header of the topogram are water equivalent estimates of the AP and LAT dimensions of the patient. As outlined in AAPM Report 204, the physical diameter (“effective diameter”) of the cross-sectional area of a patient can be calculated as the square root of the product of the physical AP and LAT dimensions of the patient [36]. If the AP and LAT attenuation data extracted from the DICOM header of the topogram are in fact water equivalent estimates of the AP and LAT dimensions of the patient, the water equivalent diameter can be calculated in a similar fashion. Using Eq. (5.3), an estimate of WED can be calculated at each location along the patient using the AP and LAT attenuation data. Figure 5.3 shows the AP and LAT attenuation-

based estimates of patient size along with $D_{w,topo}$ overlaid on the topograms of patients who received clinically indicated abdomen/pelvis (left) and chest CT examinations (right).

$$D_{w,topo} = \sqrt{AP \times LAT} \quad (5.3)$$

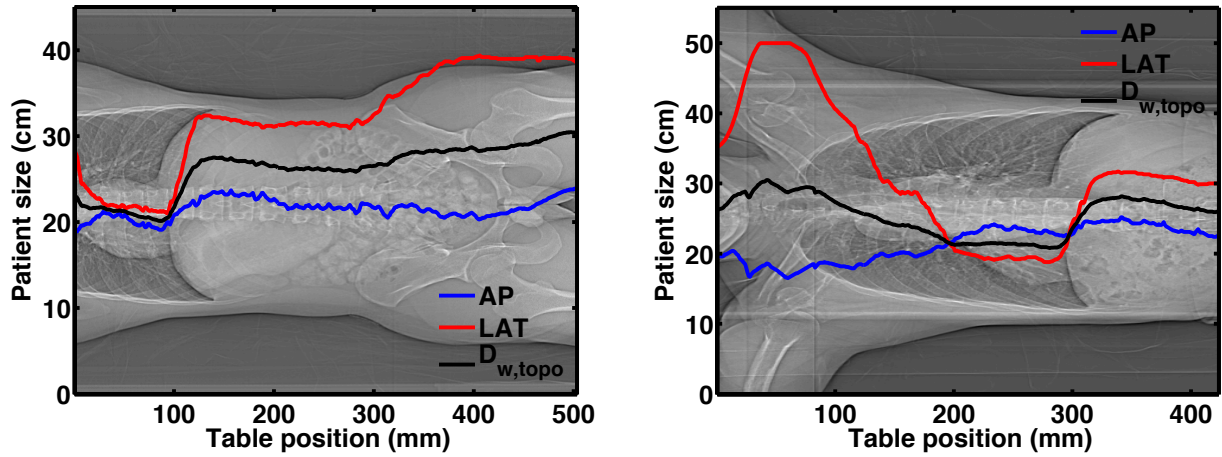


Figure 5.3. AP, LAT and $D_{w,topo}$ overlaid on topograms of patients who underwent abdomen/pelvis (left) and chest (right) CT examinations.

5.2.2 Comparison of Size Data for a Set of Patients

To verify that the values extracted from the DICOM header represent water equivalent estimates of the AP and LAT dimensions of the patient and therefore can be used to calculate water equivalent diameter, $D_{w,topo}$ was compared with $D_{w,image}$ for a set of 20 patients who received clinically indicated abdomen/pelvis (n=10) and chest (n=10) scans. Using Eq. (5.3), $D_{w,topo}$ was calculated retrospectively from the topograms of the 20 patients. $D_{w,topo}$ was calculated on a

slice-by-slice basis (1 mm resolution). Each patient was scanned on a Siemens Sensation 64 scanner, and all topograms were acquired at 120 kVp.

Using Eq. (5.1), $D_{w,image}$ was also calculated retrospectively from the axial image data of the same set of 20 patients. In order to determine an ROI that includes only the patient, a semi-automated segmentation tool was used to segment the body from the surrounding air and table [11]. $D_{w,image}$ was calculated on a slice-by-slice basis (3 mm resolution). Figure 5.4 shows $D_{w,topo}$ and $D_{w,image}$ overlaid on topograms of patients who received clinically indicated abdomen/pelvis (left) and chest CT examinations (right).

Because the topogram image is used to localize the anatomy that is to be scanned, the boundaries of the topogram image are often beyond those of the CT image data. As such, the $D_{w,topo}$ profiles shown in Fig. 5.4 extend beyond the range of the $D_{w,image}$ profiles. In order to compare $D_{w,topo}$ and $D_{w,image}$ for each of the patients, the average value of $D_{w,topo}$ was compared with the average value of $D_{w,image}$ over the range of table positions for which there were corresponding values of $D_{w,topo}$ and $D_{w,image}$.

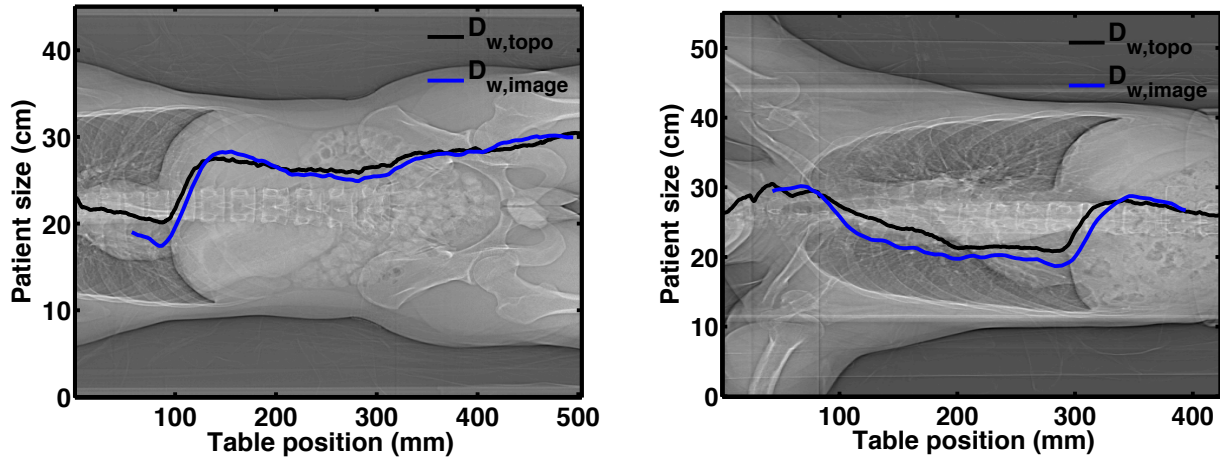


Figure 5.4. $D_{w,topo}$ and $D_{w,image}$ overlaid on topograms of patients who underwent abdomen/pelvis (left) and chest (right) CT examinations.

5.2.3 Comparison of SSDE for a Set of Patients

In addition to the direct comparison of patient size described in Section 5.2.2, an indirect comparison of patient size was performed by comparing SSDE calculated using $D_{w,topo}$ and $D_{w,image}$. SSDE was calculated according to the methodology defined in AAPM Report 204 [36]. AAPM Report 204 size-specific conversion coefficients were developed for fixed tube current (FTC) scans. Because all the scans in this investigation were performed using TCM, SSDE from a FTC of 300 effective mAs was calculated by scaling the volume CT dose index ($CTDI_{vol}$) associated with each patient scan by the ratio of 300 effective mAs and the actual (recorded) effective mAs of the scan. SSDE calculated in this investigation is defined as:

$$SSDE(Size) = CTDI_{vol}^{32\text{ cm}} \times CF_{size}^{32\text{ cm}} \times (300 \text{ effective mAs} / \text{Scan effective mAs}) \quad (5.4)$$

where $CTDI_{vol}^{32\text{ cm}}$ is the scanner-reported 32 cm $CTDI_{vol}$ and $CF_{size}^{32\text{ cm}}$ is the AAPM Report 204 size-specific $CTDI_{vol}$ -to-patient-dose conversion coefficient based on the use of the 32 cm diameter PMMA phantom for $CTDI_{vol}$. For each patient, $CF_{size}^{32\text{ cm}}$ is determined using both $D_{w,image}$ and $D_{w,topo}$. Although the conversion coefficients were originally developed using effective diameter, AAPM Report 220 indicates that it is both appropriate and more accurate to use WED to determine the conversion coefficients across multiple body regions [20]. SSDE was calculated for each patient on a slice-by-slice basis (table positions for which there were corresponding values of $D_{w,topo}$ and $D_{w,image}$) and then averaged over all slices to obtain an SSDE value for each patient and estimate of patient size.

5.3 Results

Table 5.1 shows $D_{w,image}$ and $D_{w,topo}$ for each patient. The data from Table 5.1 was used to calculate the error between $D_{w,image}$ and $D_{w,topo}$. For patients who underwent abdomen/pelvis CT examinations, the average error was 6.12%. For patients who underwent chest CT examinations, the average error was 10.19%. A collective analysis of all patients showed an average error of 8.16% between $D_{w,image}$ and $D_{w,topo}$.

Table 5.2 shows SSDE calculated using $D_{w,image}$ and $D_{w,topo}$ for each patient. The data from Table 5.2 was used to calculate the error between SSDE calculated using the two estimates of WED. For patients who underwent abdomen/pelvis CT examinations, the average error was 6.81%. For patients who underwent chest CT examinations, the average error was 8.99%. A

collective analysis of all patients showed an average error of 7.90% between SSDE($D_{w,image}$) and SSDE($D_{w,topo}$).

Table 5.1. Comparison of two estimates of WED ($D_{w,image}$ and $D_{w,topo}$).

	Patient	$D_{w,image}$ (cm)	$D_{w,topo}$ (cm)	% error
Abdomen/pelvis	FemaleAbdPel1	29.07	29.82	2.58
	FemaleAbdPel2	25.34	26.87	6.04
	FemaleAbdPel3	31.70	34.32	8.28
	FemaleAbdPel4	36.57	38.57	5.48
	FemaleAbdPel5	32.55	36.45	11.97
	MaleAbdPel1	30.00	30.28	0.91
	MaleAbdPel2	25.34	24.17	4.60
	MaleAbdPel3	37.38	39.80	6.48
	MaleAbdPel4	26.29	26.73	1.69
	MaleAbdPel5	31.36	35.51	13.21
		Average % error		
	Standard deviation			4.10
Chest	FemaleChest1	26.35	29.49	11.90
	FemaleChest2	26.63	31.16	17.00
	FemaleChest3	18.12	20.99	15.79
	FemaleChest4	20.60	22.96	11.45
	FemaleChest5	25.55	27.72	8.48
	MaleChest1	23.74	25.05	5.50
	MaleChest2	25.96	27.89	7.45
	MaleChest3	25.38	27.10	6.76
	MaleChest4	28.55	30.71	7.57
	MaleChest5	25.21	27.74	10.04
		Average % error		
	Standard deviation			3.85
	Average % error			8.16
	Standard deviation			4.40

Table 5.2. Comparison of SSDE calculated using two estimates of WED ($D_{w,image}$ and $D_{w,topo}$).

	Patient	SSDE($D_{w,image}$) (mGy)	SSDE($D_{w,topo}$) (mGy)	% error	
Abdomen/pelvis	FemaleAbdPel1	29.39	28.54	2.90	
	FemaleAbdPel2	33.78	31.91	5.53	
	FemaleAbdPel3	26.95	24.41	9.42	
	FemaleAbdPel4	22.35	20.75	7.16	
	FemaleAbdPel5	26.00	22.48	13.52	
	MaleAbdPel1	28.36	28.12	0.86	
	MaleAbdPel2	33.76	35.16	4.16	
	MaleAbdPel3	21.59	19.75	8.50	
	MaleAbdPel4	32.77	32.13	1.95	
	MaleAbdPel5	27.08	23.25	14.13	
	Average % error				6.81
	Standard deviation				4.61
Chest	FemaleChest1	32.44	28.86	11.02	
	FemaleChest2	32.27	27.20	15.71	
	FemaleChest3	44.07	39.56	10.24	
	FemaleChest4	40.40	36.92	8.60	
	FemaleChest5	33.40	30.79	7.81	
	MaleChest1	36.06	34.24	5.05	
	MaleChest2	33.10	30.72	7.20	
	MaleChest3	34.14	31.85	6.69	
	MaleChest4	30.22	27.75	8.18	
	MaleChest5	34.22	31.00	9.40	
	Average % error				8.99
	Standard deviation				2.93
Average % error				7.90	
Standard deviation				3.92	

5.4 Discussion

In this investigation, a direct comparison of $D_{w,image}$ and $D_{w,topo}$ was presented. A comparison of SSDE calculated using the various estimates of WED was also presented. WED is almost exclusively determined for the purposes of calculating SSDE, so a comparison of SSDE offers insight into how well $D_{w,image}$ and $D_{w,topo}$ agree in terms of real-world use.

As shown in Table 5.1, $D_{w,topo}$ consistently overestimates $D_{w,image}$. Because $D_{w,topo}$ is based on the topogram that includes the CT table in the attenuation measurements, this overestimation is due to the fact that the table thickness is most likely included in the AP dimension of patient size extracted from the DICOM header of the topogram. This relationship between WED determined from the topogram and CT images is consistent with the relationship between WED determined from the CT localizer radiograph and CT images presented in AAPM Report 220 [20]. As shown in Table 5.2, because $D_{w,topo}$ consistently overestimates $D_{w,image}$, $SSDE(D_{w,topo})$ consistently underestimates $SSDE(D_{w,image})$. Regardless, strong agreement was observed between both $D_{w,image}$ and $D_{w,topo}$ and $SSDE(D_{w,image})$ and $SSDE(D_{w,topo})$. The strong agreement is a direct indication that $D_{w,topo}$ is comparable to $D_{w,image}$. This in turn validates the hypothesis that the AP and LAT attenuation data extracted from the DICOM header of the Siemens topogram are water equivalent estimates of the AP and LAT dimensions of the patient. This detailed understanding of the attenuation data collected by Siemens will aid in the development of methods to reconstruct the means by which the Siemens TCM algorithm modulates tube current in response to changes in patient attenuation.

Additionally, $D_{w,image}$ is the widely accepted standard in CT imaging when it comes to determining an attenuation-based estimate of patient size. The problem with $D_{w,image}$ is that it can only be determined retrospectively from the axial images of the patient who underwent the CT scan. By demonstrating that $D_{w,topo}$ is comparable to $D_{w,image}$, it is shown that an estimate of WED can be accurately determined before that patient is even scanned. This allows for the possibility of prospective SSDE calculations directly on the scanner. Presently, the dose impact of a scan is judged prospectively on the scanner using the scanner-reported $CTDI_{vol}$, an estimate

of scanner output, not patient dose. SSDE on the scanner would serve as a useful means to prospectively understand the true impact of a scan on patient dose. The impact of changes in scan parameters on patient dose could then be reflected in real-time.

5.5 References

1. M. F. McNitt-Gray, "Tube Current Modulation Approaches: Overview, Practical Issues and Potential Pitfalls," AAPM 2011 Summit on CT Dose (2011).
2. M. K. Kalra, *et al.*, "Techniques and applications of automatic tube current modulation for CT," *Radiology* 233, 649-657 (2004).
3. J. Menke, "Comparison of Different Body Size Parameters for Individual Dose Adaptation in Body CT of Adults," *Radiology* 236, 565–571 (2005).
4. J. Wang, *et al.*, "Attenuation-based Estimation of Patient Size for the Purpose of Size Specific Dose Estimation in CT. Part I. Development and Validation of Methods Using the CT Image," *Med. Phys.* 39, 6764 (2012).
5. J. Wang, *et al.*, "Attenuation-based Determination of Patient Size for the Purpose of Size Specific Dose Estimation in CT. Part II. Implementation on Abdomen and Thorax Phantoms Using Cross Sectional CT Images and Scanned Projection Radiograph Images," *Med. Phys.* 39, 6772 (2012).
6. American Association of Physicists in Medicine, "Size-Specific Dose Estimates (SSDE) in Pediatric and Adult Body CT Examinations," AAPM Report 204 (2011).

7. W. D. Bidgood, S. C. Horii, F. W. Prior, D. E. Van Syckle, "Understanding and Using DICOM, the Data Interchange Standard for Biomedical Imaging," J. Am. Med. Inform. Assoc. **4**, 199-212 (1997).
8. American Association of Physicists in Medicine, "Use of Water Equivalent Diameter for Calculating Patient Size and Size-Specific Dose Estimates (SSDE) in CT," AAPM Report 220 (2014).
9. M. Bostani, *et al.*, "Attenuation-based size metric for estimating organ dose to patients undergoing tube current modulated CT exams," Med. Phys. **42**, 958 (2015).
10. B. Li, R. H. Behrman, A. M. Norbash, "Comparison of Topogram-based Body Size Indices for CT Dose Consideration and Scan Protocol Optimization," Med. Phys. **39**, 3456-3465 (2012).
11. M. S. Brown, *et al.*, "An architecture for computer-aided detection and radiologic measurement of lung nodules in clinical trials," Cancer Inf. **4**, 25-31 (2007).

Chapter 6: Estimating Tube Current Modulation Schemes Using Patient Size Data from Topogram

6.1 Introduction

In current clinical practice, nearly all CT exams are performed with tube current modulation (TCM), a scanning technique that adjusts scanner output according to changes in patient attenuation. Studies have shown TCM to reduce scanner output as much as 91% when compared with fixed tube current (FTC) [24,25]. The potentially large discrepancies between dose from TCM and FTC scans highlights the need to incorporate TCM into dose estimates to ensure an accurate representation of actual patient dose (and actual dose savings from TCM).

TCM simulations can be performed with the Monte Carlo CT source model described in Chapter 3 using TCM schemes extracted from the raw projection data of patients who underwent actual CT examinations. These TCM profiles are the actual TCM profiles generated for a given patient's anatomy, and therefore, organ dose estimated using these TCM schemes can be considered accurate estimates of the true organ dose for a TCM CT examination ("gold standard"). When the raw projection data is not available, Khatonabadi *et al.* described a method to use the tube current profile extracted from a patient's axial images as a surrogate for the TCM scheme extracted from the raw projection data [3]. For either scenario, organ dose estimates are limited to fully-irradiated organs that can be easily segmented from the CT image data. Doses to partially- and indirectly-irradiated organs cannot be estimated because they are not fully contained within the image volume. Without this dose information, dose metrics that require the knowledge of dose to all radiosensitive organs, such as effective dose, cannot be directly

estimated (they would require assumptions about organ placement, size and distance from the irradiated volume as well as assumptions about the tube current behavior).

The goal of this dissertation is to determine the radiation dose to any fully-, partially- or indirectly-irradiated organ for any CT exam performed with TCM. In order to do this, TCM CT exams need to be simulated for reference voxelized phantoms of various sizes that have all radiosensitive organs identified, such as the GSF and ICRP reference voxelized phantoms described in Chapter 4 [5,6]. This will allow for the identification of relationships between patient size and organ doses, similar to those observed for FTC as described in AAPM Report 204 [36]. In turn, this will also allow for the estimation of other dose/risk descriptors such as effective dose as a function of size.

However, there are no validated TCM schemes for these reference voxelized phantoms. Early efforts to model TCM concentrated on the development of idealized, attenuation-based TCM profiles [37,38]. These models were later incorporated into Monte Carlo simulations to estimate organ dose from TCM CT examinations [39-42]. Even though TCM algorithms for each major CT manufacturer are based on the idea that tube current will be adjusted in response to changes in patient attenuation, they tend to differ in implementation, so the major limitation of models of idealized TCM profiles is that they do not represent any manufacturer-specific TCM schemes [43]. Specific issues such as machine limits imposed by the scanner and scanner-specific modulation schemes (e.g. on-line modulation) are not explicitly modeled. Therefore, organ doses estimated using these TCM schemes are themselves idealized and not necessarily the organ doses the reference voxelized phantom would have received had they been scanned on an actual CT scanner. Given the limitations of current Monte Carlo-based methods to estimate organ dose from TCM CT examinations, the advancement of Monte Carlo simulations that

incorporate TCM has been recognized as a high priority. The bottleneck that remains for accurate estimates of organ dose from TCM CT exams is the ability to estimate scanner-specific TCM schemes.

The purpose of this investigation was to develop and validate methods to estimate scanner-specific TCM schemes for any voxelized patient model. Efforts concentrated on developing these methods for Siemens CT scanners. The Siemens TCM algorithm, CARE Dose4D, serves as a means to reduce patient dose while maintaining constant image quality across different body regions (i.e. different attenuation). CARE Dose4D automatically adjusts tube current to the size and shape of the patient through both longitudinal (i.e. along the length of the patient) and angular (i.e. different angles during rotation) modulation. It was determined in Chapter 5 that the patient attenuation data used to drive the Siemens TCM algorithm can be readily extracted from the topogram. Using this attenuation information, TCM schemes were generated that take into account longitudinal and angular modulation, tube current limits imposed by the scanner and Siemens-specific effects, such as reference attenuation values and on-line modulation. Unlike idealized, attenuation-based TCM profiles, these TCM schemes were generated using the actual attenuation information determined by Siemens instead of some estimate of patient attenuation [37,38]. To validate this TCM estimation method, the TCM schemes were estimated for a variety of pediatric and adult patients who underwent clinically indicated chest and abdomen/pelvis TCM CT examinations. The actual TCM schemes were extracted from the raw projection data of each patient. The average tube currents were compared between the actual and estimated TCM schemes. Additionally, Monte Carlo simulations were performed using each TCM scheme to estimate dose to the lungs and breasts (females only) for chest scans and dose to the liver, kidneys and spleen for abdomen/pelvis scans. Organ doses

from simulations using the estimated TCM schemes were compared to those using the actual TCM schemes.

6.2 Methods

6.2.1 Size Data from Topogram

For this investigation, estimates of Siemens TCM schemes were developed using patient size data extracted from the topogram. This patient size data was described at length in Chapter 5. Figure 6.1 shows an example of the anterior-posterior (AP) and lateral (LAT) water-equivalent estimates of patient size extracted from the topogram of an adult patient who underwent a clinically indicated chest CT exam. This adult chest patient will be used as an example throughout the development of the methods to estimate scanner-specific TCM schemes.

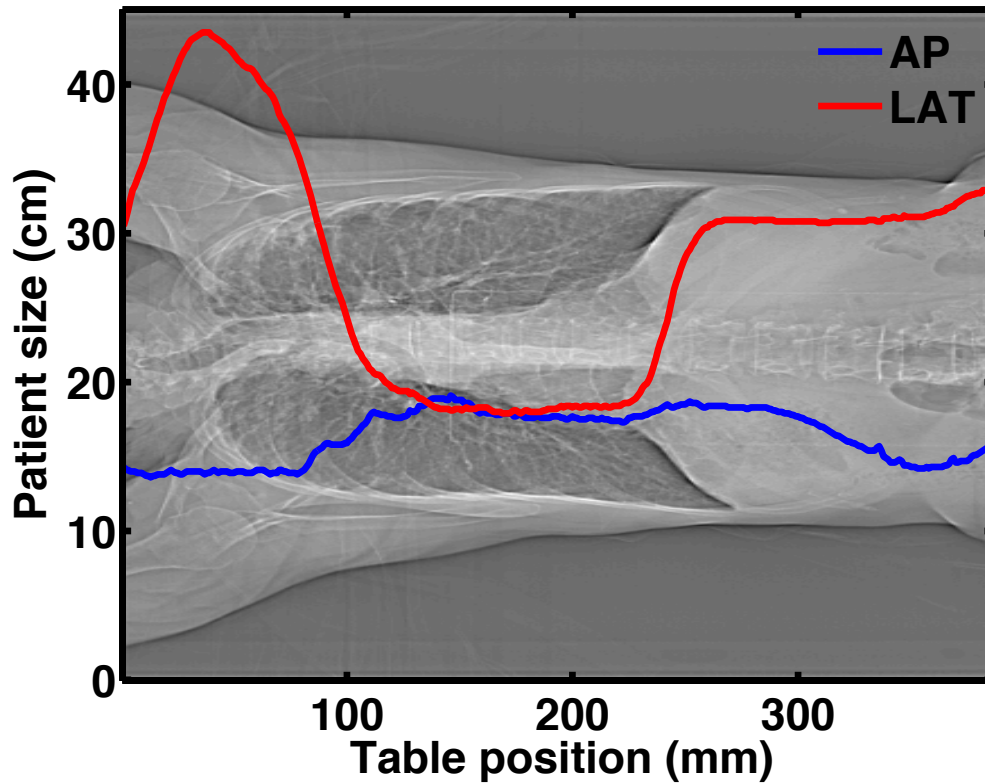


Figure 6.1. AP and LAT water-equivalent estimates of patient size extracted from the topogram of an adult patient who underwent a clinically indicated chest CT examination. This patient will be used as an example throughout the development of the methods to estimate scanner-specific TCM schemes presented in this investigation.

6.2.2 Longitudinal Modulation

In the Care Dose4D algorithm, tube current is first varied on the basis of the topogram by comparing actual patient attenuation to reference patient attenuation (i.e. longitudinal modulation) [14]. Both AP and LAT water-equivalent estimates of patient size can be extracted from the topogram of a patient scanned on a Siemens CT scanner, but longitudinal modulation works on the basis of a single estimate of patient attenuation at each table position. Siemens does

not explicitly describe how to derive a single patient attenuation estimate at each table position from two attenuation profiles. Instead, in the patent literature, Siemens describes the idea of “deep modulation” when referring to angular modulation (described in Section 6.2.3) [15]. “Deep modulation” was hypothesized to mean that modulation of tube current is always down from some maximum tube current value that would be used if angular modulation were not applied. Because a TCM scheme void of angular modulation would just be the longitudinal modulation, the longitudinal modulation was therefore considered to be based on the maximum tube current at each table position. The maximum tube current at a table position corresponds to the maximum attenuation at that table position. As such, once the patient size data was extracted from the topogram, the maximum attenuation at each table position was calculated. The maximum attenuation at each table position, i , calculated from the size data in the topogram is defined as:

$$A_{\max}(i) = \max\left(\exp\left(\mu_{\text{water},kVp} \times AP(i)\right), \exp\left(\mu_{\text{water},kVp} \times LAT(i)\right)\right) \quad (6.1)$$

where $\mu_{\text{water},kVp}$ is the linear coefficient of water for a given beam energy, $AP(i)$ is the water-equivalent estimate of AP patient dimension extracted from the topogram and $LAT(i)$ is the water-equivalent estimate of LAT patient dimension extracted from the topogram. Each topogram in this investigation was acquired at 120 kVp, so $\mu_{\text{water},kVp} = \mu_{\text{water},120\text{ kVp}} = 0.2\text{ cm}^{-1}$. Figure 6.2 shows the maximum attenuation (right) calculated from the AP and LAT size data (left) of the adult chest patient.

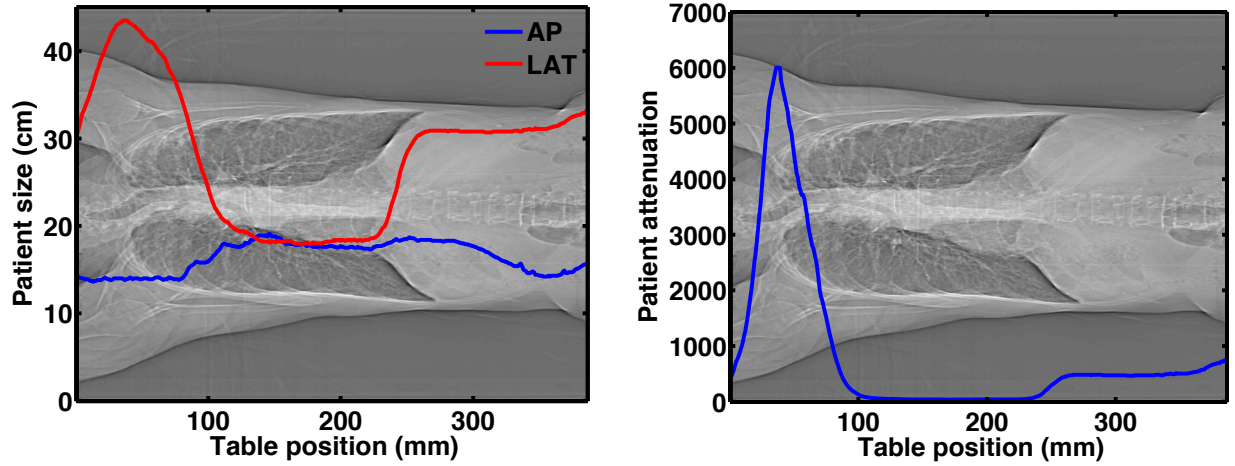


Figure 6.2. (Left) Patient size data extracted from topogram. (Right) Maximum patient attenuation at each table position calculated from patient size data using Eq. (6.1).

After the maximum attenuation at each table position was calculated, tube current values corresponding to those attenuation values were determined. Tube current (mA) at each table position, i , calculated from the corresponding patient attenuation is defined as:

$$mA(i) = \frac{QRM \times pitch}{t} \times \left(\frac{A(i)}{A_{ref}} \right)^b \quad (6.2)$$

where QRM is the quality reference tube current-time product (mAs) set directly on the scanner by the user, t is the gantry rotation time, A is the patient attenuation determined using Eq. (6.1), A_{ref} is the protocol-specific reference attenuation hard coded into the Care Dose4D algorithm and b is a strength parameter that can be set according to individual preferences for the tube current increase and decrease. The QRM represents the effective mAs (mAs/pitch) value suitable

for a standard-sized patient, and A_{ref} represents the standard-sized patient attenuation for which the QRM is specified. Protocols of interest in this investigation are: (1) Adult Chest, (2) Adult Abdomen/Pelvis, (3) Pediatric Chest and (4) Pediatric Abdomen/Pelvis. Table 6.1 lists A_{ref} for each of these protocols. These values were determined empirically (by us) and confirmed through internal communications with colleagues at the Mayo Clinic in Rochester, MN. Figure 6.3 shows an illustration of the effects of different strength parameters, b , on tube current relative to the QRM set at A_{ref} . For each strength curve, there are individual values of b for attenuation greater than and less than A_{ref} . The default strength setting on all Siemens CT scanners (including all scanners used in this investigation) is “Average.” For the “Average” strength, b is 0.33 for attenuation greater than A_{ref} and 0.5 for attenuation less than A_{ref} [16]. For pediatric chest and abdomen/pelvis scans acquired at 80 kVp, the strength parameter necessary to achieve strong agreement between estimated and actual TCM schemes was empirically determined (by us) to be 0.4 for attenuation greater than A_{ref} and 0.65 for attenuation less than A_{ref} .

Table 6.1. Protocol-specific reference attenuation for protocols of interest in this investigation. Corresponding water-equivalent length given in parentheses.

Protocol	Reference attenuation (A_{ref})
Adult Chest	600 (~32 cm)
Adult Abdomen/Pelvis	1000 (~35 cm)
Pediatric Chest	30 (~17 cm)
Pediatric Abdomen/Pelvis	40 (~18 cm)

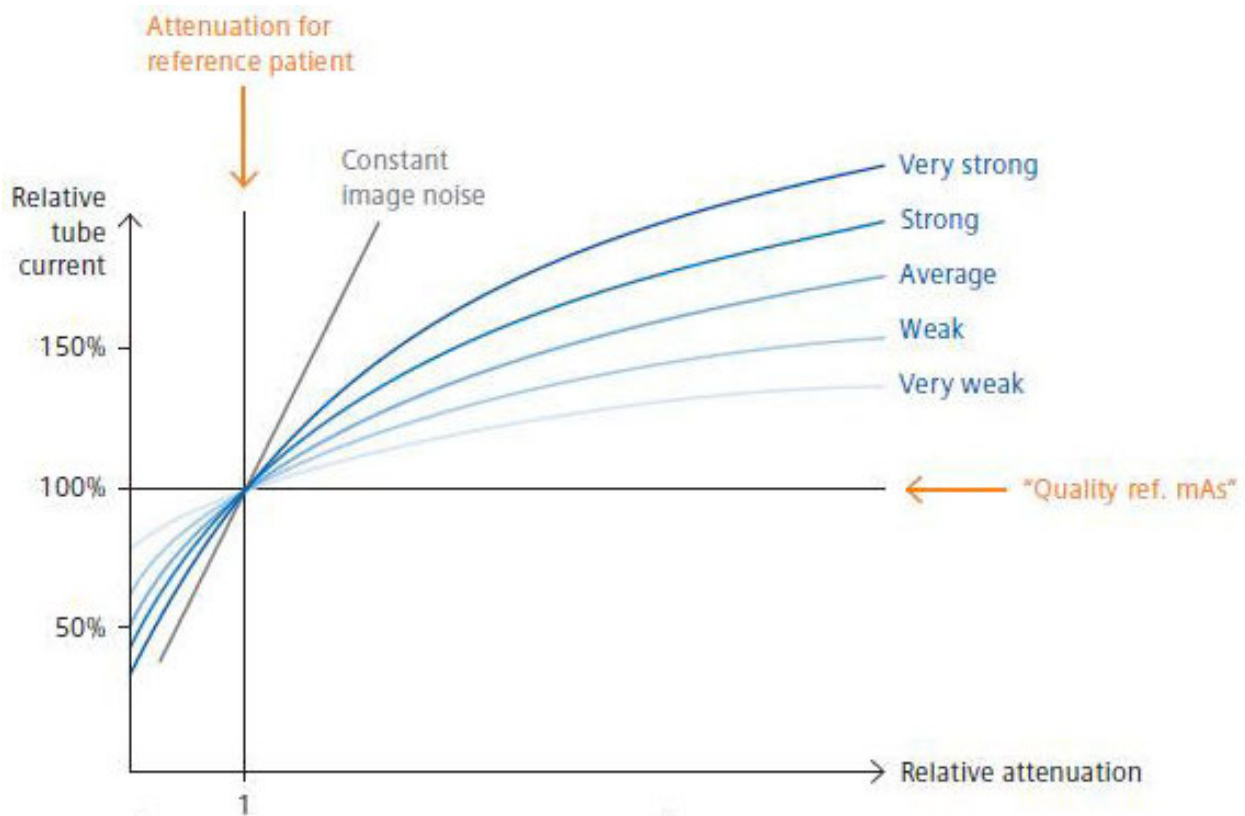


Figure 6.3. Different strength settings used by Siemens to adjust tube current relative to QRM defined at a reference patient attenuation. Image courtesy of Ronald Booiij, Department of Radiology, Erasmus MC, Rotterdam, The Netherlands.

Applying Eq. (6.2) to the patient attenuation determined at each table position along the topogram yielded an estimate of the maximum tube current at each table position along the patient. This relationship between tube current and table position is called the “control curve” and represents modulation of the tube current along the length of the patient. Figure 6.4 shows the control curve (right) calculated from the attenuation profile (left) of the adult chest patient. Because the topogram image is used to localize the anatomy that is to be scanned, the boundaries of the topogram image are often beyond those of the CT image data. As such, the control curve in Fig. 6.4 shows tube current as a function of table positions for which there are corresponding axial CT images.

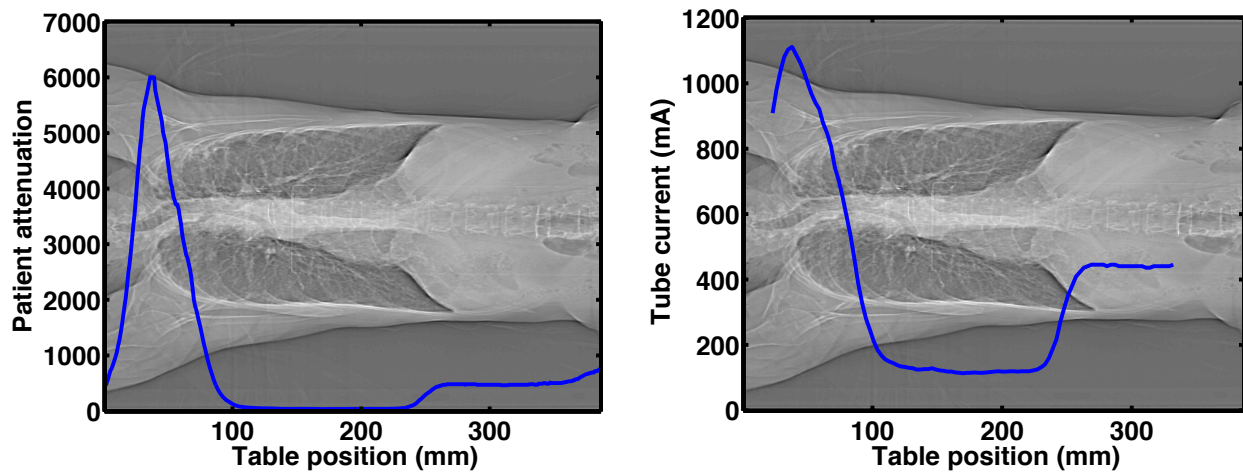


Figure 6.4. (Left) Patient attenuation calculated from size data extracted from topogram. (Right) Tube current profile calculated from patient attenuation data using Eq. (6.2) at all table positions with corresponding axial CT images.

6.2.3 Angular Modulation

In addition to modulating the tube current along the length of the patient according to the attenuation data from the topogram (i.e. longitudinal modulation), the Care Dose4D algorithm also modulates the tube current angularly according to on-line (i.e. real-time) angular attenuation measurements (i.e. angular modulation) [14]. According to Siemens, during the scan acquisition, patient attenuation is constantly measured as the tube rotates about the patient [14]. In order to set real-time tube current values in response to angular attenuation, an extrapolation method is implemented for computing an extrapolated attenuation profile for the next half rotation based on the measure angular attenuation profile for the previous half rotation [15]. The extrapolation method assumes that the angular attenuation profile of the next half rotation very closely matches the angular attenuation profile measured in the previous half rotation. For any given Siemens CT

scanner, the maximum distance between adjacent half rotations is on the order of a few centimeters.

In this investigation, the only patient attenuation data available is the attenuation data derived from the topogram. In order to model on-line angular modulation (extrapolation method), patient attenuation at each gantry angle is necessary. Taking advantage of the fact that AP attenuation is measured at tube angles of 0° and 180° and LAT attenuation is measured at tube angles of 90° and 270° , patient attenuation at any tube angle was estimated using the AP and LAT patient attenuation profiles extracted from the topogram. For a given starting table position and starting tube angle of a CT scan, the tube angle at any table position, TP , is defined as:

$$\theta(TP) = \frac{360^\circ}{NC \times Pitch} \times (TP - TP_0) + \theta_0 \quad (6.3)$$

where NC is the nominal collimation of the beam, TP_0 is the starting table position and θ_0 is the starting tube angle. The table positions at which the tube angle is in the AP (0° and 180°) and LAT (90° and 270°) locations were determined. Patient attenuation from the AP and LAT attenuation profiles at those respective table positions was then used to interpolate patient attenuation at any table position across the scan length (i.e. any tube angle). Interpolation was performed using a piecewise cubic Hermite interpolating polynomial [17]. Figure 6.5 shows the angular attenuation profile as a function of table position (right) that is calculated from the AP and LAT size data (left) of the adult chest patient.

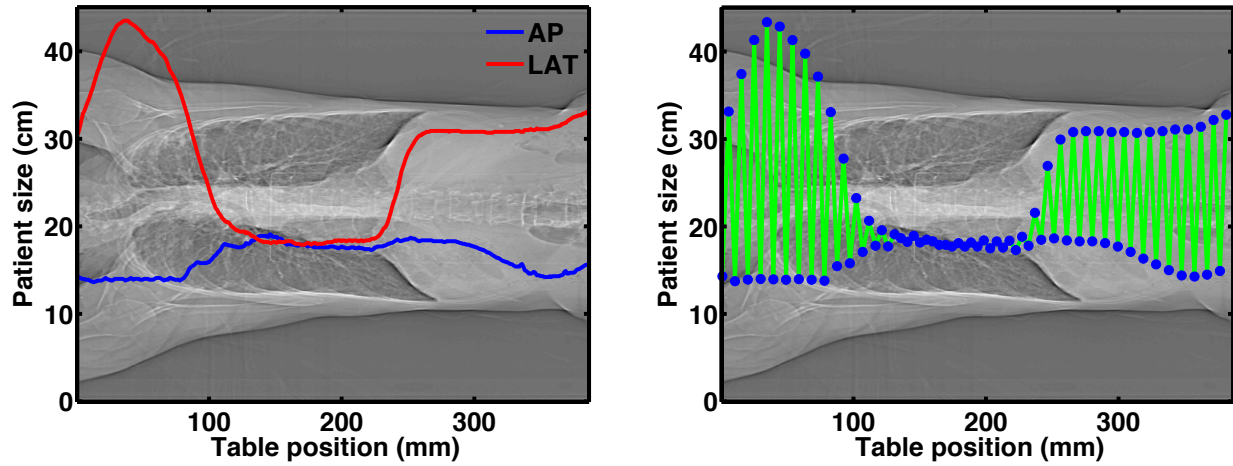


Figure 6.5. (Left) Patient size data extracted from topogram. (Right) Angular attenuation profile determined from patient size data. The blue dots are the AP and LAT locations, and the green lines are the interpolated patient size.

Once the angular attenuation was determined, the extrapolation method was implemented using equations referenced from a Siemens patent [15]. Hypothetically, the tube current at a given table position should be able to be modulated all the way down to the minimum tube current allowed by the scanner. In actuality, there are limits to the amount of modulation allowed at a given table position. The allowable modulation range at a given table position is described by a parameter called the modulation index. For each table position along the scan length, a modulation index was calculated using attenuation data from the previous half rotation of the scan. The modulation index at a table position, i , and is defined as:

$$\mu(i) = 1 - \left(\frac{A_{\min}}{A_{\max}} \right)^q \quad (6.4)$$

where A_{\min} is minimum patient attenuation over the previous half rotation, A_{\max} is the maximum patient attenuation over the previous half rotation and q is an optimization parameter between 0.5 and 1.0. When $q = 0.5$, image noise is minimized with a given dose. When $q = 1$, maximum dose savings is achieved. For this investigation q was assumed to be 0.5. The modulation index is limited as a function of the gantry rotation time. Table 6.2 outlines the modulation index limits for a set of gantry rotation times. For a given gantry rotation time, if $\mu(i) > \mu_{\max}$, then

$$\mu(i) = \mu_{\max} .$$

Table 6.2. Modulation index limits as a function of gantry rotation time.

Gantry rotation time	Maximum modulation index (μ_{\max})
2.0	0.9
1.5	0.8
1.0	0.7
0.75	0.6
0.5	0.5

Using the extrapolated attenuation data and the calculated modulation index, angular modulation at a table position, i , is defined as:

$$m(i) = 1 - \mu(i) \times \frac{A_{\max}^q - A(i - hROT)^q}{A_{\max}^q - A_{\min}^q} \quad (6.5)$$

where $hROT$ is the half rotation of the tube equal to $(NC/2) \times pitch$ and $A(i - hROT)$ is the patient attenuation at the table position a half rotation prior to the current table position. If there

is no attenuation data available in the previous half rotation, the angular modulation is set to 1 (i.e. no modulation). By Eq. (6.5), if the patient attenuation at the table position is equal to the maximum attenuation over the previous half rotation, the angular modulation at that table position is minimized (i.e. angular modulation of 1). If the patient attenuation at the table position is equal to the minimum attenuation over the previous half rotation, the angular modulation at that table position is maximized (i.e. angular modulation equal to $1 - \mu(i)$). Otherwise, the angular modulation is between 1 and $1 - \mu(i)$. Figure 6.6 shows the angular modulation scheme (right) determined from the angular attenuation profile (left) of the adult chest patient.

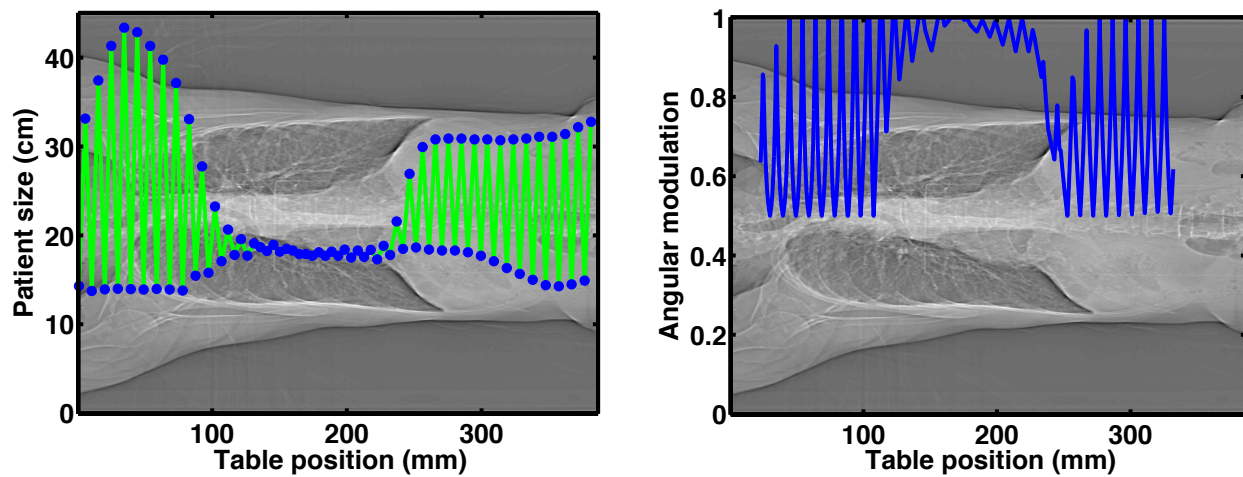


Figure 6.6. (Left) Angular attenuation profile determined from patient size data extracted from topogram. (Right) Angular modulation scheme calculated from angular attenuation data using Eq. (6.5) at all table positions with corresponding axial CT images.

6.2.4 Estimated Tube Current Modulation Scheme

Putting it all together, the control curve from Section 6.2.2 and the angular modulation scheme from Section 6.2.3 were combined to generate an estimated TCM scheme. For the estimated TCM scheme, the tube current at each table position, i , is defined as:

$$mA(i)_{TCM} = mA(i)_{control} \times m(i) \quad (6.6)$$

where $mA(i)_{control}$ is the maximum tube current at the table position calculated using Eq. (6.2) and $m(i)$ is the angular modulation at the table position calculated using Eq. (6.5). Figure 6.7 shows the estimated TCM scheme calculated from the control curve and angular modulation of the adult chest patient.

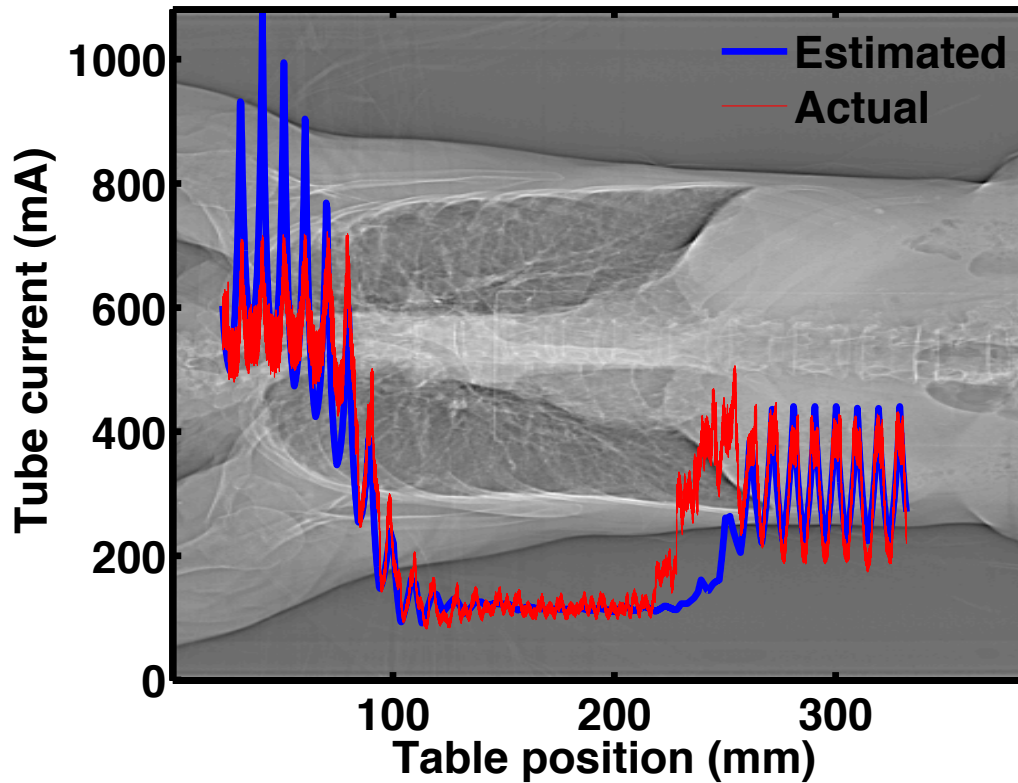


Figure 6.7. Estimated and actual TCM schemes for adult chest patient. Estimated TCM scheme calculated from control curve and angular modulation scheme from Fig. 6.4 and Fig. 6.6, respectively. Actual TCM scheme extracted from raw projection data.

6.2.5 Estimated Tube Current Modulation Scheme Modifications

Figure 6.8 shows the actual TCM scheme extracted from the raw projection data of the adult chest patient overlaid on the estimated TCM scheme for the adult chest patient. There are two clear areas of disagreement: (1) estimated tube current is too high in the shoulders (high attenuation region) and (2) tube current does not increase fast enough moving into the abdomen from the thorax.

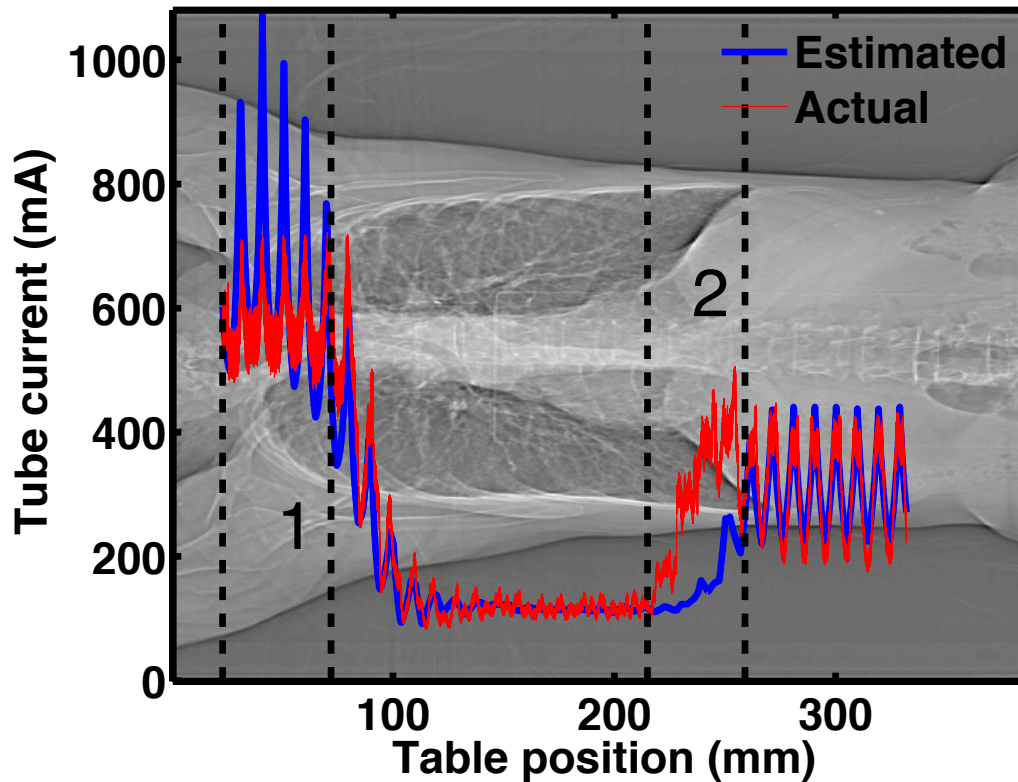


Figure 6.8. Estimated and actual TCM schemes from Fig. 6.7 with areas of disagreement labeled: (1) estimated tube current is too high in the shoulders (high attenuation region) and (2) estimated tube current does not increase fast enough moving into the abdomen from the thorax.

Correcting the first issue involves properly taking machine limits into account. Table 6.3 outlines the tube current limits for common beam energies for the Siemens Sensation 64 CT scanner, the scanner used for the CT examination of the adult chest patient [18]. At 120 kVp, the beam energy at which the images of the adult chest patient were acquired, the maximum tube current is 665 mA. There are three steps for taking machine limits into account at each table position. First, using the estimated TCM scheme calculated with Eq. (6.6), the average tube current over the previous half rotation was calculated. If that value was greater than the machine

limit, the control curve at the table position was set to the machine limit. Then, if the control curve at the table position was adjusted to the machine limit because the average tube current over the previous half rotation was greater than the machine limit, a dampened angular modulation was used. If the angular modulation at the table position was greater than the dampened angular modulation, the angular modulation was set to the dampened angular modulation. This step was motivated by observations that in regions of high attenuation, such as the shoulders in chest scans, an artificially low and uniform modulation is applied. Finally, if the average tube current over the previous half rotation was less than the machine limit but the estimated tube current at the table position was greater than the machine limit, the tube current was set to the machine limit. For example, for a 120 kVp beam on a Sensation 64, machine limits are applied to the tube current at a table position, i , as follows:

$$(1) \text{ if } \text{mean}\left(mA(i-hROT:i)_{TCM}\right) > 665, \text{ then } mA(i)_{control} = 665$$

$$(2) \text{ if } \text{mean}\left(mA(i-hROT:i)_{TCM}\right) > 665 \text{ and } m(i) < 0.8, \text{ then } m(i) = 0.8$$

$$(3) \text{ if } \text{mean}\left(mA(i-hROT:i)_{TCM}\right) < 665 \text{ and } mA(i)_{TCM} > 665, \text{ then } mA(i)_{TCM} = 665$$

where $\text{mean}\left(mA(i-hROT:i)_{TCM}\right)$ is the average tube current over the half rotation prior to the current table position. The dampened angular modulation of 0.8 appears to be applicable to all beam energies.

Table 6.3. Tube current limits for various tube voltages for the Sensation 64 CT scanner.

Tube voltage (kVp)	Tube current limit
80	500
100	500
120	665
140	500

Correcting the second issue involves applying a Siemens-specific adjustment to the TCM scheme in response to rising attenuation. Based on behaviors observed in TCM schemes from clinically indicated chest scans, it appears Siemens implemented a method to quickly ramp up the tube current as the tube moves from the thorax into the abdomen. Because the scanner has no direct knowledge of the exact anatomy being scanned at any given point, it was hypothesized that this method was developed in response to rising attenuation. A method to replicate this enhanced tube current behavior was constructed using the attenuation data extracted from the topogram. First, the attenuation at a table position was compared with the attenuation at the previous table position. If the attenuation was increasing, the enhanced behavior was applied. The enhanced behavior is applied to the control curve at a table position, i , as follows:

$$\text{if } A(i) > A(i - 1 \text{ mm}), \text{ then } mA(i)_{control} = mA(i + ROT)_{control}$$

where $A(i - 1 \text{ mm})$ is the patient attenuation at the table position immediately preceding the current table position, ROT is the full rotation of the tube equal to $NC \times pitch$ and

$mA(i + ROT)_{control}$ is the control curve tube current a full rotation in advance of the current table position. Because the control curve, according to Siemens, is estimated using attenuation data

from the topogram, tube current information a full rotation in advance of the current table position is available at the time of scanning [19]. This enhanced behavior appears to be applied to all scanning protocols in response to rising attenuation.

All corrections to the estimated TCM scheme can be applied while the estimated TCM scheme is being constructed. They are separated into individual steps for illustrative purposes only. Figure 6.9 shows the actual and estimated TCM schemes for the adult chest patient with all corrections applied to the estimated TCM scheme.

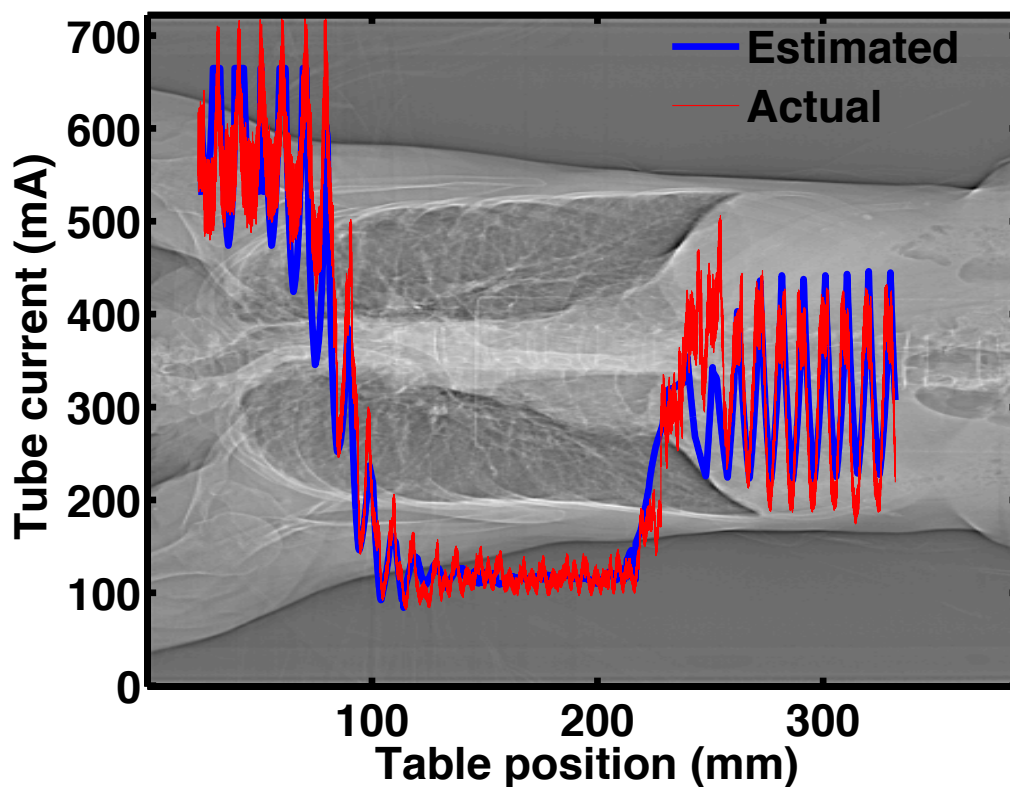


Figure 6.9. Estimated and actual TCM schemes of adult chest patient with modifications to account for tube limits and increasing attenuation applied to the estimate TCM scheme.

6.2.6 Validation – Comparing Estimated and Actual TCM Schemes in a Patient Cohort

The methods to estimate Siemens TCM schemes described above were applied to a set of pediatric and adult patients who underwent clinically indicated chest (n=20) and abdomen/pelvis (n=20) CT examinations [20]. For each patient, the topogram and axial images were acquired, and the actual TCM scheme was extracted from the raw projection data. Table 6.4 outlines the characteristics of the patients used in the validation. All patients were scanned on a Sensation 64 CT scanner, and a variety of scan techniques were used. Water equivalent diameters calculated from the central slice of the axial images using Eq. (5.1) from Chapter 5 ranged from 12.59 cm to 34.76 cm for patients who underwent chest scans and 14.11 cm to 38.4 cm for patients who underwent abdomen/pelvis scans. Figure 6.10 shows axial images of the smallest (left) and largest (right) chest patients used in this investigation. Figure 6.11 shows axial images of the smallest (left) and largest (right) abdomen/pelvis patients used in this investigation.

For each chest scan, the lungs and breasts (if female) were segmented from the axial images. For the abdomen/pelvis scans, the liver, spleen and kidneys were segmented from the images [20]. Models of patient anatomy were created from the image data, and organ dose was estimated with detailed Monte Carlo simulations using both the estimated and actual TCM schemes. The estimated TCM schemes were compared to the actual TCM scheme for each patient by comparing both the average tube current and organ dose values from each approach.

Table 6.4. Patient size and scan techniques for validation patients.

		Patient	WED (cm)	Collimation (mm)	kVp	Pitch	Rotation time (s)	QRM
Chest	Pediatric	1	21.70	28.8	120	1	0.5	55
		2	18.69	28.8	100	1	0.5	55
		3	18.29	19.2	100	1	0.5	55
		4	15.40	28.8	100	1	0.5	55
		5	12.59	28.8	80	1	0.5	55
		6	22.99	19.2	100	1	0.5	55
		7	19.36	28.8	100	1	0.5	55
		8	26.49	19.2	100	1	0.5	55
		9	19.98	28.8	100	1	0.5	55
		10	22.84	19.2	100	1	0.5	55
	Adult	1	24.74	19.2	120	1	0.5	250
		2	18.35	19.2	120	1	0.5	250
		3	20.89	19.2	120	1	0.5	250
		4	22.36	19.2	120	1	0.5	250
		5	19.34	19.2	120	1	0.5	250
		6	25.25	19.2	120	1	0.5	250
		7	13.97	19.2	120	1	0.5	250
		8	16.96	19.2	120	1	0.5	250
		9	20.48	19.2	120	1	0.5	250
		10	34.76	19.2	120	1	0.5	250
Abdomen/Pelvis	Pediatric	1	23.73	28.8	100	1	0.5	65
		2	20.1	28.8	80	1	0.5	55
		3	24.06	28.8	120	1	0.5	65
		4	20.69	28.8	100	1	0.5	65
		5	21.59	28.8	120	1	0.5	65
		6	19.66	28.8	100	1	0.5	65
		7	24.32	28.8	100	1	0.5	65
		8	22.83	28.8	100	1	0.5	35
		9	21.34	28.8	100	1	0.5	65
		10	14.11	28.8	80	1	0.5	55
	Adult	1	27.78	19.2	120	0.95	0.5	275
		2	19.97	19.2	120	1	0.5	275
		3	33.69	19.2	120	0.45	0.5	275
		4	24.57	19.2	120	1	0.5	275
		5	38.40	19.2	120	0.8	1.0	275
		6	23.87	19.2	120	1	0.5	275
		7	26.08	19.2	120	0.95	0.5	275
		8	30.77	19.2	120	1	0.5	275
		9	28.02	19.2	120	1	0.5	275
		10	37.34	19.2	120	0.75	0.5	275

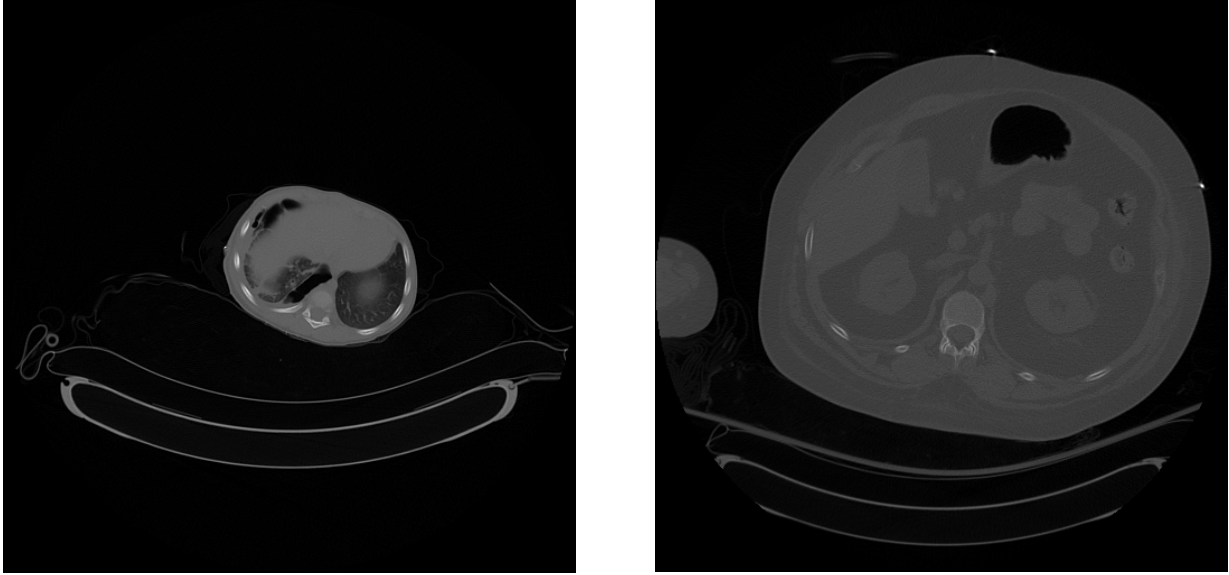


Figure 6.10. Central slice of axial images of smallest (left) and largest (right) chest patients used in the validation study. Both images were reconstructed in a 500 mm field of view.

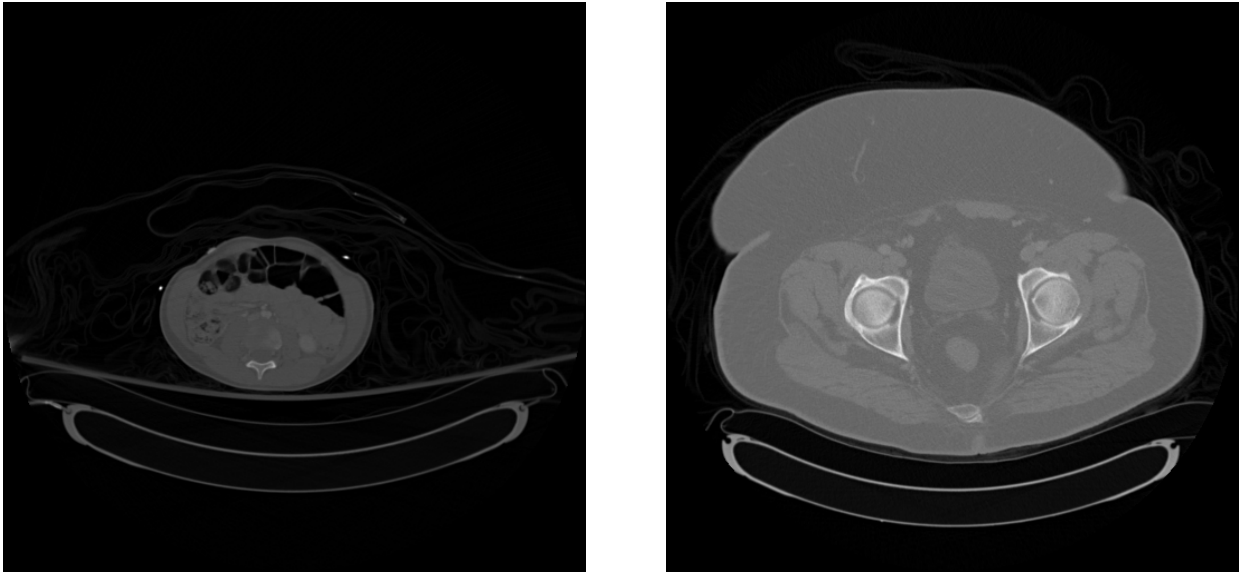


Figure 6.11. Central slice of axial images of smallest (left) and largest (right) abdomen/pelvis patients used in the validation study. Both images were reconstructed in a 500 mm field of view.

6.3 Results

A comparison of the average tube current from estimated and actual TCM schemes for all patients is tabulated in Table 6.5. Across all patients, the average error between the average tube current from estimated and actual TCM schemes is 3.82%. Table 6.6 shows a comparison of lung and breast dose estimates from Monte Carlo simulations of chest CT exams using estimated and actual TCM schemes. The average error for lung and breast dose is 4.59% and 3.36%, respectively. Figure 6.12 shows estimated and actual TCM schemes for a pediatric (left) and adult (right) patient who underwent clinically indicated chest scans. Table 6.7 shows a comparison of liver, kidney and spleen dose estimates from Monte Carlo simulations of abdomen/pelvis CT exams using estimated and actual TCM schemes. The average error for liver, kidney and spleen dose is 4.18%, 4.28% and 4.90%, respectively. Figure 6.13 shows estimated and actual TCM schemes for a pediatric (left) and adult (right) patient who underwent clinically indicated abdomen/pelvis scans.

Table 6.5. Comparison of average tube current between actual and estimated TCM schemes.

		Patient	Average mA (Actual)	Average mA (Estimated)	% error
Chest	Pediatric	1	329.2	319.0	3.10
		2	224.4	222.0	1.07
		3	257.1	230.2	10.46
		4	153.3	135.3	11.74
		5	141.6	140.0	1.13
		6	321.9	308.3	4.22
		7	296.6	273.1	7.92
		8	370.8	351.9	5.10
		9	311.3	308.0	1.06
		10	289.2	275.8	4.63
	Adult	1	418.3	401.3	4.06
		2	365.4	361.8	0.99
		3	433.3	417.8	3.58
		4	471.5	467.4	0.87
		5	381.9	383.7	0.47
		6	513.7	485.7	5.45
		7	285.5	273.7	4.13
		8	330.8	328.0	0.85
		9	381.9	377.2	1.23
		10	567.2	547.1	3.54
Abdomen/Pelvis	Pediatric	1	327.0	353.0	7.95
		2	275.9	268.7	2.61
		3	290.9	277.6	4.57
		4	253.0	274.4	8.46
		5	285.2	278.8	2.24
		6	251.2	270.6	7.72
		7	259.3	261.3	0.77
		8	282.5	309.9	6.94
		9	129.6	138.6	0.40
		10	227.0	227.9	1.67
	Adult	1	463.5	474.6	2.39
		2	502.7	495.2	6.76
		3	520.5	508.5	6.58
		4	506.2	505.1	5.81
		5	301.8	322.2	2.12
		6	418.8	439.7	4.99
		7	429.3	442.8	0.46
		8	473.9	471.7	1.40
		9	470.5	463.9	0.87
		10	435.9	447.9	7.09
Average % error					3.94
Standard deviation					3.00

Table 6.6. Comparison of lung and breast dose from Monte Carlo simulations of chest CT exams using actual and estimated TCM schemes.

		Lung (mGy)				Breast (mGy)		
		Patient	Actual	Estimated	% error	Actual	Estimated	% error
Chest	Pediatric	1	13.37	12.65	5.39	-	-	-
		2	5.57	5.36	3.77	-	-	-
		3	7.23	6.51	9.96	-	-	-
		4	5.06	4.33	14.43	-	-	-
		5	2.67	2.60	2.62	-	-	-
		6	9.18	8.85	3.59	7.60	7.40	2.63
		7	8.84	8.13	8.03	7.28	6.76	7.14
		8	9.66	9.05	6.31	8.36	7.87	5.86
		9	8.16	7.84	3.92	5.91	5.83	1.35
		10	9.00	8.33	7.44	6.10	5.76	5.57
	Adult	1	20.37	19.48	4.37	-	-	-
		2	18.10	18.09	0.06	-	-	-
		3	19.83	18.98	4.29	-	-	-
		4	21.33	20.96	1.73	-	-	-
		5	16.76	16.78	0.12	-	-	-
		6	24.62	23.15	5.97	22.83	21.40	6.26
		7	15.11	14.41	4.63	8.82	8.62	2.27
		8	16.06	15.96	0.62	10.60	10.60	0.04
		9	19.23	18.93	1.56	15.78	15.87	0.57
		10	18.67	18.13	2.89	17.43	17.09	1.95
Average % error					4.59		3.36	
Standard deviation					3.51		2.59	

Table 6.7. Comparison of liver, kidney and spleen dose from Monte Carlo simulations of abdomen/pelvis CT exams using actual and estimated TCM schemes.

		Liver (mGy)			Kidney (mGy)			Spleen (mGy)			
		Patient	Actual	Estimated	% error	Actual	Estimated	% error	Actual	Estimated	% error
Abdomen/Pelvis	Pediatric	1	7.66	8.17	6.66	7.21	7.71	6.93	7.53	8.09	7.44
		2	3.53	3.41	3.40	3.31	3.20	3.32	3.06	2.89	5.56
		3	11.93	11.47	3.86	11.83	11.10	6.17	12.13	11.61	4.29
		4	5.78	6.16	6.57	6.80	7.25	6.62	4.76	5.12	7.56
		5	13.92	13.87	0.36	10.21	9.78	4.21	11.80	11.64	1.36
		6	6.13	6.62	7.99	6.16	6.63	7.63	5.98	6.34	6.02
		7	6.37	6.45	1.26	5.77	5.72	0.87	5.95	6.04	1.51
		8	3.40	3.60	5.88	3.06	3.22	5.23	2.93	3.12	6.48
		9	6.85	6.80	0.73	6.11	6.16	0.82	6.82	6.75	1.03
		10	2.73	2.72	0.37	2.68	2.65	1.12	2.88	2.76	4.17
	Adult	1	22.27	24.37	9.43	21.34	23.16	8.53	23.85	25.95	8.81
		2	15.22	14.78	2.89	13.43	13.24	1.41	12.83	12.36	3.66
		3	23.77	22.71	4.46	26.79	25.83	3.58	26.79	25.29	5.60
		4	17.39	19.20	10.41	16.76	18.10	8.00	14.97	16.31	8.95
		5	27.66	27.22	1.59	30.30	29.65	2.15	33.46	32.62	2.51
		6	16.64	18.15	9.07	15.09	16.34	8.28	15.40	16.85	9.42
		7	19.63	19.55	0.41	20.88	20.76	0.57	21.51	22.06	2.56
		8	19.48	20.98	7.70	19.28	20.55	6.59	19.18	20.49	6.83
		9	17.87	17.92	0.28	18.37	18.41	0.22	17.87	17.74	0.73
		10	25.01	24.93	0.32	25.46	24.61	3.34	28.41	27.44	3.41
		Average % error			4.18				4.28	4.90	
		Standard deviation			3.52				2.90	2.77	

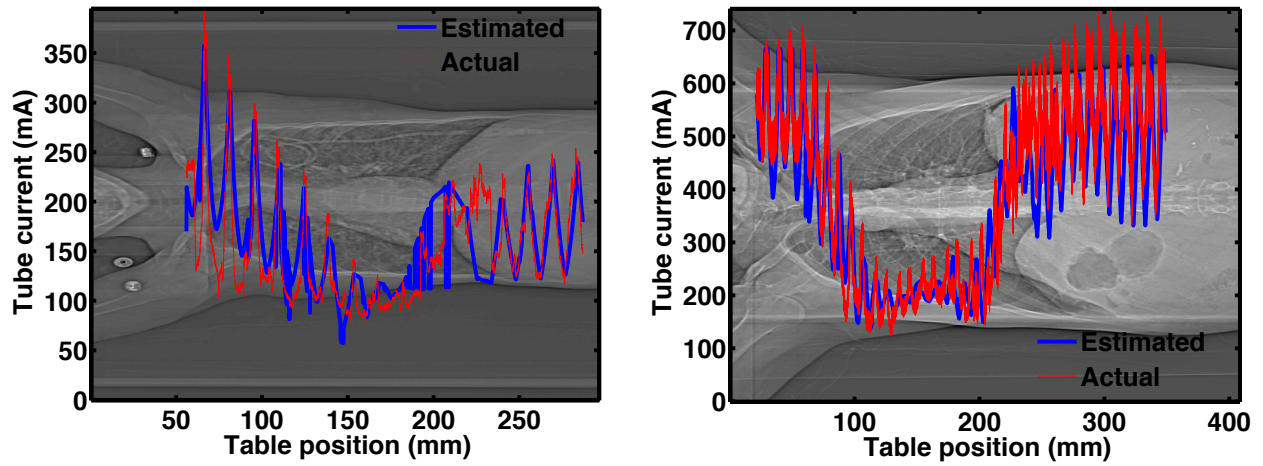


Figure 6.12. Estimated and actual TCM schemes for pediatric (left) and adult (right) chest patients.

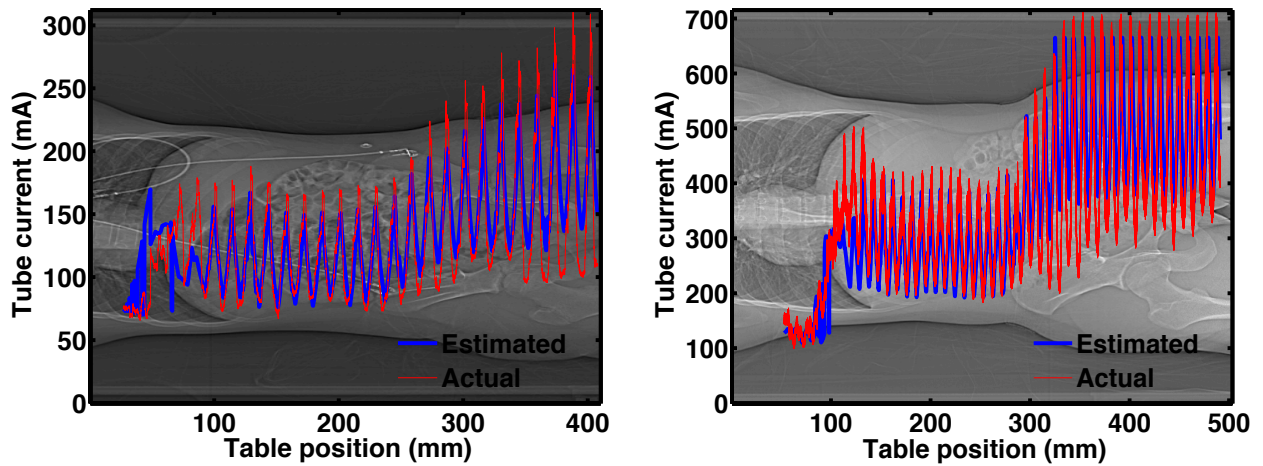


Figure 6.13. Estimated and actual TCM schemes for pediatric (left) and adult (right) abdomen/pelvis patients.

6.4 Discussion

In this chapter, a method was developed to estimate the TCM function based on size information extracted from the topogram of Siemens CT scans. This method was evaluated by comparing

estimated TCM values to actual TCM values using average tube current and organ doses estimated from Monte Carlo simulations. The results demonstrated excellent agreement and indicate that Siemens TCM schemes can be accurately estimated using the size data extracted from the topogram and the steps described in Section 6.2.

The wide varieties of scan techniques and patient sizes used in the validation study indicate that the methods to estimate TCM schemes developed in this investigation are generalizable across different scan types and patient sizes. One particular scenario, though, required adjusted parameters to generate good agreement between the estimated and actual TCM schemes. As mentioned in Section 6.2.2, for pediatric chest and abdomen/pelvis scans acquired at 80 kVp, the strength parameter in Eq. (6.2) necessary to achieve strong agreement between estimated and actual TCM schemes was empirically determined (by us) to be 0.4 for attenuation greater than A_{ref} and 0.65 for attenuation less than A_{ref} . Also mentioned in Section 6.2.2, the strength parameter for the “Average” strength setting, the default setting used on all Siemens CT scanners, was referenced to be 0.3 for attenuation greater than A_{ref} and 0.5 for attenuation less than A_{ref} . The increased strength parameter values required for 80 kVp pediatric scans indicate that the strength setting was adjusted to yield a stronger response. A stronger response means that for attenuation greater than A_{ref} , image noise is decreased at the expense of an increase in dose while for attenuation less than A_{ref} , dose is decreased at the expense of an increase in image noise. It was confirmed that the strength setting on the Sensation 64 scanner for pediatric chest and abdomen/pelvis protocols was set to “Average,” so it appears that the scanner is adjusting the strength parameter on its own in response to a particular scan technique. A reasonable explanation may be that pediatric patients scanned at 80 kVp are typically some of the smallest

patients, so the likelihood of reaching a machine limit in the TCM scheme is appreciably small. Because of this, the scanner can afford to have a stronger response to attenuation in high attenuation regions. This will result in slightly higher dose but with the benefit of reduced image noise. For an “Average” response, the dose will be less than that of a stronger response, but for patients that are small enough that 80 kVp is chosen, the tube current may be so low that image quality may be compromised in high attenuation regions like the shoulders for chest scans or pelvis for abdomen/pelvis scans. Figure 6.14 shows TCM schemes for a pediatric abdomen/pelvis patient scanned at 80 kVp estimated using both an “Average” (left) and stronger response (right). When compared to the actual TCM scheme for this patient, the TCM scheme with the “Average” response underestimates the average tube current by 22.4% while the TCM scheme with the stronger response only underestimates the average tube current by 2.6%.

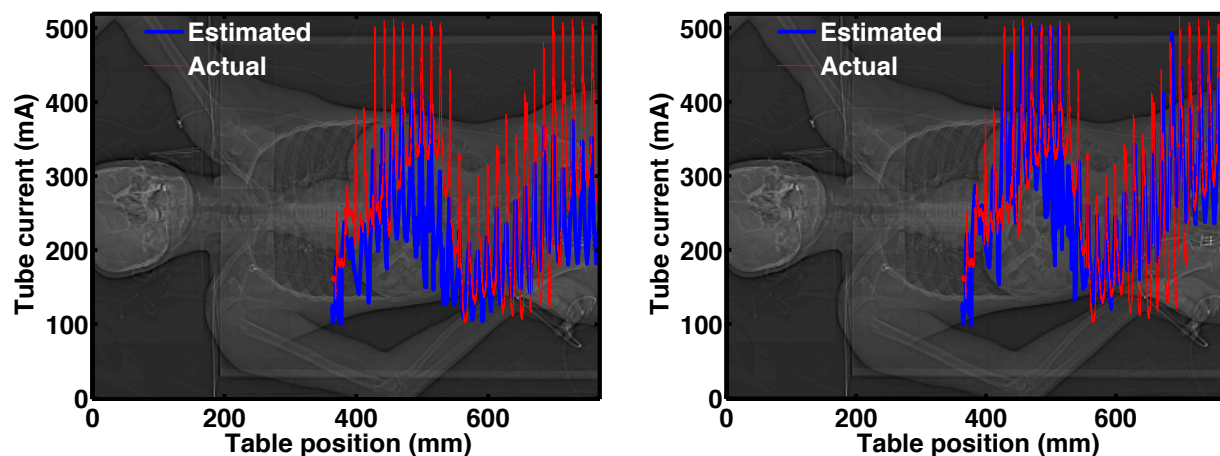


Figure 6.14. TCM schemes for 80 kVp pediatric abdomen/pelvis patient estimated using “Average” (left) and stronger response (right).

The methods to estimate Siemens TCM schemes are also generalizable to Siemens scanners beyond the Sensation 64. Figure 6.15 shows estimated and actual TCM schemes for patients who underwent clinically indicated chest CT examinations on a Sensation 16 (left) and Definition Flash (right) scanner. All methodologies described in this investigation were applied in conjunction with scanner-specific machine limits to generate the estimated TCM schemes. For the Sensation 16, the error between the average tube current from the estimated and actual TCM scheme is 0.2%. For the Definition Flash, the error between the average tube current from the estimated and actual TCM scheme is 0.8%.

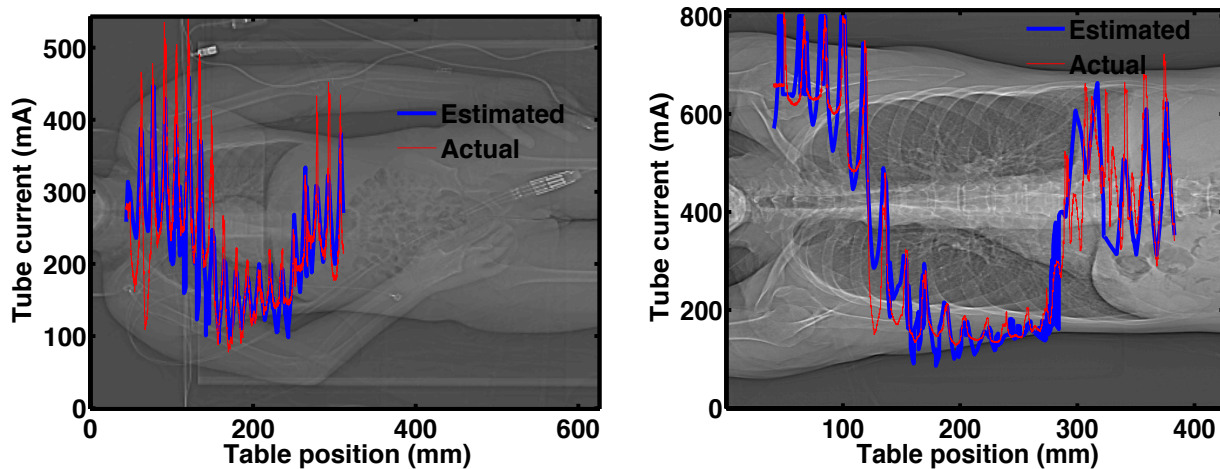


Figure 6.15. Estimated and actual TCM schemes for Sensation 16 (left) and Definition Flash (right) chest patients.

Figure 6.16 shows the various methods to obtain Siemens TCM schemes. Prior to this investigation, the only way to incorporate Siemens TCM schemes into Monte Carlo simulations was to extract the actual TCM scheme from the raw projection data. That method works well, but is limited by the fact that manufacturer cooperation is necessary to obtain the tools to properly

read the raw projection data and extract the relevant TCM information and is also limited in that it can only be applied to patients who have actually undergone a CT scan.

The methods described in this chapter extend that capability by allowing the estimation of TCM functions to patient models where only the topogram is available. In the next chapter, these capabilities will be extended further to allow TCM estimation when only a simulated topogram is available. The next chapter will show that this simulated topogram can be obtained from any voxelized model that can be expressed in terms of attenuation, tissue/material types, CT number or similar descriptors. This will in turn enable the estimation of the TCM function for voxelized reference models such as GSF and ICRP models.

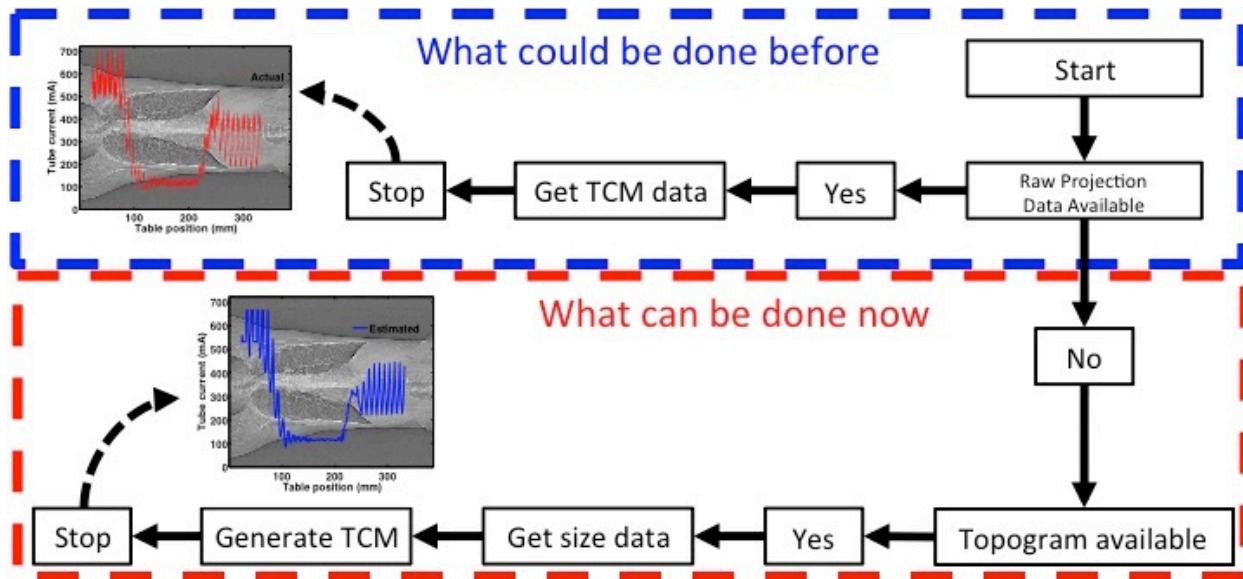


Figure 6.16. Available methods to generate Siemens TCM schemes. This investigation introduces methods to estimate TCM schemes using patient size data extracted from the topogram.

6.5 References

1. M. K. Kalra *et al.*, “Techniques and Applications of Automatic Tube Current Modulation for CT,” *Radiology* **233**, 649-657 (2004).
2. M. K. Kalra *et al.*, “Comparison of z-axis automatic tube current modulation technique with fixed tube current CT scanning of abdomen and pelvis,” *Radiology* **232**, 347-353 (2004).
3. M. Khatonabadi *et al.*, “The feasibility of a regional CTDIvol to estimate organ dose from tube current modulated CT exams,” *Med. Phys.* **40**, 051903 (2013).
4. N. Petoussi-Henss, M. Zankl, U. Fill, D. Regulla, “The GSF family of voxel phantoms,” *Phys. Med. Biol.* **47**, 89-106 (2002).
5. International Commission on Radiological Protection, “Adult Reference Computation Phantoms,” ICRP Publication 110 (2009).
6. American Association of Physicists in Medicine, “Size-Specific Dose Estimates (SSDE) in Pediatric and Adult Body CT Examinations,” AAPM Report 204 (2011).
7. M. Gies, W. A. Kalender, H. Wolf, C. Suess, “Dose reduction in CT by anatomically adapted tube current modulation. I. Simulation studies,” *Med. Phys.* **26**, 2235-2247 (1999).
8. W. A. Kalender, H. Wolf, C. Suess, “Dose reduction in CT by anatomically adapted tube current modulation. II. Phantom measurements,” *Med. Phys.* **26**, 2248-2253 (1999).
9. H. Schlattl, M. Zankl, J. Becker, C. Hoeschen, “Dose conversion coefficients for CT examinations of adults with automatic tube current modulation,” *Phys. Med. Biol.* **55**, 6243-6261 (2010).
10. H. Schlattl, M. Zankl, J. Becker, C. Hoeschen, “Dose conversion coefficient for pediatric CT examinations with automatic tube current modulation,” *Phys. Med. Biol.* **57**, 6309-6326 (2012).

11. X. Li, W. P. Segars, E. Samei, "The impact on CT dose of the variability in tube current modulation technology: a theoretical investigation," *Phys. Med. Biol.* **58**, 4525-4548 (2014).
12. X. Tian *et al.*, "Prospective estimation of organ dose in CT under tube current modulation," *Med. Phys.* **42**, 1575-1585 (2015).
13. N. Keat, "CT scanner automatic exposure control systems," MHRA Report 05016 (2005).
14. T. Flohr, "CARE Dose4D White Paper," Siemens Medical Solutions (2011).
15. S. Popescu *et al.*, US Patent No. 5,867,555, U.S. Patent and Trademark Office (1999).
16. M. Mahesh, "MDCT Physics : The Basics: Technology, Image Quality and Radiation Dose," Philadelphia: Lippincott, Williams and Wilkins, 2009.
17. F. N. Fritsch, R. E. Carlson, "Monotone Piecewise Cubic Interpolation," *SIAM J. Numerical Analysis* **17**, 238-246 (1980).
18. Centre for Evidence-based Purchasing (CEP), "64 slice CT scanners technical specifications: Comparative specifications," CEP 08027 (2009).
19. H. Wolf *et al.*, US Patent No. 20050058249 A1, U.S. Patent and Trademark Office (2005).
20. M. Bostani, *et al.*, "Attenuation-based size metric for estimating organ dose to patients undergoing tube current modulated CT exams," *Med. Phys.* **42**, 958-968 (2015).

Chapter 7: Estimating Tube Current Modulation Schemes Using Patient Size Data from Simulated Topogram

7.1 Introduction

As mentioned in previous chapters, the goal of this dissertation is to determine dose to any fully-, partially- or indirectly irradiated organ for tube current modulation (TCM) CT exams. This requires validated TCM schemes for reference voxelized phantoms that have all radiosensitive organs identified, such as the GSF and ICRP reference voxelized phantoms described in Chapter 4. Methods to estimate Siemens TCM schemes using size data from the topogram are described in Chapter 6. While these methods allow for the construction of detailed TCM schemes, they are limited to voxelized patient models for which a topogram is available. For reference voxelized phantoms, a topogram containing the attenuation data necessary to create a TCM scheme is not available. Because of this, the TCM scheme estimation methods described in Chapter 6 are not immediately applicable to any voxelized patient model, including the GSF and ICRP models, for which a topogram does not exist. In order to overcome this limitation, a method needs to be developed to simulate the topogram for these voxelized reference models and then provide the desired size information needed for the methods described in Chapter 6.

Therefore the purpose of this chapter was to develop and test a method to both simulate the topogram of a voxelized patient model and then perform the analyses on that topogram to extract the desired/required size information to generate an estimated TCM function. As described in Chapter 5, the attenuation information that can be extracted from the topogram is the patient's anterior-posterior (AP) and lateral (LAT) attenuation data. The results from Chapter 6 indicate that this is indeed the attenuation data used to drive the Siemens TCM algorithm. For

body CT exams, such as chest and abdomen/pelvis scans, an AP topogram is typically acquired. Patient attenuation is explicitly measured in the direction of the topogram (AP) and calculated in the orthogonal direction (LAT). It is this attenuation data that is used as the input to the TCM scheme estimation methods outlined in Chapter 6. In this investigation, a method was developed to estimate the AP dimension of patient size and calculate the LAT dimension of patient size at each table location from patient attenuation profiles determined from a simulated AP topogram. To validate this method to estimate patient size from a simulated topogram, patient attenuation data determined from simulated topograms was used as the input to TCM schemes estimation methods described in Chapter 6 to estimate TCM schemes for a variety of pediatric and adult patients who underwent clinically indicated chest and abdomen/pelvis TCM CT examinations. The actual TCM schemes were extracted from the raw projection data of each patient, and average tube currents were compared between the actual and estimated TCM schemes. Additionally, Monte Carlo simulations were performed using each TCM scheme to estimate dose to the lungs and breasts (females only) for chest scans and dose to the liver, kidneys and spleen for abdomen/pelvis scans. Organ doses from simulations using the estimated TCM schemes were compared to those using the actual TCM schemes.

7.2 Methods

7.2.1 Patient Attenuation Simulation – Creating a Simulated Topogram

Patient attenuation is defined as:

$$A = \frac{I_0}{I} \quad (7.1)$$

where I_0 is the intensity of the x-ray beam at the detector with no object in the scanner and I is the intensity of the x-ray beam at the detector with an object in the scanner. Eq. (7.1) describes the degree by which an object decreases the intensity of an x-ray beam. Objects with larger mass attenuation coefficients, such as bony structures, will result in higher patient attenuation values.

Patient attenuation was modeled in this investigation using Monte Carlo simulations to model the projection geometry of the topogram. Because an AP topogram is acquired for all body scans (e.g. chest and abdomen/pelvis scans) on Siemens scanners, geometry for AP projectional imaging was modeled in the Monte Carlo simulations. The CT source was fixed at the 12 o'clock position (i.e. directly above the patient) at the source-to-isocenter distance (SID) for the scanner of interest. A planar detector array consisting of 100 1 cm x 1 cm detector elements was modeled at the source-to-detector distance (SDD) for the scanner of interest. A planar detector was modeled for simplification, even though it is recognized that the actual detector design for a CT scanner will have some curvature. Because patient attenuation is based on relative measurements, a simplified planar detector array is expected to be sufficient for estimating patient attenuation. In this investigation, simulations were performed using a Sensation 64 CT source model. For a Sensation 64 scanner, the SID and SDD are 57 cm and 104 cm, respectively. A narrow beam collimation of 0.06 cm was used. Additionally, all simulations were performed with beam energy of 120 kVp. Figure 7.1 shows a diagram of the simulation setup for AP projectional imaging.

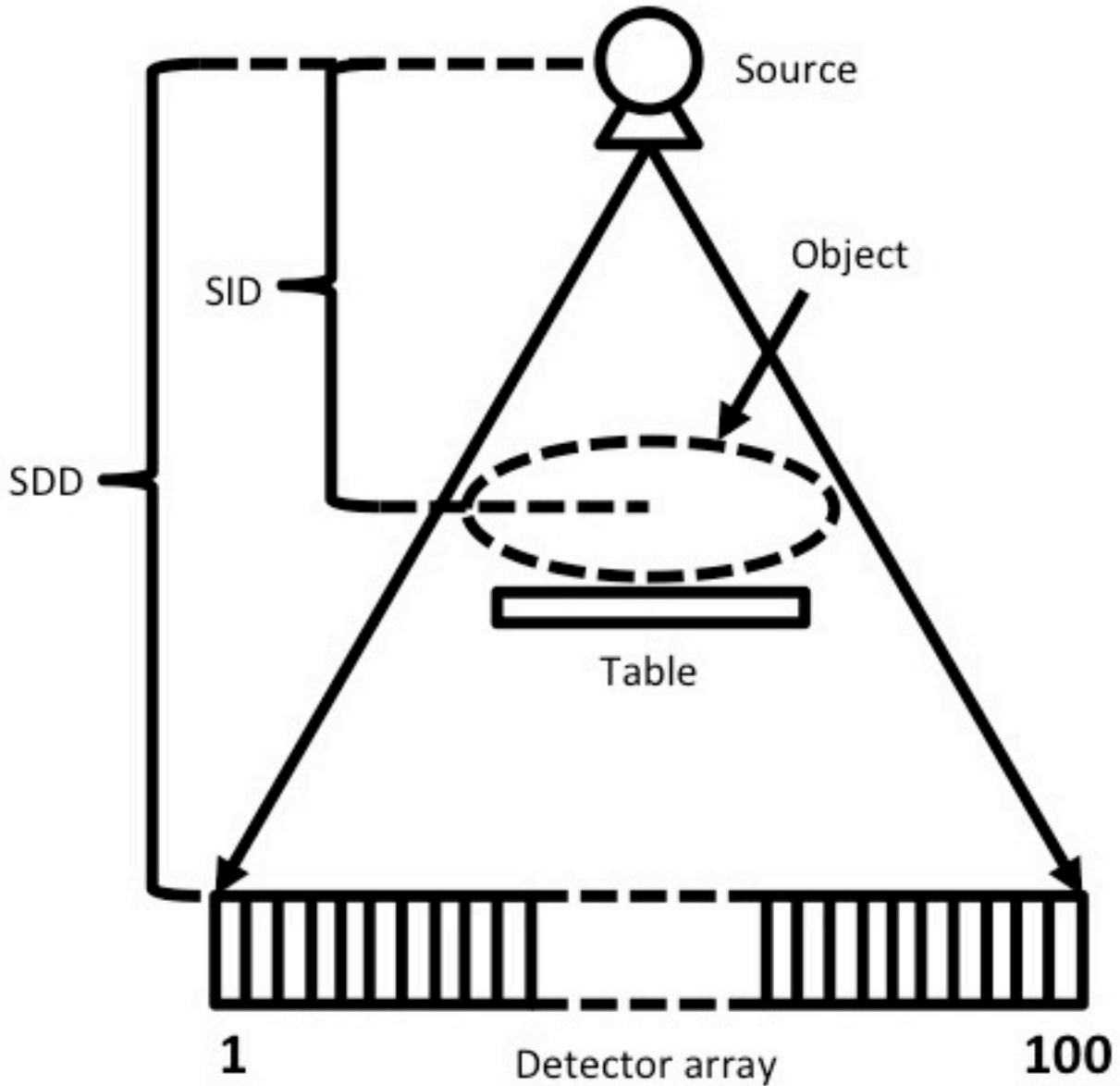


Figure 7.1. Diagram of AP projectional imaging setup.

After the simulation geometry was set up, an “air scan” was first performed. This was a simulation to determine I_0 , the intensity of the x-ray beam at the detector with no object in the scanner. With no object or table present in the simulation, photon fluence ($\#/cm^2/particle$) was tallied at each of the detector elements. This simulation only needed to be performed once. Then,

a “patient scan” was performed. This was a simulation to determine I , the intensity of the x-ray beam at the detector with an object in the scanner. With the object present in the simulation, photon fluence ($\#/cm^2/particle$) was tallied at each of the detector elements. Patient scans were performed in 1 mm increments along the length of the object. Figure 7.2 shows an example of the fluence profiles along the detector from the air and patient scans at a particular table location for an adult patient who underwent a clinically indicated chest CT exam. This adult chest patient will be used as an example throughout the development of the methods to estimate Siemens patient attenuation information. Using Eq. (7.1), patient attenuation along the detector was calculated at each table position by dividing the fluence profile from the air scan by the fluence profile from the patient scan. Figure 7.3 shows the patient attenuation profile along the detector calculated from the fluence profiles in Fig. 7.2. The determination of patient attenuation profiles at each table location is analogous to simulating an AP topogram.

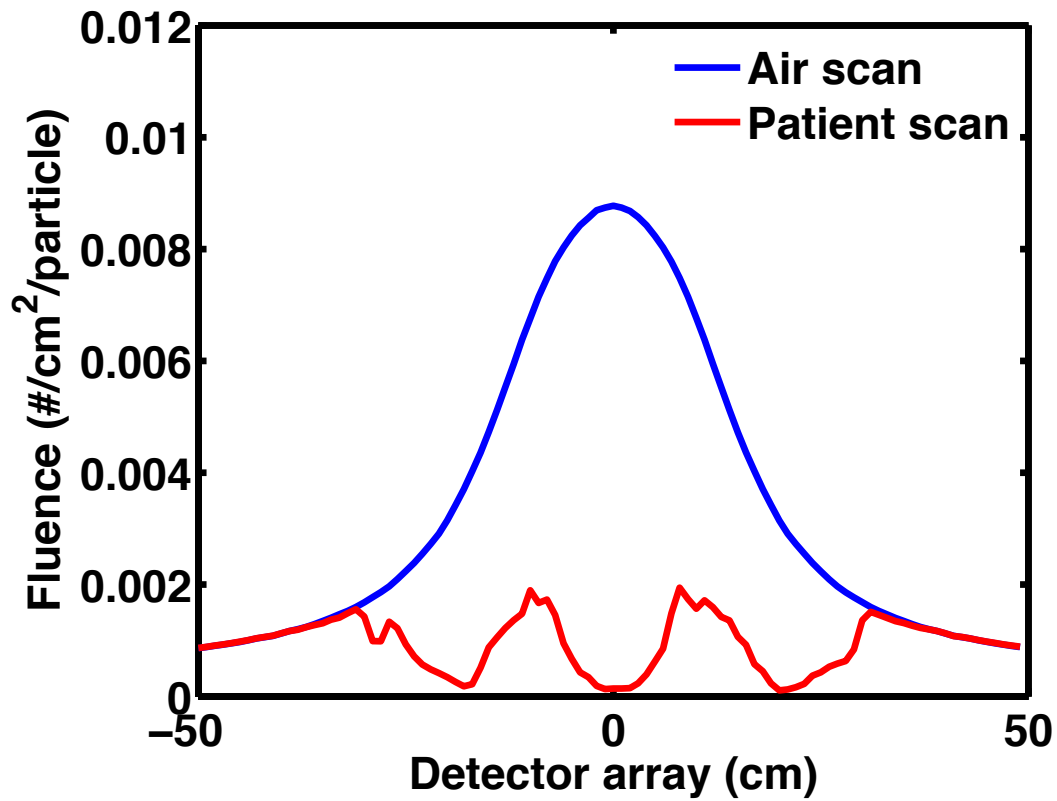


Figure 7.2. Air scan and patient scan fluence profiles at a particular table location for an adult patient who underwent a clinically indicated chest CT examination. This patient will be used as an example throughout the development of the methods to estimate Siemens patient attenuation information presented in this investigation.

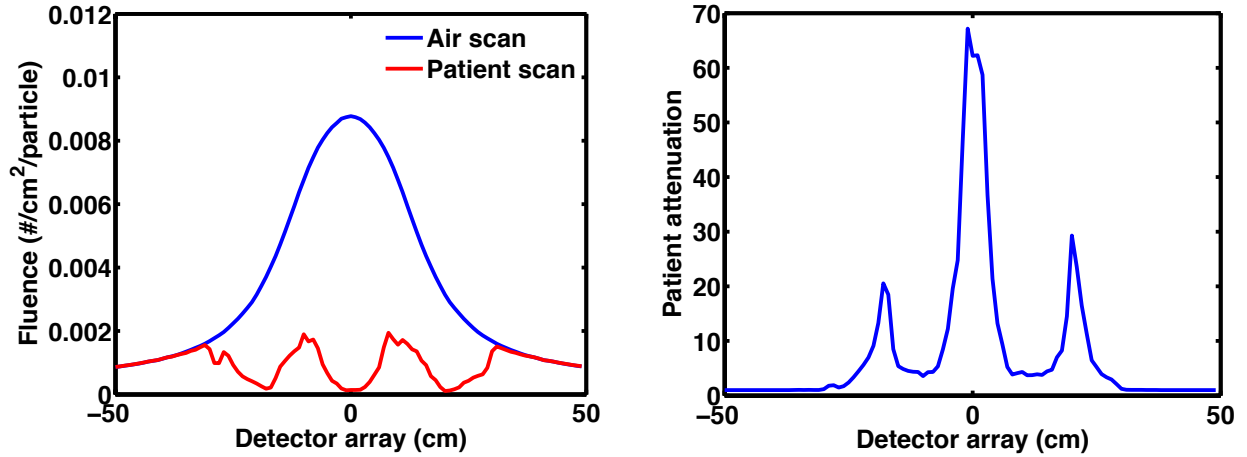


Figure 7.3. (Left) Air scan and patient scan fluence profiles. (Right) Patient attenuation profile along the detector calculated by dividing the fluence profile from the air scan by the fluence profile from the patient scan.

7.2.2 Anterior-Posterior Dimension of Patient Size

Once a patient attenuation profile was determined at each table location, the AP dimension of patient size was calculated at each table location. In order to eliminate the influence of strong local attenuations, such as metallic implants, screws or clips, on the calculation of AP size, a moving average filter was first applied to the attenuation profile [19]. The span of the moving average is 5 detector elements (5 cm). Figure 7.4 shows the patient attenuation profile before and after the moving average filter is applied. After the filter was applied, the maximum attenuation from the profile was determined. The AP dimension of patient size calculated from the maximum attenuation of the attenuation profile at each table position, i , is defined as:

$$AP(i) = \frac{1}{\mu_{water,kVp}} \times \ln(\max(A(i))) \quad (7.2)$$

where $\mu_{water,kVp}$ is the linear attenuation coefficient of water for a given beam energy and $A(i)$ is the filtered attenuation profile [2]. As mentioned in Section 7.2.1, all simulations were performed at 120 kVp, so $\mu_{water,kVp} = \mu_{water,120\text{ kVp}} = 0.2\text{ cm}^{-1}$.

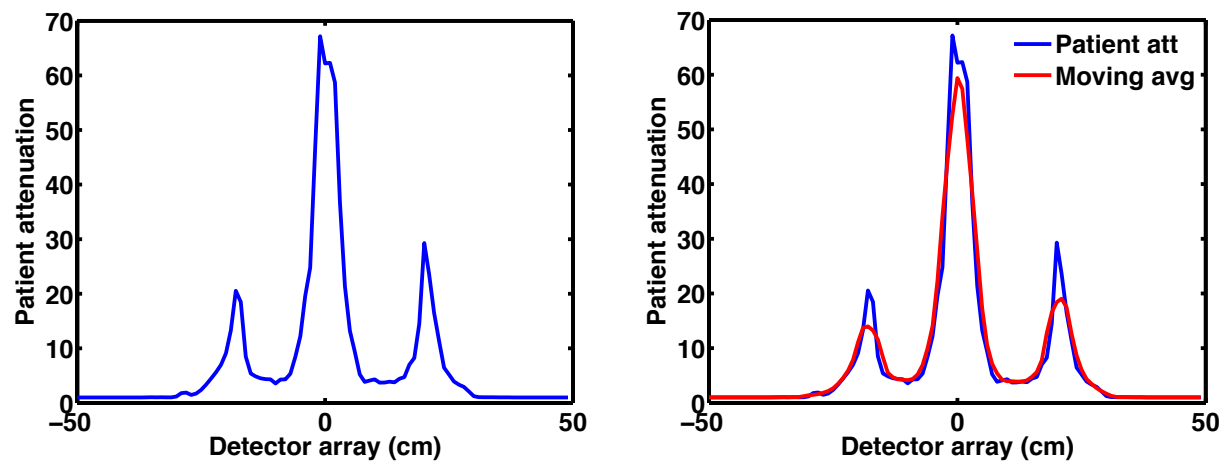


Figure 7.4. (Left) Patient attenuation profile calculated from air scan and patient scan fluence profiles. (Right) Moving average filter with span of 5 cm applied to patient attenuation profile to eliminate any spurious peaks caused by strong local attenuations.

7.2.3 Lateral Dimension of Patient Size

Only one topogram is required to generate the attenuation data necessary to drive the Siemens TCM algorithm. In this investigation, only AP topograms were simulated. As described in Section 7.2.2, the AP dimension of patient size was determined directly from the measured patient attenuation in the AP direction. The LAT dimension of patient size was estimated from the patient attenuation in the AP direction using a mathematical model [2]. According to

Siemens patents, this mathematical model involves the elimination of outside air, the CT table and low-attenuation regions through the application of thresholds to the patient attenuation profile [19]. The exact nature of these thresholds, though, was not described by Siemens in any of their patents.

First, a threshold was developed and applied to the filtered patient attenuation profile to eliminate all detectors elements whose attenuation values are consistent with outside air and the table. Failing to exclude the outside air and table from the calculation of lateral extent can lead to results that are misleading [19]. Outside air has a patient attenuation value of 1 ($I_0 = I$). From a topogram acquired with no object on the table (i.e. scan of the table), it was determined that the table had an attenuation value of approximately 1.7. By setting the threshold slightly above this value to 1.8, all outside air and table regions were eliminated from the attenuation profile. This threshold was applied to all attenuation profiles. Figure 7.5 shows how the outside air and table are eliminated from the attenuation profile by means of a threshold.

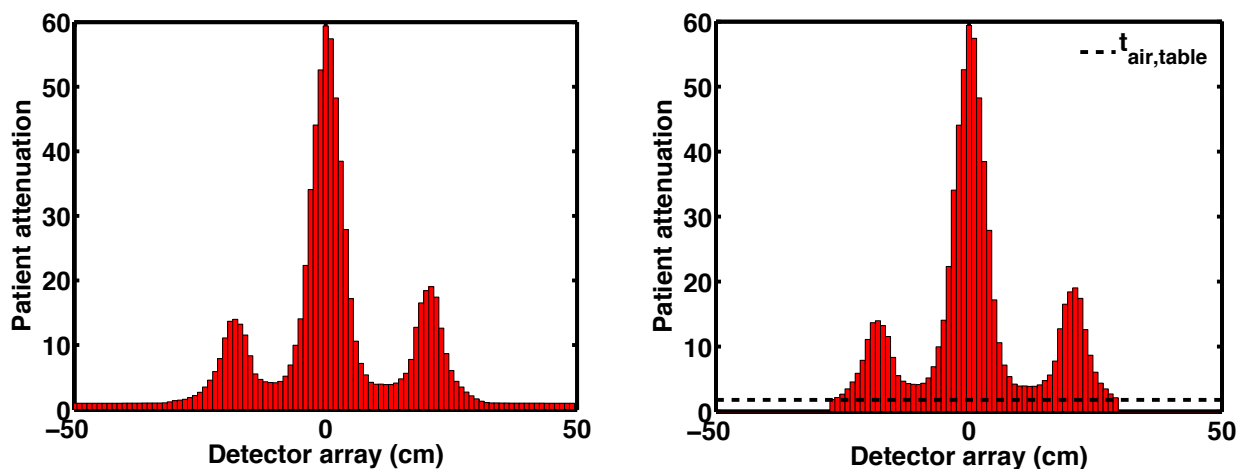


Figure 7.5. (Left) Patient attenuation profile (represented as a bar plot with each bar representing the attenuation value at each detector element) before outside air and table threshold applied. (Right) Patient attenuation profile with outside air and table detector elements eliminated by a threshold value of 1.8.

After the outside air and table were eliminated, another threshold was developed and applied to the attenuation profile to eliminate low-attenuation regions, such as the lungs [19]. Unlike the threshold to eliminate outside air and the table, this low-attenuation threshold was only applied to attenuation profiles that meet a set of criteria. First, local maxima (peaks) were identified in the attenuation profile. If two or more peaks were identified, the attenuation profile was flagged for further evaluation. If the minimum attenuation between any two peaks was less than 30, the low-attenuation threshold was applied to the attenuation profile. This step was performed to confirm that the peaks in the attenuation profile are anatomical structures that are actually surrounding low-attenuation regions rather than just symmetrical highly attenuating structures, such as the femurs found at the tail end of an abdomen/pelvis scan. The threshold value was set as a percentage of the maximum attenuation of the attenuation profile. The percentage was determined empirically (by us) to be 9%. For example, if the maximum attenuation in an attenuation profile is 100, the threshold value is 9. Figure 7.6 shows the how the low-attenuation regions are eliminated from the attenuation profile by means of a threshold.

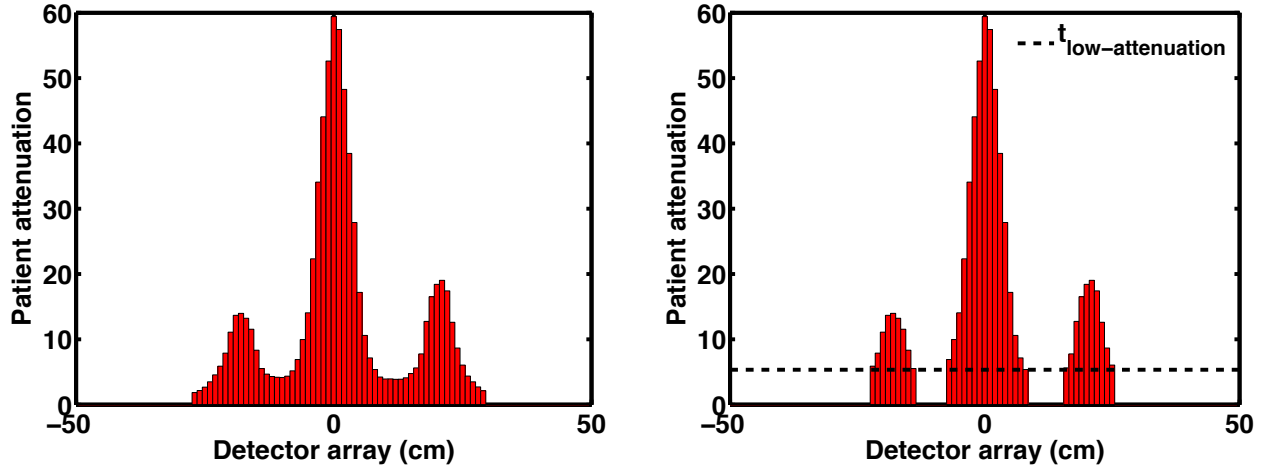


Figure 7.6. (Left) Patient attenuation profile after outside and table threshold applied. (Right) Patient attenuation profile with low-attenuation region detector elements eliminated by a threshold value of 9% of the maximum attenuation from the attenuation profile.

Once the outside air, table and low-attenuations regions were eliminated from the attenuation profile, an initial estimate of the LAT dimension of patient size was calculated by multiplying the number of detector elements with attenuations greater than the thresholds by the detector element width [19]. The initial estimate of lateral extent at each table position, i , is defined as:

$$LAT(i) = n \left\{ A(i) \mid A(i) > t_{air,table}, t_{low-attenuation} \right\} \times w_d \quad (7.3)$$

where $t_{air,table}$ is the threshold for outside air and the table, $t_{low-attenuation}$ is the threshold for low-attenuation regions, $n \left\{ A(i) \mid A(i) > t_{air,table}, t_{low-attenuation} \right\}$ is the number of detector elements with attenuations greater than the thresholds and w_d is the detector element width. In this

investigation, w_d is 1 cm. In Fig. 7.6, the number of detector elements with attenuations greater than the thresholds is 35, so the initial estimate of lateral extent is 35 cm.

This initial estimate of lateral extent was based on the “shadow” of the patient on the detector array and therefore needs to be geometrically corrected to the positioning of the patient within the within the CT scanner [2]. First, an estimate of lateral extent at the scanner isocenter at each table position, i , is defined as:

$$LAT(i)_{iso} = \frac{SID}{SDD} \times LAT(i) \quad (7.4)$$

If the patient had been perfectly aligned at isocenter, this would be the true lateral extent of the patient. As described in Section 7.2.1, the SID and SDD used in this investigation are 57 cm and 104 cm, respectively. Using Eq. (7.4), the lateral extent at isocenter calculated from the attenuation profile in Fig. 7.6 is 19.18 cm.

More often than not, the patient is not aligned perfectly at isocenter, so the off-center positioning needs to be accounted for in the calculation of lateral extent. According to Siemens patents, off-center patient positioning is explicitly accounted for in the calculation of lateral extent [2]. First, an offset correction factor quantifying the distance the table is from isocenter was calculated. The vertical position of the table at isocenter is hard coded into the CT scanner, so the scanner can readily determine the table-to-isocenter distance. In this investigation, the offset correction factor for any given patient was not explicitly known, but it can be calculated from the axial images by measuring the distance from the center of the image to the center of the table. Once the offset correction factor was calculated, the lateral extent at the offset table height at each table position, i , is defined as:

$$LAT(i)_{offset} = \frac{1}{\mu_{water,kVp}} \times \ln \left(\exp \left(\mu_{water,kVp} \times \frac{SID + OCF - \left(\frac{1}{2} \times AP(i) \right)}{SID} \times LAT(i)_{iso} \right) \right) \quad (7.5)$$

where OCF is the offset correction factor. LAT_{offset} is the LAT dimension of patient size that can be extracted from a Siemens topogram. For the attenuation profile in Fig. 7.6, the OCF for that patient is 19 cm, and at that table position, the estimate of the AP dimension of patient size is 15.81 cm. Using these values of OCF and AP with Eq. (7.5), the lateral extent at the offset table height calculated from the attenuation profile in Fig. 7.6 is 22.91 cm. Figure 7.7 provides a diagram of the scanner geometry with all components of Eq. (7.5) labeled.

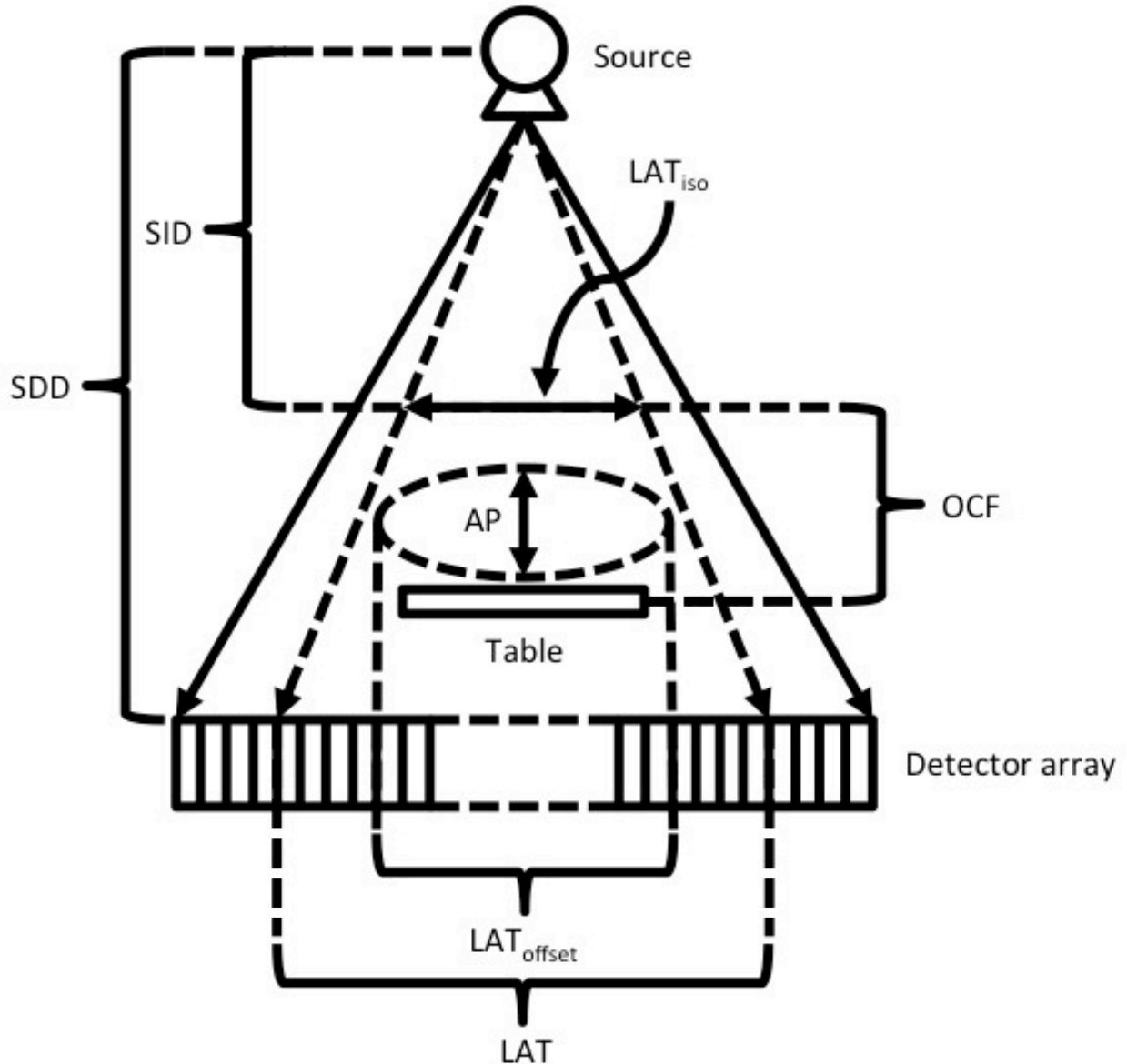


Figure 7.7. Diagram of scanner geometry with all components of Eq. (7.5) labeled.

7.2.4 Validation in Patient Datasets with Topograms and TCM Functions Available

The methods to determine patient attenuation information in the Siemens manner were applied to a set of pediatric and adult patients who underwent clinically indicated chest ($n=20$) and abdomen/pelvis ($n=20$) CT examinations [20]. This is the same set of patients used in the

validation study in Chapter 6. Characteristics of these patients were described in Section 6.2.6. For each patient, the axial images were acquired and reconstructed at full 500 mm FOV (to avoid having any anatomy outside of the image). Models of patient anatomy were created from the image data and used as the patient geometry in the patient attenuation simulations described in Section 7.2.1. AP and LAT dimensions of patient size were estimated for each patient and then used as the inputs to the methods to estimate Siemens TCM schemes described in Chapter 6.

As described previously, for the chest scans, the lungs and breasts (if female) were segmented from the axial images. For the abdomen/pelvis scans, the liver, spleen and kidneys were segmented from the images [20]. For each patient, the actual TCM scheme was then extracted from the raw projection data. Organ doses were estimated with detailed Monte Carlo simulations using both the estimated and actual TCM schemes. The estimated TCM schemes were validated against the actual TCM scheme for each patient by comparing average tube current and organ dose estimates.

7.3 Results

Figure 7.8 shows AP and LAT dimensions of patient size extracted from the simulated topogram compared with AP and LAT dimensions of patient size extracted from the actual topogram for patients who underwent clinically indicated chest (left) and abdomen/pelvis (right) scans. For the same patients from Fig. 7.8, Fig. 7.9 shows estimated TCM schemes derived from the estimated AP and LAT dimensions of patient size compared with actual TCM schemes extracted from the raw projection data. A comparison of the average tube current from estimated and actual TCM schemes for all patients is tabulated in Table 7.1. Across all patients, the average difference

between the average tube current from estimated and actual TCM schemes is 5.77%. Table 7.2 outlines a comparison of lung and breast dose estimates from Monte Carlo simulations of chest CT exams using estimated and actual TCM schemes. The average difference for lung and breast dose is 6.64% and 4.49%, respectively. Table 7.3 outlines a comparison of liver, kidney and spleen dose estimates from Monte Carlo simulations of abdomen/pelvis CT exams using estimated and actual TCM schemes. The average difference for liver, kidney and spleen dose is 5.14%, 5.07% and 5.27%, respectively.

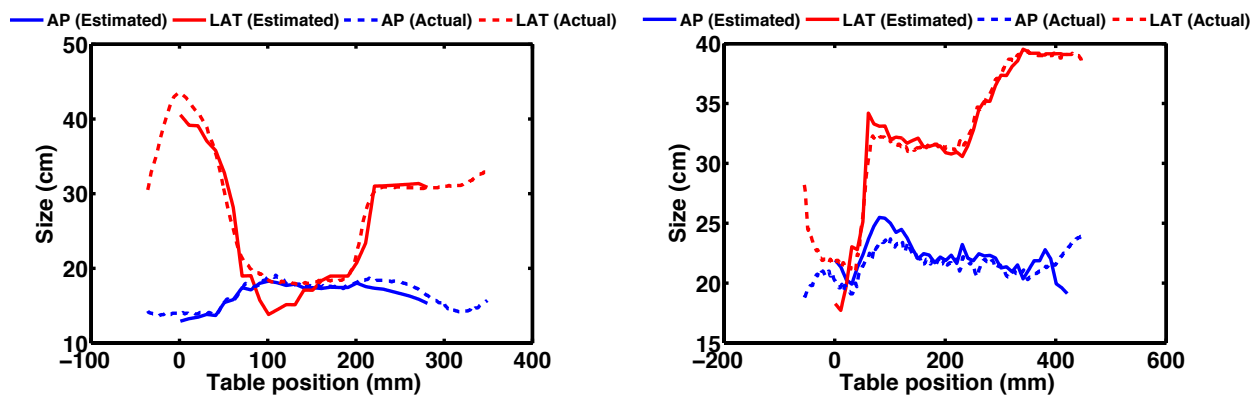


Figure 7.8. (Left) Estimated AP and LAT dimensions of patient size compared with AP and LAT dimensions of patient size extracted from the topogram of a patient who underwent a clinically indicated chest CT exam. (Right) Estimated AP and LAT dimensions of patient size compared with AP and LAT dimensions of patient size extracted from the topogram of a patient who underwent a clinically indicated abdomen/pelvis CT exam. (Note: The estimated patient attenuation data (solid lines) was derived from the patient’s axial image data and therefore does not include the extra anatomy before and after the scan range in the patient’s actual topogram (dashed lines).)

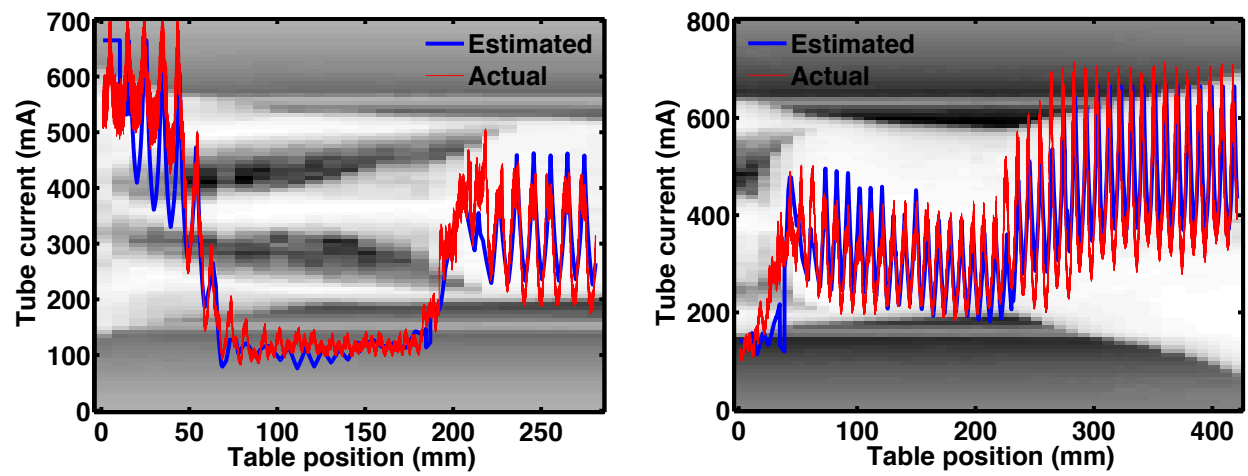


Figure 7.9. (Left) TCM from simulated topogram and actual TCM scheme for chest patient. (Right) TCM from simulated topogram and actual TCM scheme for abdomen/pelvis patient.

Table 7.1. Comparison of average tube current between actual and estimated TCM schemes.

		Patient	Average mA (Actual)	Average mA (Estimated)	% error
Chest	Pediatric	1	329.2	321.7	2.28
		2	224.4	201.2	10.34
		3	257.1	227.8	11.40
		4	153.3	134.7	12.13
		5	141.6	147.6	4.24
		6	321.9	309.0	4.01
		7	296.6	265.8	10.38
		8	370.8	338.6	8.68
		9	311.3	314.5	1.03
		10	289.2	283.5	1.97
	Adult	1	418.3	360.5	13.82
		2	365.4	395.6	8.26
		3	433.3	384.4	11.29
		4	471.5	428.4	9.14
		5	381.9	361.1	5.45
		6	513.7	526.9	2.57
		7	285.5	287.3	0.63
		8	330.8	338.9	2.45
		9	381.9	363.5	4.82
		10	567.2	588.4	3.74
Abdomen/Pelvis	Pediatric	1	327.0	338.5	3.52
		2	275.9	290.4	5.26
		3	290.9	268.7	7.63
		4	253.0	274.7	8.58
		5	285.2	262.9	7.82
		6	251.2	259.8	3.42
		7	259.3	240.4	7.29
		8	129.6	128.5	0.85
		9	227.0	235.4	3.70
		10	185.5	175.0	5.66
	Adult	1	463.5	502.6	8.44
		2	301.8	337.1	11.70
		3	323.7	329.2	1.70
		4	357.7	378.5	5.81
		5	392.2	402.1	2.52
		6	418.8	405.8	3.10
		7	473.9	461.3	2.66
		8	470.5	452.8	3.76
		9	450.4	414.1	8.06
		10	334.4	337.7	0.99
Average % error					5.78
Standard deviation					3.65

Table 7.2. Comparison of lung and breast dose from Monte Carlo simulations of chest CT exams using actual and estimated TCM schemes.

		Lung (mGy)				Breast (mGy)		
		Patient	Actual	Estimated	% error	Actual	Estimated	% error
Chest	Pediatric	1	13.37	13.53	1.22	-	-	-
		2	5.57	4.91	11.94	-	-	-
		3	7.23	6.39	11.59	-	-	-
		4	5.06	4.21	16.86	-	-	-
		5	2.67	2.74	2.75	-	-	-
		6	9.18	8.54	7.01	7.60	7.70	1.32
		7	8.84	7.96	9.92	7.28	6.87	5.63
		8	9.66	8.89	8.00	8.36	7.79	6.82
		9	8.16	7.98	2.22	5.91	5.75	2.71
		10	9.00	9.20	2.20	6.10	5.77	5.41
	Adult	1	20.37	18.45	9.43	-	-	-
		2	18.10	19.78	9.28	-	-	-
		3	19.83	17.54	11.55	-	-	-
		4	21.33	19.56	8.30	-	-	-
		5	16.76	15.58	7.04	-	-	-
		6	24.62	24.94	1.30	22.83	24.52	7.40
		7	15.11	15.52	2.71	8.82	9.37	6.24
		8	16.06	16.56	3.11	10.60	11.09	4.62
		9	19.23	18.21	5.30	15.78	15.72	0.38
		10	18.67	18.46	1.12	17.43	18.19	4.36
Average % error					6.64		4.49	
Standard deviation					4.50		2.34	

Table 7.3. Comparison of liver, kidney and spleen dose from Monte Carlo simulations of abdomen/pelvis CT exams using actual and estimated TCM schemes.

		Liver (mGy)			Kidney (mGy)			Spleen (mGy)			
		Patient	Actual	Estimated	% error	Actual	Estimated	% error	Actual	Estimated	% error
Abdomen/Pelvis	Pediatric	1	7.66	7.71	0.65	7.21	7.31	1.39	7.53	7.76	3.05
		2	3.53	3.76	6.52	3.31	3.46	4.53	3.06	3.27	6.86
		3	11.93	10.88	8.80	11.83	11.02	6.85	12.13	11.36	6.35
		4	5.78	6.22	7.61	6.80	7.43	9.26	4.76	5.13	7.77
		5	13.92	12.80	8.05	10.21	9.46	7.35	11.80	11.04	6.44
		6	6.13	6.27	2.28	6.16	6.38	3.57	5.98	6.07	1.51
		7	6.37	5.84	8.32	5.77	5.48	5.03	5.95	5.44	8.57
		8	3.40	3.44	1.18	3.06	3.02	1.31	2.93	2.86	2.39
		9	6.85	7.26	5.99	6.11	6.44	5.40	6.82	7.14	4.69
		10	2.73	2.49	8.79	2.68	2.55	4.85	2.88	2.70	6.25
	Adult	1	22.27	24.43	9.70	21.34	23.09	8.20	23.85	26.12	9.52
		2	15.22	16.63	9.26	13.43	14.77	9.98	12.83	14.11	9.98
		3	23.77	23.63	0.59	26.79	27.90	4.14	26.79	27.00	0.78
		4	17.39	18.07	3.91	16.76	17.63	5.19	14.97	15.92	6.35
		5	27.66	28.75	3.94	30.30	31.12	2.71	33.46	33.66	0.60
		6	16.64	16.03	3.67	15.09	14.44	4.31	15.40	14.72	4.42
		7	19.63	19.67	0.20	20.88	20.07	3.88	21.51	20.33	5.49
		8	19.48	18.83	3.34	19.28	18.39	4.62	19.18	18.42	3.96
		9	17.87	16.63	6.94	18.37	17.40	5.28	17.87	16.62	6.99
		10	25.01	25.77	3.04	25.46	26.37	3.57	28.41	29.36	3.34
		Average % error			5.14				5.07		
		Standard deviation			3.22				2.31		

7.4 Discussion

In this chapter, methods were developed to simulate a topogram in the Siemens manner to determine patient attenuation information for any voxelized patient model that matches the attenuation data that would have been determined by the scanner. Using this attenuation data, TCM schemes were estimated for a set of pediatric and adult patients who underwent clinically indicated chest and abdomen/pelvis CT examinations. The collective method of simulating

topograms and estimating TCM schemes using patient attenuation derived from the simulated topograms was evaluated by comparing estimated TCM values to actual TCM values using average tube current and organ doses estimated from Monte Carlo simulations. The results demonstrated excellent agreement and indicate that Siemens TCM schemes can be accurately estimated using the size data determined from a simulated topogram and the TCM scheme estimation methods described in Chapter 6.

In this investigation patient attenuation information was determined from a simulated AP topogram. In some scenarios, a posterior-anterior (PA) topogram may be acquired on a Siemens scanner. Because of the offset correction factor described in Section 7.2.3 used to account for off-center patient positioning in the calculation of lateral extent, estimated patient attenuation from AP and PA topograms should be approximately equivalent. For those instances where a lateral topogram is used (not common in body imaging), these results may be different because what is being measured (lateral direction attenuation) and what is being calculated (AP direction attenuation) are reversed from the AP or PA topogram and may be affected by table height, etc. For manufacturers other than Siemens, it is not clear that an offset correction is applied to account for off-center patient positioning. Because of that, table height may be an important factor in the determination of TCM schemes for other manufacturers. In addition, if a table height correction is not being used, the results from an AP topogram may not be the same as the results from a PA topogram.

Figure 7.10 shows the various methods to obtain Siemens TCM schemes. Prior to the work presented in this dissertation, the only way to incorporate Siemens TCM schemes into Monte Carlo simulations was to extract the actual TCM scheme from the raw projection data. Chapter 6 introduced methods to accurately estimate Siemens TCM schemes with patient size

data extracted from the actual topogram. The application of these methods, though, was limited to voxelized patient models for which a topogram exists. This excludes reference voxelized phantoms such as the GSF and ICRP models. From this investigation, the new state of the art is the ability to accurately estimate Siemens TCM schemes using patient size data determined from either an actual or a simulated topogram. TCM schemes can now be generated for any voxelized patient model, including reference voxelized phantoms in which a voxelized (or geometric) representation exists and from which a simulated topogram can be generated. This enables the extraction of the size data required to accurately estimate TCM. This in turns allows the estimation of TCM schemes for reference voxelized phantoms and will facilitate the assessment of fully-, partially- or indirectly-irradiated organ for TCM CT exams.

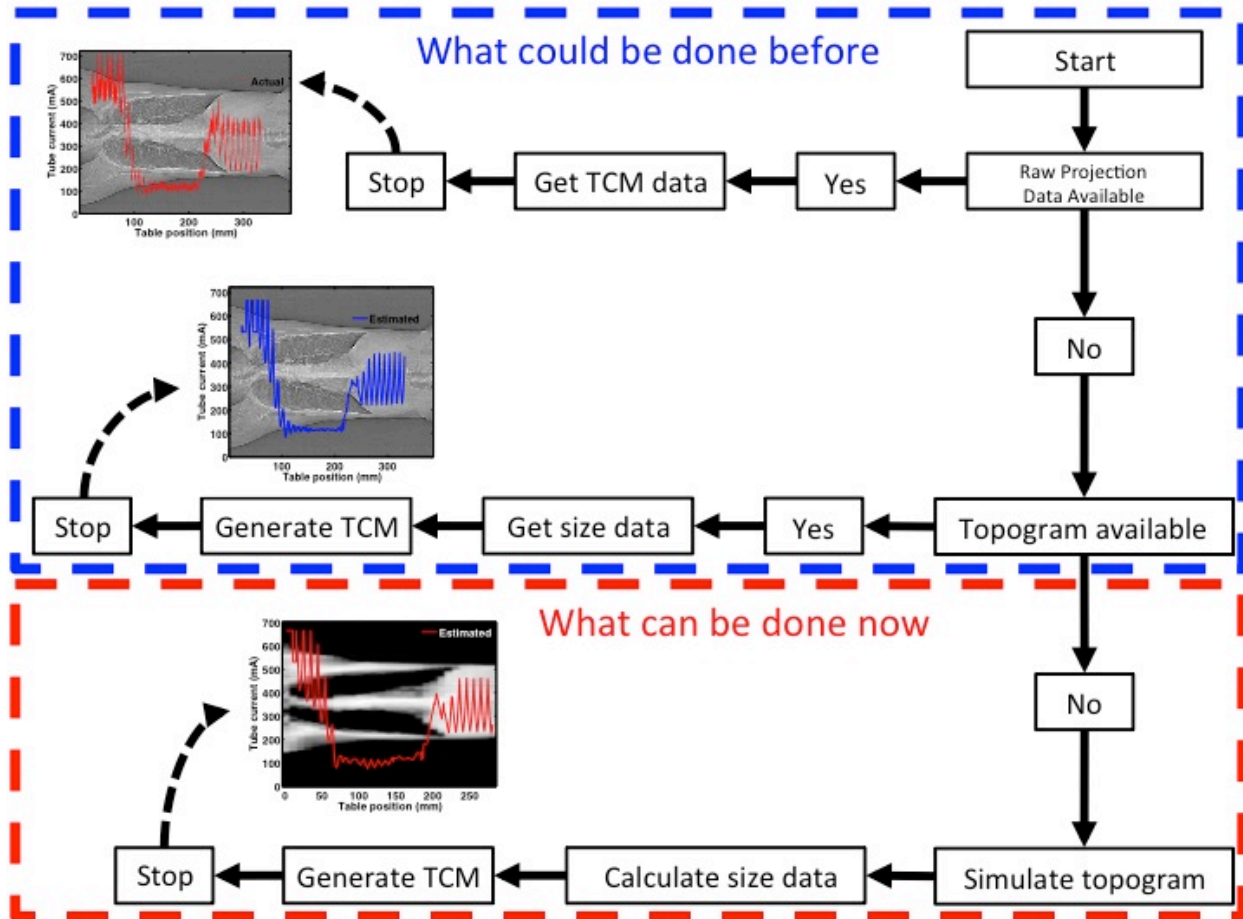


Figure 7.10. Available methods to generate Siemens TCM schemes. This investigation introduces methods to estimate TCM schemes using patient size calculated from a simulated topogram.

7.5 References

1. H. Wolf *et al.*, US Patent No. 20050058249 A1, U.S. Patent and Trademark Office (2005).
2. R. Raupach *et al.*, US Patent No. 7,289,595 B2, U.S. Patent and Trademark Office (2007).
3. M. Bostani, *et al.*, "Attenuation-based size metric for estimating organ dose to patients undergoing tube current modulated CT exams," *Med. Phys.* **42**, 958-968 (2015).

Chapter 8: Tube Current Modulation Monte Carlo Dose Simulations with GSF and ICRP Reference Voxelized Phantoms

8.1 Introduction

The goal of this dissertation is to determine dose to any fully-, partially- or indirectly irradiated organ for CT exams that use tube current modulation (TCM). As stated previously, this requires validated TCM schemes for reference voxelized phantoms that have all radiosensitive organs identified, such as the GSF and ICRP reference voxelized phantoms described in Chapter 4 [5,22]. Currently, there are no such validated TCM schemes for these patient models, nor are there available estimates of patient size (i.e. attenuation information) or even estimated topograms from which size data could be estimated. However, the investigations in Chapter 7 demonstrated the ability to estimate the TCM function for any patient model, even when no size data or topogram data existed. This approach can be applied to the GSF and ICRP models to estimate TCM schemes, which in turn would allow the estimation of organ and effective doses using Monte Carlo simulation techniques.

The purpose of this chapter was to estimate organ and effective doses for several clinical CT protocols that use TCM and to do this for a range of patient models of different sizes. To accomplish this, the GSF and ICRP reference voxelized phantoms described in Chapter 4 were used as they have all radiosensitive organs identified, which allowed for the estimation of both organ doses and effective doses (using both ICRP Report 60 and ICRP Report 103 definitions). Because no TCM function, size data or topogram data exists for these models, the TCM function for each protocol and each patient model was based on: (1) the methods for developing TCM schemes from size data described in Chapter 6, (2) the size data described in Chapter 5 and (3)

the methods for simulating a topogram and estimating size data described in Chapter 7. When put together, these methods allowed for the estimation of TCM schemes which were included in Monte Carlo simulations to estimate doses to fully-, partially- and indirectly-irradiated organs for TCM CT examinations. Effective doses were then calculated from the organ dose estimates. As a comparative reference, organ doses and effective dose were also estimated from fixed tube current (FTC) simulations.

8.2 Methods

8.2.1 Topogram Simulations and Estimation of Patient Size Information

For each of the GSF and ICRP reference voxelized phantoms, patient attenuation profiles in the anterior-posterior (AP) direction were simulated using the methods described in Section 7.2.1. Patient attenuation profiles were determined along the length of each phantom at increments equal to the phantom-specific slice thicknesses presented in Table 4.2. As mentioned in Chapter 7, the determination of patient attenuation profiles at each table location is analogous to simulating an AP topogram.

From the simulated topogram, estimates of the AP and LAT dimensions of patient size were calculated using the methods described in Section 7.2.2 and Section 7.2.3, respectively. Clinically, nearly all topograms are acquired at 120 kVp, even for pediatric patients, so in this investigation, all simulations were performed using a beam energy of 120 kVp. Estimates of patient size, though, are independent of the beam energy used in the simulation. Because the calculations of AP and LAT dimension of patient size (Eq. 7.2 and Eq. 7.5) include the linear

attenuation coefficient of water at the prescribed beam energy, any beam energy can be used to simulate patient attenuation for these voxelized phantoms. Figure 8.1 shows the AP and LAT dimensions of patient size determined from the whole body simulated topogram of the Visible Human reference voxelized phantom. This attenuation data is completely independent of the CT imaging protocol, so this attenuation data can be used to generate TCM schemes for any set of technical parameters within the boundaries of the voxelized phantom anatomy.

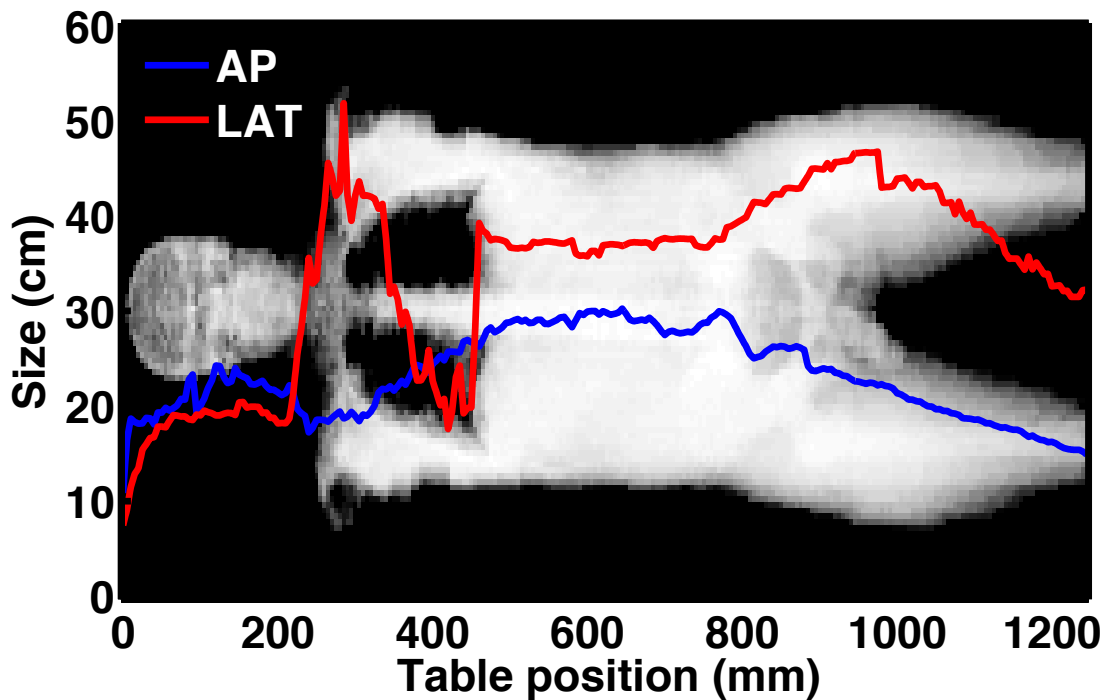


Figure 8.1. AP and LAT dimensions of patient size determined from the whole body simulated topogram of the Visible Human reference voxelized phantom.

8.2.2 Tube Current Modulation Schemes

For each of the GSF and ICRP reference voxelized phantoms, estimates of AP and LAT dimensions of patient size were used as the inputs to the methods to estimate Siemens TCM schemes described in Chapter 6. TCM schemes were generated for four routine body CT protocols: (1) Abdomen, (2) Abdomen/Pelvis, (3) Chest and (4) Chest/Abdomen/Pelvis (CAP). Table 8.1 outlines the prescribed scan ranges for each of these simulated protocols. These scan ranges were based on CT scan protocols published by the American Association of Physicists in Medicine (AAPM) [23-25].

Table 8.1. Scan ranges for protocols used in this investigation.

Protocol	Scan start	Scan end
Abdomen	Top of liver	Iliac crest
Abdomen/pelvis	Top of liver	Pubic symphysis
Chest	Top of lung	Top of adrenals
Chest/abdomen/pelvis (CAP)	Top of lung	Pubic symphysis

All simulations were performed using a model of a Siemens Definition Flash CT scanner, which was determined using the approach described by Turner *et al.* [21]. Table 8.2 outlines the technical parameters used in the Monte Carlo simulations. At 120 kVp, the Definition Flash has a tube limit of 800 mA [18]. For FTC scans, a tube current of 400 mA was used (200 QRM with 0.5 s rotation time). For each simulation, in order to model some form of z-axis over-ranging/over-prescription, a single beam width (nominal collimation listed in Table 8.2) was added to each side of the scan range. Protocol-specific adult reference patient attenuation, A_{ref} , values are listed in Table 8.3. Figure 8.2 shows TCM schemes for each protocol of interest for the Visible Human reference voxelized phantom. Each TCM schemes was determined using the

attenuation data shown in Figure 8.1, the technical settings presented in Table 8.2 and the respective A_{ref} values indexed in Table 8.3.

Table 8.2. Technical settings used for all Monte Carlo simulations.

Parameter	Setting
kVp	120
Quality reference mAs (QRM)	200
Rotation time (s)	0.5
Pitch	1
Collimation (mm)	38.4
Bowtie filter	W1+W3

Table 8.3. Protocol-specific adult reference attenuation values for protocols of interest in this investigation. Corresponding water-equivalent length given in parentheses. For Siemens Definition class scanners, both pediatric and adult patients are scanned with the same set of reference attenuation values. For Siemens Sensation class scanners, pediatric patients are scanned with a different set of reference attenuation values. In this investigation, a Definition Flash scanner model was used in the simulations, so both pediatric and adult reference voxelized phantoms were scanned with this set of reference attenuation values.

Protocol	Reference attenuation (A_{ref})
Abdomen	1000 (~35 cm)
Abdomen/pelvis	1000 (~35 cm)
Chest	600 (~32 cm)
Chest/abdomen/pelvis (CAP)	600 (~32 cm)

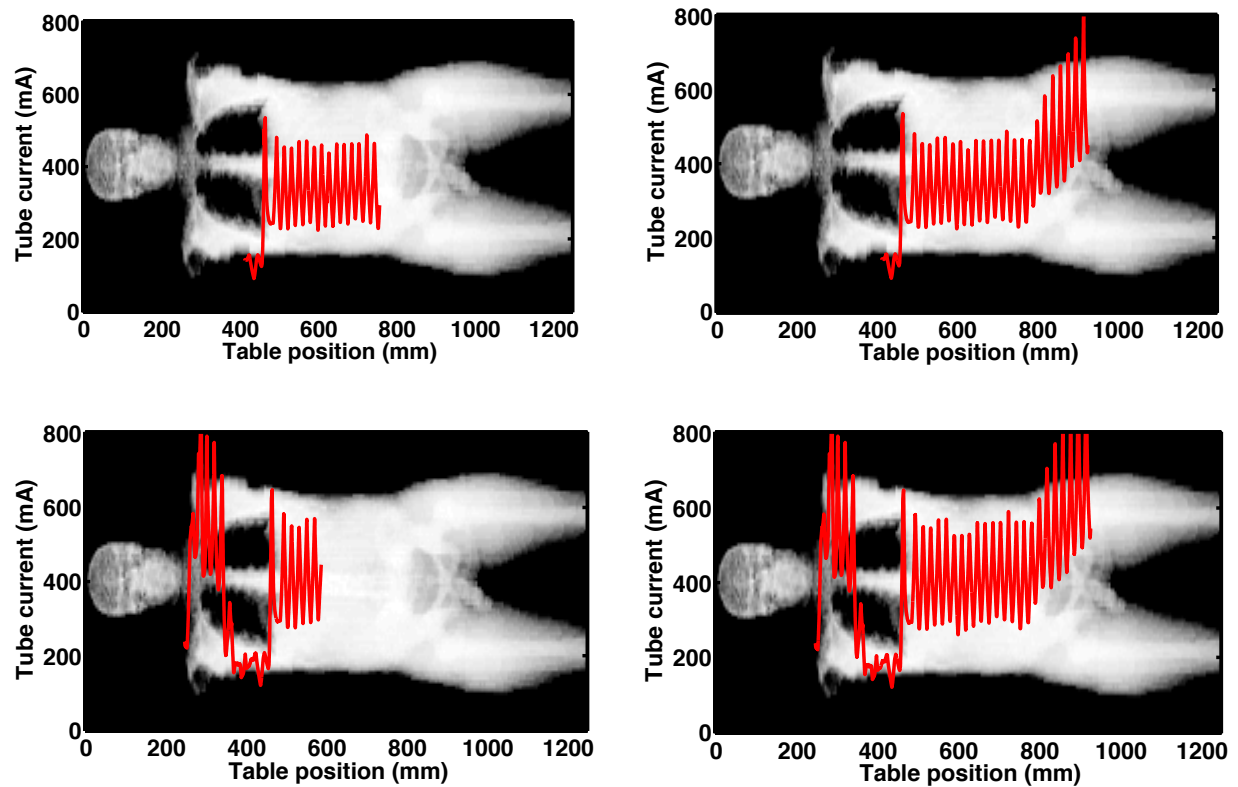


Figure 8.2. Visible Human reference voxelized phantom TCM schemes for abdomen (top left), abdomen/pelvis (top right), chest (bottom left) and CAP (bottom right) protocols.

8.2.3 Organ Dose and Effective Dose

Once TCM schemes were determined for each combination of voxelized phantom and scan protocol, doses to all radiosensitive organs were estimated using detailed Monte Carlo simulations of TCM and FTC CT exams. Table 8.4 lists all organs of interest whose doses are tallied within each of the Monte Carlo simulations in this investigation. This list includes all organs in the ICRP Publication 103 and ICRP Publication 60 calculations of effective dose [11,10]. As described in Section 4.4, if any organs of interest were not explicitly identified in all reference voxelized phantoms, appropriate anatomical substitutes were suggested based on relative anatomical location. Any anatomical substitutes are given in parentheses in Table 8.4.

For each combination of voxelized phantom and scan protocol, ICRP Publication 103 and ICRP Publication 60 estimates of effective dose were also calculated.

Table 8.4. Organs of interest whose doses are tallied within each of the Monte Carlo simulations in this investigation. Anatomical substitutes are given in parentheses.

Organ (Organ substitute)
Breast
Colon
Lung
Red bone marrow
Stomach
Gonads (Prostate/Uterus)
Bladder
Esophagus (Thymus)
Liver
Thyroid
Bone surface
Brain
Salivary glands (Brain)
Skin
Adrenals
Extrathoracic (ET) region (Thyroid)
Gall Bladder (Pancreas)
Heart
Kidneys
Lymphatic nodes (Muscle)
Muscle
Oral mucosa (Brain)
Pancreas
Prostate/Uterus
Small intestine (Stomach)
Spleen
Thymus

The novelty of Monte Carlo simulations of TCM CT exams for whole body reference voxelized phantoms is the ability to estimate dose to any of the organs listed in Table 8.4, even if they are partially within or completely outside of the scan range. For each voxelized phantom

and scan protocol, individual organs were irradiated to different extents. In this investigation, for a given protocol, if an organ was 100% irradiated (i.e. all voxels are within the scan range) in all reference voxelized phantoms, that organ was considered to be fully-irradiated for that protocol. If the organ was irradiated any percentage greater than 0% and less than 100% in any reference voxelized phantom for a given protocol, that organ was considered to be partially-irradiated for that protocol. Finally, if, for a given protocol, the organ was 0% irradiated in all reference voxelized phantoms, that organ was considered to be indirectly-irradiated for that protocol. Table 8.5 outlines the criteria for each classification of organ irradiation. For each voxelized phantom and protocol, the irradiation percentage for each organ was determined by dividing the number of organ voxels within the scan range by the total number of voxels for the organ. Organ irradiation percentages for each voxelized phantom and protocol can be found in Appendix A. Table 8.6-Table 8.9 present organ irradiation classifications for each organ for all protocols used in this investigation. These organ irradiation classifications were determined according to the criteria presented in Table 8.5.

Table 8.5. Criteria for organ irradiation classification for each organ for a given protocol.

Organ irradiation classification	Criteria
Fully-irradiated	Organ 100% irradiated in all reference voxelized phantoms
Partially-irradiated	Organ irradiated any percentage greater than 0% and less than 100% in any reference voxelized phantom
Indirectly-irradiated	Organ 0% irradiated in all reference voxelized phantoms

Table 8.6. Organ irradiation classifications for abdomen protocol. ICRP Publication 103 and ICRP Publication 60 tissue weighting factors for each organ are also presented.

Organ	Organ irradiation classification	ICRP 103 Tissue weighting factor	ICRP 60 Tissue weighting factor
Adrenals	Fully	Remainder (0.12)	Remainder (0.05)
Gall Bladder	Fully	Remainder (0.12)	---
Kidneys	Fully	Remainder (0.12)	Remainder (0.05)
Liver	Fully	0.04	0.05
Pancreas	Fully	Remainder (0.12)	Remainder (0.05)
Spleen	Fully	Remainder (0.12)	Remainder (0.05)
Stomach	Fully	0.12	0.12
Bladder	Partially	0.04	0.05
Bone surface	Partially	0.01	0.01
Breast	Partially	0.12	0.05
Colon	Partially	0.12	0.12
Esophagus	Partially	0.04	0.05
Gonads	Partially	0.08	0.2
Heart	Partially	Remainder (0.12)	---
Lung	Partially	0.12	0.12
Lymphatic nodes	Partially	Remainder (0.12)	---
Muscle	Partially	Remainder (0.12)	Remainder (0.05)
Prostate/Uterus	Partially	Remainder (0.12)	Remainder (0.05)
Red bone marrow	Partially	0.12	0.12
Skin	Partially	0.01	0.01
Small intestine	Partially	Remainder (0.12)	Remainder (0.05)
Thymus	Partially	Remainder (0.12)	Remainder (0.05)
Brain	Indirectly	0.01	Remainder (0.05)
ET region	Indirectly	Remainder (0.12)	---
Oral mucosa	Indirectly	Remainder (0.12)	---
Salivary glands	Indirectly	0.01	---
Thyroid	Indirectly	0.04	0.05

Table 8.7. Organ irradiation classifications for abdomen/pelvis protocol. ICRP Publication 103 and ICRP Publication 60 tissue weighting factors for each organ are also presented.

Organ	Organ irradiation classification	ICRP 103 Tissue weighting factor	ICRP 60 Tissue weighting factor
Adrenals	Fully	Remainder (0.12)	Remainder (0.05)
Bladder	Fully	0.04	0.05
Colon	Fully	0.12	0.12
Gall Bladder	Fully	Remainder (0.12)	---
Kidneys	Fully	Remainder (0.12)	Remainder (0.05)
Liver	Fully	0.04	0.05
Pancreas	Fully	Remainder (0.12)	Remainder (0.05)
Prostate/Uterus	Fully	Remainder (0.12)	Remainder (0.05)
Small intestine	Fully	Remainder (0.12)	Remainder (0.05)
Spleen	Fully	Remainder (0.12)	Remainder (0.05)
Stomach	Fully	0.12	0.12
Bone surface	Partially	0.01	0.01
Breast	Partially	0.12	0.05
Esophagus	Partially	0.04	0.05
Gonads	Partially	0.08	0.2
Heart	Partially	Remainder (0.12)	---
Lung	Partially	0.12	0.12
Lymphatic nodes	Partially	Remainder (0.12)	---
Muscle	Partially	Remainder (0.12)	Remainder (0.05)
Red bone marrow	Partially	0.12	0.12
Skin	Partially	0.01	0.01
Thymus	Partially	Remainder (0.12)	Remainder (0.05)
Brain	Indirectly	0.01	Remainder (0.05)
ET region	Indirectly	Remainder (0.12)	---
Oral mucosa	Indirectly	Remainder (0.12)	---
Salivary glands	Indirectly	0.01	---
Thyroid	Indirectly	0.04	0.05

Table 8.8. Organ irradiation classifications for chest protocol. ICRP Publication 103 and ICRP Publication 60 tissue weighting factors for each organ are also presented.

Organ	Organ irradiation classification	ICRP 103 Tissue weighting factor	ICRP 60 Tissue weighting factor
Breast	Fully	0.12	0.05
Heart	Fully	Remainder (0.12)	---
Lung	Fully	0.12	0.12
Thymus	Fully	Remainder (0.12)	Remainder (0.05)
Adrenals	Partially	Remainder (0.12)	Remainder (0.05)
Bone surface	Partially	0.01	0.01
Colon	Partially	0.12	0.12
Esophagus	Partially	0.04	0.05
ET region	Partially	Remainder (0.12)	---
Gall Bladder	Partially	Remainder (0.12)	---
Kidneys	Partially	Remainder (0.12)	Remainder (0.05)
Liver	Partially	0.04	0.05
Lymphatic nodes	Partially	Remainder (0.12)	---
Muscle	Partially	Remainder (0.12)	Remainder (0.05)
Pancreas	Partially	Remainder (0.12)	Remainder (0.05)
Red bone marrow	Partially	0.12	0.12
Skin	Partially	0.01	0.01
Small intestine	Partially	Remainder (0.12)	Remainder (0.05)
Spleen	Partially	Remainder (0.12)	Remainder (0.05)
Stomach	Partially	0.12	0.12
Thyroid	Partially	0.04	0.05
Bladder	Indirectly	0.04	0.05
Brain	Indirectly	0.01	Remainder (0.05)
Gonads	Indirectly	0.08	0.2
Oral mucosa	Indirectly	Remainder (0.12)	---
Prostate/Uterus	Indirectly	Remainder (0.12)	Remainder (0.05)
Salivary glands	Indirectly	0.01	---

Table 8.9. Organ irradiation classifications for CAP protocol. ICRP Publication 103 and ICRP Publication 60 tissue weighting factors for each organ are also presented.

Organ	Organ irradiation classification	ICRP 103 Tissue weighting factor	ICRP 60 Tissue weighting factor
Adrenals	Fully	Remainder (0.12)	Remainder (0.05)
Bladder	Fully	0.04	0.05
Breast	Fully	0.12	0.05
Colon	Fully	0.12	0.12
Gall Bladder	Fully	Remainder (0.12)	---
Heart	Fully	Remainder (0.12)	---
Kidneys	Fully	Remainder (0.12)	Remainder (0.05)
Liver	Fully	0.04	0.05
Lung	Fully	0.12	0.12
Pancreas	Fully	Remainder (0.12)	Remainder (0.05)
Prostate/Uterus	Fully	Remainder (0.12)	Remainder (0.05)
Small intestine	Fully	Remainder (0.12)	Remainder (0.05)
Spleen	Fully	Remainder (0.12)	Remainder (0.05)
Stomach	Fully	0.12	0.12
Thymus	Fully	Remainder (0.12)	Remainder (0.05)
Bone surface	Partially	0.01	0.01
Esophagus	Partially	0.04	0.05
ET region	Partially	Remainder (0.12)	---
Gonads	Partially	0.08	0.2
Lymphatic nodes	Partially	Remainder (0.12)	---
Muscle	Partially	Remainder (0.12)	Remainder (0.05)
Red bone marrow	Partially	0.12	0.12
Skin	Partially	0.01	0.01
Thyroid	Partially	0.04	0.05
Brain	Indirectly	0.01	Remainder (0.05)
Oral mucosa	Indirectly	Remainder (0.12)	---
Salivary glands	Indirectly	0.01	---

8.3 Results

Table 8.10 lists simulated organ doses and ICRP Publication 103 calculations of effective dose for both TCM and FTC for all protocols for the Visible Human reference voxelized phantom.

The TCM organ doses were based on simulations using the TCM schemes shown in Figure 8.2.

Because of the extensive nature of this data, organ doses and ICRP Publication 103 calculations of effective dose for all other reference voxelized phantoms can be found in Appendix B. Organ doses and ICRP Publication 60 calculations of effective dose for all reference voxelized phantoms can be found in Appendix C.

Table 8.10. Simulated organ doses and ICRP Publication 103 calculations of effective dose for the Visible Human reference voxelized phantom. Values are tabulated for both TCM and FTC for all protocols used in this investigation.

Organ	ICRP 103 Tissue weighting factor (w_T)	Dose (mGy)								
		FTC				TCM				
		Abd	AbdPel	Chest	CAP	Abd	AbdPel	Chest	CAP	
Primary organs	Breast	0.12	0.00	0.00	0.00	0.00	0.00	0.00	0.00	0.00
	Colon	0.12	12.83	16.44	4.57	16.65	10.88	15.46	5.26	18.61
	Lung	0.12	7.30	7.32	15.44	15.71	5.95	5.99	14.18	14.48
	Red bone marrow	0.12	2.37	3.95	3.25	5.74	1.94	4.13	3.40	6.75
	Stomach	0.12	14.38	14.46	14.10	15.82	12.14	12.21	14.46	15.99
	Gonads	0.08	0.10	2.97	0.01	2.31	0.07	5.90	0.01	6.01
	Bladder	0.04	0.69	11.74	0.04	11.63	0.56	17.31	0.03	18.49
	Esophagus	0.04	6.34	6.39	15.07	15.33	5.15	5.19	16.47	16.78
	Liver	0.04	13.94	14.00	13.00	15.18	11.69	11.77	12.88	15.34
	Thyroid	0.04	0.72	0.72	20.56	20.62	0.58	0.58	32.37	32.58
	Bone surface	0.01	11.56	18.93	15.52	27.42	9.48	19.73	16.20	32.13
	Brain	0.01	0.02	0.03	0.21	0.21	0.02	0.02	0.26	0.27
	Salivary glands	0.01	0.15	0.16	1.54	1.55	0.13	0.14	1.92	1.94
	Skin	0.01	4.50	8.29	3.30	9.58	3.77	8.70	3.55	11.66
Remainder organs	Adrenals		10.73	10.87	8.99	11.70	9.00	9.05	8.50	11.48
	ET region		0.72	0.72	20.56	20.62	0.58	0.58	32.37	32.58
	Gall Bladder		16.65	16.80	13.11	16.23	13.38	13.56	14.10	16.90
	Heart		11.46	11.47	18.51	18.83	10.25	10.29	17.44	17.78
	Kidneys		14.12	14.43	5.59	14.69	12.08	12.47	5.04	15.30
	Lymphatic nodes		3.78	6.29	4.44	8.77	3.11	6.78	4.61	10.48
	Muscle	0.12	3.78	6.29	4.44	8.77	3.11	6.78	4.61	10.48
	Oral mucosa		0.02	0.03	0.21	0.21	0.02	0.02	0.26	0.27
	Pancreas		12.91	13.03	9.90	13.71	10.80	10.93	10.33	13.88
	Prostate/Uterus		0.31	7.45	0.02	7.61	0.25	12.09	0.02	12.56
	Small intestine		14.22	16.45	3.50	16.63	11.88	14.64	3.82	17.76
	Spleen		13.43	13.54	12.72	14.46	11.47	11.62	12.85	14.88
	Thymus		1.03	1.01	22.47	22.41	0.82	0.83	32.69	32.56
Effective dose (mSv)			6.41	7.98	7.78	11.17	5.37	7.70	8.52	12.88

8.4 Discussion

The results from this investigation indicate that TCM schemes can be reasonably estimated for the GSF and ICRP reference voxelized phantoms using the methods described in Chapter 6 and 7. These TCM schemes were used in Monte Carlo simulations to estimate dose to 27 individual organs for a variety of routine body CT protocols. ICRP Publication 103 and ICRP Publication 60 effective dose estimate were also calculated using these organ doses and the appropriate tissue weighting factors.

While this investigation provided an expansive set of organ dose and effective dose estimates for a variety of protocols and patient sizes, this work was limited to absolute organ doses determined for the exact scanning conditions prescribed in this investigation for patients of equivalent size to the reference voxelized phantoms only. As mentioned in Section 8.2.2, a uniform set of technical parameters was used for each simulation (Table 8.2), even though in the clinic, parameters may be adjusted according to the clinical indication, patient size or patient age. Because of this, the absolute organ doses from this investigation are not necessarily reflective of the organ doses a patient of equivalent size to any one of the reference voxelized phantoms would have received. Because TCM adjusts for patient size, this effect was most pronounced for FTC organ doses. For example, for the Baby reference voxelized phantom, the colon dose was 35.62 mGy (Section B.1 from Appendix B) for the FTC abdomen/pelvis simulation and only 3.10 mGy for the TCM abdomen/pelvis simulation. In the clinic, the technical settings would be adjusted to account for the Baby's small size, so the FTC colon dose would not actually be more than 10 times the TCM colon dose.

That being said, in Chapter 9, the effects of patient size on scanner output-normalized organ dose estimates will be explored, so in order to allow the simulations results to be as comparable as possible across all voxelized phantoms so that the effects of patient size can be isolated, the simulations needed to be performed with a constant set of technical parameters. Therefore, the organ doses determined in this investigation will serve as the raw organ dose data for the size-specific, scan technique-independent organ dose estimates that will be described in Chapter 9 [31-33].

8.5 References

21. N. Petoussi-Henss, M. Zankl, U. Fill, D. Regulla, "The GSF family of voxel phantoms," *Phys. Med. Biol.* 47, 89-106 (2002).
22. International Commission on Radiological Protection, "Adult Reference Computation Phantoms," ICRP Publication 110 (2009).
23. American Association of Physicists in Medicine, "Adult Routine Abdomen/Pelvis CT Protocols Version 1.1," AAPM (2015).
24. American Association of Physicists in Medicine, "Adult Routine Chest CT Protocols Version 1.0," AAPM (2012).
25. American Association of Physicists in Medicine, "Adult Routine Chest-Abdomen-Pelvis CT Protocols Version 1.0," AAPM (2014).
26. A. C. Turner *et al.*, "A method to generate equivalent energy spectra and filtration models based on measurements for multidetector CT Monte Carlo dosimetry simulations," *Med. Phys.* **36**, 2154-2164 (2009).

27. Centre for Evidence-based Purchasing (CEP), “128 to 320 slice CT scanners technical specifications: Comparative specifications,” CEP 08028 (2009).
28. International Commission on Radiological Protection, “The 2007 Recommendations of the International Commission on Radiological Protection,” ICRP Publication 103 (2007).
29. International Commission on Radiological Protection, “1990 Recommendations of the International Commission on Radiological Protection,” ICRP Publication 60 (1991).
30. A. C. Turner *et al.*, “The feasibility of a scanner-independent technique to estimate organ dose from MDCT scans: Using CTDIvol to account for differences between scanners,” *Med. Phys.* **37**, 1816-1825 (2010).
31. A. C. Turner *et al.*, “The feasibility of patient size-corrected, scanner-independent organ dose estimates for abdominal CT exams,” *Med. Phys.* **38**, 820-829 (2011).
32. K. McMillan *et al.*, “Size-specific, scanner-independent organ dose estimates in contiguous axial and helical head CT examinations,” *Med. Phys.* **41**, 121909 (2014).

Chapter 9: Size-Specific, Scan Technique-Independent Organ Dose and Effective Dose Estimates in Tube Current Modulation CT Examinations

9.1 Introduction

In Chapter 8, absolute estimates of organ dose (in mGy) and effective dose (in mSv) were determined for the GSF and ICRP reference voxelized phantoms using Monte Carlo simulations of tube current modulation (TCM) CT examinations. These dose estimates, though, were limited to a single set of technical parameter settings (specified kV, mA, etc.). Therefore, the application of those dose estimates is limited to patients of the same size as the reference voxelized phantoms who are scanned using the exact conditions prescribed in the Monte Carlo simulations. Given the limitations of the dose estimates presented in Chapter 8, methods to account for variation in patient size and scan technique in organ dose estimates for TCM CT exams are necessary.

Previous work by Turner *et al.* using the GSF reference voxelized phantoms suggested that scan technique-independent organ dose estimates can be determined by normalizing organ doses by a scanner output metric [31]. That work focused on fixed tube current (FTC) CT examinations, and the scanner output metric was the scanner-reported volume CT dose index ($CTDI_{vol}$). $CTDI_{vol}$ is directly related to technique settings, such as nominal collimation, beam energy, pitch, rotation time and tube current, but it is independent of the scan range. By normalizing an individual organ dose by $CTDI_{vol}$, a $CTDI_{vol}$ -to-organ-dose conversion coefficient is created that can be used to estimate dose to that organ for a similar scan range using any technique. The dose estimate, though, does not take different patient sizes into account. Expanding this idea of scan technique-independent organ dose estimates to TCM,

Khatonabadi *et al.* demonstrated that scanner-reported $CTDI_{vol}$ weighted by the average tube current over a specific organ ($CTDI_{vol,organ}$) or region of the scan range ($CTDI_{vol,regional}$) could be used to reasonably determine scan technique-independent organ dose estimates from TCM CT exams [46]. Unlike scanner-reported $CTDI_{vol}$, which is based on the average tube current over the entire scan range, these modified versions of $CTDI_{vol}$ take into account local variations in the tube current profile from a TCM CT exam. That work was based on Monte Carlo simulation of models of actual patient anatomy, so its application was limited to a select few fully-irradiated organs.

Further work by Turner *et al.* using the GSF reference voxelized phantoms suggested that relationships between scan technique-independent organ dose and patient size can be used to estimate organ dose for any patient size using any set of technical parameters [32]. Strongly correlated exponential relationships between $CTDI_{vol}$ -to-organ-dose conversion coefficients and a measure of patient perimeter were demonstrated for a wide variety of organs for FTC abdomen/pelvis CT exams. The concept of correcting dose for patient size was further investigated in AAPM Report 204 [36]. In that report, conversion coefficients were determined to correct $CTDI_{vol}$ for patient size ($CTDI_{vol}$ -to-patient-dose conversion coefficients). These $CTDI_{vol}$ -to-patient-dose conversion coefficients were determined as a function of effective diameter. Effective diameter is the diameter of a circle that has the same cross-sectional area as the patient. Beyond being limited to FTC, the major limitation of the work by Turner *et al.* and AAPM Report 204 is the use of size metrics based only on the physical dimensions of a patient and which did not account for a patient's attenuation. Differences in attenuation properties across different regions of the body cannot be accounted for by a geometric measure of size. For example, while regions of the thorax and abdomen may have the same the same physical

dimensions, the composition and density of tissue within each region is drastically different. This will result in different absorbed doses within each region for scans performed at the same $CTDI_{vol}$. Because of this, an attenuation-based size metric is needed to truly capture the differences in attenuation properties across different regions of the body.

A recently proposed attenuation-based patient size metric in diagnostic CT is water-equivalent diameter (WED) [13]. Because water is a major component of the human body, for dose purposes, patient anatomy can be modeled as a cylindrical water phantom. Often measured retrospectively from the topogram or axial image data, WED expresses patient attenuation in terms of the diameter of a cylinder of water having the same average attenuation as the patient. This accounts for the lower attenuation observed in the chest region due to air-filled lungs as well as increased attenuation due to bone in the pelvic region. Work by Bostani *et al.* demonstrated strong correlation between $CTDI_{vol,regional}$ -to-organ-dose conversion coefficients and WED for TCM chest and abdomen/pelvis CT examinations [6]. That work, though, was limited to a select few fully-irradiated organs.

As described in Chapter 5, size data extracted from the DICOM header of the topogram can be used to calculate a reasonable estimate of WED. Therefore, using the size data estimated from the simulated topograms of the GSF and ICRP reference voxelized phantoms, estimates of WED can be determined for each voxelized phantom.

Using the organ doses determined for the GSF and ICRP reference voxelized phantoms in Chapter 8, the purpose of this investigation was to develop size-specific, scan technique-independent organ dose estimates for all radiosensitive organs for TCM CT examinations. Estimates were developed using two approaches: (1) Protocol-specific and (2) organ-specific. For the protocol-specific approach, organ doses were first normalized by $CTDI_{vol}$ based on the

average tube current across the entire scan range ($CTDI_{vol,protocol}$). Then, correlations between $CTDI_{vol,protocol}$ -normalized organ doses and WED determined at the center of the scan range ($WED_{protocol}$) were established. For the organ-specific approach, organ doses were first normalized by $CTDI_{vol}$ based on the average tube current across all slices containing the organ of interest ($CTDI_{vol,organ}$). Then, correlations between $CTDI_{vol,organ}$ -normalized organ doses and the average WED across all slices containing the organ of interest (WED_{organ}) were established. Exponential regression equations describing these correlations serve as the means to generate scan technique-independent organ dose estimates for any patient size. Regression equations were determined for each combination of organ and scan protocol used in this investigation. Additionally, because size-specific, scan technique-independent organ dose estimates were developed for all fully-, partially- and indirectly-irradiated radiosensitive organs, this allows size-specific, scan technique-independent effective dose estimates to be developed. As a comparative reference, size-specific, scan technique-independent organ dose and effective dose estimates were also developed for FTC CT exams.

9.2 Methods

9.2.1 Overview of Monte Carlo Simulations

Organ doses and effective doses used in this investigation are the result of the Monte Carlo simulations described in Chapter 8. Simulations were performed for four routine body CT protocols: (1) Abdomen, (2) Abdomen/Pelvis, (3) Chest and (4) Chest/Abdomen/Pelvis (CAP). Scan ranges for these protocols are presented in Table 8.1.

As described in Chapter 8, all simulations were performed using an equivalent source model of the Siemens Definition Flash CT scanner. The technical settings for the simulations are presented in Table 8.2. A uniform set of technical parameters was used for all simulations so that the effects of patient size under constant technical parameters could be isolated. Using the technical settings outlined in Table 8.2, $CTDI_{vol}$ measured on a Definition Flash scanner with the body (32 cm diameter) CTDI phantom was 0.068 mGy/mAs. By recording the measured $CTDI_{vol}$ on a per tube current time product basis, $CTDI_{vol}$ can be estimated for any tube current. For example, for the FTC scenario ($400 \text{ mA} \times 0.5 \text{ s}$), the $CTDI_{vol}$ is 13.60 mGy.

Organs of interest whose doses were tallied in the Monte Carlo simulations are presented in Table 8.4. This list includes all organs in the ICRP Publication 103 and ICRP Publication 60 calculations of effective dose [11,10]. For each combination of voxelized phantom and scan scenario, ICRP Publication 103 and ICRP Publication 60 estimates of effective dose were calculated. For each protocol, organ irradiation classification (fully-, partially- and indirectly-irradiated) as defined in Table 8.5, is tabulated in Table 8.6 – Table 8.9.

9.2.2 Patient Size Metrics – $WED_{protocol}$ and WED_{organ}

For each GSF and ICRP reference voxelized phantom protocol, two estimates of patient size were determined: (1) protocol-specific patient size and (2) organ-specific patient size. Protocol-specific patient size was determined as the WED in the central slice of the scan range ($WED_{protocol}$). This protocol-specific estimate characterizes the patient size for a given protocol. This method for determining patient size is in line with the recommendations of AAPM Report 220 [13]. An organ-specific estimate of patient size was determined as the average WED across

all slices containing the organ of interest (WED_{organ}). This organ-specific estimate characterizes patient size at the anatomical location of a particular organ. In order to determine WED_{organ} , the organ of interest must be fully within the scan range. Therefore, size-specific organ dose estimates determined using WED_{organ} could only be determined for fully-irradiated organs.

Figure 9.1 shows the anterior-posterior (AP) and lateral (LAT) estimates of patient size determined from the simulated topogram of the Visible Human reference voxelized phantom. Also shown is an estimate of WED calculated at each table position using Eq. 5.3. As an example of how $WED_{protocol}$ and WED_{organ} are calculated for the lungs for a chest protocol, the chest scan range, the center of the scan range and the anatomical extent of the lungs are all annotated on the size data. $WED_{protocol}$ is calculated as the WED at the table location at the center of the scan range. WED_{organ} is calculated as the average WED over all table positions within the anatomical extent of the lungs.

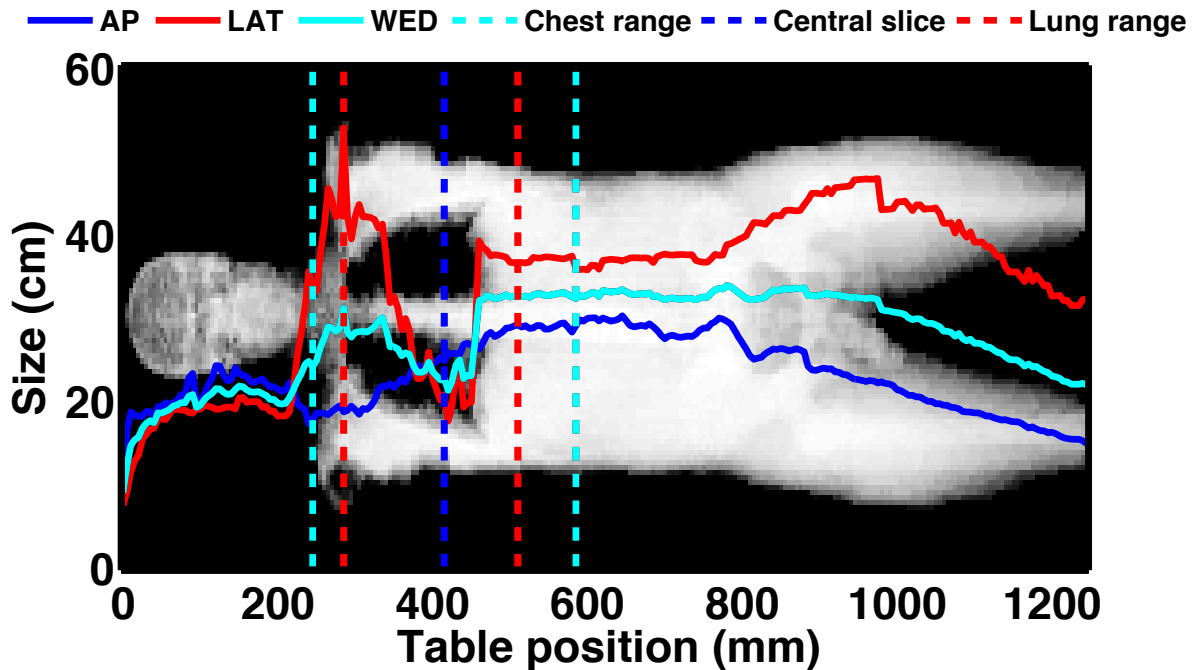


Figure 9.1. Patient size data for Visible Human reference voxelized phantom. Chest protocol scan range, central table position of scan range and lung extent annotated on size data. WED_{protocol} calculated as the WED at the table location at the center of the scan range. WED_{organ} calculated as the average WED over all table positions within the anatomical extent of the lungs.

9.2.3 Scanner Output

For each GSF and ICRP reference voxelized phantom and protocol, two estimates of scanner output were determined: (1) protocol-specific scanner output and (2) organ-specific scanner output. Protocol-specific scanner output was determined as $CTDI_{\text{vol}}$ based on the average tube current across the entire scan range ($CTDI_{\text{vol,protocol}}$). This is the same value of $CTDI_{\text{vol}}$ that would be displayed on the scanner console at the conclusion of a CT scan. Organ-specific scanner output was determined as $CTDI_{\text{vol}}$ based on the average tube current across all slices containing the organ of interest ($CTDI_{\text{vol,organ}}$). This organ-specific estimate better characterizes local

changes in the tube current profile. As with WED_{organ} , $CTDI_{vol,organ}$ is only available for organs that are fully-irradiated within the scan range.

Figure 9.2 shows the chest TCM scheme and FTC profile for the Visible Human reference voxelized phantom. As an example of how $CTDI_{vol,protocol}$ and $CTDI_{vol,organ}$ are calculated for the lungs for a chest protocol, the chest scan range and the anatomical extent of the lungs are annotated on the TCM scheme. $CTDI_{vol,protocol}$ is calculated as $CTDI_{vol}$ based on the average tube current across all table positions within the chest scan range. $CTDI_{vol,organ}$ is calculated as $CTDI_{vol}$ based on the average tube current over all table positions within the anatomical extent of the lungs. For the FTC scenario, $CTDI_{vol,protocol}$ is equal to $CTDI_{vol,organ}$.

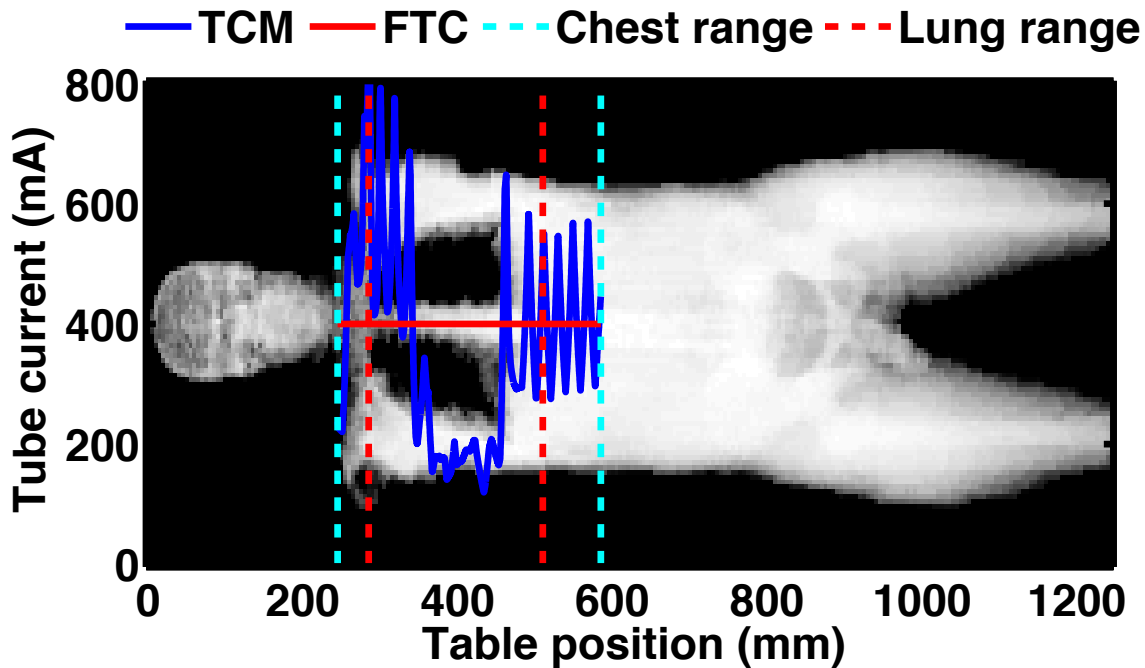


Figure 9.2. Chest protocol TCM scheme and FTC profile for Visible Human reference voxelized phantom. Chest protocol scan range and lung extent annotated on tube current profiles. $CTDI_{vol,protocol}$ based on the average tube current across the entire chest scan range. $CTDI_{vol,organ}$ based on the average tube current across all slices containing the lungs.

9.2.4 Size-Specific, Scan Technique-Independent Organ Dose Estimates

For each combination of organ and protocol, the size-specific, scan technique-independent organ dose estimates are determined using: (1) A protocol-specific approach and (2) an organ-specific approach. For the protocol-specific approach, organ doses for each of the GSF and ICRP voxelized phantoms were first normalized by the corresponding $CTDI_{vol,protocol}$. Because both organ dose and $CTDI_{vol,protocol}$ are quoted in units of mGy, this normalization results in a unitless value. Then, correlations between $CTDI_{vol,protocol}$ -normalized organ doses and $WED_{protocol}$ were established. Correlations were established for both FTC and TCM organ doses.

For the organ-specific approach, organ doses for each of the GSF and ICRP voxelized phantoms were first normalized by the corresponding $CTDI_{vol,organ}$. Like the protocol-specific approach, this normalization produces a unitless value. Then, correlations between $CTDI_{vol,organ}$ -normalized organ doses and WED_{organ} were established. Correlations were established for both FTC and TCM organ doses. Because $CTDI_{vol,organ}$ and WED_{organ} can only be determined for fully-irradiated organs, size-specific, scan technique-independent organ dose estimates determined using the organ-specific approach can only be determined for fully-irradiated organs.

It should be emphasized that organ doses for all patient models, including pediatric patients (i.e. Baby and Child), were normalized by $CTDI_{vol}$ measured with the 32 cm diameter body CTDI phantom. This was done to hold all parameters constant except for patient size. Additionally, all manufactures have agreed (through the International Electrotechnical Commission) to move to the 32 cm diameter body CTDI phantom for all body scans regardless of the patient size or age. This, though, will take time to be implemented in the clinic.

Regression equations describing the correlations between $CTDI_{vol,protocol/organ}$ -normalized organ dose and $WED_{protocol/organ}$ served as the means to generate scan technique-independent organ dose estimates for any patient size (size-specific, scan technique-independent $CTDI_{vol,protocol/organ}$ -to-organ-dose conversion coefficients). Because of the exponential relationship between x-ray beam intensity and patient size observed in previous investigations, an exponential relationship between $CTDI_{vol}$ -normalized organ dose and patient size was used for all organs and protocols for both the protocol-specific and organ-specific approaches [32,9]. For size-specific, scan technique-independent organ dose estimates using the protocol-specific approach, the exponential relationship between $CTDI_{vol}$ -normalized organ dose and patient size is defined as:

$$\frac{D_{organ,protocol}}{CTDI_{vol,protocol}} = A_0 \times \exp(-B_0 \times WED_{protocol}) \quad (9.1)$$

where A_0 and B_0 are exponential regression coefficients specific to the combination of organ and protocol. For size-specific, scan technique-independent organ dose estimates using the organ-specific approach, the exponential relationship between $CTDI_{vol}$ -normalized organ dose and patient size is defined as:

$$\frac{D_{organ,protocol}}{CTDI_{vol,organ}} = A_0 \times \exp(-B_0 \times WED_{organ}) \quad (9.2)$$

where A_0 and B_0 are exponential regression coefficients specific to the combination of organ and protocol. In order to gauge the strength of these correlations, the coefficient of determination (R^2) was tabulated for each combination of organ and protocol.

9.2.5 Size-Specific, Scan Technique-Independent Effective Dose Estimates

Because effective dose is a weighted average of multiple organ doses, in order to create size-specific effective dose estimates as a function of a single estimate of patient size, size-specific, scan technique-independent effective dose estimates were determined using a protocol-specific approach only. For each protocol, ICRP Publication 103 and ICRP Publication 60 calculations of effective dose for each of the GSF and ICRP voxelized phantoms were first normalized by the corresponding $CTDI_{vol,protocol}$. This normalization results in a value with units of mSv/mGy. Then, correlations between $CTDI_{vol,protocol}$ -normalized effective doses and $WED_{protocol}$ were established. Correlations were established for effective doses calculated using both FTC and TCM organ doses.

As with the organ dose normalization, it should be emphasized that effective doses for all patient models, including pediatric patients (i.e. Baby and Child), were normalized by $CTDI_{vol}$ measured with the 32 cm diameter body CTDI phantom. This was done to hold all parameters constant except for patient size.

Regression equations describing the correlations between $CTDI_{vol,protocol}$ -normalized effective dose and $WED_{protocol}$ served as the means to generate scan technique-independent effective dose estimates for any patient size (size-specific, scan technique-independent $CTDI_{vol,protocol}$ -to-effective-dose conversion coefficients). Because effective dose is based on

organ dose, which correlates with patient size in an exponential fashion, an exponential relationship between $CTDI_{vol}$ -normalized effective dose and patient size was used for all protocols. For size-specific, scan technique-independent effective dose estimates using the protocol-specific approach, the exponential relationship between $CTDI_{vol}$ -normalized effective dose and patient size is defined as:

$$\frac{ED_{protocol}}{CTDI_{vol,protocol}} = A_0 \times \exp(-B_0 \times WED_{protocol}) \quad (9.3)$$

where A_0 and B_0 are exponential regression coefficients specific to the combination of effective dose calculation (i.e. ICRP Publication 103 or ICRP Publication 60) and protocol. In order to gauge the strength of these correlations, the coefficient of determination (R^2) was tabulated for each combination of organ and protocol.

9.2.6 Comparison of Methods to Estimate Effective Dose

A common method to estimate effective dose from a clinically indicated CT examination is to multiply the scanner-reported dose length product (DLP) by a DLP-to-effective-dose conversion factor (k-factor) that is a function of the patient's age and the region of the body that was scanned [10]. DLP is the product of the scanner-reported $CTDI_{vol}$ and the scan length. Because $CTDI_{vol}$ and the scan length can be calculated from the simulated scans, DLP was calculated for each of the scan scenarios described in this investigation. These DLP values were then multiplied by the appropriate k-factor values to calculate estimates of effective dose. Table 9.1 shows the k-

factor values for a variety of patient ages for all protocols of interest in this investigation [10]. For all pediatric protocols, the k-factor values assume the use of the 16 cm diameter head CTDI phantom for the determination of $CTDI_{vol}$. Because all $CTDI_{vol}$ values used in this investigation are based on the 32 cm diameter body CTDI phantom, for Baby and Child, $CTDI_{vol}$ values are multiplied by two to provide an estimate of the corresponding $CTDI_{vol}$ values based on the 16 cm diameter head CTDI phantom. Adult k-factor values assume the use of the 32 cm diameter body CTDI phantom. As tabulated in Table 4.1, Baby is based on an 8 week old patient, so k-factor values for the “0 year old” were used. Child is based on a 7 year old patient, so k-factor values for the “5 year old” were used. For all other voxelized phantoms, k-factor values for the “Adult” were used.

Table 9.1. Age-specific k-factor values for protocols of interest in this investigation.

Region of body	k-factor ($mSv\ mGy^{-1}\ cm^{-1}$)				
	0 year old	1 year old	5 year old	10 year old	Adult
Chest	0.039	0.026	0.018	0.013	0.014
Abdomen (and Abdomen/Pelvis)	0.049	0.030	0.020	0.015	0.015
CAP	0.044	0.028	0.019	0.014	0.015

Multiple methods to estimate effective dose were described in this investigation. For each of the scan scenarios in this investigation, effective dose was estimated using the following methods: (1) $DLP \times k$ -factor, (2) size-specific, scan technique-independent $CTDI_{vol,protocol}$ -to-effective-dose conversion coefficients (Size-Specific Method 1) and (3) weighted average of organ doses estimated using size-specific scan technique-independent $CTDI_{vol,protocol}$ -to-organ-dose conversion coefficients (Size-Specific Method 2). In an effort to understand the accuracy of the various methods to estimate effective dose, effective doses were calculated directly from

simulated organ doses to provide a “gold standard” estimate. For each protocol, the mean error across all reference voxelized phantoms between the “gold standard” and estimated effective doses was then calculated.

9.3 Results

WED_{protocol} values for each voxelized phantom and protocol as well as WED_{organ} values for each fully-irradiated organ can be referenced in Appendix D. For the abdomen protocol, WED_{protocol} across all reference voxelized phantoms ranges from 10.49 cm to 37.62 cm. For the abdomen/pelvis protocol, WED_{protocol} across all reference voxelized phantoms ranges from 10.02 cm to 37.41 cm. For the chest protocol, WED_{protocol} across all reference voxelized phantoms ranges from 9.12 cm to 26.10 cm. For the CAP protocol, WED_{protocol} across all reference voxelized phantoms ranges from 10.32 cm to 37.62 cm.

$CTDI_{\text{vol,protocol}}$ values for each voxelized phantom and protocol as well as $CTDI_{\text{vol,organ}}$ values for each fully-irradiated organ can be referenced in Appendix E. For FTC CT exams, $CTDI_{\text{vol,protocol}}$ is 13.60 mGy for all protocols and reference voxelized phantoms. For the TCM abdomen protocol, $CTDI_{\text{vol,protocol}}$ across all reference voxelized phantoms ranges from 1.16 to 18.77. For the TCM abdomen/pelvis protocol, $CTDI_{\text{vol,protocol}}$ across all reference voxelized phantoms ranges from 1.22 to 18.09. For the TCM chest protocol, $CTDI_{\text{vol,protocol}}$ across all reference voxelized phantoms ranges from 1.46 to 15.85. For the TCM CAP protocol, $CTDI_{\text{vol,protocol}}$ across all reference voxelized phantoms ranges from 1.60 to 18.57.

For size-specific, scan technique-independent organ dose estimates using the protocol-specific (Eq. (9.1)) and organ-specific (Eq. 9.2)) approaches, the exponential regression

coefficients, R^2 and organ irradiation classification for each organ are shown for the abdomen, abdomen/pelvis, chest and CAP protocols in Table 9.2, Table 9.3, Table 9.4 and Table 9.5, respectively. For size-specific, scan technique-independent effective dose estimates using the protocol-specific approach (Eq. (9.3)), the exponential regression coefficients and R^2 for each protocol are shown for ICRP Publication 103 and ICRP Publication 60 calculations of effective dose in Table 9.6 and Table 9.7, respectively. For ICRP Publication 103 effective dose estimates, R^2 across all protocols ranges from 0.79 to 0.90 for both the FTC and TCM scenarios. For ICRP Publication 60 effective dose estimates, R^2 across all protocols ranges from 0.84 to 0.88 and 0.80 to 0.87 for the FTC and TCM scenarios, respectively.

Table 9.2. Exponential regression coefficients and R^2 for each organ for abdomen protocol.

Organ	Organ irradiation classification	FTC						TCM					
		Protocol-specific			Organ-specific			Protocol-specific			Organ-specific		
		A_0	B_0	R^2	A_0	B_0	R^2	A_0	B_0	R^2	A_0	B_0	R^2
Adrenals	Fully	3.87	0.045	0.95	3.91	0.045	0.96	3.27	0.040	0.85	3.76	0.045	0.95
Gall Bladder	Fully	4.06	0.040	0.95	4.03	0.040	0.98	3.56	0.036	0.85	4.21	0.041	0.95
Kidneys	Fully	4.41	0.045	0.98	4.30	0.044	0.99	3.93	0.040	0.91	4.33	0.044	0.98
Liver	Fully	4.17	0.042	0.98	4.31	0.044	0.99	3.63	0.039	0.95	4.30	0.045	0.99
Pancreas	Fully	4.24	0.045	0.98	4.27	0.045	0.99	3.71	0.040	0.94	3.72	0.041	0.95
Spleen	Fully	3.85	0.041	0.94	3.91	0.041	0.98	3.37	0.036	0.84	4.16	0.043	0.98
Stomach	Fully	4.00	0.040	0.98	4.02	0.040	0.99	3.51	0.036	0.95	4.24	0.043	0.98
Bladder	Partially	3.09	0.124	0.62	-	-	-	4.82	0.135	0.68	-	-	-
Bone surface	Partially	3.84	0.050	0.71	-	-	-	4.00	0.053	0.73	-	-	-
Breast	Partially	3.18	0.061	0.46	-	-	-	1.79	0.050	0.23	-	-	-
Colon	Partially	3.32	0.038	0.85	-	-	-	3.50	0.036	0.94	-	-	-
Esophagus	Partially	1.35	0.035	0.38	-	-	-	1.18	0.037	0.36	-	-	-
Gonads	Partially	8.95	0.191	0.44	-	-	-	13.53	0.202	0.47	-	-	-
Heart	Partially	3.20	0.043	0.70	-	-	-	3.04	0.047	0.64	-	-	-
Lung	Partially	2.71	0.050	0.73	-	-	-	2.45	0.054	0.68	-	-	-
Lymphatic nodes	Partially	1.17	0.044	0.62	-	-	-	1.18	0.044	0.62	-	-	-
Muscle	Partially	1.17	0.044	0.62	-	-	-	1.18	0.044	0.62	-	-	-
Prostate/Uterus	Partially	8.59	0.173	0.69	-	-	-	11.96	0.180	0.73	-	-	-
Red bone marrow	Partially	0.81	0.051	0.75	-	-	-	0.85	0.054	0.77	-	-	-
Skin	Partially	0.93	0.038	0.48	-	-	-	0.96	0.039	0.52	-	-	-
Small intestine	Partially	3.62	0.046	0.67	-	-	-	3.81	0.045	0.75	-	-	-
Thymus	Partially	1.19	0.061	0.29	-	-	-	1.04	0.066	0.37	-	-	-
Brain	Indirectly	0.03	0.082	0.50	-	-	-	0.03	0.084	0.49	-	-	-
ET region	Indirectly	0.31	0.061	0.55	-	-	-	0.26	0.060	0.49	-	-	-
Oral mucosa	Indirectly	0.03	0.082	0.50	-	-	-	0.03	0.084	0.49	-	-	-
Salivary glands	Indirectly	0.02	0.033	0.16	-	-	-	0.02	0.035	0.17	-	-	-
Thyroid	Indirectly	0.31	0.061	0.55	-	-	-	0.26	0.060	0.49	-	-	-

Table 9.3. Exponential regression coefficients and R^2 for each organ for abdomen/pelvis protocol.

Organ	Organ irradiation classification	FTC						TCM					
		Protocol-specific			Organ-specific			Protocol-specific			Organ-specific		
		A_0	B_0	R^2	A_0	B_0	R^2	A_0	B_0	R^2	A_0	B_0	R^2
Adrenals	Fully	3.75	0.044	0.95	3.91	0.045	0.96	2.67	0.039	0.61	3.80	0.045	0.95
Bladder	Fully	4.46	0.045	0.96	4.45	0.044	0.96	6.17	0.049	0.87	3.90	0.042	0.93
Colon	Fully	3.57	0.033	0.99	3.62	0.034	0.99	3.33	0.033	0.86	3.04	0.030	0.98
Gall Bladder	Fully	3.95	0.039	0.94	4.07	0.040	0.98	2.91	0.035	0.63	4.27	0.041	0.95
Kidneys	Fully	4.21	0.042	0.98	4.26	0.042	0.99	3.21	0.038	0.71	4.38	0.043	0.99
Liver	Fully	4.03	0.041	0.97	4.34	0.044	0.99	2.94	0.038	0.71	4.35	0.045	0.99
Pancreas	Fully	4.05	0.042	0.98	4.23	0.044	0.99	2.99	0.039	0.71	3.74	0.040	0.95
Prostate/Uterus	Fully	5.12	0.059	0.89	5.05	0.058	0.85	6.48	0.058	0.87	4.82	0.060	0.83
Small intestine	Fully	3.85	0.036	0.98	4.02	0.038	0.99	3.86	0.038	0.95	4.13	0.040	0.99
Spleen	Fully	3.74	0.039	0.94	3.92	0.041	0.98	2.75	0.036	0.57	4.21	0.043	0.98
Stomach	Fully	3.87	0.039	0.99	4.02	0.040	0.99	2.84	0.035	0.66	4.27	0.043	0.98
Bone surface	Partially	4.31	0.037	0.73	-	-	-	4.31	0.037	0.75	-	-	-
Breast	Partially	3.01	0.058	0.44	-	-	-	1.32	0.046	0.22	-	-	-
Esophagus	Partially	1.30	0.034	0.37	-	-	-	0.94	0.035	0.25	-	-	-
Gonads	Partially	4.57	0.076	0.24	-	-	-	5.85	0.074	0.27	-	-	-
Heart	Partially	3.17	0.043	0.74	-	-	-	2.44	0.046	0.50	-	-	-
Lung	Partially	2.67	0.049	0.76	-	-	-	1.96	0.052	0.53	-	-	-
Lymphatic nodes	Partially	1.51	0.034	0.62	-	-	-	1.54	0.033	0.66	-	-	-
Muscle	Partially	1.51	0.034	0.62	-	-	-	1.54	0.033	0.66	-	-	-
Red bone marrow	Partially	0.91	0.037	0.77	-	-	-	0.91	0.037	0.79	-	-	-
Skin	Partially	1.11	0.027	0.41	-	-	-	1.14	0.027	0.44	-	-	-
Thymus	Partially	1.16	0.060	0.30	-	-	-	0.84	0.065	0.32	-	-	-
Brain	Indirectly	0.03	0.079	0.51	-	-	-	0.02	0.082	0.46	-	-	-
ET region	Indirectly	0.31	0.061	0.58	-	-	-	0.21	0.059	0.41	-	-	-
Oral mucosa	Indirectly	0.03	0.079	0.51	-	-	-	0.02	0.082	0.46	-	-	-
Salivary glands	Indirectly	0.02	0.030	0.15	-	-	-	0.02	0.032	0.15	-	-	-
Thyroid	Indirectly	0.31	0.061	0.58	-	-	-	0.21	0.059	0.41	-	-	-

Table 9.4. Exponential regression coefficients and R^2 for each organ for chest protocol.

Organ	Organ irradiation classification	FTC						TCM					
		Protocol-specific			Organ-specific			Protocol-specific			Organ-specific		
		A_0	B_0	R^2	A_0	B_0	R^2	A_0	B_0	R^2	A_0	B_0	R^2
Breast	Fully	3.48	0.048	0.88	3.35	0.045	0.93	2.61	0.046	0.40	3.29	0.042	0.89
Heart	Fully	4.33	0.047	0.74	4.31	0.046	0.95	3.93	0.051	0.62	4.12	0.039	0.96
Lung	Fully	4.22	0.051	0.78	4.30	0.047	0.99	4.03	0.055	0.68	4.50	0.052	0.98
Thymus	Fully	3.80	0.040	0.71	3.26	0.032	0.93	3.13	0.036	0.18	3.80	0.037	0.93
Adrenals	Partially	4.26	0.074	0.68	-	-	-	4.23	0.076	0.72	-	-	-
Bone surface	Partially	6.71	0.078	0.92	-	-	-	6.77	0.078	0.93	-	-	-
Colon	Partially	1.38	0.088	0.27	-	-	-	1.47	0.092	0.24	-	-	-
Esophagus	Partially	4.30	0.054	0.79	-	-	-	4.25	0.054	0.67	-	-	-
ET region	Partially	3.48	0.036	0.33	-	-	-	3.55	0.025	0.11	-	-	-
Gall Bladder	Partially	3.11	0.065	0.36	-	-	-	2.61	0.056	0.26	-	-	-
Kidneys	Partially	2.73	0.080	0.65	-	-	-	2.99	0.086	0.76	-	-	-
Liver	Partially	3.86	0.058	0.67	-	-	-	3.69	0.058	0.61	-	-	-
Lymphatic nodes	Partially	2.60	0.093	0.96	-	-	-	2.58	0.092	0.94	-	-	-
Muscle	Partially	2.60	0.093	0.96	-	-	-	2.58	0.092	0.94	-	-	-
Pancreas	Partially	4.65	0.081	0.82	-	-	-	4.94	0.087	0.78	-	-	-
Red bone marrow	Partially	1.35	0.076	0.93	-	-	-	1.36	0.076	0.93	-	-	-
Skin	Partially	1.62	0.076	0.82	-	-	-	1.64	0.076	0.84	-	-	-
Small intestine	Partially	1.26	0.104	0.23	-	-	-	1.25	0.107	0.21	-	-	-
Spleen	Partially	4.22	0.060	0.78	-	-	-	4.19	0.061	0.89	-	-	-
Stomach	Partially	3.73	0.055	0.80	-	-	-	3.59	0.056	0.80	-	-	-
Thyroid	Partially	3.48	0.036	0.33	-	-	-	3.55	0.025	0.11	-	-	-
Bladder	Indirectly	0.73	0.227	0.79	-	-	-	0.78	0.234	0.74	-	-	-
Brain	Indirectly	0.15	0.088	0.54	-	-	-	0.17	0.086	0.50	-	-	-
Gonads	Indirectly	1.99	0.295	0.54	-	-	-	2.03	0.296	0.55	-	-	-
Oral mucosa	Indirectly	0.15	0.088	0.54	-	-	-	0.17	0.086	0.50	-	-	-
Prostate/Uterus	Indirectly	1.25	0.259	0.70	-	-	-	1.44	0.267	0.70	-	-	-
Salivary glands	Indirectly	0.07	0.002	0.01	-	-	-	0.08	0.001	0.01	-	-	-

Table 9.5. Exponential regression coefficients and R^2 for each organ for CAP protocol.

Organ	Organ irradiation classification	FTC						TCM					
		Protocol-specific			Organ-specific			Protocol-specific			Organ-specific		
		A_0	B_0	R^2	A_0	B_0	R^2	A_0	B_0	R^2	A_0	B_0	R^2
Adrenals	Fully	3.81	0.042	0.95	3.87	0.043	0.96	2.66	0.035	0.59	3.83	0.043	0.96
Bladder	Fully	4.48	0.045	0.94	4.37	0.043	0.95	6.22	0.049	0.93	3.87	0.041	0.94
Breast	Fully	2.87	0.030	0.85	3.32	0.044	0.92	2.53	0.041	0.67	3.25	0.040	0.89
Colon	Fully	3.63	0.033	0.97	3.63	0.033	0.99	3.22	0.029	0.83	3.06	0.030	0.99
Gall Bladder	Fully	4.00	0.038	0.96	4.00	0.038	0.98	2.89	0.032	0.64	4.29	0.041	0.95
Heart	Fully	3.95	0.033	0.97	4.36	0.045	0.96	3.29	0.038	0.80	4.19	0.039	0.97
Kidneys	Fully	4.33	0.042	0.98	4.27	0.042	0.99	3.15	0.035	0.70	4.39	0.042	0.99
Liver	Fully	4.12	0.039	0.98	4.29	0.041	0.99	2.95	0.033	0.69	4.40	0.043	0.99
Lung	Fully	3.66	0.034	0.93	4.35	0.047	0.99	3.35	0.041	0.90	4.53	0.051	0.98
Pancreas	Fully	4.09	0.041	0.98	4.15	0.042	0.99	2.97	0.035	0.69	3.74	0.039	0.96
Prostate/Uterus	Fully	5.11	0.059	0.88	4.86	0.056	0.84	6.68	0.059	0.91	4.74	0.059	0.84
Small intestine	Fully	3.93	0.037	0.97	4.03	0.038	0.99	3.71	0.034	0.94	4.15	0.040	0.99
Spleen	Fully	3.82	0.037	0.94	3.89	0.038	0.98	2.79	0.031	0.57	4.32	0.042	0.99
Stomach	Fully	3.92	0.037	0.99	3.96	0.037	0.99	2.82	0.031	0.66	4.27	0.041	0.98
Thymus	Fully	3.41	0.028	0.87	3.32	0.032	0.93	3.31	0.036	0.41	3.90	0.038	0.93
Bone surface	Partially	5.71	0.034	0.68	-	-	-	5.86	0.035	0.74	-	-	-
Esophagus	Partially	3.57	0.035	0.90	-	-	-	3.45	0.040	0.90	-	-	-
ET region	Partially	4.15	0.035	0.82	-	-	-	4.48	0.034	0.53	-	-	-
Gonads	Partially	5.69	0.084	0.28	-	-	-	6.80	0.079	0.29	-	-	-
Lymphatic nodes	Partially	2.07	0.035	0.62	-	-	-	2.10	0.034	0.63	-	-	-
Muscle	Partially	2.07	0.035	0.62	-	-	-	2.10	0.034	0.63	-	-	-
Red bone marrow	Partially	1.20	0.033	0.72	-	-	-	1.23	0.035	0.79	-	-	-
Skin	Partially	1.38	0.025	0.40	-	-	-	1.43	0.026	0.43	-	-	-
Thyroid	Partially	4.15	0.035	0.82	-	-	-	4.48	0.034	0.53	-	-	-
Brain	Indirectly	0.16	0.070	0.86	-	-	-	0.18	0.075	0.94	-	-	-
Oral mucosa	Indirectly	0.16	0.070	0.86	-	-	-	0.18	0.075	0.94	-	-	-
Salivary glands	Indirectly	0.08	0.006	0.01	-	-	-	0.10	0.011	0.01	-	-	-

Table 9.6. Exponential regression coefficients and R^2 for ICRP 103 calculation of effective dose.

Protocol	Protocol-specific					
	FTC			TCM		
	A_0	B_0	R^2	A_0	B_0	R^2
Abd	2.64	0.050	0.88	2.53	0.050	0.86
AbdPel	2.70	0.043	0.90	2.40	0.042	0.85
Chest	2.49	0.056	0.79	2.37	0.055	0.79
CAP	3.24	0.038	0.89	3.07	0.039	0.90

Table 9.7. Exponential regression coefficients and R^2 for ICRP 60 calculation of effective dose.

Protocol	Protocol-specific					
	FTC			TCM		
	A_0	B_0	R^2	A_0	B_0	R^2
Abd	2.95	0.057	0.87	3.05	0.059	0.85
AbdPel	3.08	0.046	0.85	3.01	0.047	0.80
Chest	2.26	0.057	0.84	2.20	0.056	0.85
CAP	3.62	0.042	0.88	3.64	0.043	0.87

Table 9.8 shows a summary of errors between ICRP Publication 103 calculations of effective dose from the simulated organ doses (Appendix B) and effective doses determined using the various estimation methods. Table 9.9 shows a summary of errors between ICRP Publication 60 calculations of effective dose from the simulated organ doses (Appendix C) and effective doses determined using the various estimation methods. For the $DLP \times k$ -factor method, estimates of the ICRP 60 calculations of effective dose were slightly better than estimates of the ICRP 103 calculations of effective dose. This makes sense because the k-factor values were originally developed using ICRP 60 calculations of effective dose [10]. For all scan scenarios, the two size-specific effective dose estimate methods provided effective dose estimates that were both consistent with one another and consistently better than the $DLP \times k$ -factor method.

Table 9.8. Mean error across all reference voxelized phantoms between ICRP Publication 103 calculations of effective dose from the simulated organ doses (Appendix B) and effective doses determined using the various estimation methods.

Estimation method	Mean error (%)									
	FTC					TCM				
	Abd	AbdPel	Chest	CAP	Avg	Abd	AbdPel	Chest	CAP	Avg
$DLP \times k$	18.32	16.70	31.39	13.98	20.10	16.51	17.04	29.39	13.22	19.04
Size-Specific Method 1	12.17	9.29	11.48	8.13	10.27	13.29	12.07	11.78	7.67	11.20
Size-Specific Method 2	11.70	8.96	11.83	7.85	10.09	12.56	11.39	11.65	7.45	10.77

Table 9.9. Mean error across all reference voxelized phantoms between ICRP Publication 60 calculations of effective dose from the simulated organ doses (Appendix C) and effective doses determined using the various estimation methods.

Estimation method	Mean error (%)									
	FTC					TCM				
	Abd	AbdPel	Chest	CAP	Avg	Abd	AbdPel	Chest	CAP	Avg
DLP x k	13.59	13.88	23.94	12.28	15.92	12.32	16.18	23.32	12.97	16.20
Size-Specific Method 1	13.81	12.18	9.38	9.91	11.32	15.33	14.74	8.98	10.29	12.34
Size-Specific Method 2	12.20	13.13	9.07	10.22	11.16	12.95	15.92	8.75	11.16	12.19

9.4 Discussion

In this chapter, size-specific, scan technique-independent organ dose and effective dose estimates were determined from Monte Carlo-based estimates of organ dose for the GSF and ICRP reference voxelized phantoms. Exponential relationships between $CTDI_{vol}$ -normalized organ dose and patient size were observed for all scan scenarios. Exponential relationships between $CTDI_{vol}$ -normalized effective dose and patient size were also observed for all scan scenarios.

Using the appropriate exponential regression coefficients presented in Table 9.2 – Table 9.5 in conjunction with Eq. (9.1) (protocol-specific approach) and Eq. (9.2) (organ-specific approach), size-specific, scan technique-independent $CTDI_{vol}$ -to-organ-dose conversion coefficients can be generated using a measure of patient size. Eq. (9.1) can be used to generate conversion coefficients for any fully-, partially- or indirectly-irradiated radiosensitive organ. Eq. (9.2) can be used to generate conversion coefficients for fully-irradiated radiosensitive organs only. Beyond being applicable to any fully-, partially- or indirectly-irradiated radiosensitive organ, Eq. (9.1) can be readily applied to estimate organ dose using inputs already available on Siemens scanners. $CTDI_{vol,protocol}$ is the same value of $CTDI_{vol}$ that would be displayed on the

scanner console at the conclusion of a CT scan. It could also be referenced from the structured dose report. As was described in Chapter 5, WED along the length of the patient can be calculated from the AP and LAT dimensions of patient size found in the DICOM header of the topogram. WED_{protocol} can be determined from this WED profile. Therefore, all inputs necessary to calculate estimates of organ dose using Eq. (9.1) are already available on Siemens CT scanners. Although Eq. (9.2) only requires the identification of the slices containing the organ of interest to determine $CTDI_{\text{vol,organ}}$ and WED_{organ} , this would require manual input or the development of some automated system to identify the correct slices.

Because of the ease in calculating organ dose using the protocol-specific approach, conditions need to be established for when the organ-specific approach is necessary to ensure accurate qualification of fully-irradiated organ dose. Evaluating R^2 for fully-irradiated organs across the various protocols, values are appreciable high (i.e. close to 1.0) and comparable for both the protocol-specific and organ-specific approaches for organs in regions of the body where attenuation is fairly constant. For example, the liver has R^2 greater than 0.7 for all scan scenarios and organ dose estimation approaches for the abdomen, abdomen/pelvis and CAP protocols. On the other hand, R^2 is distinctly different between protocol-specific and organ-specific approaches for organs in regions of the body where there is local variation in attenuation. For example, for the TCM chest protocol, the thymus, which would be in the low-attenuation region of the chest scan, has R^2 equal to 0.18 for the protocol-specific approach and R^2 equal to 0.93 for the organ-specific approach. For this particular organ, local variations in patient attenuation need to be accounted for with organ-specific values of $CTDI_{\text{vol}}$ and WED in order to determine a reliable estimate of organ dose.

An added benefit to the organ-specific approach is the generalizability of organ dose estimates across different protocols for the same fully-irradiated organ. Using the liver example mentioned previously, for both FTC and TCM scan scenarios for the abdomen, abdomen/pelvis and CAP protocols, exponential regression coefficients (i.e. A_0 and B_0) are nearly identical. This makes sense because WED_{organ} is organ-specific, not protocol-specific, and $CTDI_{vol,organ}$ normalizes out any local variations in the tube current profile that exist from protocol to protocol. This means that a single set of exponential regression coefficients can be used to estimate the organ dose for any protocol. Additionally, this indicates that the organ-specific dose estimates may be applicable to other manufacturers' TCM schemes. FTC is basically a form of TCM without any modulation. Because exponential regression coefficients for the organ-specific approach are nearly identical for both FTC and TCM scan scenarios, this means that organ dose can be estimated for multiple TCM schemes using the same set of exponential regression coefficients. This concept will be explored in more detail in Chapter 10 when exponential regression coefficients from this investigation are used to estimate organ dose for patient who underwent clinically indicated TCM CT examinations on GE and Toshiba CT scanners.

Using the appropriate exponential regression coefficients outlined in Table 9.6 (ICRP Publication 103) and Table 9.7 (ICRP Publication 60) in conjunction with Eq. (9.3), size-specific, scan technique-independent $CTDI_{vol,protocol}$ -to-effective-dose conversion coefficients can be generated for any body CT protocol using a measure of $WED_{protocol}$. Multiplying the conversion coefficients by $CTDI_{vol,protocol}$ yields an estimate of patient-specific effective dose calculated according to either ICRP Publication 103 or ICRP Publication 60. Table 9.8 and Table 9.9 indicate that effective dose estimated this way is within approximately 10% of calculations of effective dose values calculated directly from the simulated organ doses (Appendix B and C).

This means that a measure of scanner output, $CTDI_{vol,protocol}$, and patient size, $WED_{protocol}$, can provide a reasonable estimate of a dose metric that otherwise requires knowledge of dose to all radiosensitive organs. As mentioned previously, both $CTDI_{vol,protocol}$ and $WED_{protocol}$ can be readily accessed on Siemens scanners, so all inputs necessary to calculate estimates of effective dose using Eq. (9.3) are already available on Siemens CT scanners.

$DLP \times k$ -factor is a common method to estimate effective dose using information reported at the end of a CT scan. As shown in Table 9.8 and Table 9.9, compared to the size-specific effective dose estimates, $DLP \times k$ -factor provides the worst estimate of effective dose and is especially bad for the chest protocol. The k -factor values used in the calculation of $DLP \times k$ -factor are pseudo-size-dependent because they are a function of age, but there is only one set of k -factor values for adults. In the chest, patient attenuation can vary greatly, so a size component to the effective dose estimates in that region is important. By taking patient size into account within the size-specific effective dose estimates, accuracy is improved for the chest protocol.

While the exponential regression coefficient listed in Table 9.2 – Table 9.7 can be used to generate a variety of size-specific, scan technique-independent $CTDI_{vol}$ -to-organ-dose and $CTDI_{vol}$ -to-effective-dose conversion coefficients, it should be emphasized that the protocol-specific conversion coefficients are only applicable to dose estimates for patients scanned on Siemens scanners. Because the scanner output metric, $CTDI_{vol,protocol}$, is based on the tube current from the entire scan range, it is very much dependent upon the TCM algorithm used to generate the tube current profile. In Chapter 10, conversion coefficients developed in this investigation will be used to estimate organ dose to a variety of pediatric and adult patients who underwent clinically indicated chest and abdomen/pelvis TCM CT examinations on a variety of Siemens

scanners. By comparing dose estimates derived from these conversion coefficients with dose estimates from detailed Monte Carlo simulations, the accuracy and applicability of these conversion coefficients will be tested. As mentioned previously, organ doses for patients who underwent clinically indicated CT examinations on GE and Toshiba CT scanners will also be explored to understand the applicability of the conversion coefficients for estimating organ dose for TCM CT exams for other manufacturers.

9.5 References

1. A. C. Turner *et al.*, “The feasibility of a scanner-independent technique to estimate organ dose from MDCT scans: Using CTDIvol to account for differences between scanners,” *Med. Phys.* **37**, 1816-1825 (2010).
2. M. Khatonabadi *et al.*, “The feasibility of a regional CTDIvol to estimate organ dose from tube current modulated CT exams,” *Med. Phys.* **40**, 051903 (2013).
3. A. C. Turner *et al.*, “The feasibility of patient size-corrected, scanner-independent organ dose estimates for abdominal CT exams,” *Med. Phys.* **38**, 820-829 (2011).
4. American Association of Physicists in Medicine, “Size-Specific Dose Estimates (SSDE) in Pediatric and Adult Body CT Examinations,” AAPM Report 204 (2011).
5. American Association of Physicists in Medicine, “Use of Water Equivalent Diameter for Calculating Patient Size and Size-Specific Dose Estimates (SSDE) in CT,” AAPM Report 220 (2014).
6. M. Bostani *et al.*, “Attenuation-based size metric for estimating organ dose to patients undergoing tube current modulated CT exams,” *Med. Phys.* **42**, 958-968 (2015).

7. International Commission on Radiological Protection, “The 2007 Recommendations of the International Commission on Radiological Protection,” ICRP Publication 103 (2007).
8. International Commission on Radiological Protection, “1990 Recommendations of the International Commission on Radiological Protection,” ICRP Publication 60 (1991).
9. K. McMillan *et al.*, “Size-specific, scanner-independent organ dose estimates in contiguous axial and helical head CT examinations,” *Med. Phys.* **41**, 121909 (2014).
10. American Association of Physicists in Medicine, “The Measurement, Reporting, and Management of Radiation Dose in CT,” AAPM Report 96 (2008).

Chapter 10: Accuracy and Generalizability of Size-Specific, Scan Technique-Independent Organ Dose Estimates In Tube Current Modulation CT Examinations

10.1 Introduction

In Chapter 9, size-specific, scan technique-independent organ dose estimates were developed for tube current modulation (TCM) CT examinations. Size-specific, scan technique-independent organ dose estimates were also developed for fixed tube current (FTC) CT exams. These dose estimates were developed from Monte Carlo-based estimates of organ dose for the GSF and ICRP reference voxelized phantoms. Exponential relationships between $CTDI_{vol}$ -normalized organ dose and patient size were observed for all scan scenarios. Exponential regression coefficients presented in Table 9.2 – Table 9.5 serve as the means to generate scan technique-independent organ dose estimates for any patient size (size-specific, scan technique-independent $CTDI_{vol}$ -to-organ-dose conversion coefficients).

The purpose of this chapter was to evaluate both the accuracy and generalizability of these conversion coefficients. The accuracy of the conversion coefficients, which were based on organ doses for the GSF and ICRP reference voxelized phantoms, was evaluated by comparing them to a set of reference organ dose estimates using an independent set of detailed patient models described previously by Khatonabadi *et al.* [46]. This set of patient models includes pediatric and adult patients who underwent clinically indicated abdomen/pelvis and chest CT examinations. For each patient, protocol-specific and organ-specific estimates of patient size and scanner output were determined. For abdomen/pelvis exams, liver, kidney and spleen doses were determined using detailed Monte Carlo simulations. For chest exams, lung and breast doses were determined using detailed Monte Carlo simulations. Using the patient size and scanner output

metrics in conjunction with the appropriate exponential regression coefficients from Chapter 9, dose estimates were determined for each patient and organ of interest. In an effort to understand the importance of using conversion coefficients specifically determined for TCM dose estimation, organ dose estimates were generated using both FTC and TCM conversion coefficients. Additionally, dose estimates were calculated using size-specific dose estimate (SSDE) conversion coefficients from AAPM Report 204 [2]. Although not intended to be used as a surrogate for organ dose, SSDE conversion coefficients are widely used as a means for determining patient dose (i.e. dose at the center of the scan range), so applying these conversion coefficients to estimate organ dose in the investigation offered a better understanding of the correlation between organ dose and patient dose. Organ doses from detailed Monte Carlo simulations (“gold standard”) were then compared with dose estimates calculated using the various conversion coefficients. Patients used in this investigation were scanned on Siemens, GE and Toshiba scanners. Even though the conversion coefficients from Chapter 9 were developed using a Siemens scanner and the Siemens TCM algorithm, by including other manufacturers in the test set, an understanding of the generalizability of the conversion coefficients for estimating TCM organ dose for other TCM algorithms was developed.

10.2 Methods

10.2.1 Patient Cohort

Patient image data was previously collected for a set of patients scanned on CT scanners from three major CT manufacturers (Siemens, GE and Toshiba). Images were collected from: (1)

Siemens CT scanners (Sensation 64) at the University of California, Los Angeles (UCLA), (2) GE CT scanners (LightSpeed VCT) at University of Texas-MD Anderson Cancer Center in Houston, TX and (3) Toshiba CT scanners (Aquilion 64) at University of Texas Southwestern Medical Center in Dallas, TX as well as Arkansas Children’s Hospital in Little Rock, AR [46]. Patient dose reports were collected for each patient. For patients scanned on Siemens scanners, raw projection data was also collected.

Image data was collected for pediatric and adult patients who underwent clinically indicated abdomen/pelvis and chest CT examinations. Table 10.1 summarizes the patient image data used in this investigation. A total of 313 patients were used in this investigation.

Table 10.1. Summary of patient image data used in this investigation.

Patient	Siemens		GE		Toshiba	
	AbdPel	Chest	AbdPel	Chest	AbdPel	Chest
Adult	62	71	19	19	23	40
Pediatric	20	30	1	3	12	13
Total	82	101	20	22	35	53

For each abdomen/pelvis scan, the liver, kidneys and spleen were segmented from the axial images. For the chest scans, the lungs and breasts (if female) were segmented from the images. These organs were identified because they are fully-irradiated organs within the scan range for each patient.

10.2.2 Monte Carlo Simulations

Models of patient anatomy were created from the image data, and organ dose was estimated with detailed Monte Carlo simulations of TCM CT examinations. For patients scanned on Siemens scanners, detailed TCM information (longitudinal and angular modulation) extracted from the raw projection data collected for each patient was used within the Monte Carlo simulations. For patients scanned on GE and Toshiba scanners, tube current information extracted from the image data of each patient (longitudinal modulation only) was used within the Monte Carlo simulations [3]. Validated equivalent source models of each CT scanner were used in the organ dose simulations [21].

10.2.3 Size-Specific, Scan Technique-Independent Organ Dose Estimates

For each patient and protocol, two estimates of patient size were determined: (1) protocol-specific patient size and (2) organ-specific patient size. As described in Section 9.2.2, protocol-specific patient size was determined as the WED in the central slice of the scan range (WED_{protocol}). An organ-specific estimate of patient size was determined as the average WED across all slices containing the organ of interest (WED_{organ}).

For each patient and protocol, two estimates of scanner output were determined: (1) protocol-specific scanner output and (2) organ-specific scanner output. As described in Section 9.2.3, protocol-specific scanner output was determined as $CTDI_{\text{vol}}$ based on the average tube current across the entire scan range ($CTDI_{\text{vol,protocol}}$). Organ-specific scanner output was determined as $CTDI_{\text{vol}}$ based on the average tube current across all slices containing the organ of interest ($CTDI_{\text{vol,organ}}$). For both adult and pediatric patients, the various scanner output metrics are based on $CTDI_{\text{vol}}$ measured with the body (32 cm diameter) CTDI phantom.

For each combination of organ and protocol, size-specific, scan technique-independent organ dose estimates were determined using: (1) A protocol-specific approach and (2) an organ-specific approach. The development of the size-specific, scan technique-independent organ dose estimates is described in detail in Section 9.2.4. Estimates were developed for both FTC and TCM organ doses. For size-specific, scan technique-independent organ dose estimates using the protocol-specific approach, the exponential relationship between $CTDI_{vol}$ -normalized organ dose and patient size is defined in Eq. (9.1). For size-specific, scan technique-independent organ dose estimates using the organ-specific approach, the exponential relationship between $CTDI_{vol}$ -normalized organ dose and patient size is defined in Eq. (9.2). Referenced from Table 9.3, exponential regression coefficients and R^2 for organs of interest within the abdomen/pelvis protocol are presented in Table 10.2. Referenced from Table 9.4, exponential regression coefficients and R^2 for organs of interest within the chest protocol are presented in Table 10.3.

Table 10.2. Exponential regression coefficients and R^2 for organs of interest within the abdomen/pelvis protocol.

Organ	FTC						TCM					
	Protocol-specific			Organ-specific			Protocol-specific			Organ-specific		
	A_0	B_0	R^2	A_0	B_0	R^2	A_0	B_0	R^2	A_0	B_0	R^2
Liver	4.03	0.041	0.97	4.34	0.044	0.99	2.94	0.038	0.71	4.35	0.045	0.99
Kidneys	4.21	0.042	0.98	4.26	0.042	0.99	3.21	0.038	0.71	4.38	0.043	0.99
Spleen	3.74	0.039	0.94	3.92	0.041	0.98	2.75	0.036	0.57	4.21	0.043	0.98

Table 10.3. Exponential regression coefficients and R^2 for organs of interest within the chest protocol.

Organ	FTC						TCM					
	Protocol-specific			Organ-specific			Protocol-specific			Organ-specific		
	A_0	B_0	R^2	A_0	B_0	R^2	A_0	B_0	R^2	A_0	B_0	R^2

Lung	4.22	0.051	0.78	4.30	0.047	0.99	4.03	0.055	0.68	4.50	0.052	0.98
Breast	3.48	0.048	0.88	3.35	0.045	0.93	2.61	0.046	0.40	3.29	0.042	0.89

Using the appropriate exponential regression coefficients presented in Table 10.2 (abdomen/pelvis) and Table 10.3 (chest) in conjunction with Eq. (9.1) (protocol-specific approach) and Eq. (9.2) (organ-specific approach), size-specific, scan technique-independent $CTDI_{vol}$ -to-organ-dose conversion coefficients can be generated using a measure of patient size. Multiplying the conversion coefficients by the appropriate value of $CTDI_{vol}$ yields an estimate of patient-specific organ dose.

10.2.4 AAPM Report 204 Size-Specific Dose Estimates

Size-specific dose estimates (SSDE) were presented in AAPM Report 204 as a set of conversion coefficients that can be applied to a patient's $CTDI_{vol}$ to allow for the estimation of patient dose [2]. For $CTDI_{vol}$ measured with the body (32 cm diameter) CTDI phantom, the exponential relationship between $CTDI_{vol}$ -normalized patient dose and patient size is defined as:

$$\frac{Patient\ dose}{CTDI_{vol}} = 3.70 \times \exp(-0.037 \times ED) \quad (10.1)$$

where ED is effective diameter (i.e. diameter of a circle that has the same cross-sectional area as the patient). Although the conversion coefficients were originally developed using ED, AAPM Report 220 indicated that it is both appropriate and more accurate to use WED to determine the

conversion coefficients across multiple body regions [13]. Therefore, for this investigation, Eq. (10.1) is rewritten as:

$$\frac{\text{Patient dose}}{CTDI_{vol}} = 3.70 \times \exp(-0.037 \times WED) \quad (10.2)$$

where WED was originally defined in the center of the scan range. In this work, two forms of WED were calculated: WED_{protocol} for the protocol-specific approach and WED_{organ} for the organ-specific approach (Section 9.2.2). $CTDI_{vol, \text{protocol}}$ was used as the measure of $CTDI_{vol}$ for the protocol-specific approach, and $CTDI_{vol, \text{organ}}$ was used as the measure of $CTDI_{vol}$ for the organ-specific approach (Section 9.2.3).

10.2.5 Comparison of Organ Dose Estimates

For each patient, organ doses were estimated for the protocol-specific and organ-specific approaches using the following methods: (1) Detailed Monte Carlo simulations, (2) TCM size-specific, scan technique-independent $CTDI_{vol}$ -to-organ-dose conversion coefficients, (3) FTC size-specific, scan technique-independent $CTDI_{vol}$ -to-organ-dose conversion coefficients and (4) SSDE conversion coefficients. Because organ doses determined from detailed Monte Carlo simulations are based on actual patient anatomy and actual TCM schemes, those organ doses were considered to be the “gold standard” to which organ doses estimated using the other methods were compared. The mean error and standard deviation (SD) of the error across scanner-specific and pooled (i.e. all scanners) patients between organ doses from detailed Monte

Carlo simulations and organ doses estimated using TCM, FTC and SSDE conversion coefficients were calculated to determine the accuracy and generalizability of the estimation methods. Errors were evaluated for conversion coefficients determined using the protocol-specific and organ-specific approaches. Therefore, a total of 6 comparisons were made to the reference organ doses.

10.3 Results

For patients who underwent clinically indicated abdomen/pelvis scans, a comparison of organ doses determined from detailed Monte Carlo simulations and organ doses estimated using the various estimation methods is presented for the liver, kidneys and spleen in Table 10.4, Table 10.5 and Table 10.6, respectively. For the protocol-specific approach to estimating organ doses from abdominal scans (e.g. liver, kidney, spleen), the mean error across Siemens patients ranged from 9.85% - 24.94% for TCM, FTC and SSDE conversion coefficients. For the organ-specific approach, the mean error ranged from 6.25% - 12.93%. The mean error across pooled patients ranged from 13.62% - 19.68% and 6.27% - 11.00% for the protocol-specific and organ-specific approaches, respectively. For both the protocol-specific and organ-specific approaches, a graphical comparison of $CTDI_{vol}$ -normalized organ doses determined from detailed Monte Carlo simulations and $CTDI_{vol}$ -normalized organ doses estimated using the various estimation methods is shown for the liver, kidneys and spleen in Fig. 10.1, Fig. 10.2 and Fig. 10.3, respectively.

Table 10.4. Mean error and SD of error across scanner-specific and pooled patients between simulated liver dose for an abdomen/pelvis scan and liver dose estimated using TCM, FTC and SSDE conversion coefficients for the same scan. Errors evaluated for conversion coefficients determined using the protocol-specific and organ-specific approaches.

Scanner	Liver dose % error											
	Protocol-specific						Organ-specific					
	TCM		FTC		SSDE		TCM		FTC		SSDE	
	Mean	SD	Mean	SD	Mean	SD	Mean	SD	Mean	SD	Mean	SD
Siemens	9.85	6.29	20.21	13.43	23.47	13.33	6.25	5.63	8.26	6.19	12.20	7.11
GE	29.02	7.98	13.42	8.84	9.82	7.74	7.53	5.13	5.60	5.14	7.93	6.36
Toshiba	17.99	8.21	10.49	9.76	12.32	10.87	5.60	5.38	6.25	6.15	8.97	8.60
Pooled	14.72	9.82	16.73	12.69	18.63	13.40	6.27	5.49	7.36	6.10	10.75	7.58

Table 10.5. Mean error and SD of error across scanner-specific and pooled patients between simulated kidney dose for an abdomen/pelvis scan and kidney dose estimated using TCM, FTC and SSDE conversion coefficients for the same scan. Errors evaluated for conversion coefficients determined using the protocol-specific and organ-specific approaches.

Scanner	Kidney dose % error											
	Protocol-specific						Organ-specific					
	TCM		FTC		SSDE		TCM		FTC		SSDE	
	Mean	SD	Mean	SD	Mean	SD	Mean	SD	Mean	SD	Mean	SD
Siemens	11.65	8.68	22.75	17.27	23.84	15.85	11.56	9.15	10.37	8.66	12.31	8.36
GE	22.82	8.40	12.59	8.70	9.48	7.56	5.71	5.22	5.95	5.66	7.12	4.02
Toshiba	12.95	8.01	10.02	9.05	10.88	9.65	8.03	7.36	7.51	7.37	9.42	9.17
Pooled	13.62	9.26	18.01	15.59	18.43	15.00	9.81	8.51	8.99	8.11	10.81	8.29

Table 10.6. Mean error and SD of error across scanner-specific and pooled patients between simulated spleen dose for an abdomen/pelvis scan and spleen dose estimated using TCM, FTC and SSDE conversion coefficients for the same scan. Errors evaluated for conversion coefficients determined using the protocol-specific and organ-specific approaches.

Scanner	Spleen dose % error											
	Protocol-specific						Organ-specific					
	TCM		FTC		SSDE		TCM		FTC		SSDE	
	Mean	SD	Mean	SD	Mean	SD	Mean	SD	Mean	SD	Mean	SD
Siemens	12.05	8.52	20.15	16.25	24.94	17.87	9.42	9.24	8.42	9.22	12.93	9.62
GE	30.52	9.29	15.31	11.07	11.71	9.38	8.96	6.50	9.44	6.73	7.22	4.78
Toshiba	21.61	10.08	11.05	8.68	11.92	10.58	7.62	5.88	8.26	6.37	8.64	8.38
Pooled	17.11	11.30	17.12	14.45	19.68	16.49	8.89	8.13	8.53	7.54	11.00	9.04

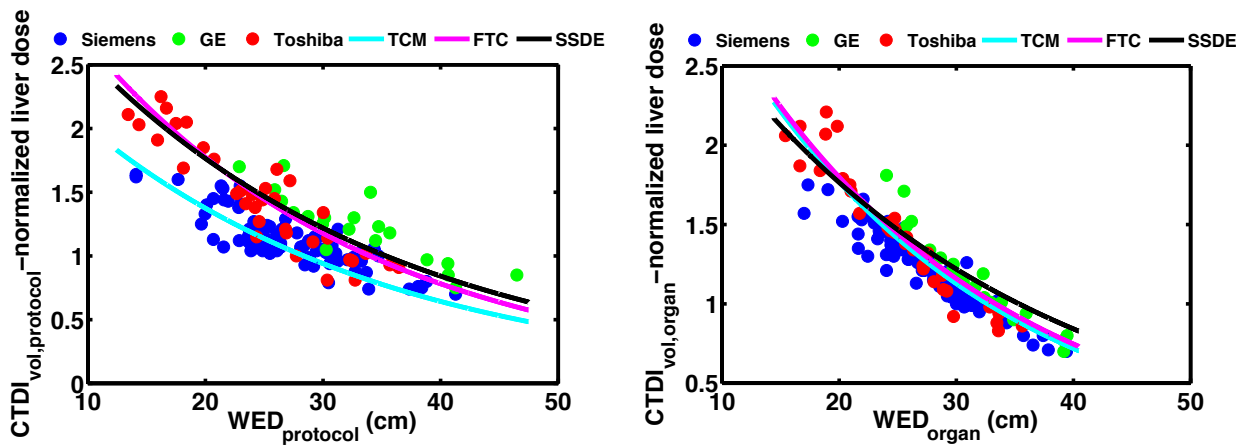


Figure 10.1. Comparison of simulated liver dose for patients scanned on Siemens, GE and Toshiba scanners and liver dose estimated using TCM, FTC and SSDE conversion coefficients for the protocol-specific (left) and organ-specific (right) approaches.

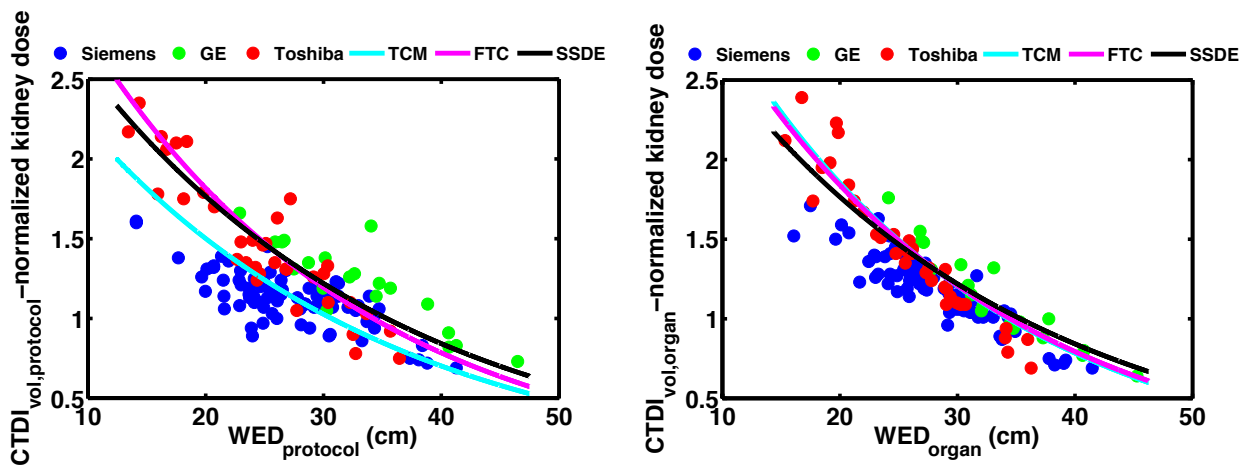


Figure 10.2. Comparison of simulated kidney dose for patients scanned on Siemens, GE and Toshiba scanners and kidney dose estimated using TCM, FTC and SSDE conversion coefficients for the protocol-specific (left) and organ-specific (right) approaches.

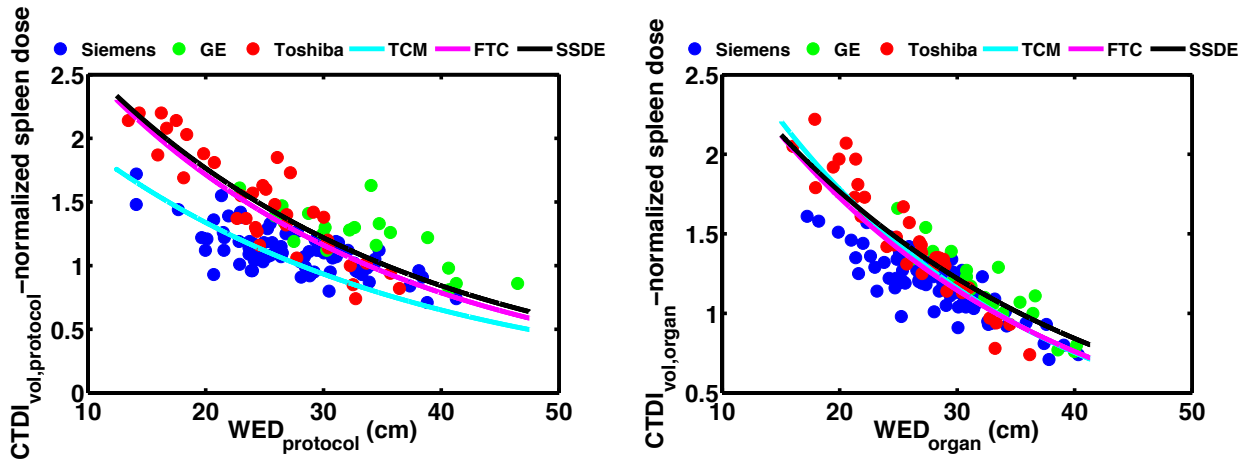


Figure 10.3. Comparison of simulated spleen dose for patients scanned on Siemens, GE and Toshiba scanners and spleen dose estimated using TCM, FTC and SSDE conversion coefficients for the protocol-specific (left) and organ-specific (right) approaches.

For patients who underwent clinically indicated chest scans, a comparison of organ doses determined from detailed Monte Carlo simulations and organ doses estimated using the various estimation methods is presented for the lungs and breasts in Table 10.7 and Table 10.8, respectively. For the protocol-specific approach to estimating organ doses from chest scans (e.g. lung, breast), the mean error across Siemens patients ranged from 14.15% - 69.25% for TCM, FTC and SSDE conversion coefficients. For the organ-specific approach, the mean error ranged from 10.04% - 38.82%. The mean error across pooled patients ranged from 14.72% - 54.33% and 10.22% - 31.72% for the protocol-specific and organ-specific approaches, respectively. For both the protocol-specific and organ-specific approaches, a graphical comparison of $CTDI_{vol}$ -normalized organ doses determined from detailed Monte Carlo simulations and $CTDI_{vol}$ -normalized organ doses estimated using the various estimation methods is shown for the lungs and breasts in Fig. 10.4 and Fig. 10.5, respectively.

Table 10.7. Mean error and SD of error across scanner-specific and pooled patients between simulated lung dose for a chest scan and lung dose estimated using TCM, FTC and SSDE conversion coefficients for the same scan. Errors evaluated for conversion coefficients determined using the protocol-specific and organ-specific approaches.

Scanner	Lung dose % error											
	Protocol-specific						Organ-specific					
	TCM		FTC		SSDE		TCM		FTC		SSDE	
	Mean	SD	Mean	SD	Mean	SD	Mean	SD	Mean	SD	Mean	SD
Siemens	14.15	9.60	18.13	14.19	35.53	15.93	11.52	9.51	14.09	11.40	22.54	10.78
GE	24.49	9.33	12.92	9.41	10.45	6.58	12.15	9.02	6.80	6.26	7.19	3.99
Toshiba	11.93	7.33	9.76	8.60	23.53	11.73	6.99	4.91	4.34	5.38	11.64	5.98
Pooled	14.72	9.65	14.97	12.75	28.89	16.35	10.22	8.55	10.26	10.41	17.40	10.83

Table 10.8. Mean error and SD of error across scanner-specific and pooled patients between simulated breast dose for a chest scan and breast dose estimated using TCM, FTC and SSDE conversion coefficients for the same scan. Errors evaluated for conversion coefficients determined using the protocol-specific and organ-specific approaches.

Scanner	Breast dose % error											
	Protocol-specific						Organ-specific					
	TCM		FTC		SSDE		TCM		FTC		SSDE	
	Mean	SD	Mean	SD	Mean	SD	Mean	SD	Mean	SD	Mean	SD
Siemens	21.47	15.53	29.67	30.91	69.25	40.66	12.38	8.94	10.04	8.20	38.82	13.51
GE	31.78	8.01	13.54	10.31	20.86	12.46	13.54	10.07	17.55	10.42	14.75	9.67
Toshiba	19.32	11.17	14.30	11.38	41.24	20.19	8.48	5.38	9.24	5.26	25.88	13.29
Pooled	22.00	13.91	22.73	25.27	54.33	37.04	11.25	8.26	10.67	8.02	31.72	15.53

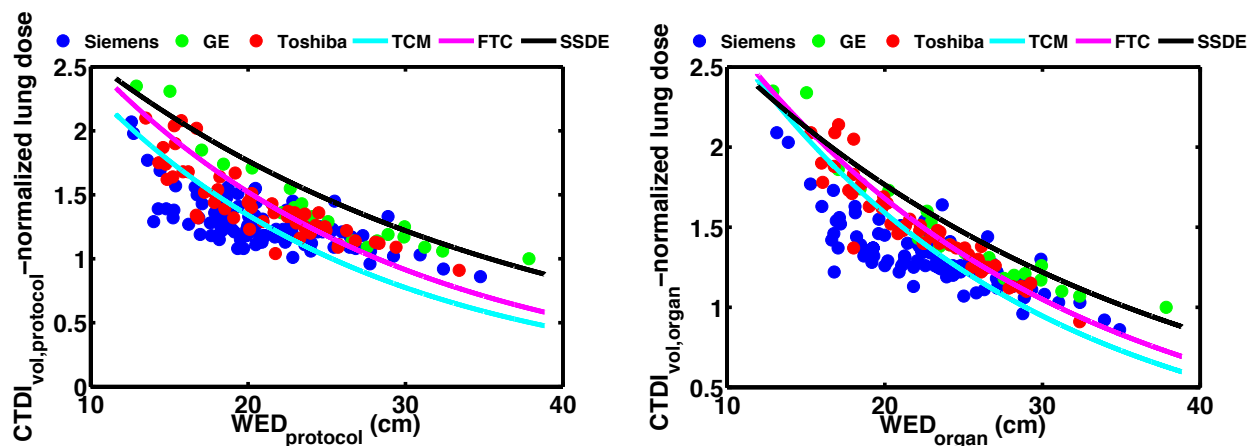


Figure 10.4. Comparison of simulated lung dose for patients scanned on Siemens, GE and Toshiba scanners and lung dose estimated using TCM, FTC and SSDE conversion coefficients for the protocol-specific (left) and organ-specific (right) approaches.

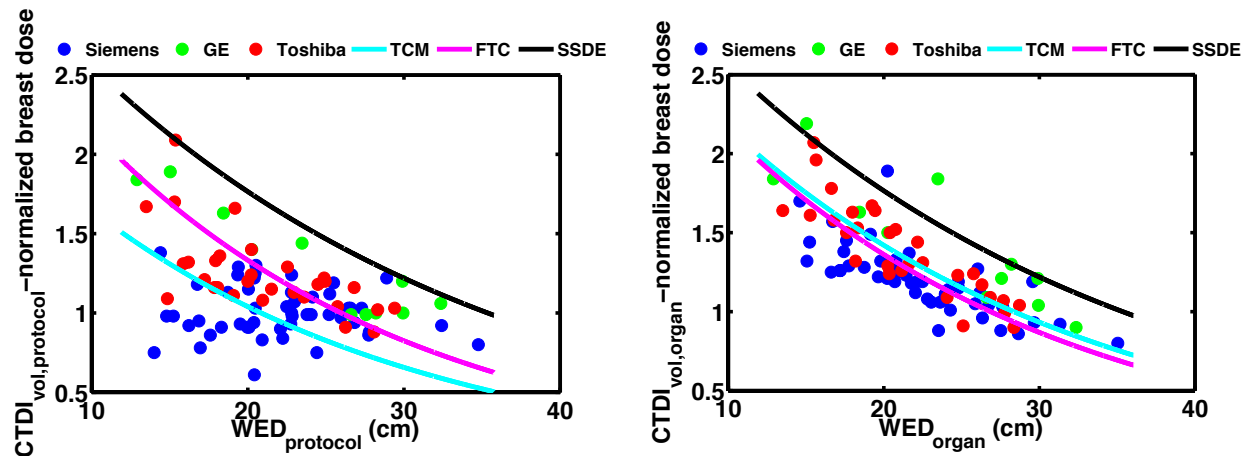


Figure 10.5. Comparison of simulated breast dose for patients scanned on Siemens, GE and Toshiba scanners and breast dose estimated using TCM, FTC and SSDE conversion coefficients for the protocol-specific (left) and organ-specific (right) approaches.

10.4 Discussion

In this chapter, size-specific, scan technique-independent $CTDI_{vol}$ -to-organ-dose conversion coefficients developed in Chapter 9 were applied to estimate organ doses for pediatric and adult patient who underwent clinically indicated abdomen/pelvis and chest TCM CT examinations on Siemens, GE and Toshiba scanners. SSDE conversion coefficients from AAPM Report 204 were also applied. A comparison of organ doses determined from detailed Monte Carlo simulations and organ doses estimated using the various estimation methods was performed to determine the accuracy and generalizability of the estimation methods for estimating organ doses.

In AAPM Report 204, the acceptable tolerance for differences between estimated and actual patient dose was 10% to 20% [2]. This tolerance level was established for size-specific, scan technique-independent patient dose estimates. Given the similarities to the conversion

coefficients used in this investigation to estimate organ dose (i.e. size-specific and scan technique-independent), errors within this range were considered to be indicative of reasonably accurate organ dose estimates.

For Siemens patients, organ doses could be reasonably estimated for all organs, except the breast, using protocol-specific TCM conversion coefficients. Protocol-specific TCM conversion coefficients were consistently more accurate than FTC and SSDE conversion coefficients. For all organs, the estimates improved when using organ-specific TCM conversion coefficients, but this improvement comes at the cost of having to identify organ-specific regions from the image data. For abdomen/pelvis organ dose estimation, organ-specific FTC and SSDE conversion coefficients were comparable to TCM conversion coefficients. As discussed in Chapter 9, when local variations in the tube current profile are taken into account in the organ-specific estimate of scanner output, TCM and FTC conversion coefficient for each organ are appreciably close. SSDE conversion coefficients were based, in part, on the average dose to organs in the abdomen (e.g. liver, kidney, spleen) determined using Monte Carlo simulations of FTC abdomen protocols for a set of reference voxelized phantoms [2]. Therefore, SSDE conversion coefficients are similar to the organ-specific FTC conversion coefficients for the liver, kidney and spleen. For chest organ dose estimation, only organ-specific FTC conversion coefficients were comparable to TCM conversion coefficients.

For the breast, only organ-specific conversion coefficients (both TCM and FTC) provided reasonable accuracy in dose estimation. Across different patients, the breast has a lot of variability in both shape and size. Therefore, an organ-specific determination of both the scanner output and patient size at the level of the breast is necessary to account for this variability. As shown in Fig. 10.5, even after accounting for local variation in the tube current profile and

patient size (i.e. organ-specific approach), there is still variation in the $CTDI_{vol}$ -normalized breast dose that is not observed for other organs. The breast is a superficial organ, so unlike other organs that are at depth within the patient, the breast is more susceptible to variation in dose caused by patient positioning (i.e. off-centered positioning).

For patients pooled across Siemens, GE and Toshiba scanners, organ dose estimation trends were similar to those for Siemens-only patients. Organ doses could be reasonably estimated for all organs, except the breast, using protocol-specific TCM conversion coefficients. The error and SD of the error, though, were greater for the pooled patients compared to the Siemens patients. This is expected because the protocol-specific approach is very much dependent upon the TCM algorithm for which the conversion coefficients were developed (i.e. Siemens Care Dose4D). Protocol-specific TCM conversion coefficients were actually comparable to FTC conversion coefficients, although the SD of the error was greater for the FTC conversion coefficients. For all organs, the estimates improved when using organ-specific TCM conversion coefficients. The mean error and SD of the error were comparable for organ-specific TCM and FTC conversion coefficients.

Results from this investigation indicate that the TCM conversion coefficients presented in Chapter 9 can be used to reasonably estimate organ dose for patients who underwent clinically indicated abdomen/pelvis and chest TCM CT examinations. The TCM conversion coefficients are also generalizable in that they can be used to reasonably estimate organ dose for patients scanned on Siemens, GE and Toshiba scanners. Organ-specific TCM conversion coefficients provide consistently more accurate dose estimates, but they require the determination of organ-specific regions from the image data. In regions of the body where attenuation is fairly constant, such as the abdomen, protocol-specific TCM conversion coefficients yielded strong agreement

for Siemens patients. Agreement within 20% was also observed for abdominal organs for the pooled patients, but estimates for Siemens-only patients were better in terms of mean error and SD of the error. For pooled patients, in order to estimate dose with mean error and SD of the error comparable to Siemens-only patients, organ-specific TCM conversion coefficients are necessary. In regions of the body where there is local variation in attenuation, such as the chest, protocol-specific conversion coefficients provide reasonable agreement for the lungs only. Like abdominal organs, dose estimation improved for the lungs when using organ-specific conversion coefficients. For the breast, only organ-specific conversion coefficients provided reasonable agreement. This indicates that the organ-specific approach is especially necessary for organs with large patient-to-patient variation in shape and size.

10.5 References

1. M. Khatonabadi *et al.*, “Predictive Models for Estimating Dose from Tube Current Modulation CT Scans Using Regional $CTDI_{vol}$ and Water Equivalent Diameter (WED),” 99th Scientific Assembly and Annual Meeting of the Radiological Society of North America, Chicago, IL, December 1-6, 2013.
2. American Association of Physicists in Medicine, “Size-Specific Dose Estimates (SSDE) in Pediatric and Adult Body CT Examinations,” AAPM Report 204 (2011).
3. M. Khatonabadi *et al.*, “A comparison of methods to estimate organ doses in CT when utilizing approximations to the tube current modulation function,” *Med. Phys.* **39**, 5212-5228 (2012).

4. A. C. Turner *et al.*, “A method to generate equivalent energy spectra and filtration models based on measurements for multidetector CT Monte Carlo dosimetry simulations,” *Med. Phys.* **36**, 2154-2164 (2009).
5. American Association of Physicists in Medicine, “Use of Water Equivalent Diameter for Calculating Patient Size and Size-Specific Dose Estimates (SSDE) in CT,” AAPM Report 220 (2014).

Chapter 11: Size-Specific Fetal Dose Estimates in Tube Current Modulation CT Examinations of Pregnant Patients

11.1 Introduction

In Chapter 9, size-specific, scan technique-independent $CTDI_{vol}$ -to-organ-dose conversion coefficients were determined for a variety of radiosensitive organs. While conversion coefficients were presented for all organs included in the ICRP Publication 103 and ICRP Publication 60 calculation of effective dose, there are additional patient doses of interest not represented in that dataset. Of significant interest is fetal dose for pregnant patients undergoing CT examinations.

CT examinations of pregnant patients are sometimes necessary, especially in the case of trauma such as a car accident. In order to determine if the diagnostic benefit of the CT scan outweighs the risk of radiation exposure for the fetus, accurate estimates of radiation dose to the fetus are necessary. Early efforts to quantify the dose a fetus receives during a CT examination were based on phantom measurements and/or geometric phantom simulation methods [1-28]. These efforts were limited by simplified geometries and the assumption of early term pregnancy in a single-size patient model with an average, non-varying maternal anatomy.

In an effort to overcome these limitations, Angel *et al.* investigated the effects of maternal and fetal characteristics (i.e. maternal size, gestational age and fetal presentation) on Monte Carlo-based fetal dose estimates for a set of pregnant patient who underwent clinically indicated abdominal and pelvic CT examinations [5]. While the results of that work provided size-specific fetal dose estimates based on actual patient anatomy, dose estimates were limited to fixed tube current (FTC) CT exams of pregnant patients. The limitation of FTC dose was also

true for the previously mentioned investigations of fetal dose [1-28]. In current clinical practice, nearly all CT exams are performed with using tube current modulation (TCM).

A study by Gu *et al.* attempted to evaluate the effects of TCM on fetal doses [6]. Fetal doses were evaluated for three computational phantoms designed to represent pregnant patients of gestational ages of 3, 6 and 9 months [7]. In order to model TCM for these computational phantoms for which no TCM data exists, TCM schemes (longitudinal modulation only) were selected that were applied to actual patients of gestational ages of 15, 20 and 31 weeks, respectively. In other words, the TCM schemes incorporated into Monte Carlo simulations of fetal dose were not based on the computational phantom attenuation properties but rather on a best match of gestational age between the computational phantom and an actual patient who was scanned in the clinic. As demonstrated in the work by Angel *et al.*, fetal dose and patient size correlate strongly but fetal dose and gestational age do not [5]. Consequently, the selection of TCM schemes based on gestational age rather than patient size may not be appropriate. Additionally, because fetal dose was only evaluated for three computational phantoms, no relationships between fetal dose and patient size for TCM CT exams were presented.

Given the collective limitations of previous work to determine dose to the fetus, the purpose of this investigation was to develop patient size-specific, scan technique-independent $CTDI_{vol}$ -to-fetal-dose conversion coefficients for abdominal/pelvic CT examinations of pregnant patients of various gestational ages that use TCM. For a set of pregnant patients who underwent clinically indicated abdomen/pelvis CT examinations, models of maternal and fetal anatomy were created from the image data [5]. Using the methods described in Chapter 7, patient attenuation information was estimated for each pregnant patient model from a simulated topogram. This patient attenuation data was then used as the input to the TCM scheme estimation

methods described in Chapter 6. TCM schemes created for each pregnant patient model were then used in Monte Carlo simulations of TCM scans to estimate fetal dose. Fetal doses were normalized by scan-specific $CTDI_{vol}$ values based on the average tube current across the entire scan to obtain scan technique-independent $CTDI_{vol}$ -to-fetal-dose conversion coefficients for each patient. Patient size was described using water equivalent diameter (WED) measured at the image containing the three-dimensional geometric centroid of the fetus. The correlation between the WED patient size metric and $CTDI_{vol}$ -to-fetal-dose conversion coefficients was then established. An exponential regression equation describing this correlation serves as the means to generate scan technique-independent fetal dose estimates for any patient size. As a comparative reference, size-specific, scan technique-independent fetal dose estimates were also developed for FTC CT exams. Additionally, fetal dose estimates were calculated using size-specific dose estimate (SSDE) conversion coefficients from AAPM Report 204 [36].

11.2 Methods

11.2.1 Patient Cohort

Patient image data was previously collected for a set of 18 pregnant patients of gestational ages ranging from 12 to 36 weeks who underwent clinically indicated abdomen/pelvis FTC CT examinations [3]. The pregnant patients were originally scanned on the following GE scanners: (1) HighSpeed CT/I, (2) LightSpeed QX/i, (3) Light Speed Ultra, (4) Light Speed PRO, (5) LightSpeed 16 and (6) LightSpeed VCT. For each patient, the image data included, at a minimum,

patient anatomy from the lower thorax to the pubic symphysis. Figure 11.1 shows axial (left) and sagittal (right) images of a pregnant patient at a gestational age of 24 weeks.

For each patient, an estimate of patient size was determined. Consistent with the size measurement location used by Angel *et al.*, patient size was determined as the WED measured at the image containing the three-dimensional geometric centroid of the fetus [5]. WED was calculated from the image data using Eq. (5.1).

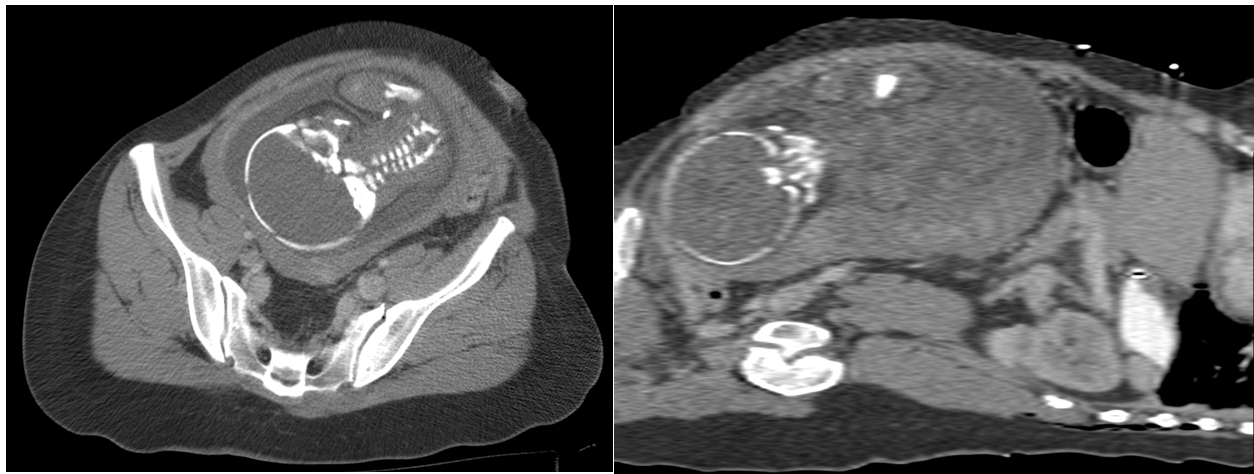


Figure 11.1. Axial (left) and sagittal (right) images of a pregnant patient at a gestational age of 24 weeks who underwent a clinically indicated abdomen/pelvis CT examination.

11.2.2 Creation of Voxelized Models

For each patient, the gestational sac, uterus and fetus were segmented from the axial images. Voxels within the fetus were modeled as soft tissue or bone depending on the Hounsfield number. The voxels in the gestational sac were modeled as water, and the voxels in the uterus were modeled as soft tissue. All voxels outside of the contoured regions were identified as a specific tissue type (lung, fat, water, muscle, bone, air) using a Hounsfield number lookup table [15]. Models of

maternal and fetal anatomy were created from the image data for use as the patient geometry for Monte Carlo simulations. Figure 11.2 shows an example of the gestational sac, uterus and fetus segmented from the axial images of a pregnant patient (center) and the Monte Carlo representation of the patient with all non-contoured regions identified as a specific tissue type (right).



Figure 11.2. (Center) Gestational sac (yellow), uterus (pink) and fetus (red) segmented from the images of a pregnant patient. (Right) Monte Carlo representation of the patient with all voxels assigned to a specific tissue type [5].

11.2.3 Creation of TCM Functions

For each of the pregnant patient models, patient attenuation profiles in the anterior-posterior (AP) direction were simulated using the methods described in Section 7.2.1. Patient attenuation profiles were determined along the length of each patient in 1 mm increments. As mentioned in Chapter 7, the determination of patient attenuation profiles at each table location is analogous to simulating an AP topogram.

From the simulated topogram, estimates of the AP and LAT dimensions of patient size were calculated using the methods described in Section 7.2.2 and Section 7.2.3, respectively. The

estimates of AP and LAT dimensions of patient size were used as the inputs to the methods to estimate Siemens TCM schemes described in Chapter 6. Even though the pregnant patient were originally scanned on GE scanners, the novelty of the TCM scheme estimation methods presented in this dissertation is that it does not matter what scanner was used to acquire the CT images. The attenuation data used as the input to the Siemens TCM scheme estimation methods can be determined from a simulated topogram using any set of CT images.

11.2.4 Monte Carlo Simulations

Using the models of patient anatomy created from the image data, dose to the fetus was estimated with detailed Monte Carlo simulations of TCM and FTC CT examinations. All simulations were performed using an equivalent source model of a Siemens Sensation 64 CT scanner. Table 11.1 outlines the technical parameters used in the Monte Carlo simulations. For TCM scans, the estimated TCM schemes were used. Estimated TCM schemes were generated using an adult reference attenuation value of 1000 (abdomen/pelvis protocol). For FTC scans, a tube current of 400 mA was used (200 effective mAs with 0.5 s rotation time). Figure 11.3 shows the estimated TCM scheme for a pregnant patient who underwent a clinically indicated abdomen/pelvis CT examination.

Table 11.1. Technical settings used for all Monte Carlo simulations.

Parameter	Setting
kVp	120
Quality reference mAs (QRM)	200
Rotation time (s)	0.5
Pitch	1
Collimation (mm)	19.2
Bowtie filter	Standard

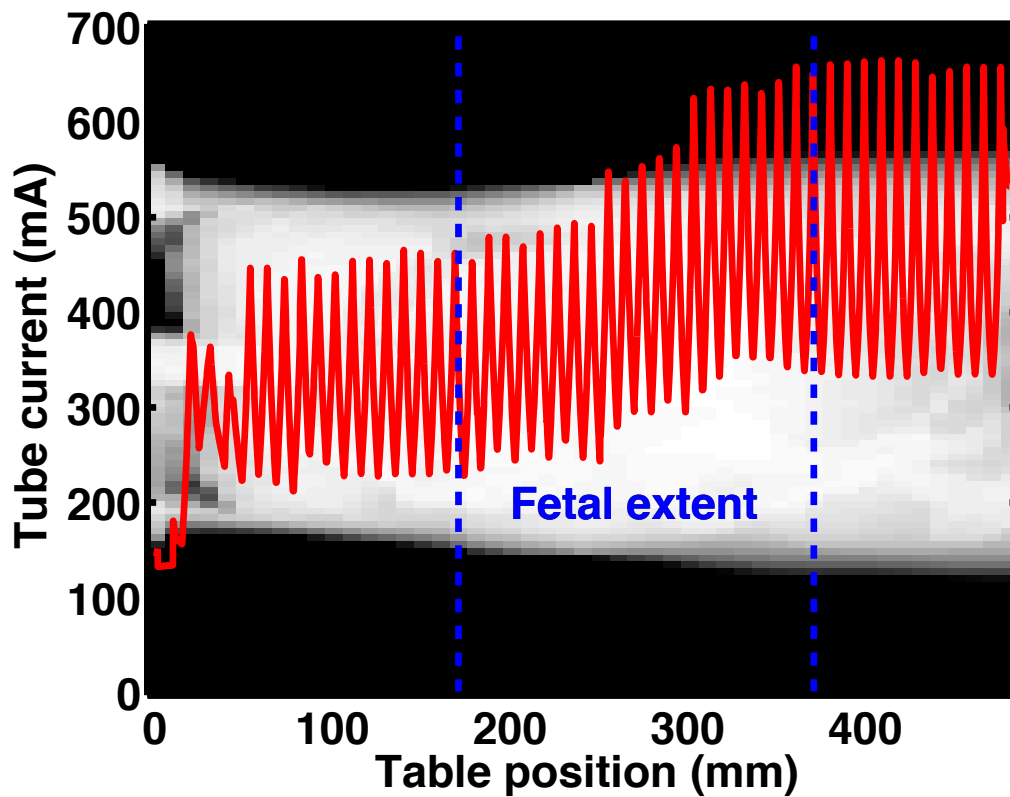


Figure 11.3. Estimated TCM scheme for a pregnant patient who received a clinically indicated CT examination. The TCM scheme is overlaid on an image of the simulated CT localizer radiograph of the pregnant patient. The portion of the scan range in which the fetus is located is indicated with blue dashed lines.

11.2.5 Size-Specific, Scan Technique-Independent Fetal Dose Estimates

In addition to the estimate of patient size described in Section 11.2.1, for each patient, an estimate of scanner output was determined. Scanner output was determined as $CTDI_{vol}$ based on the average tube current across the entire scan range. The scanner output metric is based on $CTDI_{vol}$ measured with the body (32 cm diameter) CTDI phantom.

Using the patient size and scanner output data determined for each patient, size-specific, scan technique-independent fetal dose estimates were determined. Fetal doses for each patient were first normalized by the corresponding $CTDI_{vol}$ values. Then correlations between $CTDI_{vol}$ -normalized fetal dose and WED were established. Correlations were established separately for both FTC and TCM fetal doses.

Regression equations describing the correlations between $CTDI_{vol}$ -normalized organ dose and WED served as the means to generate scan technique-independent fetal dose estimates for any patient size (size-specific, scan technique-independent $CTDI_{vol}$ -to-organ-dose conversion coefficients). An exponential relationship between $CTDI_{vol}$ -normalized fetal dose and patient size was used for FTC and TCM fetal doses. This is consistent with the observed exponential relationships between $CTDI_{vol}$ -normalized organ dose and patient size presented in Chapter 9. The exponential relationship between $CTDI_{vol}$ -normalized fetal dose and patient size is defined as:

$$\frac{D_{fetus}}{CTDI_{vol}} = A_0 \times \exp(-B_0 \times WED) \quad (11.1)$$

where A_0 and B_0 are exponential regression coefficients specific to FTC and TCM. In order to gauge the strength of these correlations, the coefficient of determination (R^2) was tabulated for each correlation.

11.2.6 Comparison of Fetal Dose Estimates

For each pregnant patient model, fetal doses were estimated using the following methods: (1) Detailed Monte Carlo simulations using the estimated TCM schemes, (2) TCM size-specific, scan technique-independent $CTDI_{vol}$ -to-organ-dose conversion coefficients, (3) FTC size-specific, scan technique-independent $CTDI_{vol}$ -to-organ-dose conversion coefficients and (4) SSDE conversion coefficients. SSDE conversion coefficients were calculated for each patient using Eq. (10.2) described in Section 10.2.4. Because fetal doses determined from detailed Monte Carlo simulations are based on actual patient anatomy and estimated TCM schemes determined using validated methods, those fetal doses were considered the “gold standard.” For each patient, the error between the “gold standard” and estimated fetal doses was then calculated.

11.3 Results

Table 11.2 shows the gestational age, estimate of patient size (WED) and fetal dose and $CTDI_{vol}$ for both the FTC and TCM simulations for each of the pregnant patient models used in this investigation. Fetal dose ranges from 16.94 to 29.76 mGy for FTC simulations and 12.17 to 22.11 mGy for TCM simulations.

Table 11.2. Patient characteristics and fetal doses for pregnant patients used in this investigation.

Patient	Gestational age (wk)	WED (cm)	FTC		TCM	
			Fetal dose (mGy)	CTDI _{vol}	Fetal dose (mGy)	CTDI _{vol}
1	12.1	25.34	29.76	15.36	21.12	12.78
2	14.3	31.99	22.72	15.36	21.69	16.30
3	17.0	29.53	23.83	15.36	18.71	13.27
4	17.1	25.93	25.75	15.36	17.25	11.44
5	18.5	26.55	29.47	15.36	15.58	9.54
6	20.3	34.59	17.99	15.36	17.29	16.99
7	22.0	30.63	22.71	15.36	21.65	17.58
8	23.7	35.62	16.94	15.36	17.91	17.88
9	24.0	29.65	24.14	15.36	16.81	11.44
10	24.4	28.16	24.05	15.36	16.68	12.19
11	25.0	27.93	25.23	15.36	22.11	14.71
12	27.0	27.88	23.61	15.36	12.17	9.30
13	27.4	30.84	24.30	15.36	19.76	14.20
14	27.4	35.55	18.03	15.36	21.82	20.88
15	28.3	33.97	19.84	15.36	20.63	17.58
16	29.4	31.67	20.00	15.36	19.23	17.90
17	35.0	28.48	21.71	15.36	17.62	14.04
18	35.9	35.27	18.49	15.36	18.88	17.03

Figure 11.4 shows FTC and TCM CTDI_{vol}-normalized fetal doses determined from detail Monte Carlo simulations (fetal dose divided by CTDI_{vol} from Table 11.2) as well as the exponential regression equations for the FTC and TCM size-specific, scan technique-independent fetal dose estimates. Also shown is the exponential regression equation for SSDE from AAPM Report 204 (Eq. (10.2)). The exponential regression coefficients and R² for FTC and TCM fetal dose estimates are shown in Table 11.3. R² greater than 0.8 for the FTC and TCM scenarios indicates that fetal dose from FTC and TCM CT examinations of pregnant patients of various gestational ages can be reasonably estimated using CTDI_{vol}-to-fetal-dose conversion coefficients. Table 11.4 shows the comparison of fetal dose from detailed Monte Carlo simulations of TCM CT exams (“gold standard”) and fetal dose estimated using the TCM, FTC

and SSDE conversion coefficients. The mean error across all patients between the “gold standard” and the estimation methods was 6.36%, 12.32% and 8.21% for TCM, FTC and SSDE conversion coefficients, respectively.

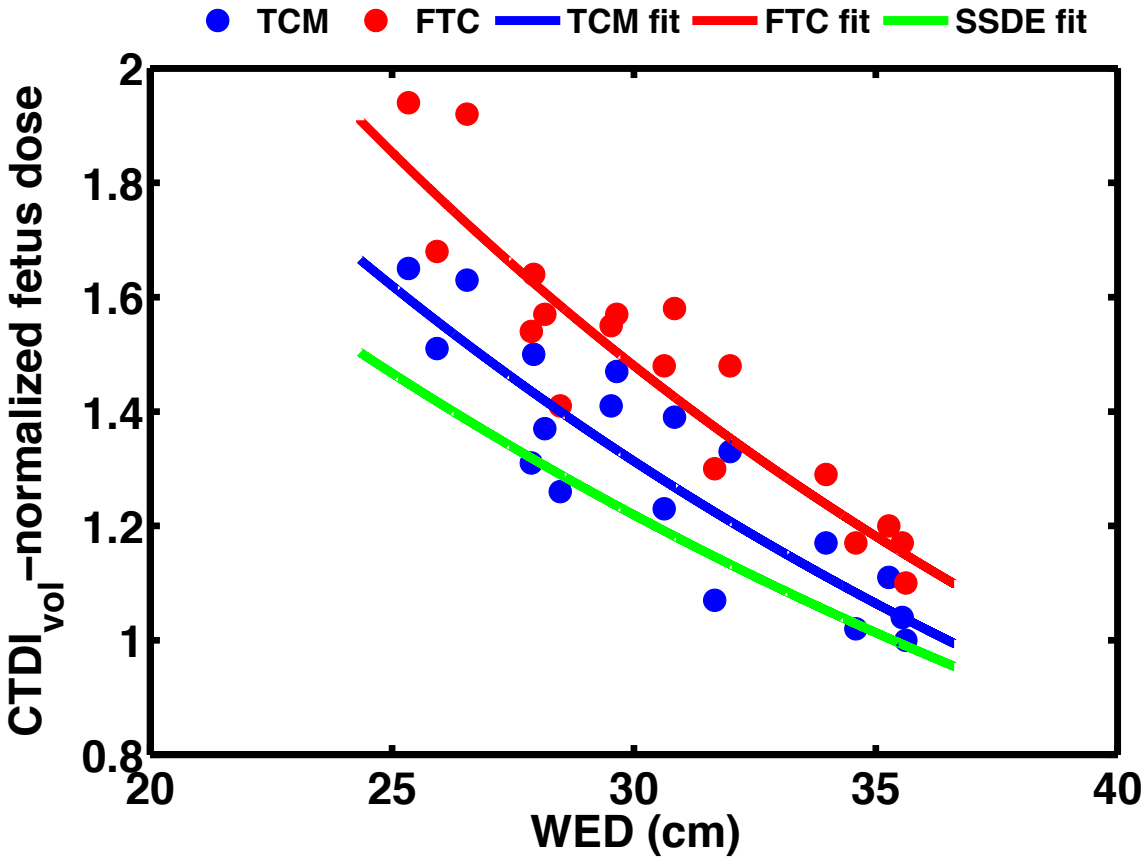


Figure 11.4. FTC and TCM CTDI_{vol}-normalized fetal doses determined from detail Monte Carlo simulations as well as TCM, FTC and SSDE conversion coefficients (fits).

Table 11.3. Exponential regression coefficients and R² for fetal dose estimation.

Organ	FTC			TCM		
	A ₀	B ₀	R ²	A ₀	B ₀	R ²
Fetus	5.71	0.045	0.86	4.63	0.042	0.81

Table 11.4. Error between simulated fetal dose and fetal dose estimated using TCM, FTC and SSDE conversion coefficients.

Patient	Fetal dose (mGy)						
	Simulation	TCM	% error	FTC	% error	SSDE	% error
1	21.12	20.42	3.32	23.32	10.44	18.55	12.18
2	21.69	19.69	9.21	22.05	1.66	18.49	14.75
3	18.71	17.77	5.01	20.05	7.15	16.49	11.89
4	17.25	17.83	3.36	20.33	17.86	16.24	5.84
5	15.58	14.48	7.07	16.48	5.77	13.23	15.08
6	17.29	18.40	6.44	20.45	18.26	17.51	1.26
7	21.65	22.49	3.88	25.29	16.79	20.97	3.12
8	17.91	18.54	3.51	20.53	14.64	17.73	1.02
9	16.81	15.24	9.34	17.18	2.23	14.14	15.85
10	16.68	17.29	3.67	19.59	17.42	15.93	4.50
11	22.11	21.08	4.67	23.89	8.05	19.39	12.28
12	12.17	13.35	9.69	15.13	24.34	12.28	0.91
13	19.76	18.00	8.92	20.22	2.33	16.80	14.97
14	21.82	21.72	0.48	24.06	10.25	20.76	4.87
15	20.63	19.54	5.31	21.74	5.40	18.53	10.20
16	19.23	21.91	13.92	24.55	27.67	20.54	6.80
17	17.62	19.65	11.53	22.24	26.21	18.13	2.91
18	18.88	17.92	5.10	19.87	5.22	17.10	9.41
Average % error			6.36		12.32		8.21
Standard deviation			3.44		8.40		5.34

11.4 Discussion

In this chapter, the methods for estimating dose to patient models without TCM, size or even topogram data (that is, voxel representation only) were applied to 18 pregnant patient models to estimate fetal dose from CT abdomen/pelvis exams using TCM. These fetal dose estimates were obtained using methods to simulate a topogram, estimate the required patient size information and create the TCM function, which were used in Monte Carlo simulations. The resulting fetal doses were normalized by scanner output ($CTDI_{vol}$) and correlated with patient size (WED) to create size-specific, scan technique-independent fetal dose estimates. As described in Section

11.2.1, WED was measured at the image containing the three-dimensional geometric centroid of the fetus. For a handful of the patient models, there was some anatomy outside of the field of view (FOV). Therefore, for these patients, the calculated WED was a slight underestimate of the actual WED. Anatomy outside of the FOV also impacted the estimates of AP and LAT dimensions of patient size used as the inputs to the methods to estimate Siemens TCM schemes. Underestimated patient size results in artificially low tube current values, but the resulting $CTDI_{vol}$ based on the average tube current across the entire scan range is also underestimated, so the effect of slightly underestimated patient size on $CTDI_{vol}$ -normalized fetal dose should be minimal. Collectively, the result of anatomy outside of the FOV was a slightly conservative estimate of size-specific fetal dose.

Using the appropriate exponential regression coefficients presented in Table 11.3 in conjunction with Eq. (11.1), size-specific, scan technique-independent $CTDI_{vol}$ -to-fetal-dose conversion coefficients can be generated using a measure of WED. As shown in Fig. 11.4, for a given patient size, FTC conversion coefficients are slightly greater than TCM conversion coefficients. In this investigation, the FTC and TCM conversion coefficients are pseudo-protocol-specific. The scanner output, $CTDI_{vol}$ based on the average tube current across the entire scan range, is protocol-specific whereas the patient size metric, WED measured at the image containing the three-dimensional geometric centroid of the fetus, is more organ-specific. As such, local variations in the tube current profile are not accounted for in the estimate of $CTDI_{vol}$. Because of the inclusion of both the tail end of the low-attenuation (i.e. low tube current) thorax region (right side of Figure 11.3) and the high-attenuation (i.e. high tube current) pelvic region (left side of Figure 11.3) in the scan range, the average tube current for TCM scans can be either greater than or less than that for FTC scans. The fetal anatomy, though, is centrally

located within the scan range, so for TCM scans, the fetus is subjected to an average tube current different than the average tube current across the entire scan range. Therefore, the increase or decrease of $CTDI_{vol}$ for TCM scans relative to $CTDI_{vol}$ for FTC scans will not necessarily translate into an equivalent increase or decrease of fetal dose for TCM scans relative to fetal dose for FTC scans. As shown in Table 11.2, even though the $CTDI_{vol}$ values for TCM scans are both greater than and less than the $CTDI_{vol}$ values for FTC scans (8 greater than and 10 less than), TCM fetal doses are consistently less than the FTC fetal doses such that $CTDI_{vol}$ -normalized fetal doses for TCM scans that are less than $CTDI_{vol}$ -normalized fetal doses for FTC scans. In Chapter 10, a similar relationship was observed for conversion coefficients determined using the protocol-specific approach for fully-irradiated organs within the abdomen/pelvis protocol (Fig. 10.1 – Fig. 10.3).

Also shown in Fig. 11.4, for a given patient size, both FTC and TCM conversion coefficients are greater than SSDE conversion coefficients. SSDE conversion coefficients were based, in part, on the average dose to organs in the abdomen (e.g. liver, kidney, spleen) determined using Monte Carlo simulations of FTC abdomen protocols for a set of reference voxelized phantoms [36]. These soft tissue organs are essentially water-equivalent in composition. In this investigation, fetal dose is tallied in fetal anatomy consisting of both soft tissue and bone voxels. Because the ratio of mass energy-absorption coefficients for bone to water is greater than unity, absorbed dose to the fetus will be greater than absorbed dose to any of the abdominal organs [17]. As such, for an equivalent $CTDI_{vol}$, the $CTDI_{vol}$ -normalized fetal dose will be greater than $CTDI_{vol}$ -normalized organ dose for abdominal organs.

As presented in Table 11.4, TCM conversion coefficients provided the best estimate of fetal doses from detailed Monte Carlo simulations of TCM scans. While it is recognized that this

is somewhat of a “circular” comparison because the TCM conversion coefficients were generated using the fetal doses from detailed Monte Carlo simulations to which they are being compared, the comparison is used primarily to quantify the accuracy of the TCM conversion coefficients relative to the FTC and SSDE conversion coefficients. In AAPM Report 204, the acceptable tolerance for differences between estimated and actual patient dose was 10% to 20% [36]. This tolerance level was established for size-specific, scan technique-independent patient dose estimates. Given the similarities to the conversion coefficients used in this investigation to estimate fetal dose (i.e. size-specific and scan technique-independent), errors within this range were considered to be indicative of reasonably accurate fetal dose estimates. The mean errors across all patients between the “gold standard” and the FTC and SSDE conversion coefficient estimation methods were within the 20% tolerance. This indicates that FTC and SSDE conversion coefficients, which were generated from FTC data, can provide reasonable accuracy in estimating fetal doses from TCM scans.

Although the maternal and fetal anatomy used in this work was the same as that used in the work by Angel *et al.*, there are distinct differences between fetal dose normalization and patient size from the two investigations [5]. In the investigation by Angel *et al.*, the correlation between fetal dose normalized on the basis of 100 mAs and maternal perimeter was presented for FTC scans only. In the investigation described in this chapter, correlations between $CTDI_{vol}$ -normalized fetal dose and WED were presented for FTC and TCM scans. Those differences aside, Angel *et al.* estimated the average fetal dose from FTC scans to be 10.8 mGy per 100 mAs. In this investigation, 200 effective mAs was used to determine FTC doses shown in Table 11.2, so multiplying the average, normalized fetal dose determined by Angel *et al.* by 200 effective mAs yields an average, absolute fetal dose of 21.6 mGy. In this investigation, the

average fetal dose from FTC scans is 22.7 mGy, so the error between the FTC fetal dose estimates in this investigation and those in the investigation by Angel *et al.* is 4.84%. Angel *et al.* used a model of a GE LightSpeed 16 scanner in the Monte Carlo simulations used to determine fetal doses. At the scanner settings described in that investigation, the $CTDI_{vol}$ was approximately 0.080 mGy per mAs. In this investigation, a model of a Siemens Sensation 64 scanner was used in the Monte Carlo simulations used to determine fetal doses. At the scanner settings presented in Table 11.1, the $CTDI_{vol}$ was approximately 0.077 mGy per mAs. Because the $CTDI_{vol}$ values for the scanner models used in both investigations are nearly identical, scanner-specific effects are minimal between these two sets of simulated fetal doses. Therefore, the simulations are comparable, and the resultant doses are appreciably close.

Results from this investigation indicate that fetal dose from TCM CT examinations of pregnant patients of various gestational ages may be reasonably estimated with: (a) fetal dose normalized by scanner-reported $CTDI_{vol}$ to account for scan technique variation and (b) a WED patient size metric to account for patient size variation. Results from this work can be used to readily estimate fetal dose for TCM CT exams of pregnant patients given only the scanner-reported $CTDI_{vol}$ and an attenuation-based estimate of patient size.

11.5 References

1. J. P. Felmlee, J. E. Gray, M. L. Leetzow, J. C. Price, "Estimated fetal radiation dose from multi-slice CT studies," *Am. J. Roentgenol.* **154**, 185-190 (1990).
2. L. M. Hurwitz *et al.*, "Radiation dose to the fetus from body MDCT during early gestation," *Am. J. Roentgenol.* **8**, 488-495 (1981).

3. D. G. Jones, P. C. Shrimpton, "Normalised organ doses for X-ray computed tomography calculated using Monte Carlo techniques," NRPB-SR250 (1993).
4. G. Stamm, H. D. Nagel, "CT-expo – a novel program for dose evaluation in CT," *Rofo*. **174**, 1570-1576 (2002).
5. E. Angel *et al.*, "Radiation dose to the fetus for pregnant patients undergoing multidetector CT imaging: Monte Carlo simulations estimating fetal dose for a range of gestational age and patient size," *Radiology* **249**, 220-227 (2010).
6. J. Gu, X. G. Xu, P. F. Caracappa, B. Liu, "Fetal doses to pregnant patients from CT with tube current modulation calculated using Monte Carlo simulation and realistic phantoms," *Radiat. Prot. Dosimetry* **155**, 64-72 (2013).
7. X. G. Xu, V. Taranenko, J. Zhang, C. Shi, "A boundary-representation method for designing whole-body radiation dosimetry: pregnant females at the ends of three gestational periods – RPI-P3, -P6 and -P9," *Phys. Med. Biol.* **52**, 7023-7044 (2007).
8. American Association of Physicists in Medicine, "Size-Specific Dose Estimates (SSDE) in Pediatric and Adult Body CT Examinations," AAPM Report 204 (2011).
9. J. J. DeMarco, T.D. Solberg, J. B. Smathers, "A CT-based Monte Carlo simulation tool for dosimetry planning and analysis," *Med. Phys.* **25**, 1-11 (1998).
10. J. H. Hubbell and S. M. Seltzer, "Tables of x-ray mass attenuation coefficients and mass energy-absorption coefficients," available at:
<http://physics.nist.gov/PhysRefData/XrayMassCoef/cover.html> (2004).

Chapter 12: Conclusion

12.1 Contributions

First, methods to estimate Siemens tube current modulation (TCM) schemes for any voxelized patient model were developed. Patient size data calculated by the CT scanner was shown to be stored in the DICOM header of the Siemens CT localizer radiograph (i.e. topogram). This size data was determined to be water-equivalent estimates of the anterior-posterior (AP) and lateral (LAT) dimensions of the patient. These AP and LAT dimensions of patient size were used as the inputs to methods to estimate TCM schemes that account for patient attenuation, on-line modulation and machine limits imposed by the scanner. TCM schemes were estimated for a set of pediatric and adult patients who underwent clinically indicated abdomen/pelvis and chest TCM CT examinations. Estimated TCM schemes were validated against actual TCM schemes extracted from the raw projection data of each patient by comparing average tube current and Monte Carlo-based organ dose estimates. Strong agreement between both average tube current and organ dose estimates demonstrated the utility of the methods to accurately estimate Siemens TCM schemes. For voxelized patient models, such as reference voxelized phantoms, for which a topogram is not available, methods were developed to determine patient attenuation information that matches the attenuation data that would have been determined by the scanner. Using the same set of pediatric and adult patients used in the validation of the TCM scheme estimation methods, simulated topograms were determined for each patient. AP and LAT dimensions of patient size were calculated from the simulated topograms and used as the input to the TCM scheme estimation methods. Estimated TCM schemes based on patient size data calculated from simulated topograms were validated against actual TCM schemes by comparing average tube

current and Monte Carlo-based organ dose estimates. Strong agreement demonstrated the accuracy of the end-to-end system to estimate patient size data in the Siemens manner and then use that size data as the inputs to TCM scheme estimation methods. This validated end-to-end system is generalizable to any voxelized patient model, so other researchers could use these methods to estimate TCM schemes for any patient model or computation phantom of interest.

Next, a comprehensive set of patient-specific dose estimates from TCM CT exams was developed. Simulated whole-body topograms were used to determine patient attenuation information for pediatric and adult reference voxelized phantoms from the GSF and ICRP family of reference voxelized phantoms. For each reference voxelized phantom, TCM schemes were generated for four routine body CT protocols: (1) Abdomen, (2) Abdomen/Pelvis, (3) Chest and (4) Chest/Abdomen/Pelvis (CAP). The TCM schemes were used in detailed Monte Carlo simulations to estimate dose to all radiosensitive organs for all reference voxelized phantoms and protocols. Protocol-specific and organ-specific estimates of patient size and scanner output were used to develop size-specific, scan technique-independent organ dose estimates for TCM CT exams. Correlations between $CTDI_{vol}$ -normalized organ dose and patient size served as the means to generate scan technique-independent organ dose estimates for any patient size (size-specific, scan technique-independent $CTDI_{vol}$ -to-organ-dose conversion coefficients).

Correlations between $CTDI_{vol}$ -normalized effective dose and patient size were also developed and served as the means to generate scan technique-independent effective dose estimates for any patient size (size-specific, scan technique-independent $CTDI_{vol}$ -to-effective-dose conversion coefficients). $CTDI_{vol}$ -to-organ-dose conversion coefficients determined using the protocol-specific approach could be used to estimate dose to any fully-, partially- or indirectly-irradiated organ. $CTDI_{vol}$ -to-organ-dose conversion coefficients determined using the organ-specific

approach could only be used to estimate dose to fully-irradiated organs, but a comparison of organ doses from detailed Monte Carlo simulations of patients scanned on Siemens, GE and Toshiba scanners and organ doses estimated using the organ-specific $CTDI_{vol}$ -to-organ-dose conversion coefficients demonstrated that organ dose for any TCM algorithm could be reasonably estimated using the organ-specific conversion coefficients. Protocol-specific conversion coefficients, on the other hand, were best used to estimate organ doses for the TCM algorithm used in their development.

Finally, size-specific, scan technique-independent fetal dose estimates for TCM CT examinations of pregnant patients were developed. Demonstrating the generalizability of the methods to estimate TCM schemes for any voxelized patient model, TCM schemes were estimated for a set of pregnant patients scanned on GE scanners. Fetal dose estimates were determined from detailed Monte Carlo simulations using the estimated TCM schemes. Patient size and scanner output estimates were determined for each pregnant patient and used to develop size-specific, scan technique-independent fetal dose estimates. Correlations between $CTDI_{vol}$ -normalized fetal dose and patient size served as the means to generate scan technique-independent fetal dose estimates for any patient size (size-specific, scan technique-independent $CTDI_{vol}$ -to-fetal-dose conversion coefficients). These conversion coefficients could be used to estimate fetal dose for TCM CT exams for any patient size or scan technique.

12.2 Future Work

The work presented in this dissertation can be extended in a handful of ways. TCM scheme estimation methods in this dissertation were developed explicitly for the Siemens TCM

algorithm, Care Dose4D. The foundation of these methods was knowledge of the patient attenuation data determined by Siemens and a conceptual understanding of the various components of the Siemens TCM algorithm referenced from the patent literature. Through an understanding of the attenuation data determined by other manufacturers and an in-depth inspection of the patent literature, TCM scheme estimation methods could be developed for other manufacturers, such as GE, Toshiba and Philips. This would extend organ dose estimates for partially- and indirectly-irradiated organs to scanners beyond Siemens CT scanners.

In this dissertation, size-specific, scan technique-independent organ dose and effective dose estimates were presented for four routine body CT protocols. While these protocols constitute a majority of body scanning done for pediatric and adult patients, organ doses from an arbitrary scan range may be of interest. Organ dose estimates for any arbitrary scan range could be generated by performing Monte Carlo simulations for every combination of scan start and stop locations for the set of reference voxelized phantoms used in this dissertation. This would create a complete set of organ dose and effective dose estimates for any patient size, scan technique and scan range.

Appendix A: Organ Irradiation Percentages for Protocols of Interest

A.1 Abdomen

Organ	Irradiation (%)									
	Reference Voxelized Phantom									
	Baby	Child	Donna	Frank	Golem	Helga	Irene	ICRP Female (Regina)	ICRP Male (Rex)	Visible Human
Adrenals	100.00	100.00	100.00	100.00	100.00	100.00	100.00	100.00	100.00	100.00
Gall bladder	100.00	100.00	100.00	100.00	100.00	100.00	100.00	100.00	100.00	100.00
Kidneys	100.00	100.00	100.00	100.00	100.00	100.00	100.00	100.00	100.00	100.00
Liver	100.00	100.00	100.00	100.00	100.00	100.00	100.00	100.00	100.00	100.00
Pancreas	100.00	100.00	100.00	100.00	100.00	100.00	100.00	100.00	100.00	100.00
Spleen	100.00	100.00	100.00	100.00	100.00	100.00	100.00	100.00	100.00	100.00
Stomach	100.00	100.00	100.00	100.00	100.00	100.00	100.00	100.00	100.00	100.00
Bladder	100.00	16.47	0.00	0.00	0.00	0.00	0.00	0.00	0.00	0.00
Bone surface	29.50	22.79	21.01	22.15	18.90	30.19	18.40	18.14	18.42	25.62
Breast	100.00	0.00	100.00	0.00	0.00	77.92	40.25	38.13	100.00	0.00
Colon	91.17	94.16	82.17	81.90	81.67	97.64	76.99	70.18	88.24	76.93
Gonads	100.00	64.71	0.00	0.00	0.00	0.00	0.00	0.00	0.00	0.00
Heart	100.00	100.00	79.09	80.72	71.76	86.71	42.83	52.48	63.67	72.42
Lung	87.38	65.94	46.64	45.57	43.07	60.53	31.63	36.11	42.75	44.85
Lymphatic nodes	37.72	30.91	22.48	31.17	20.36	28.37	20.78	16.81	19.77	23.33
Muscle	37.72	30.91	22.48	31.17	20.36	28.37	20.78	16.81	19.77	23.33
Oesophagus	70.00	0.00	41.30	50.00	33.33	52.27	19.86	29.58	36.69	43.75
Prostate/Uterus	100.00	94.00	0.00	0.00	0.00	0.00	0.00	0.00	0.00	0.00
Red bone marrow	29.50	22.79	21.01	22.15	18.90	30.19	18.40	18.14	18.42	25.62
Skin	38.46	26.51	20.00	32.90	21.29	18.73	16.93	18.50	21.53	26.29
Small intestine	100.00	98.07	65.32	65.82	80.49	88.71	39.43	58.98	79.06	91.39
Thymus	49.25	0.00	0.00	11.11	0.00	0.00	0.00	0.00	0.00	0.00
Brain	0.00	0.00	0.00	0.00	0.00	0.00	0.00	0.00	0.00	0.00
ET region	0.00	0.00	0.00	0.00	0.00	0.00	0.00	0.00	0.00	0.00
Oral mucosa	0.00	0.00	0.00	0.00	0.00	0.00	0.00	0.00	0.00	0.00
Salivary glands	0.00	0.00	0.00	0.00	0.00	0.00	0.00	0.00	0.00	0.00
Thyroid	0.00	0.00	0.00	0.00	0.00	0.00	0.00	0.00	0.00	0.00

A.2 Abdomen/Pelvis

Organ	Irradiation (%)									
	Reference Voxelized Phantom									
	Baby	Child	Donna	Frank	Golem	Helga	Irene	ICRP Female (Regina)	ICRP Male (Rex)	Visible Human
Adrenals	100.00	100.00	100.00	100.00	100.00	100.00	100.00	100.00	100.00	100.00
Bladder	100.00	100.00	100.00	100.00	100.00	100.00	100.00	100.00	100.00	100.00
Colon	100.00	100.00	100.00	100.00	100.00	100.00	100.00	100.00	100.00	100.00
Gall bladder	100.00	100.00	100.00	100.00	100.00	100.00	100.00	100.00	100.00	100.00
Kidneys	100.00	100.00	100.00	100.00	100.00	100.00	100.00	100.00	100.00	100.00
Liver	100.00	100.00	100.00	100.00	100.00	100.00	100.00	100.00	100.00	100.00
Pancreas	100.00	100.00	100.00	100.00	100.00	100.00	100.00	100.00	100.00	100.00
Prostate/Uterus	100.00	100.00	100.00	100.00	100.00	100.00	100.00	100.00	100.00	100.00
Small intestine	100.00	100.00	100.00	100.00	100.00	100.00	100.00	100.00	100.00	100.00
Spleen	100.00	100.00	100.00	100.00	100.00	100.00	100.00	100.00	100.00	100.00
Stomach	100.00	100.00	100.00	100.00	100.00	100.00	100.00	100.00	100.00	100.00
Bone surface	36.08	34.45	39.65	47.05	37.41	54.52	34.97	34.96	36.73	51.68
Breast	100.00	0.00	100.00	0.00	0.00	77.92	40.25	38.13	100.00	0.00
Gonads	100.00	100.00	100.00	100.00	0.00	100.00	100.00	100.00	0.00	0.00
Heart	100.00	100.00	79.09	80.72	71.76	86.71	42.83	52.48	63.67	72.42
Lung	87.38	65.94	46.64	45.57	43.07	60.53	31.63	36.11	42.75	44.85
Lymphatic nodes	49.98	50.88	41.89	63.67	35.54	51.29	43.54	36.72	37.97	41.67
Muscle	49.98	50.88	41.89	63.67	35.54	51.29	43.54	36.72	37.97	41.67
Oesophagus	70.00	0.00	41.30	50.00	33.33	52.27	19.86	29.58	36.69	43.75
Red bone marrow	36.08	34.45	39.65	47.05	37.41	54.52	34.97	34.96	36.73	51.68
Skin	49.14	39.82	33.67	54.08	31.74	34.45	31.01	30.80	33.57	51.04
Thymus	49.25	0.00	0.00	11.11	0.00	0.00	0.00	0.00	0.00	0.00
Brain	0.00	0.00	0.00	0.00	0.00	0.00	0.00	0.00	0.00	0.00
ET region	0.00	0.00	0.00	0.00	0.00	0.00	0.00	0.00	0.00	0.00
Oral mucosa	0.00	0.00	0.00	0.00	0.00	0.00	0.00	0.00	0.00	0.00
Salivary glands	0.00	0.00	0.00	0.00	0.00	0.00	0.00	0.00	0.00	0.00
Thyroid	0.00	0.00	0.00	0.00	0.00	0.00	0.00	0.00	0.00	0.00

A.3 Chest

Organ	Irradiation (%)									
	Reference Voxelized Phantom									
	Baby	Child	Donna	Frank	Golem	Helga	Irene	ICRP Female (Regina)	ICRP Male (Rex)	Visible Human
Breast	100.00	-	100.00	100.00	-	100.00	100.00	100.00	100.00	-
Heart	100.00	100.00	100.00	100.00	100.00	100.00	100.00	100.00	100.00	100.00
Lung	100.00	100.00	100.00	100.00	100.00	100.00	100.00	100.00	100.00	100.00
Thymus	100.00	100.00	100.00	100.00	100.00	100.00	100.00	100.00	100.00	100.00
Adrenals	100.00	100.00	58.33	87.84	100.00	90.91	73.33	100.00	100.00	100.00
Bone surface	32.06	22.91	23.24	33.37	22.31	29.92	29.28	20.69	22.53	31.92
Colon	18.95	0.00	3.10	17.62	13.35	10.73	0.30	0.00	13.32	29.63
ET region	100.00	100.00	100.00	52.85	100.00	100.00	100.00	100.00	100.00	100.00
Gall bladder	100.00	100.00	100.00	100.00	66.67	100.00	8.70	100.00	100.00	100.00
Kidneys	63.59	36.89	51.15	12.51	34.93	12.56	26.93	26.03	47.08	34.47
Liver	97.91	95.17	91.85	96.98	95.26	88.73	63.61	91.56	96.08	96.66
Lymphatic nodes	46.67	26.92	21.94	35.07	23.14	22.41	22.59	20.56	21.38	29.37
Muscle	46.67	26.92	21.94	35.07	23.14	22.41	22.59	20.56	21.38	29.37
Oesophagus	100.00	100.00	100.00	92.35	91.67	97.73	100.00	93.66	89.93	99.31
Pancreas	100.00	100.00	100.00	100.00	67.77	100.00	90.69	24.63	76.99	100.00
Red bone marrow	32.06	22.91	23.24	33.37	22.31	29.92	29.28	20.69	22.53	31.92
Skin	35.02	22.48	15.92	38.19	20.43	21.08	19.83	19.55	21.07	19.67
Small intestine	22.83	7.14	0.00	4.52	7.90	8.83	0.00	4.89	5.65	18.65
Spleen	100.00	90.77	94.29	99.18	100.00	91.72	92.82	100.00	100.00	99.68
Stomach	100.00	84.48	92.07	100.00	93.11	100.00	84.15	71.12	98.59	100.00
Thyroid	100.00	100.00	100.00	52.85	100.00	100.00	100.00	100.00	100.00	100.00
Bladder	0.00	0.00	0.00	0.00	0.00	0.00	0.00	0.00	0.00	0.00
Brain	0.00	0.00	0.00	0.00	0.00	0.00	0.00	0.00	0.00	0.00
Gonads	0.00	0.00	0.00	0.00	0.00	0.00	0.00	0.00	0.00	0.00
Oral mucosa	0.00	0.00	0.00	0.00	0.00	0.00	0.00	0.00	0.00	0.00
Prostate/Uterus	0.00	0.00	0.00	0.00	0.00	0.00	0.00	0.00	0.00	0.00
Salivary glands	0.00	0.00	0.00	0.00	0.00	0.00	0.00	0.00	0.00	0.00

**No breast voxels were identified in the Child, Golem and Visible Human reference voxelized phantoms.

A.4 Chest/Abdomen/Pelvis (CAP)

Organ	Irradiation (%)									
	Reference Voxelized Phantom									
	Baby	Child	Donna	Frank	Golem	Helga	Irene	ICRP Female (Regina)	ICRP Male (Rex)	Visible Human
Adrenals	100.00	100.00	100.00	100.00	100.00	100.00	100.00	100.00	100.00	100.00
Bladder	100.00	100.00	100.00	100.00	100.00	100.00	100.00	100.00	100.00	100.00
Breast	100.00	-	100.00	100.00	-	100.00	100.00	100.00	100.00	-
Colon	100.00	100.00	100.00	100.00	100.00	100.00	100.00	100.00	100.00	100.00
Gall bladder	100.00	100.00	100.00	100.00	100.00	100.00	100.00	100.00	100.00	100.00
Heart	100.00	100.00	100.00	100.00	100.00	100.00	100.00	100.00	100.00	100.00
Kidneys	100.00	100.00	100.00	100.00	100.00	100.00	100.00	100.00	100.00	100.00
Liver	100.00	100.00	100.00	100.00	100.00	100.00	100.00	100.00	100.00	100.00
Lung	100.00	100.00	100.00	100.00	100.00	100.00	100.00	100.00	100.00	100.00
Pancreas	100.00	100.00	100.00	100.00	100.00	100.00	100.00	100.00	100.00	100.00
Prostate/Uterus	100.00	100.00	100.00	100.00	100.00	100.00	100.00	100.00	100.00	100.00
Small intestine	100.00	100.00	100.00	100.00	100.00	100.00	100.00	100.00	100.00	100.00
Spleen	100.00	100.00	100.00	100.00	100.00	100.00	100.00	100.00	100.00	100.00
Stomach	100.00	100.00	100.00	100.00	100.00	100.00	100.00	100.00	100.00	100.00
Thymus	100.00	100.00	100.00	100.00	100.00	100.00	100.00	100.00	100.00	100.00
Bone surface	48.06	45.13	53.37	67.61	50.34	70.38	55.49	47.39	49.55	69.48
ET region	100.00	100.00	100.00	52.85	100.00	100.00	100.00	100.00	100.00	100.00
Gonads	100.00	100.00	100.00	100.00	0.00	100.00	100.00	100.00	0.00	0.00
Lymphatic nodes	73.52	62.47	54.11	84.19	49.84	62.36	57.86	51.54	50.88	59.31
Muscle	73.52	62.47	54.11	84.19	49.84	62.36	57.86	51.54	50.88	59.31
Oesophagus	100.00	100.00	100.00	92.35	91.67	97.73	100.00	93.66	89.93	99.31
Red bone marrow	48.06	45.13	53.37	67.61	50.34	70.38	55.49	47.39	49.55	69.48
Skin	61.04	48.13	40.91	72.51	41.22	45.94	43.06	41.81	43.83	59.29
Thyroid	100.00	100.00	100.00	52.85	100.00	100.00	100.00	100.00	100.00	100.00
Brain	0.00	0.00	0.00	0.00	0.00	0.00	0.00	0.00	0.00	0.00
Oral mucosa	0.00	0.00	0.00	0.00	0.00	0.00	0.00	0.00	0.00	0.00
Salivary glands	0.00	0.00	0.00	0.00	0.00	0.00	0.00	0.00	0.00	0.00

**No breast voxels were identified in the Child, Golem and Visible Human reference voxelized phantoms.

Appendix B: Estimates of Organ Dose and ICRP Publication 103 Calculations of Effective Dose for GSF and ICRP Reference Voxelized Phantoms

B.1 Baby

Organ	ICRP 103 Tissue weighting factor (w_T)	Dose (mGy)								
		FTC				TCM				
		Abd	AbdPel	Chest	CAP	Abd	AbdPel	Chest	CAP	
Primary organs	Breast	0.12	20.54	20.00	30.67	30.85	1.00	1.01	3.05	3.06
	Colon	0.12	32.50	35.62	9.79	35.84	2.78	3.10	1.19	4.15
	Lung	0.12	28.93	29.03	35.93	36.68	2.14	2.14	3.64	3.73
	Red bone marrow	0.12	8.96	10.70	9.72	14.43	0.76	0.94	1.04	1.67
	Stomach	0.12	35.23	35.33	32.17	36.10	2.93	2.95	3.58	3.99
	Gonads	0.08	34.63	38.07	1.93	37.72	3.83	4.13	0.22	5.50
	Bladder	0.04	30.31	38.51	1.36	37.81	3.63	4.23	0.15	5.65
	Esophagus	0.04	24.11	24.26	33.98	34.79	1.84	1.85	3.56	3.64
	Liver	0.04	35.80	36.09	32.93	36.92	2.93	2.95	3.55	4.05
	Thyroid	0.04	3.27	3.35	34.84	34.62	0.23	0.23	3.88	3.90
	Bone surface	0.01	43.96	52.32	47.62	70.58	3.73	4.57	5.10	8.17
	Brain	0.01	0.26	0.26	1.11	1.15	0.02	0.02	0.13	0.13
	Salivary glands	0.01	0.26	0.26	1.11	1.15	0.02	0.02	0.13	0.13
	Skin	0.01	12.89	16.31	11.52	20.17	1.12	1.48	1.25	2.42
Remainder organs	Adrenals		34.10	34.42	29.42	34.74	2.78	2.82	3.21	3.80
	ET region		3.27	3.35	34.84	34.62	0.23	0.23	3.88	3.90
	Gall Bladder		36.88	37.40	27.98	37.30	3.03	3.05	3.00	4.14
	Heart		33.83	33.83	37.61	38.36	2.53	2.53	3.77	3.86
	Kidneys		36.38	37.04	19.55	37.36	3.00	3.06	2.21	4.11
	Lymphatic nodes		13.94	17.72	15.90	25.09	1.20	1.59	1.71	2.97
	Muscle	0.12	13.94	17.72	15.90	25.09	1.20	1.59	1.71	2.97
	Oral mucosa		0.26	0.26	1.11	1.15	0.02	0.02	0.13	0.13
	Pancreas		35.99	36.12	30.07	36.18	2.95	2.97	3.38	4.02
	Prostate/Uterus		34.67	38.48	1.90	37.72	3.74	4.09	0.22	5.45
	Small intestine		35.87	36.82	10.88	37.11	3.07	3.16	1.27	4.24
	Spleen		35.49	35.69	32.83	36.47	2.94	2.98	3.67	4.05
	Thymus		19.14	19.19	35.42	35.86	1.15	1.16	3.52	3.56
Effective dose (mSv)			25.30	26.72	21.80	32.03	2.11	2.25	2.32	3.67

B.2 Child

Organ		ICRP 103 Tissue weighting factor (w_T)	Dose (mGy)									
			FTC				TCM					
			Abd	AbdPel	Chest	CAP	Abd	AbdPel	Chest	CAP		
Primary organs	Breast	0.12	0.00	0.00	0.00	0.00	0.00	0.00	0.00	0.00	0.00	0.00
	Colon	0.12	24.20	26.45	5.09	26.70	5.33	5.92	1.23	7.92		
	Lung	0.12	16.24	16.29	25.12	25.65	3.28	3.29	7.16	7.33		
	Red bone marrow	0.12	3.98	5.97	4.37	8.07	0.86	1.39	1.30	2.53		
	Stomach	0.12	26.17	26.42	19.48	26.94	5.45	5.52	4.93	7.53		
	Gonads	0.08	14.03	25.19	0.72	26.23	3.19	6.23	0.19	8.32		
	Bladder	0.04	5.00	26.54	0.29	26.49	1.10	6.77	0.08	9.02		
	Esophagus	0.04	5.84	5.87	25.96	26.09	1.16	1.16	7.80	7.87		
	Liver	0.04	25.25	25.47	21.42	26.44	5.36	5.41	6.36	7.52		
	Thyroid	0.04	1.75	1.79	29.15	29.30	0.35	0.35	9.23	9.29		
	Bone surface	0.01	19.01	28.41	20.70	38.24	4.10	6.62	6.17	11.97		
	Brain	0.01	0.14	0.14	0.62	0.64	0.03	0.03	0.19	0.20		
	Salivary glands	0.01	0.14	0.14	0.62	0.64	0.03	0.03	0.19	0.20		
	Skin	0.01	6.22	9.37	5.31	11.51	1.36	2.22	1.55	3.64		
Remainder organs	Adrenals		22.17	22.43	19.62	23.18	4.70	4.74	5.44	6.57		
	ET region		1.75	1.79	29.15	29.30	0.35	0.35	9.23	9.29		
	Gall Bladder		24.45	24.70	18.02	25.48	5.21	5.28	5.03	7.25		
	Heart		23.77	23.81	28.17	28.88	4.72	4.72	7.67	7.87		
	Kidneys		25.63	26.21	9.45	26.54	5.66	5.81	2.82	7.87		
	Lymphatic nodes		7.77	12.60	6.63	15.47	1.69	2.99	1.94	4.91		
	Muscle	0.12	7.77	12.60	6.63	15.47	1.69	2.99	1.94	4.91		
	Oral mucosa		0.14	0.14	0.62	0.64	0.03	0.03	0.19	0.20		
	Pancreas		24.45	24.70	18.02	25.48	5.21	5.28	5.03	7.25		
	Prostate/Uterus		12.95	25.42	0.55	24.80	2.80	6.24	0.16	8.34		
	Small intestine		24.04	27.37	3.35	27.44	5.29	6.24	0.76	8.36		
	Spleen		25.11	25.36	21.33	26.14	5.51	5.58	5.30	7.69		
	Thymus		5.84	5.87	25.96	26.09	1.16	1.16	7.80	7.87		
Effective dose (mSv)			13.26	15.95	11.62	20.15	2.82	3.54	3.28	6.03		

B.3 Donna

Organ	ICRP 103 Tissue weighting factor (w_T)	Dose (mGy)								
		FTC				TCM				
		Abd	AbdPel	Chest	CAP	Abd	AbdPel	Chest	CAP	
Primary organs	Breast	0.12	13.61	13.64	15.33	15.72	12.92	12.98	17.54	18.06
	Colon	0.12	14.26	17.32	1.70	17.48	12.98	18.01	1.69	20.88
	Lung	0.12	8.26	8.29	17.88	18.39	6.46	6.53	16.22	16.78
	Red bone marrow	0.12	2.16	3.70	2.83	5.43	1.84	4.42	3.04	6.84
	Stomach	0.12	16.71	16.79	13.73	18.09	13.87	14.03	13.17	18.10
	Gonads	0.08	1.50	13.23	0.09	13.40	1.42	20.83	0.08	21.37
	Bladder	0.04	0.96	16.65	0.05	16.74	0.96	27.26	0.04	27.48
	Esophagus	0.04	6.81	6.81	17.07	17.55	5.33	5.35	16.98	17.48
	Liver	0.04	16.49	16.59	14.51	18.00	13.13	13.31	13.04	17.40
	Thyroid	0.04	0.69	0.70	23.37	23.49	0.53	0.56	30.23	30.51
	Bone surface	0.01	10.63	17.99	13.51	26.15	9.06	21.44	14.37	32.81
	Brain	0.01	0.05	0.05	0.27	0.29	0.04	0.04	0.32	0.34
	Salivary glands	0.01	0.05	0.05	0.27	0.29	0.04	0.04	0.32	0.34
	Skin	0.01	3.50	5.93	2.93	7.42	3.14	7.31	3.06	9.64
Remainder organs	Adrenals		14.83	15.02	7.55	15.64	12.19	12.47	6.92	15.54
	ET region		0.69	0.70	23.37	23.49	0.53	0.56	30.23	30.51
	Gall Bladder		17.03	17.16	11.35	17.90	13.66	13.94	8.92	17.38
	Heart		12.84	12.86	20.21	20.82	10.68	10.73	18.58	19.25
	Kidneys		15.10	15.41	7.09	15.95	12.38	12.84	6.54	15.91
	Lymphatic nodes		3.98	6.81	3.82	8.92	3.43	8.20	3.87	11.21
	Muscle	0.12	3.98	6.81	3.82	8.92	3.43	8.20	3.87	11.21
	Oral mucosa		0.05	0.05	0.27	0.29	0.04	0.04	0.32	0.34
	Pancreas		15.63	15.83	9.55	16.54	12.63	12.89	8.57	16.19
	Prostate/Uterus		0.99	14.17	0.06	14.33	0.97	22.94	0.06	23.17
	Small intestine		11.03	17.44	0.47	17.49	10.65	20.82	0.42	22.98
	Spleen		15.62	15.73	12.63	17.14	13.33	13.56	13.50	17.60
	Thymus		3.89	3.86	21.07	21.36	2.83	2.81	17.08	17.28
Effective dose (mSv)			8.93	11.41	9.67	15.29	7.70	11.82	9.89	17.55

B.4 Frank

Organ		ICRP 103 Tissue weighting factor (w _T)	Dose (mGy)							
			FTC				TCM			
			Abd	AbdPel	Chest	CAP	Abd	AbdPel	Chest	CAP
Primary organs	Breast	0.12	1.96	1.98	15.05	15.27	1.57	1.63	8.05	8.34
	Colon	0.12	11.71	14.86	3.59	15.12	18.41	21.97	4.91	23.63
	Lung	0.12	7.74	7.79	15.66	16.21	7.27	7.33	12.85	13.71
	Red bone marrow	0.12	2.01	3.57	3.60	5.85	2.48	4.43	3.57	6.88
	Stomach	0.12	12.54	12.77	11.37	13.93	18.34	18.61	14.64	20.35
	Gonads	0.08	0.43	8.21	0.05	8.20	0.61	10.42	0.08	11.59
	Bladder	0.04	1.18	12.43	0.13	12.53	1.68	14.54	0.19	16.73
	Esophagus	0.04	7.50	7.59	14.17	14.94	7.81	7.85	13.09	14.27
	Liver	0.04	12.32	12.51	11.58	13.82	17.88	18.10	15.33	20.27
	Thyroid	0.04	0.46	0.45	11.54	11.56	0.49	0.50	13.36	13.45
	Bone surface	0.01	9.93	17.26	17.19	27.99	12.37	21.48	17.15	33.06
	Brain	0.01	0.02	0.02	0.14	0.14	0.02	0.02	0.14	0.15
	Salivary glands	0.01	0.07	0.07	0.84	0.85	0.08	0.09	0.89	0.91
	Skin	0.01	5.11	8.45	6.20	11.77	6.78	10.81	6.52	14.67
Remainder organs	Adrenals		10.63	11.03	7.70	11.97	16.84	17.33	11.03	18.48
	ET region		0.46	0.45	11.54	11.56	0.49	0.50	13.36	13.45
	Gall Bladder		12.26	12.55	9.52	13.67	19.55	19.93	9.92	21.04
	Heart		10.63	10.68	15.90	16.52	9.23	9.30	12.95	14.06
	Kidneys		11.56	12.58	3.55	12.94	19.00	20.14	5.51	21.29
	Lymphatic nodes		4.70	8.62	5.39	11.80	6.82	11.72	6.07	15.74
	Muscle	0.12	4.70	8.62	5.39	11.80	6.82	11.72	6.07	15.74
	Oral mucosa		0.02	0.02	0.14	0.14	0.02	0.02	0.14	0.15
	Pancreas		11.02	11.43	8.04	12.27	17.32	17.84	11.00	19.11
	Prostate/Uterus		0.43	8.21	0.05	8.20	0.61	10.42	0.08	11.59
	Small intestine		8.57	13.73	1.80	13.90	12.85	18.52	2.40	20.51
	Spleen		13.19	13.36	12.15	14.90	20.04	20.28	18.29	22.00
	Thymus		5.12	5.23	16.03	16.25	3.84	3.78	9.97	10.38
Effective dose (mSv)			6.22	8.23	8.55	12.58	8.35	10.77	8.20	14.63

B.5 Golem

Organ	ICRP 103 Tissue weighting factor (w_T)	Dose (mGy)									
		FTC				TCM					
		Abd	AbdPel	Chest	CAP	Abd	AbdPel	Chest	CAP		
Primary organs	Breast	0.12	0.00	0.00	0.00	0.00	0.00	0.00	0.00	0.00	0.00
	Colon	0.12	16.16	19.41	3.65	19.62	11.91	15.06	3.12	18.39	
	Lung	0.12	8.32	8.37	18.38	18.83	4.27	4.30	14.20	14.61	
	Red bone marrow	0.12	2.27	3.91	2.83	5.55	1.51	3.30	2.57	5.71	
	Stomach	0.12	17.73	17.80	14.30	18.96	11.70	11.79	11.96	15.39	
	Gonads	0.08	0.06	1.19	0.01	1.14	0.05	1.60	0.01	1.94	
	Bladder	0.04	1.56	17.85	0.06	17.96	1.16	17.56	0.05	21.11	
	Esophagus	0.04	5.82	5.82	16.34	16.73	3.28	3.30	15.13	15.56	
	Liver	0.04	16.90	16.98	14.09	18.18	11.09	11.18	12.24	14.85	
	Thyroid	0.04	0.63	0.64	21.38	21.50	0.35	0.37	27.56	27.67	
	Bone surface	0.01	10.90	18.52	13.30	26.14	7.31	15.58	12.03	26.85	
	Brain	0.01	0.05	0.05	0.28	0.29	0.03	0.03	0.30	0.31	
	Salivary glands	0.01	0.05	0.05	0.28	0.29	0.03	0.03	0.30	0.31	
	Skin	0.01	3.84	5.79	3.70	7.62	2.64	4.85	3.27	7.80	
Remainder organs	Adrenals		15.93	16.17	12.86	16.83	10.89	11.03	10.31	14.10	
	ET region		0.63	0.64	21.38	21.50	0.35	0.37	27.56	27.67	
	Gall Bladder		18.61	18.73	5.81	19.43	12.87	13.05	9.74	16.07	
	Heart		12.70	12.73	20.68	21.32	6.64	6.67	14.31	14.84	
	Kidneys		18.31	18.68	6.63	19.07	13.17	13.50	5.24	16.70	
	Lymphatic nodes		3.93	6.44	4.05	8.82	2.69	5.56	3.70	9.21	
	Muscle	0.12	3.93	6.44	4.05	8.82	2.69	5.56	3.70	9.21	
	Oral mucosa		0.05	0.05	0.28	0.29	0.03	0.03	0.30	0.31	
	Pancreas		16.84	17.05	8.02	17.50	11.43	11.53	7.65	14.51	
	Prostate/Uterus		0.45	11.82	0.04	11.86	0.35	14.00	0.03	16.61	
	Small intestine		15.60	19.30	2.58	19.50	11.22	15.15	2.04	18.49	
	Spleen		16.10	16.21	15.79	17.72	11.02	11.09	12.81	14.87	
	Thymus		1.57	1.55	20.86	21.04	0.84	0.84	21.07	21.13	
Effective dose (mSv)			7.64	9.27	8.08	12.85	5.04	6.76	7.27	11.96	

B.6 Helga

Organ		ICRP 103 Tissue weighting factor (w_T)	Dose (mGy)							
			FTC				TCM			
			Abd	AbdPel	Chest	CAP	Abd	AbdPel	Chest	CAP
Primary organs	Breast	0.12	9.21	9.26	11.83	12.26	9.67	9.77	12.70	13.25
	Colon	0.12	14.87	15.85	2.69	16.02	16.27	17.90	3.67	21.13
	Lung	0.12	8.33	8.36	14.33	14.93	8.04	8.09	14.54	15.35
	Red bone marrow	0.12	2.90	4.64	3.25	6.41	3.22	6.12	3.73	8.63
	Stomach	0.12	14.29	14.39	12.50	15.41	17.64	17.72	16.94	20.45
	Gonads	0.08	1.54	11.81	0.05	11.92	1.92	18.96	0.07	19.71
	Bladder	0.04	0.76	13.33	0.03	13.21	0.92	21.75	0.03	22.04
	Esophagus	0.04	6.76	6.84	13.97	14.41	6.78	6.75	15.27	15.96
	Liver	0.04	13.44	13.52	10.34	14.47	15.77	15.93	14.19	18.81
	Thyroid	0.04	1.03	1.03	17.79	17.92	1.00	1.01	22.50	22.62
	Bone surface	0.01	14.29	22.57	15.52	30.89	15.86	29.71	17.80	41.51
	Brain	0.01	0.07	0.07	0.32	0.34	0.07	0.07	0.36	0.38
	Salivary glands	0.01	0.29	0.30	2.08	2.09	0.29	0.29	2.40	2.46
	Skin	0.01	3.02	5.72	3.45	7.72	3.49	8.16	3.97	10.78
Remainder organs	Adrenals		11.65	11.64	8.35	12.21	12.66	12.81	10.43	15.60
	ET region		1.03	1.03	17.79	17.92	1.00	1.01	22.50	22.62
	Gall Bladder		13.95	14.12	7.58	14.67	15.12	15.32	11.56	18.28
	Heart		11.35	11.38	16.22	16.85	10.99	11.03	15.88	16.69
	Kidneys		13.44	13.71	3.77	14.00	14.31	14.72	4.31	17.74
	Lymphatic nodes		4.50	7.61	3.36	9.23	4.98	10.25	3.89	12.85
	Muscle	0.12	4.50	7.61	3.36	9.23	4.98	10.25	3.89	12.85
	Oral mucosa		0.07	0.07	0.32	0.34	0.07	0.07	0.36	0.38
	Pancreas		13.52	13.59	8.79	14.23	14.77	14.99	11.50	17.89
	Prostate/Uterus		1.07	12.44	0.05	12.44	1.39	20.36	0.06	20.66
	Small intestine		12.85	15.31	1.75	15.41	14.01	17.87	2.39	20.61
	Spleen		13.33	13.43	10.99	14.43	15.48	15.64	12.92	18.81
	Thymus		4.20	4.29	16.04	16.30	3.54	3.61	14.78	15.04
Effective dose (mSv)			8.10	10.09	8.16	13.11	8.96	12.23	9.58	16.70

B.7 Irene

Organ	ICRP 103 Tissue weighting factor (w_T)	Dose (mGy)								
		FTC				TCM				
		Abd	AbdPel	Chest	CAP	Abd	AbdPel	Chest	CAP	
Primary organs	Breast	0.12	6.87	6.91	18.47	18.78	2.10	2.13	6.18	6.36
	Colon	0.12	17.42	21.87	1.43	22.07	7.26	10.95	0.64	14.22
	Lung	0.12	7.72	7.76	21.55	22.03	2.27	2.30	9.77	10.02
	Red bone marrow	0.12	2.67	4.50	4.29	7.44	0.98	2.55	2.64	5.30
	Stomach	0.12	20.87	20.86	17.64	22.57	7.19	7.28	7.81	10.34
	Gonads	0.08	0.63	18.40	0.03	18.45	0.29	15.43	0.01	18.76
	Bladder	0.04	0.64	21.21	0.03	21.34	0.29	17.71	0.02	21.48
	Esophagus	0.04	5.74	5.76	22.10	22.45	1.64	1.65	12.95	13.07
	Liver	0.04	21.55	21.83	12.50	22.90	7.45	7.67	5.30	10.68
	Thyroid	0.04	0.43	0.44	26.17	26.15	0.13	0.14	25.74	25.74
	Bone surface	0.01	12.68	21.31	19.76	34.69	4.65	12.05	12.03	24.62
	Brain	0.01	0.02	0.02	0.29	0.29	0.01	0.01	0.25	0.26
	Salivary glands	0.01	0.10	0.10	1.75	1.77	0.03	0.04	1.73	1.75
	Skin	0.01	3.58	6.38	4.04	8.88	1.35	3.86	2.30	6.50
Remainder organs	Adrenals		16.93	17.13	12.04	18.13	5.74	5.83	5.23	8.18
	ET region		0.43	0.44	26.17	26.15	0.13	0.14	25.74	25.74
	Gall Bladder		23.81	24.20	4.81	24.61	8.54	8.88	2.01	11.95
	Heart		11.04	11.06	25.15	25.70	3.48	3.50	9.48	9.74
	Kidneys		21.40	21.84	6.70	22.37	7.73	8.08	3.04	10.97
	Lymphatic nodes		4.69	8.83	4.58	11.59	1.78	5.36	2.59	8.54
	Muscle	0.12	4.69	8.83	4.58	11.59	1.78	5.36	2.59	8.54
	Oral mucosa		0.02	0.02	0.29	0.29	0.01	0.01	0.25	0.26
	Pancreas		18.86	18.90	14.00	19.89	6.49	6.60	6.15	9.22
	Prostate/Uterus		0.63	18.40	0.03	18.45	0.29	15.43	0.01	18.76
	Small intestine		10.13	21.29	0.26	21.38	4.31	13.21	0.11	16.54
	Spleen		19.88	19.92	17.93	21.60	6.88	6.99	8.15	10.02
	Thymus		2.96	2.97	24.69	25.04	0.92	0.94	8.60	8.75
Effective dose (mSv)			9.26	12.75	11.60	19.07	3.28	6.25	5.85	11.58

B.8 ICRP Female (Regina)

Organ	ICRP 103 Tissue weighting factor (w_T)	Dose (mGy)								
		FTC				TCM				
		Abd	AbdPel	Chest	CAP	Abd	AbdPel	Chest	CAP	
Primary organs	Breast	0.12	7.41	7.44	17.72	17.96	2.22	2.24	9.55	9.73
	Colon	0.12	13.76	20.26	0.52	20.30	10.40	17.82	0.29	21.45
	Lung	0.12	8.92	8.96	21.87	22.34	3.49	3.53	13.68	14.04
	Red bone marrow	0.12	2.52	4.17	3.17	6.07	1.38	3.60	2.25	5.87
	Stomach	0.12	20.25	20.43	14.65	21.36	9.90	10.06	7.82	13.89
	Gonads	0.08	0.89	15.06	0.05	15.13	0.73	20.72	0.03	23.72
	Bladder	0.04	0.85	19.21	0.04	19.12	0.73	26.30	0.02	30.34
	Esophagus	0.04	6.32	6.34	18.86	19.32	2.53	2.54	14.15	14.46
	Liver	0.04	21.18	21.30	17.74	22.66	9.59	9.73	10.23	13.84
	Thyroid	0.04	0.66	0.66	23.70	23.85	0.27	0.27	24.41	24.48
	Bone surface	0.01	11.79	19.34	14.56	27.98	6.47	16.60	10.31	27.00
	Brain	0.01	0.03	0.03	0.36	0.36	0.01	0.01	0.33	0.34
	Salivary glands	0.01	0.15	0.15	2.02	2.05	0.06	0.07	1.97	2.01
	Skin	0.01	3.89	6.32	4.02	8.58	2.18	5.51	2.81	8.43
Remainder organs	Adrenals		16.84	17.03	12.70	17.96	7.92	8.07	7.71	11.12
	ET region		0.66	0.66	23.70	23.85	0.27	0.27	24.41	24.48
	Gall Bladder		18.65	18.78	12.93	19.42	8.79	8.93	7.29	12.24
	Heart		11.57	11.60	22.80	23.31	4.74	4.77	13.58	13.97
	Kidneys		21.23	21.65	6.94	22.01	11.13	11.60	4.29	15.38
	Lymphatic nodes		3.77	7.16	4.13	9.85	2.19	6.76	3.11	10.36
	Muscle	0.12	3.77	7.16	4.13	9.85	2.19	6.76	3.11	10.36
	Oral mucosa		0.03	0.03	0.36	0.36	0.01	0.01	0.33	0.34
	Pancreas		20.76	21.05	8.27	21.32	10.54	10.86	3.94	14.48
	Prostate/Uterus		0.82	14.47	0.04	14.48	0.68	19.60	0.03	22.47
	Small intestine		12.80	19.85	2.00	19.98	8.56	16.53	1.11	20.16
	Spleen		19.30	19.45	18.34	20.90	8.95	9.10	11.03	13.03
	Thymus		1.57	1.58	21.37	21.58	0.63	0.64	16.48	16.58
Effective dose (mSv)			8.95	12.20	10.85	17.64	4.57	8.86	7.03	15.10

B.9 ICRP Male (Rex)

Organ	ICRP 103 Tissue weighting factor (w_T)	Dose (mGy)								
		FTC				TCM				
		Abd	AbdPel	Chest	CAP	Abd	AbdPel	Chest	CAP	
Primary organs	Breast	0.12	15.03	15.03	16.31	16.50	7.36	7.39	10.44	10.59
	Colon	0.12	17.31	19.80	4.10	19.95	11.62	13.86	2.66	16.93
	Lung	0.12	8.01	8.04	17.86	18.24	3.78	3.80	12.93	13.23
	Red bone marrow	0.12	2.14	3.74	2.74	5.31	1.25	2.73	2.20	4.78
	Stomach	0.12	17.94	18.00	15.93	19.06	11.00	11.10	10.96	14.51
	Gonads	0.08	0.05	1.34	0.01	1.43	0.03	1.37	0.00	1.65
	Bladder	0.04	1.23	18.07	0.05	18.08	0.90	15.53	0.03	18.87
	Esophagus	0.04	5.73	5.74	14.95	15.32	2.80	2.80	11.93	12.24
	Liver	0.04	17.07	17.16	14.95	18.34	10.02	10.10	10.81	13.43
	Thyroid	0.04	0.65	0.68	22.51	22.44	0.32	0.32	22.00	22.13
	Bone surface	0.01	9.91	17.06	12.47	24.14	5.81	12.42	9.99	21.66
	Brain	0.01	0.02	0.02	0.26	0.26	0.01	0.01	0.25	0.25
	Salivary glands	0.01	0.13	0.13	1.30	1.32	0.06	0.07	1.24	1.26
	Skin	0.01	3.93	6.19	3.77	8.09	2.41	4.55	2.97	7.29
Remainder organs	Adrenals		14.72	14.91	12.11	15.56	8.75	8.81	8.97	11.35
	ET region		0.65	0.68	22.51	22.44	0.32	0.32	22.00	22.13
	Gall Bladder		17.31	17.40	10.41	17.94	10.72	10.86	8.12	13.56
	Heart		11.63	11.66	19.72	20.22	5.97	6.00	13.77	14.21
	Kidneys		17.34	17.59	6.93	17.96	11.02	11.27	5.83	13.99
	Lymphatic nodes		3.75	6.64	3.66	8.74	2.31	5.08	2.98	8.13
	Muscle	0.12	3.75	6.64	3.66	8.74	2.31	5.08	2.98	8.13
	Oral mucosa		0.02	0.02	0.26	0.26	0.01	0.01	0.25	0.25
	Pancreas		16.97	17.14	10.20	17.70	10.42	10.60	6.67	13.30
	Prostate/Uterus		0.41	12.06	0.02	11.73	0.29	10.82	0.02	13.07
	Small intestine		15.69	19.95	2.20	20.06	10.72	14.43	1.50	17.58
	Spleen		15.23	15.37	15.12	16.73	8.93	9.02	11.12	12.44
	Thymus		1.51	1.52	20.64	20.62	0.73	0.73	17.57	17.56
Effective dose (mSv)			9.48	11.07	10.29	14.74	5.52	6.95	7.58	11.84

B.10 Visible Human

Organ	ICRP 103 Tissue weighting factor (w_T)	Dose (mGy)									
		FTC				TCM					
		Abd	AbdPel	Chest	CAP	Abd	AbdPel	Chest	CAP		
Primary organs	Breast	0.12	0.00	0.00	0.00	0.00	0.00	0.00	0.00	0.00	0.00
	Colon	0.12	12.83	16.44	4.57	16.65	10.88	15.46	5.26	18.61	
	Lung	0.12	7.30	7.32	15.44	15.71	5.95	5.99	14.18	14.48	
	Red bone marrow	0.12	2.37	3.95	3.25	5.74	1.94	4.13	3.40	6.75	
	Stomach	0.12	14.38	14.46	14.10	15.82	12.14	12.21	14.46	15.99	
	Gonads	0.08	0.10	2.97	0.01	2.31	0.07	5.90	0.01	6.01	
	Bladder	0.04	0.69	11.74	0.04	11.63	0.56	17.31	0.03	18.49	
	Esophagus	0.04	6.34	6.39	15.07	15.33	5.15	5.19	16.47	16.78	
	Liver	0.04	13.94	14.00	13.00	15.18	11.69	11.77	12.88	15.34	
	Thyroid	0.04	0.72	0.72	20.56	20.62	0.58	0.58	32.37	32.58	
	Bone surface	0.01	11.56	18.93	15.52	27.42	9.48	19.73	16.20	32.13	
	Brain	0.01	0.02	0.03	0.21	0.21	0.02	0.02	0.26	0.27	
	Salivary glands	0.01	0.15	0.16	1.54	1.55	0.13	0.14	1.92	1.94	
	Skin	0.01	4.50	8.29	3.30	9.58	3.77	8.70	3.55	11.66	
Remainder organs	Adrenals		10.73	10.87	8.99	11.70	9.00	9.05	8.50	11.48	
	ET region		0.72	0.72	20.56	20.62	0.58	0.58	32.37	32.58	
	Gall Bladder		16.65	16.80	13.11	16.23	13.38	13.56	14.10	16.90	
	Heart		11.46	11.47	18.51	18.83	10.25	10.29	17.44	17.78	
	Kidneys		14.12	14.43	5.59	14.69	12.08	12.47	5.04	15.30	
	Lymphatic nodes		3.78	6.29	4.44	8.77	3.11	6.78	4.61	10.48	
	Muscle	0.12	3.78	6.29	4.44	8.77	3.11	6.78	4.61	10.48	
	Oral mucosa		0.02	0.03	0.21	0.21	0.02	0.02	0.26	0.27	
	Pancreas		12.91	13.03	9.90	13.71	10.80	10.93	10.33	13.88	
	Prostate/Uterus		0.31	7.45	0.02	7.61	0.25	12.09	0.02	12.56	
	Small intestine		14.22	16.45	3.50	16.63	11.88	14.64	3.82	17.76	
	Spleen		13.43	13.54	12.72	14.46	11.47	11.62	12.85	14.88	
	Thymus		1.03	1.01	22.47	22.41	0.82	0.83	32.69	32.56	
Effective dose (mSv)			6.41	7.98	7.78	11.17	5.37	7.70	8.52	12.88	

Appendix C: Estimates of Organ Dose and ICRP Publication 60 Calculations of Effective Dose for GSF and ICRP Reference Voxelized Phantoms

C.1 Baby

Organ		ICRP 60 Tissue weighting factor (w_T)	Dose (mGy)							
			FTC				TCM			
			Abd	AbdPel	Chest	CAP	Abd	AbdPel	Chest	CAP
Primary organs	Gonads	0.20	34.63	38.07	1.93	37.72	3.83	4.13	0.22	5.50
	Colon	0.12	32.50	35.62	9.79	35.84	2.78	3.10	1.19	4.15
	Lung	0.12	28.93	29.03	35.93	36.68	2.14	2.14	3.64	3.73
	Red bone marrow	0.12	8.96	10.70	9.72	14.43	0.76	0.94	1.04	1.67
	Stomach	0.12	35.23	35.33	32.17	36.10	2.93	2.95	3.58	3.99
	Bladder	0.05	30.31	38.51	1.36	37.81	3.63	4.23	0.15	5.65
	Breast	0.05	20.54	20.00	30.67	30.85	1.00	1.01	3.05	3.06
	Esophagus	0.05	24.11	24.26	33.98	34.79	1.84	1.85	3.56	3.64
	Liver	0.05	35.80	36.09	32.93	36.92	2.93	2.95	3.55	4.05
	Thyroid	0.05	3.27	3.35	34.84	34.62	0.23	0.23	3.88	3.90
	Bone surface	0.01	43.96	52.32	47.62	70.58	3.73	4.57	5.10	8.17
Skin	0.01	12.89	16.31	11.52	20.17	1.12	1.48	1.25	2.42	
Remainder organs	Adrenals		34.10	34.42	29.42	34.74	2.78	2.82	3.21	3.80
	Brain		0.26	0.26	1.11	1.15	0.02	0.02	0.13	0.13
	Kidneys		36.38	37.04	19.55	37.36	3.00	3.06	2.21	4.11
	Muscle		13.94	17.72	15.90	25.09	1.20	1.59	1.71	2.97
	Pancreas	0.05	35.99	36.12	30.07	36.18	2.95	2.97	3.38	4.02
	Prostate/Uterus		34.67	38.48	1.90	37.72	3.74	4.09	0.22	5.45
	Small intestine		35.87	36.82	10.88	37.11	3.07	3.16	1.27	4.24
	Spleen		35.49	35.69	32.83	36.47	2.94	2.98	3.67	4.05
	Thymus		19.14	19.19	35.42	35.86	1.15	1.16	3.52	3.56
Effective dose (mSv)			27.24	29.11	19.17	33.53	2.44	2.62	2.06	4.03

C.2 Child

Organ	ICRP 60 Tissue weighting factor (w_T)	Dose (mGy)								
		FTC				TCM				
		Abd	AbdPel	Chest	CAP	Abd	AbdPel	Chest	CAP	
Primary organs	Gonads	0.20	14.03	25.19	0.72	26.23	3.19	6.23	0.19	8.32
	Colon	0.12	24.20	26.45	5.09	26.70	5.33	5.92	1.23	7.92
	Lung	0.12	16.24	16.29	25.12	25.65	3.28	3.29	7.16	7.33
	Red bone marrow	0.12	3.98	5.97	4.37	8.07	0.86	1.39	1.30	2.53
	Stomach	0.12	26.17	26.42	19.48	26.94	5.45	5.52	4.93	7.53
	Bladder	0.05	5.00	26.54	0.29	26.49	1.10	6.77	0.08	9.02
	Breast	0.05	0.00	0.00	0.00	0.00	0.00	0.00	0.00	0.00
	Esophagus	0.05	5.84	5.87	25.96	26.09	1.16	1.16	7.80	7.87
	Liver	0.05	25.25	25.47	21.42	26.44	5.36	5.41	6.36	7.52
	Thyroid	0.05	1.75	1.79	29.15	29.30	0.35	0.35	9.23	9.29
	Bone surface	0.01	19.01	28.41	20.70	38.24	4.10	6.62	6.17	11.97
Skin	0.01	6.22	9.37	5.31	11.51	1.36	2.22	1.55	3.64	
Remainder organs	Adrenals		22.17	22.43	19.62	23.18	4.70	4.74	5.44	6.57
	Brain		0.14	0.14	0.62	0.64	0.03	0.03	0.19	0.20
	Kidneys		25.63	26.21	9.45	26.54	5.66	5.81	2.82	7.87
	Muscle		7.77	12.60	6.63	15.47	1.69	2.99	1.94	4.91
	Pancreas	0.05	24.45	24.70	18.02	25.48	5.21	5.28	5.03	7.25
	Prostate/Uterus		12.95	25.42	0.55	24.80	2.80	6.24	0.16	8.34
	Small intestine		24.04	27.37	3.35	27.44	5.29	6.24	0.76	8.36
	Spleen		25.11	25.36	21.33	26.14	5.51	5.58	5.30	7.69
	Thymus		5.84	5.87	25.96	26.09	1.16	1.16	7.80	7.87
Effective dose (mSv)			14.24	18.36	11.32	22.73	3.06	4.16	3.21	6.87

C.3 Donna

Organ	ICRP 60 Tissue weighting factor (w_T)	Dose (mGy)								
		FTC				TCM				
		Abd	AbdPel	Chest	CAP	Abd	AbdPel	Chest	CAP	
Primary organs	Gonads	0.20	1.50	13.23	0.09	13.40	1.42	20.83	0.08	21.37
	Colon	0.12	14.26	17.32	1.70	17.48	12.98	18.01	1.69	20.88
	Lung	0.12	8.26	8.29	17.88	18.39	6.46	6.53	16.22	16.78
	Red bone marrow	0.12	2.16	3.70	2.83	5.43	1.84	4.42	3.04	6.84
	Stomach	0.12	16.71	16.79	13.73	18.09	13.87	14.03	13.17	18.10
	Bladder	0.05	0.96	16.65	0.05	16.74	0.96	27.26	0.04	27.48
	Breast	0.05	13.61	13.64	15.33	15.72	12.92	12.98	17.54	18.06
	Esophagus	0.05	6.81	6.81	17.07	17.55	5.33	5.35	16.98	17.48
	Liver	0.05	16.49	16.59	14.51	18.00	13.13	13.31	13.04	17.40
	Thyroid	0.05	0.69	0.70	23.37	23.49	0.53	0.56	30.23	30.51
	Bone surface	0.01	10.63	17.99	13.51	26.15	9.06	21.44	14.37	32.81
Skin	0.01	3.50	5.93	2.93	7.42	3.14	7.31	3.06	9.64	
Remainder organs	Adrenals		14.83	15.02	7.55	15.64	12.19	12.47	6.92	15.54
	Brain		0.05	0.05	0.27	0.29	0.04	0.04	0.32	0.34
	Kidneys		15.10	15.41	7.09	15.95	12.38	12.84	6.54	15.91
	Muscle		3.98	6.81	3.82	8.92	3.43	8.20	3.87	11.21
	Pancreas	0.05	15.63	15.83	9.55	16.54	12.63	12.89	8.57	16.19
	Prostate/Uterus		0.99	14.17	0.06	14.33	0.97	22.94	0.06	23.17
	Small intestine		11.03	17.44	0.47	17.49	10.65	20.82	0.42	22.98
	Spleen		15.62	15.73	12.63	17.14	13.33	13.56	13.50	17.60
	Thymus		3.89	3.86	21.07	21.36	2.83	2.81	17.08	17.28
Effective dose (mSv)			7.79	11.72	8.38	15.43	6.65	13.18	8.49	18.54

C.4 Frank

Organ	ICRP 60 Tissue weighting factor (w_T)	Dose (mGy)								
		FTC				TCM				
		Abd	AbdPel	Chest	CAP	Abd	AbdPel	Chest	CAP	
Primary organs	Gonads	0.20	0.43	8.21	0.05	8.20	0.61	10.42	0.08	11.59
	Colon	0.12	11.71	14.86	3.59	15.12	18.41	21.97	4.91	23.63
	Lung	0.12	7.74	7.79	15.66	16.21	7.27	7.33	12.85	13.71
	Red bone marrow	0.12	2.01	3.57	3.60	5.85	2.48	4.43	3.57	6.88
	Stomach	0.12	12.54	12.77	11.37	13.93	18.34	18.61	14.64	20.35
	Bladder	0.05	1.18	12.43	0.13	12.53	1.68	14.54	0.19	16.73
	Breast	0.05	1.96	1.98	15.05	15.27	1.57	1.63	8.05	8.34
	Esophagus	0.05	7.50	7.59	14.17	14.94	7.81	7.85	13.09	14.27
	Liver	0.05	12.32	12.51	11.58	13.82	17.88	18.10	15.33	20.27
	Thyroid	0.05	0.46	0.45	11.54	11.56	0.49	0.50	13.36	13.45
	Bone surface	0.01	9.93	17.26	17.19	27.99	12.37	21.48	17.15	33.06
Skin	0.01	5.11	8.45	6.20	11.77	6.78	10.81	6.52	14.67	
Remainder organs	Adrenals		10.63	11.03	7.70	11.97	16.84	17.33	11.03	18.48
	Brain		0.02	0.02	0.14	0.14	0.02	0.02	0.14	0.15
	Kidneys		11.56	12.58	3.55	12.94	19.00	20.14	5.51	21.29
	Muscle		4.70	8.62	5.39	11.80	6.82	11.72	6.07	15.74
	Pancreas	0.05	11.02	11.43	8.04	12.27	17.32	17.84	11.00	19.11
	Prostate/Uterus		0.43	8.21	0.05	8.20	0.61	10.42	0.08	11.59
	Small intestine		8.57	13.73	1.80	13.90	12.85	18.52	2.40	20.51
	Spleen		13.19	13.36	12.15	14.90	20.04	20.28	18.29	22.00
	Thymus		5.12	5.23	16.03	16.25	3.84	3.78	9.97	10.38
Effective dose (mSv)			5.85	8.79	7.28	12.14	7.90	11.49	7.43	14.97

C.5 Golem

Organ	ICRP 60 Tissue weighting factor (w_T)	Dose (mGy)								
		FTC				TCM				
		Abd	AbdPel	Chest	CAP	Abd	AbdPel	Chest	CAP	
Primary organs	Gonads	0.20	0.06	1.19	0.01	1.14	0.05	1.60	0.01	1.94
	Colon	0.12	16.16	19.41	3.65	19.62	11.91	15.06	3.12	18.39
	Lung	0.12	8.32	8.37	18.38	18.83	4.27	4.30	14.20	14.61
	Red bone marrow	0.12	2.27	3.91	2.83	5.55	1.51	3.30	2.57	5.71
	Stomach	0.12	17.73	17.80	14.30	18.96	11.70	11.79	11.96	15.39
	Bladder	0.05	1.56	17.85	0.06	17.96	1.16	17.56	0.05	21.11
	Breast	0.05	0.00	0.00	0.00	0.00	0.00	0.00	0.00	0.00
	Esophagus	0.05	5.82	5.82	16.34	16.73	3.28	3.30	15.13	15.56
	Liver	0.05	16.90	16.98	14.09	18.18	11.09	11.18	12.24	14.85
	Thyroid	0.05	0.63	0.64	21.38	21.50	0.35	0.37	27.56	27.67
	Bone surface	0.01	10.90	18.52	13.30	26.14	7.31	15.58	12.03	26.85
Skin	0.01	3.84	5.79	3.70	7.62	2.64	4.85	3.27	7.80	
Remainder organs	Adrenals		15.93	16.17	12.86	16.83	10.89	11.03	10.31	14.10
	Brain		0.05	0.05	0.28	0.29	0.03	0.03	0.30	0.31
	Kidneys		18.31	18.68	6.63	19.07	13.17	13.50	5.24	16.70
	Muscle		3.93	6.44	4.05	8.82	2.69	5.56	3.70	9.21
	Pancreas	0.05	16.84	17.05	8.02	17.50	11.43	11.53	7.65	14.51
	Prostate/Uterus		0.45	11.82	0.04	11.86	0.35	14.00	0.03	16.61
	Small intestine		15.60	19.30	2.58	19.50	11.22	15.15	2.04	18.49
	Spleen		16.10	16.21	15.79	17.72	11.02	11.09	12.81	14.87
	Thymus		1.57	1.55	20.86	21.04	0.84	0.84	21.07	21.13
Effective dose (mSv)			7.23	9.08	7.86	12.58	4.77	6.74	7.08	11.89

C.6 Helga

Organ	ICRP 60 Tissue weighting factor (w_T)	Dose (mGy)								
		FTC				TCM				
		Abd	AbdPel	Chest	CAP	Abd	AbdPel	Chest	CAP	
Primary organs	Gonads	0.20	1.54	11.81	0.05	11.92	1.92	18.96	0.07	19.71
	Colon	0.12	14.87	15.85	2.69	16.02	16.27	17.90	3.67	21.13
	Lung	0.12	8.33	8.36	14.33	14.93	8.04	8.09	14.54	15.35
	Red bone marrow	0.12	2.90	4.64	3.25	6.41	3.22	6.12	3.73	8.63
	Stomach	0.12	14.29	14.39	12.50	15.41	17.64	17.72	16.94	20.45
	Bladder	0.05	0.76	13.33	0.03	13.21	0.92	21.75	0.03	22.04
	Breast	0.05	9.21	9.26	11.83	12.26	9.67	9.77	12.70	13.25
	Esophagus	0.05	6.76	6.84	13.97	14.41	6.78	6.75	15.27	15.96
	Liver	0.05	13.44	13.52	10.34	14.47	15.77	15.93	14.19	18.81
	Thyroid	0.05	1.03	1.03	17.79	17.92	1.00	1.01	22.50	22.62
	Bone surface	0.01	14.29	22.57	15.52	30.89	15.86	29.71	17.80	41.51
Skin	0.01	3.02	5.72	3.45	7.72	3.49	8.16	3.97	10.78	
Remainder organs	Adrenals		11.65	11.64	8.35	12.21	12.66	12.81	10.43	15.60
	Brain		0.07	0.07	0.32	0.34	0.07	0.07	0.36	0.38
	Kidneys		13.44	13.71	3.77	14.00	14.31	14.72	4.31	17.74
	Muscle		4.50	7.61	3.36	9.23	4.98	10.25	3.89	12.85
	Pancreas	0.05	13.52	13.59	8.79	14.23	14.77	14.99	11.50	17.89
	Prostate/Uterus		1.07	12.44	0.05	12.44	1.39	20.36	0.06	20.66
	Small intestine		12.85	15.31	1.75	15.41	14.01	17.87	2.39	20.61
	Spleen		13.33	13.43	10.99	14.43	15.48	15.64	12.92	18.81
	Thymus		4.20	4.29	16.04	16.30	3.54	3.61	14.78	15.04
Effective dose (mSv)			7.30	10.54	7.13	13.32	8.15	13.52	8.47	17.74

C.7 Irene

Organ		ICRP 60 Tissue weighting factor (w_T)	Dose (mGy)							
			FTC				TCM			
			Abd	AbdPel	Chest	CAP	Abd	AbdPel	Chest	CAP
Primary organs	Gonads	0.20	0.63	18.40	0.03	18.45	0.29	15.43	0.01	18.76
	Colon	0.12	17.42	21.87	1.43	22.07	7.26	10.95	0.64	14.22
	Lung	0.12	7.72	7.76	21.55	22.03	2.27	2.30	9.77	10.02
	Red bone marrow	0.12	2.67	4.50	4.29	7.44	0.98	2.55	2.64	5.30
	Stomach	0.12	20.87	20.86	17.64	22.57	7.19	7.28	7.81	10.34
	Bladder	0.05	0.64	21.21	0.03	21.34	0.29	17.71	0.02	21.48
	Breast	0.05	6.87	6.91	18.47	18.78	2.10	2.13	6.18	6.36
	Esophagus	0.05	5.74	5.76	22.10	22.45	1.64	1.65	12.95	13.07
	Liver	0.05	21.55	21.83	12.50	22.90	7.45	7.67	5.30	10.68
	Thyroid	0.05	0.43	0.44	26.17	26.15	0.13	0.14	25.74	25.74
	Bone surface	0.01	12.68	21.31	19.76	34.69	4.65	12.05	12.03	24.62
Skin	0.01	3.58	6.38	4.04	8.88	1.35	3.86	2.30	6.50	
Remainder organs	Adrenals		16.93	17.13	12.04	18.13	5.74	5.83	5.23	8.18
	Brain		0.02	0.02	0.29	0.29	0.01	0.01	0.25	0.26
	Kidneys		21.40	21.84	6.70	22.37	7.73	8.08	3.04	10.97
	Muscle		4.69	8.83	4.58	11.59	1.78	5.36	2.59	8.54
	Pancreas	0.05	18.86	18.90	14.00	19.89	6.49	6.60	6.15	9.22
	Prostate/Uterus		0.63	18.40	0.03	18.45	0.29	15.43	0.01	18.76
	Small intestine		10.13	21.29	0.26	21.38	4.31	13.21	0.11	16.54
	Spleen		19.88	19.92	17.93	21.60	6.88	6.99	8.15	10.02
	Thymus		2.96	2.97	24.69	25.04	0.92	0.94	8.60	8.75
Effective dose (mSv)			8.42	14.08	10.04	19.48	3.01	7.83	5.35	13.22

C.8 ICRP Female (Regina)

Organ	ICRP 60 Tissue weighting factor (w_T)	Dose (mGy)								
		FTC				TCM				
		Abd	AbdPel	Chest	CAP	Abd	AbdPel	Chest	CAP	
Primary organs	Gonads	0.20	0.89	15.06	0.05	15.13	0.73	20.72	0.03	23.72
	Colon	0.12	13.76	20.26	0.52	20.30	10.40	17.82	0.29	21.45
	Lung	0.12	8.92	8.96	21.87	22.34	3.49	3.53	13.68	14.04
	Red bone marrow	0.12	2.52	4.17	3.17	6.07	1.38	3.60	2.25	5.87
	Stomach	0.12	20.25	20.43	14.65	21.36	9.90	10.06	7.82	13.89
	Bladder	0.05	0.85	19.21	0.04	19.12	0.73	26.30	0.02	30.34
	Breast	0.05	7.41	7.44	17.72	17.96	2.22	2.24	9.55	9.73
	Esophagus	0.05	6.32	6.34	18.86	19.32	2.53	2.54	14.15	14.46
	Liver	0.05	21.18	21.30	17.74	22.66	9.59	9.73	10.23	13.84
	Thyroid	0.05	0.66	0.66	23.70	23.85	0.27	0.27	24.41	24.48
	Bone surface	0.01	11.79	19.34	14.56	27.98	6.47	16.60	10.31	27.00
Skin	0.01	3.89	6.32	4.02	8.58	2.18	5.51	2.81	8.43	
Remainder organs	Adrenals		16.84	17.03	12.70	17.96	7.92	8.07	7.71	11.12
	Brain		0.03	0.03	0.36	0.36	0.01	0.01	0.33	0.34
	Kidneys		21.23	21.65	6.94	22.01	11.13	11.60	4.29	15.38
	Muscle		3.77	7.16	4.13	9.85	2.19	6.76	3.11	10.36
	Pancreas	0.05	20.76	21.05	8.27	21.32	10.54	10.86	3.94	14.48
	Prostate/Uterus		0.82	14.47	0.04	14.48	0.68	19.60	0.03	22.47
	Small intestine		12.80	19.85	2.00	19.98	8.56	16.53	1.11	20.16
	Spleen		19.30	19.45	18.34	20.90	8.95	9.10	11.03	13.03
	Thymus		1.57	1.58	21.37	21.58	0.63	0.64	16.48	16.58
Effective dose (mSv)			8.15	13.15	9.34	17.77	4.30	11.08	6.21	17.06

C.9 ICRP Male (Rex)

Organ	ICRP 60 Tissue weighting factor (w_T)	Dose (mGy)								
		FTC				TCM				
		Abd	AbdPel	Chest	CAP	Abd	AbdPel	Chest	CAP	
Primary organs	Gonads	0.20	0.05	1.34	0.01	1.43	0.03	1.37	0.00	1.65
	Colon	0.12	17.31	19.80	4.10	19.95	11.62	13.86	2.66	16.93
	Lung	0.12	8.01	8.04	17.86	18.24	3.78	3.80	12.93	13.23
	Red bone marrow	0.12	2.14	3.74	2.74	5.31	1.25	2.73	2.20	4.78
	Stomach	0.12	17.94	18.00	15.93	19.06	11.00	11.10	10.96	14.51
	Bladder	0.05	1.23	18.07	0.05	18.08	0.90	15.53	0.03	18.87
	Breast	0.05	15.03	15.03	16.31	16.50	7.36	7.39	10.44	10.59
	Esophagus	0.05	5.73	5.74	14.95	15.32	2.80	2.80	11.93	12.24
	Liver	0.05	17.07	17.16	14.95	18.34	10.02	10.10	10.81	13.43
	Thyroid	0.05	0.65	0.68	22.51	22.44	0.32	0.32	22.00	22.13
	Bone surface	0.01	9.91	17.06	12.47	24.14	5.81	12.42	9.99	21.66
Skin	0.01	3.93	6.19	3.77	8.09	2.41	4.55	2.97	7.29	
Remainder organs	Adrenals		14.72	14.91	12.11	15.56	8.75	8.81	8.97	11.35
	Brain		0.02	0.02	0.26	0.26	0.01	0.01	0.25	0.25
	Kidneys		17.34	17.59	6.93	17.96	11.02	11.27	5.83	13.99
	Muscle		3.75	6.64	3.66	8.74	2.31	5.08	2.98	8.13
	Pancreas	0.05	16.97	17.14	10.20	17.70	10.42	10.60	6.67	13.30
	Prostate/Uterus		0.41	12.06	0.02	11.73	0.29	10.82	0.02	13.07
	Small intestine		15.69	19.95	2.20	20.06	10.72	14.43	1.50	17.58
	Spleen		15.23	15.37	15.12	16.73	8.93	9.02	11.12	12.44
	Thymus		1.51	1.52	20.64	20.62	0.73	0.73	17.57	17.56
Effective dose (mSv)			8.06	9.87	8.87	13.37	4.77	6.42	6.65	11.01

C.10 Visible Human

Organ	ICRP 60 Tissue weighting factor (w_T)	Dose (mGy)								
		FTC				TCM				
		Abd	AbdPel	Chest	CAP	Abd	AbdPel	Chest	CAP	
Primary organs	Gonads	0.20	0.10	2.97	0.01	2.31	0.07	5.90	0.01	6.01
	Colon	0.12	12.83	16.44	4.57	16.65	10.88	15.46	5.26	18.61
	Lung	0.12	7.30	7.32	15.44	15.71	5.95	5.99	14.18	14.48
	Red bone marrow	0.12	2.37	3.95	3.25	5.74	1.94	4.13	3.40	6.75
	Stomach	0.12	14.38	14.46	14.10	15.82	12.14	12.21	14.46	15.99
	Bladder	0.05	0.69	11.74	0.04	11.63	0.56	17.31	0.03	18.49
	Breast	0.05	0.00	0.00	0.00	0.00	0.00	0.00	0.00	0.00
	Esophagus	0.05	6.34	6.39	15.07	15.33	5.15	5.19	16.47	16.78
	Liver	0.05	13.94	14.00	13.00	15.18	11.69	11.77	12.88	15.34
	Thyroid	0.05	0.72	0.72	20.56	20.62	0.58	0.58	32.37	32.58
	Bone surface	0.01	11.56	18.93	15.52	27.42	9.48	19.73	16.20	32.13
Skin	0.01	4.50	8.29	3.30	9.58	3.77	8.70	3.55	11.66	
Remainder organs	Adrenals		10.73	10.87	8.99	11.70	9.00	9.05	8.50	11.48
	Brain		0.02	0.03	0.21	0.21	0.02	0.02	0.26	0.27
	Kidneys		14.12	14.43	5.59	14.69	12.08	12.47	5.04	15.30
	Muscle		3.78	6.29	4.44	8.77	3.11	6.78	4.61	10.48
	Pancreas	0.05	12.91	13.03	9.90	13.71	10.80	10.93	10.33	13.88
	Prostate/Uterus		0.31	7.45	0.02	7.61	0.25	12.09	0.02	12.56
	Small intestine		14.22	16.45	3.50	16.63	11.88	14.64	3.82	17.76
	Spleen		13.43	13.54	12.72	14.46	11.47	11.62	12.85	14.88
	Thymus		1.03	1.01	22.47	22.41	0.82	0.83	32.69	32.56
Effective dose (mSv)			6.08	8.03	7.48	11.05	5.09	8.18	8.20	13.22

Appendix D: Estimates of WED_{protocol} and WED_{organ} for Protocols of Interest

D.1 WED_{protocol} – All Protocols

Protocol	WED_{protocol} (cm)									
	Reference Voxelized Phantom									
	Baby	Child	Donna	Frank	Golem	Helga	Irene	ICRP Female (Regina)	ICRP Male (Rex)	Visible Human
Abd	10.49	20.00	30.08	37.62	28.14	31.80	22.96	24.25	27.53	32.33
AbdPel	10.02	18.88	30.80	37.41	27.39	32.31	23.43	25.17	26.95	32.88
Chest	9.12	18.71	24.13	21.26	22.75	26.10	19.46	23.28	24.38	22.69
CAP	10.32	19.81	29.99	37.62	28.14	32.80	23.38	24.46	27.74	32.33

D.2 WED_{organ} – Abdomen

Organ	WED _{organ} (cm)									
	Reference Voxelized Phantom									
	Baby	Child	Donna	Frank	Golem	Helga	Irene	ICRP Female (Regina)	ICRP Male (Rex)	Visible Human
Adrenals	10.55	19.47	29.68	37.45	28.81	31.66	23.50	24.76	27.98	32.79
Gall bladder	10.39	19.66	29.70	37.58	28.70	31.64	22.77	24.79	27.92	32.76
Kidneys	10.18	19.45	29.83	37.53	28.29	32.06	23.03	24.63	27.58	32.89
Liver	10.26	19.29	29.69	34.79	28.01	31.97	22.98	24.34	27.50	32.38
Pancreas	10.46	19.66	29.74	37.45	28.50	31.68	23.50	24.60	27.78	32.83
Spleen	10.49	19.36	29.57	36.85	28.24	32.45	23.22	24.69	27.67	32.65
Stomach	10.57	19.67	29.51	37.26	28.50	32.78	23.20	24.54	27.83	32.61

D.3 WED_{organ} – Abdomen/Pelvis

Organ	WED _{organ} (cm)									
	Reference Voxelized Phantom									
	Baby	Child	Donna	Frank	Golem	Helga	Irene	ICRP Female (Regina)	ICRP Male (Rex)	Visible Human
Adrenals	10.55	19.47	29.68	37.45	28.81	31.66	23.50	24.76	27.98	32.79
Bladder	8.60	18.75	31.92	33.47	28.79	33.04	26.36	28.88	28.16	33.49
Colon	9.21	19.03	30.60	36.24	28.13	32.11	24.22	26.87	27.34	32.79
Gall bladder	10.39	19.66	29.70	37.58	28.70	31.64	22.77	24.79	27.92	32.76
Kidneys	10.18	19.45	29.83	37.53	28.29	32.06	23.03	24.63	27.58	32.89
Liver	10.26	19.29	29.69	34.79	28.01	31.97	22.98	24.34	27.50	32.38
Pancreas	10.46	19.66	29.74	37.45	28.50	31.68	23.50	24.60	27.78	32.83
Prostate/Uterus	8.03	19.34	31.84	33.40	28.67	32.54	26.07	28.77	28.25	32.75
Small intestine	9.85	19.30	30.68	36.03	28.00	32.10	24.46	26.25	27.33	32.81
Spleen	10.49	19.36	29.57	36.85	28.24	32.45	23.22	24.69	27.67	32.65
Stomach	10.57	19.67	29.51	37.26	28.50	32.78	23.20	24.54	27.83	32.61

D.4 WED_{organ} – Chest

Organ	WED _{organ} (cm)									
	Reference Voxelized Phantom									
	Baby	Child	Donna	Frank	Golem	Helga	Irene	ICRP Female (Regina)	ICRP Male (Rex)	Visible Human
Breast	9.27	-	26.86	22.14	-	28.61	19.49	22.72	23.02	-
Heart	9.27	18.44	24.36	21.46	24.39	26.30	19.32	22.63	24.81	24.54
Lung	9.38	18.26	25.96	26.41	25.26	28.25	20.88	22.92	25.21	27.31
Thymus	9.39	18.31	24.86	21.46	25.83	26.83	19.72	22.92	25.09	28.23

**No breast voxels were identified in the Child, Golem and Visible Human reference voxelized phantoms.

D.5 WED_{organ} – Chest/Abdomen/Pelvis (CAP)

Organ	WED _{organ} (cm)									
	Reference Voxelized Phantom									
	Baby	Child	Donna	Frank	Golem	Helga	Irene	ICRP Female (Regina)	ICRP Male (Rex)	Visible Human
Adrenals	10.55	19.47	29.68	37.45	28.81	31.66	23.50	24.76	27.98	32.79
Bladder	8.60	18.75	31.92	33.47	28.79	33.04	26.36	28.88	28.16	33.49
Breast	9.27	-	26.86	22.14	-	28.61	19.49	22.72	23.02	-
Colon	9.21	19.03	30.60	36.24	28.13	32.11	24.22	26.87	27.34	32.79
Gall bladder	10.39	19.66	29.70	37.58	28.70	31.64	22.77	24.79	27.92	32.76
Heart	9.27	18.44	24.36	21.46	24.39	26.30	19.32	22.63	24.81	24.54
Kidneys	10.18	19.45	29.83	37.53	28.29	32.06	23.03	24.63	27.58	32.89
Liver	10.26	19.29	29.69	34.79	28.01	31.97	22.98	24.34	27.50	32.38
Lung	9.38	18.26	25.96	26.41	25.26	28.25	20.88	22.92	25.21	27.31
Pancreas	10.46	19.66	29.74	37.45	28.50	31.68	23.50	24.60	27.78	32.83
Prostate/Uterus	8.03	19.34	31.84	33.40	28.67	32.54	26.07	28.77	28.25	32.75
Small intestine	9.85	19.30	30.68	36.03	28.00	32.10	24.46	26.25	27.33	32.81
Spleen	10.49	19.36	29.57	36.85	28.24	32.45	23.22	24.69	27.67	32.65
Stomach	10.57	19.67	29.51	37.26	28.50	32.78	23.20	24.54	27.83	32.61
Thymus	9.39	18.31	24.86	21.46	25.83	26.83	19.72	22.92	25.09	28.23

**No breast voxels were identified in the Child, Golem and Visible Human reference voxelized phantoms.

Appendix E: Estimates of $CTDI_{vol,protocol}$ and $CTDI_{vol,organ}$ for Protocols of Interest

E.1 $CTDI_{vol,protocol}$ – All Protocols

E.1.1 TCM

Protocol	$CTDI_{vol,protocol}$ (mGy)									
	Reference Voxelized Phantom									
	Baby	Child	Donna	Frank	Golem	Helga	Irene	ICRP Female (Regina)	ICRP Male (Rex)	Visible Human
Abd	1.16	2.92	11.83	18.77	9.32	15.20	5.07	7.55	8.30	11.26
AbdPel	1.22	3.16	15.95	18.09	11.29	17.85	7.85	11.46	9.89	13.87
Chest	1.46	3.98	13.84	14.52	12.17	15.85	7.79	9.49	10.85	14.08
CAP	1.60	4.25	16.93	17.51	13.77	18.57	9.69	13.09	12.21	15.74

E.1.2 FTC

Protocol	$CTDI_{vol,protocol}$ (mGy)									
	Reference Voxelized Phantom									
	Baby	Child	Donna	Frank	Golem	Helga	Irene	ICRP Female (Regina)	ICRP Male (Rex)	Visible Human
Abd	13.60	13.60	13.60	13.60	13.60	13.60	13.60	13.60	13.60	13.60
AbdPel	13.60	13.60	13.60	13.60	13.60	13.60	13.60	13.60	13.60	13.60
Chest	13.60	13.60	13.60	13.60	13.60	13.60	13.60	13.60	13.60	13.60
CAP	13.60	13.60	13.60	13.60	13.60	13.60	13.60	13.60	13.60	13.60

E.2 CTDI_{vol,organ} – Abdomen

E.2.1 TCM

Organ	CTDI _{vol,organ} (mGy)									
	Reference Voxelized Phantom									
	Baby	Child	Donna	Frank	Golem	Helga	Irene	ICRP Female (Regina)	ICRP Male (Rex)	Visible Human
Adrenals	1.14	3.06	10.75	23.46	9.66	13.71	4.92	6.11	8.58	11.61
Gall bladder	1.11	2.96	9.95	24.19	8.04	14.58	4.96	6.52	8.81	11.56
Kidneys	1.15	2.97	11.27	23.42	9.54	14.16	4.94	6.88	8.50	11.57
Liver	1.14	2.93	11.03	21.19	9.21	16.01	4.80	6.04	8.24	11.48
Pancreas	1.33	2.96	10.09	24.19	9.51	14.26	4.92	6.72	8.62	11.57
Spleen	1.13	2.89	10.69	21.84	9.32	16.84	4.54	6.11	7.74	11.36
Stomach	1.15	2.93	10.55	22.67	9.30	19.12	4.62	6.35	8.29	10.92

E.2.2 FTC

Organ	CTDI _{vol,organ} (mGy)									
	Reference Voxelized Phantom									
	Baby	Child	Donna	Frank	Golem	Helga	Irene	ICRP Female (Regina)	ICRP Male (Rex)	Visible Human
Adrenals	13.60	13.60	13.60	13.60	13.60	13.60	13.60	13.60	13.60	13.60
Gall bladder	13.60	13.60	13.60	13.60	13.60	13.60	13.60	13.60	13.60	13.60
Kidneys	13.60	13.60	13.60	13.60	13.60	13.60	13.60	13.60	13.60	13.60
Liver	13.60	13.60	13.60	13.60	13.60	13.60	13.60	13.60	13.60	13.60
Pancreas	13.60	13.60	13.60	13.60	13.60	13.60	13.60	13.60	13.60	13.60
Spleen	13.60	13.60	13.60	13.60	13.60	13.60	13.60	13.60	13.60	13.60
Stomach	13.60	13.60	13.60	13.60	13.60	13.60	13.60	13.60	13.60	13.60

E.3 CTDI_{vol,organ} – Abdomen/Pelvis

E.3.1 TCM

Organ	CTDI _{vol,organ} (mGy)									
	Reference Voxelized Phantom									
	Baby	Child	Donna	Frank	Golem	Helga	Irene	ICRP Female (Regina)	ICRP Male (Rex)	Visible Human
Adrenals	1.14	3.06	10.75	23.46	9.66	13.71	4.92	6.11	8.58	11.61
Bladder	1.69	3.64	23.46	15.42	14.04	23.47	12.98	20.23	12.90	23.26
Colon	1.31	3.27	15.82	19.76	11.52	15.90	8.37	13.34	9.94	13.01
Gall bladder	1.11	2.96	9.95	24.19	8.04	14.58	4.96	6.52	8.81	11.56
Kidneys	1.15	2.97	11.27	23.42	9.54	14.16	4.94	6.88	8.50	11.57
Liver	1.14	2.93	11.03	21.19	9.21	16.01	4.80	6.04	8.24	11.48
Pancreas	1.33	2.96	10.09	24.19	9.51	14.26	4.92	6.72	8.62	11.57
Prostate/Uterus	1.54	3.40	23.55	19.98	19.46	23.48	13.42	20.63	13.70	23.51
Small intestine	1.13	3.14	16.25	19.08	11.12	16.98	9.06	11.46	9.88	11.90
Spleen	1.13	2.89	10.69	21.84	9.32	16.84	4.54	6.11	7.74	11.36
Stomach	1.15	2.93	10.55	22.67	9.30	19.12	4.62	6.35	8.29	10.92

E.3.2 FTC

Organ	CTDI _{vol,organ} (mGy)									
	Reference Voxelized Phantom									
	Baby	Child	Donna	Frank	Golem	Helga	Irene	ICRP Female (Regina)	ICRP Male (Rex)	Visible Human
Adrenals	13.60	13.60	13.60	13.60	13.60	13.60	13.60	13.60	13.60	13.60
Bladder	13.60	13.60	13.60	13.60	13.60	13.60	13.60	13.60	13.60	13.60
Colon	13.60	13.60	13.60	13.60	13.60	13.60	13.60	13.60	13.60	13.60
Gall bladder	13.60	13.60	13.60	13.60	13.60	13.60	13.60	13.60	13.60	13.60
Kidneys	13.60	13.60	13.60	13.60	13.60	13.60	13.60	13.60	13.60	13.60
Liver	13.60	13.60	13.60	13.60	13.60	13.60	13.60	13.60	13.60	13.60
Pancreas	13.60	13.60	13.60	13.60	13.60	13.60	13.60	13.60	13.60	13.60
Prostate/Uterus	13.60	13.60	13.60	13.60	13.60	13.60	13.60	13.60	13.60	13.60
Small intestine	13.60	13.60	13.60	13.60	13.60	13.60	13.60	13.60	13.60	13.60
Spleen	13.60	13.60	13.60	13.60	13.60	13.60	13.60	13.60	13.60	13.60
Stomach	13.60	13.60	13.60	13.60	13.60	13.60	13.60	13.60	13.60	13.60

E.4 CTDI_{vol,organ} – Chest

E.4.1 TCM

Organ	CTDI _{vol,organ} (mGy)									
	Reference Voxelized Phantom									
	Baby	Child	Donna	Frank	Golem	Helga	Irene	ICRP Female (Regina)	ICRP Male (Rex)	Visible Human
Breast	1.36	-	14.11	5.88	-	14.49	4.52	7.96	7.89	-
Heart	1.34	3.68	10.86	10.13	9.16	10.96	4.27	7.37	9.42	10.55
Lung	1.37	3.96	13.49	12.69	11.30	14.95	6.88	8.93	10.21	13.19
Thymus	1.38	4.39	9.41	6.69	15.07	12.33	3.29	10.96	12.47	22.78

**No breast voxels were identified in the Child, Golem and Visible Human reference voxelized phantoms.

E.4.2 FTC

Organ	CTDI _{vol,organ} (mGy)									
	Reference Voxelized Phantom									
	Baby	Child	Donna	Frank	Golem	Helga	Irene	ICRP Female (Regina)	ICRP Male (Rex)	Visible Human
Breast	13.60	-	13.60	13.60	-	13.60	13.60	13.60	13.60	-
Heart	13.60	13.60	13.60	13.60	13.60	13.60	13.60	13.60	13.60	13.60
Lung	13.60	13.60	13.60	13.60	13.60	13.60	13.60	13.60	13.60	13.60
Thymus	13.60	13.60	13.60	13.60	13.60	13.60	13.60	13.60	13.60	13.60

**No breast voxels were identified in the Child, Golem and Visible Human reference voxelized phantoms.

E.5 CTDI_{vol,organ} – Chest/Abdomen/Pelvis (CAP)

E.5.1 TCM

Organ	CTDI _{vol,organ} (mGy)									
	Reference Voxelized Phantom									
	Baby	Child	Donna	Frank	Golem	Helga	Irene	ICRP Female (Regina)	ICRP Male (Rex)	Visible Human
Adrenals	1.53	4.09	13.00	23.66	11.69	16.59	6.56	8.15	10.38	14.05
Bladder	2.26	4.85	23.46	18.10	16.82	23.47	15.70	23.46	15.61	24.07
Breast	1.36	-	14.11	5.88	-	14.49	4.52	7.96	7.89	-
Colon	1.74	4.36	17.77	21.39	13.91	18.50	10.54	16.02	12.02	15.44
Gall bladder	1.48	3.95	12.03	24.22	9.73	17.64	6.62	8.70	10.66	13.99
Heart	1.34	3.68	10.86	10.13	9.16	10.96	4.27	7.37	9.42	10.55
Kidneys	1.53	3.96	13.64	23.97	11.54	17.13	6.60	9.10	10.28	14.00
Liver	1.52	3.91	13.34	21.98	11.35	18.19	6.40	8.06	10.19	13.95
Lung	1.37	3.96	13.49	12.69	11.30	14.95	6.88	8.93	10.21	13.19
Pancreas	1.78	3.95	12.21	24.27	11.51	17.25	6.56	8.96	10.43	14.00
Prostate/Uterus	2.06	4.54	23.55	21.56	22.71	23.51	16.23	23.56	16.58	23.51
Small intestine	1.51	4.19	18.18	20.93	13.45	19.30	11.32	13.98	11.96	14.40
Spleen	1.50	3.85	12.93	22.87	11.43	18.90	6.06	8.16	9.60	13.74
Stomach	1.54	3.92	12.76	23.75	11.26	20.68	6.16	8.48	10.14	13.21
Thymus	1.38	4.39	9.41	6.69	15.07	12.33	3.29	10.96	12.47	22.78

**No breast voxels were identified in the Child, Golem and Visible Human reference voxelized phantoms.

E.5.2 FTC

Organ	CTDI _{vol,organ} (mGy)									
	Reference Voxelized Phantom									
	Baby	Child	Donna	Frank	Golem	Helga	Irene	ICRP Female (Regina)	ICRP Male (Rex)	Visible Human
Adrenals	13.60	13.60	13.60	13.60	13.60	13.60	13.60	13.60	13.60	13.60
Bladder	13.60	13.60	13.60	13.60	13.60	13.60	13.60	13.60	13.60	13.60
Breast	13.60	-	13.60	13.60	-	13.60	13.60	13.60	13.60	-
Colon	13.60	13.60	13.60	13.60	13.60	13.60	13.60	13.60	13.60	13.60
Gall bladder	13.60	13.60	13.60	13.60	13.60	13.60	13.60	13.60	13.60	13.60
Heart	13.60	13.60	13.60	13.60	13.60	13.60	13.60	13.60	13.60	13.60
Kidneys	13.60	13.60	13.60	13.60	13.60	13.60	13.60	13.60	13.60	13.60
Liver	13.60	13.60	13.60	13.60	13.60	13.60	13.60	13.60	13.60	13.60
Lung	13.60	13.60	13.60	13.60	13.60	13.60	13.60	13.60	13.60	13.60
Pancreas	13.60	13.60	13.60	13.60	13.60	13.60	13.60	13.60	13.60	13.60
Prostate/Uterus	13.60	13.60	13.60	13.60	13.60	13.60	13.60	13.60	13.60	13.60
Small intestine	13.60	13.60	13.60	13.60	13.60	13.60	13.60	13.60	13.60	13.60
Spleen	13.60	13.60	13.60	13.60	13.60	13.60	13.60	13.60	13.60	13.60
Stomach	13.60	13.60	13.60	13.60	13.60	13.60	13.60	13.60	13.60	13.60
Thymus	13.60	13.60	13.60	13.60	13.60	13.60	13.60	13.60	13.60	13.60

**No breast voxels were identified in the Child, Golem and Visible Human reference voxelized phantoms.